2000

A Study of the Effect of Alpha-Nucleus Potential on Alpha-Induced Transfer Reactions in the Sci-Shell.

Das, Susanta Kumar

University of Rajshahi

DEDICATED TO
MY DEPARTED PARENTS
AND
THE MARTYRS OF
LIBERATION WAR
AND THEIR FAMILIES

A STUDY OF THE EFFECT OF ALPHA-NUCLEUS POTENTIAL ON ALPHA-INDUCED TRANSFER REACTIONS IN THE sd-SHELL

Ph.D. Thesis
By

SUSANTA KUMAR DAS

B. Sc. (Honors), M. Sc. (Physics),
University of Rajshahi, Bangladesh.

Nuclear Research Laboratory
Department of Physics
Rajshahi University
Bangladesh.

JUNE 2000.

A STUDY OF THE EFFECT OF ALPHA-NUCLEUS POTENTIAL ON ALPHA-INDUCED TRANSFER REACTIONS IN THE sd-SHELL

A DISSERTATION

SUBMITTED TO THE DEPARTMENT OF PHYSICS, UNIVERSITY OF RAJSHAHI, IN FULFILMENT OF THE REQUIREMENTS FOR THE DEGREE OF DOCTOR OF PHILOSOPHY

IN PHYSICS

BY

SUSANTA KUMAR DAS

PHYSICS BUILDING,
JUNE, 2000.

Nuclear Research Lab.,
Department of Physics.
Rajshahi University,
Rajshahi,
Bangladesh.

DECLARATION

I, **Susanta Kumar Das,** hereby declare that the whole of the work now submitted as a thesis towards the fulfillment for the degree of Doctor of Philosophy in Physics at the Rajshahi University , is the result of my own investigation.

Susanta Das 11.06.2000.

(Susanta Kumar Das)
Signature of the candidate

11.6.2000

(Dr. Arun Kumar Basak)
Professor, Department of Physics,
University of Rajshahi,
Rajshahi, Bangladesh.

Countersigned by Supervisor.

CERTIFICATE

I, **Susanta Kumar Das,** hereby certify that the work contained in this thesis has not been accepted in substance for any degree, and is not being concurrently submitted in the candidature for any other degree.

Susanta Das 11.06.2000.

(Susanta Kumar Das)
Signature of the candidate

11.6.2000

(Dr. Arun Kumar Basak)
Professor, Department of Physics,
Rajshahi University,
Rajshahi, Bangladesh.

Countersigned by Supervisor.

ACKNOWLEDGMENT

This is a privilege for me to express my sincerest gratitude to my supervisor Professor Arun Kumar Basak, department of Physics, Rajshahi University for his constant vigilance, direction, constructive criticism and propelling intuitive initiatives in pursuing the whole investigations. Words are always insufficient to express his working capabilities and unending enthusiasm for scientific rigorousness for innovative investigations. This always becomes the everlasting source of inspiration for his students.

I extend my tribute to Prof. H. M. Sen Gupta, department of Physics, Dhaka University and Prof. F. B. Malik, department of Physics, Southern Illinois University at Carbondale for their constant encouragement.

I must extend my appreciation to Prof. Sayeedur Rahman Khan, the Vice-chancellor, Rajshahi University and Mrs. Khan for their loving care and keen interest in the progress of my work.

I wish to thank my teachers, Prof. Abdus Salam Mondal and Prof. Nazrul Islam, present and former Chairman, department of Physics, Rajshahi University for providing a beautiful scientific environment for research for the entire period of my work and for showing positive interest into the study. I also extend my deep respect for my other teachers, Prof. M. M. Haque, Prof. G. S. Islam, Prof. G. Mahtaboally, Prof. A.K. M. A. Islam, Prof. K. Banu, Prof. Shamsunnahar Islam, my friends Prof. S. Bhattacharjee, Prof. E. Haque, Mr. A. Uddin and other esteemed teachers of the department for encouraging me constantly.

I am also thankful to all the staffs and employees of Physics department for the all out help and cooperation they offered me.

I wish to thank Prof. M. Raquib Ahmed, administrator, Computer Center, Mr. S. Rahman, M. Zakir Hossain and other staffs of CC for their cordial and sincere help.

It's a pleasure for me to express my thanks to other members of our Nuclear Research group, A. S. B. Tariq, A. F. M. M. Rahman, P. K. Roy, M. S. Hossain and

Ms. M. Haque for their cooperative, positive and enthusiastic attitude to create a scientific environment in the Lab. for exploring new ideas. I enjoyed it thoroughly all the time and it will remain ever bright in my memory as a source of inspiration for my future work.

This work is partially supported by Grant No. INT-9808892 of the US National Science Foundation. I thankfully acknowledge and appreciate the US National Science Foundation for this grant.

I express my sincerest gratitude to American Institute of Bangladesh Studies (AIBS) and its chairman, Dr. Sayedur Rahman to offer me the fellowship for visiting Southern Illinois University at Carbondale, USA. It made a substantial help to complete my work successfully. I am also thankful to Centre for Developement Research, Bangladeh (CDRB) for all possible help for my travel to the USA on behalf of AIBS.

It is a great pleasure for me to remember and mention the unforgettable and cordial hospitality, I was offered by the department of Physics of SIUC. I am thankful to Prof. R. Tao, Chairman and other members of the faculty for all kinds of spontaneous support they provided for pursuing my research.

I will remain ever grateful to Mrs. Akemi Malik for the cordial hospitality and care she extended for me during my stay at SIUC. I will also remain thankful for her earnest feelings and well wishes for my children and family.

I especially like to appreciate Mrs. Sylvia Shaw, Mrs. S. Pleasure and other staffs of the office of the department of Physics, SIUC, providing me of every official support I needed, even before I mentioned it. I also express my appreciation for Mr. W. Walker for his sincere help in using computational facilities in the computer center without any hindrance. I will be simply ungrateful if I don't express my gratitude for all the staffs of the library of SIUC for their earnest and ardent help.

I got a loving touch of the hearts of a flock of young gems of Bangladesh, who have been pursuing their higher studies in different Universities in USA, during the days I stayed at SIUC. My young friends, Ali A. Shams and his wife Fonty, Shyamal K. Das and his wife Jhumur, M. Fhokrul Islam and M. Masudul Haque, whom I like

to be proud of, as my former students, Kalyani Rama and her husband, Shusmi and her husband and many others whose names are impossible to mention within this short space, all of them, extended their all out help for everything I needed to continue my work smoothly. Probably, the most suitable words my weak pen can express to convey my gratitude are, 'They made a piece of Bangladesh for me abroad'

It's a pleasure for me to mention my gratitude to my friends Prof. R. N. Bose, department of chemistry, Kent State University, Ohio and Mrs. A. Bose for their wishes and encouragement for the completion of the work.

I thankfully acknowledge the grants and study leave from Shahjalal University of Science and Technology, Sylhet. It made a great help to complete my works without practical difficulties. I like to express my gratitude and thanks to Prof. Habibur Rahman, the Vice-Chancellor of Shahjalal University of Science and Technology for his personal initiatives for valuable helps he provided me for time to time I needed.

No words are sufficient enough to express my appreciation and gratitude for Dr. Yasmeen Haque and Prof. Zafar Iqbal, my friends and colleagues for their enthusiastic suggestions, guidance, inspiration and concrete help to achieve my goal. I will remain ever grateful to them.

I like to thank all of my colleagues of Physics and other departments, the officers and staffs of SUST, for their constant encouragement and wishes for me.

It is a special gratitude to Mrs. Devika Basak for her loving care to me and for her constant encouragement for my work. She always stood steadfastly beside me with her affectionate help during my hard days.

Among my well-wishers, I must mention the names of Mr. Saranan Pramanik, his family, Mrs. N. Bhattacharjee, wife of my friend, Prof. S. Bhattacharjee for their constant inspiration.

I also thankfully acknowledge the wishes of my relatives, well-wishers and innumerable friends. I felt greatly encouraged when all of them showed keen interests in the progress of my works.

At last, I must admit that I have no words to express my gratitude for my sons Arka and Joy and for my wife Promila for their sacrifice and help. My wife has taken over all the responsibilities of my family and children on her shoulder with courage and borne it efficiently to set me free from all agonies for pursuing my research. I will never be able to repay my debt to them by any means.

The author.
June 2000.

Title: A study of the effect of alpha-nucleus potential on alpha-induced transfer reactions in the sd-shell

Table of contents: **Page**

ABSTRACT

Effects of the molecular, normal optical Woods-Saxon and squared Woods-Saxon (Michel) α-nucleus potentials on the $^{27}Al(\alpha,t)^{28}Si$, $^{28,29,30}Si(\alpha,d)^{30,31,32}P$ and $^{28}S(\alpha,p)^{31}P$ reactions have been studied. The parameters of the molecular and Michel α-^{27}Al potential have been generated by fitting the α-elastic data on ^{27}Al at the incident energy E_α=64.5 MeV. The potential parameters of molecular, normal optical and Michel potential at E_α=25 MeV have been determined by analyzing of α-$^{29,30}Si$ elastic data. The elastic fits in these cases, seem to be of similar quality for all three forms of potentials.

Full-finite range (FFR) distorted wave Born approximation (DWBA) calculations have been performed using the molecular, Michel and normal optical potentials to analyze the angular distributions of cross-section for the 53 transitions populating the bound and unbound states of ^{28}Si *via* the (α,t) reaction. The molecular, Michel and optical potentials are found to produce satisfactory fits to the reaction data. For all the three potentials in the entrance channel, the deduced *l*-transfers for the transitions to the 15.02, 15.85 and 16.11 MeV states, differ from the assignments previously reported. The extracted spectroscopic factors are compared with shell-model predictions.

FFR macroscopic and zero-range (ZR) microscopic distorted wave Born approximation calculations have been performed using molecular, normal optical and Michel potentials to analyze the angular distributions of cross-section for 12 transitions populating 0.0, 0.709, 1.454, 1.974, 2.538, 2.72, 2.84, 3.02, 3.93, 4.62, 5.42 and 7.20 MeV. states of ^{30}P *via* the (α,d) reaction. Only the molecular potential has been able to reproduce satisfactorily the angular distribution and order of magnitude of cross-sections

for different transitions, but the normal optical potential is found to be inadequate in accounting the large angle data. The Michel potential is unsatisfactory in relation to both reproducing angular distribution at large angles and the correct order of magnitude of cross-section. The macroscopic spectroscopic factors for the d-cluster transfer have been deduced from the full finite-range (FFR) distorted-wave Born approximation (DWBA) and compared to the shell-model predictions for the even parity states. The assignment of the spin-parity of the 3.93 MeV state is confirmed.

Angular distributions of cross-sections of 9 transitions of ^{31}P populated through ^{29}Si(α,d)^{31}P reaction have also been analyzed by both macroscopic FFR DWBA and microscopic ZR DWBA using the molecular, normal optical and Michel potentials. The spectroscopic factors yielded by the macroscopic calculations have been compared to the theoretical spectroscopic factors, calculated from spectroscopic amplitudes of three different interactions. Normalization constants for the (α,d) reaction in the ZR DWBA calculations have been extracted. Spectroscopic factors yielded by molecular potential are found to comparable to the corresponding theoretical spectroscopic factors, whereas, those for normal optical and Michel potentials are found to be 1-2 orders higher in magnitude.

The macroscopic FFR DWBA and microscopic ZR DWBA analyses performed using the molecular, normal optical and Michel potentials for 8 transitions of ^{32}P excited *via* ^{30}Si(α,d)^{32}P reaction have been compared to the experimental data. The experimental spectroscopic factors and normalization constants are extracted from the macroscopic and microscopic calculations, respectively. The overall fits using the molecular potential are found reasonable. The normal optical and Michel potentials fit reasonably for most of the

states only at the forward angle region, but underestimates the magnitude of the cross-sections by same order as mentioned in the case of $^{28,29}Si(\alpha,d)^{30,31}P$ reactions.

The best fit value for the finite-range parameter for the zero-range DWBA calculations for (α,d) reaction has also been deduced and found to be 0.7 fm.

The $^{28}Si(\alpha,p)^{31}P$ differential cross-section at 26 MeV incident energy has been analyzed in DWBA with zero and full-finite range and CCBA. Parameters of deep and shallow optical, Michel and molecular potentials in the incident channel are determined from the elastic scattering data. The calculations done with the deep optical and Michel potentials reproduce the structure of the angular distributions reasonably well, but fail to account for the absolute magnitudes by a few orders. The shallow optical one is satisfactory up to about $\theta_{cm}=100^0$. The molecular potential, on the other hand, reproduces both the correct magnitude of absolute cross-sections and the pattern of the angular distributions. CCBA calculations improve fits to the data over the DWBA predictions.

LIST OF TABLES

LIST OF FIGURES

CHAPTER 1

INTRODUCTION

1.1. *Preamble and Rationale*

Through the decades, the nucleon transfer reactions have established themselves as useful tools in the study of spectroscopy of the nuclei. The interaction of various kinds of projectiles with different nuclei as targets have been extensively studied using different form of scattering and reaction data. A significant improvement has been achieved in the knowledge of the light particle wave functions and of potentials of proton, neutron, deuteron, triton and hellion-nucleus system. The situation is, however, not satisfactory with the interactions of alpha-particles with other nuclei, and hence still leaves some questions to be answered.

Since the first observation of anomalous large angle scattering (ALAS) by Correlli *et al.* [1] in the elastic scattering of α-particles by ^{16}O and ^{32}S, it has also been found to occur in other elastic and non-elastic processes [2–21] induced by α-particles. The normal optical model potentials are found to be inadequate in reproducing ALAS in elastic, inelastic and transfer reactions involving α-particles [10–13,18]. Hodgson [22] has also pointed out the problems to have a really satisfactory global α-nucleus potential.

The ALAS problem, from the very beginning of its discovery invoked the researchers to float different *ad hoc* models to explain it. But the models suggesting the inclusion of Hauser-Feshbach resonance contribution [9,23], the use of *l*-dependent absorption [10], or the use of arbitrary WS^n (n>2) form factors [12] have not been able to give a consistent and theoretically sound description of alpha-elastic scattering over a

significant range of targets and energies. Two alternative type of potentials have been proposed to explain ALAS. The one, advocated by Michel *et al.*[20–21,24], is a special type of optical potential with a squared Woods-Saxon (WS) geometry. The another one is a molecular type of complex potential suggested by Block and Malik [25] and developed through a series of works [26–29], having a repulsive core in its real part. Both the potentials have been successful in reproducing the ALAS in the scattering of α- particles [19–21, 28–29] by some 2s-1d nuclei. On the other hand, Schmittroth *et al.* [16] have established that the use of a complex molecular potential could enhance the back angle scattering in a single-nucleon transfer reaction involving heavy ion.

Non-elastic processes have so far been, in most cases, treated within the framework of direct reaction theory using the normal optical potential (WS type) in the distorted channels. The ALAS in the data of (α,d) and (α,p) reactions on ^{28}Si [18], have been analyzed by Jankowski *et al.* [18] in terms of incoherent sum of the distorted wave Born approximation (DWBA) contribution calculated with the normal optical potentials and the compound nucleus contribution calculated on the basis of the Hauser-Feshbach model [30]. In addition, the elastic and the transfer data could not be fitted with the same optical potential. Above all, at the incident energy more than 20 MeV, the compound nucleus effect is expected to be highly improbable. In spite of all these inconsistencies within, the method has, however, enjoyed a limited success. So, the ALAS problem for the (α,d) and (α,p) reaction remains yet to be resolved.

1.2. *Object of the present study*

To the best of our knowledge there is no available report dealing with the description of transfer reactions using either of the molecular and Michel type of potentials, although these potentials could reproduce successfully the elastic α-scattering data for a number of 2s-1d targets [19]. But the normal optical potential has failed to account for the same.

The present study is the first attempt to perform a comparative study of the effect of three forms of α-nucleus potentials obtained from the corresponding elastic scattering on the single, two, and three nucleon transfer reactions. There is a well-known contention [31] that the potentials capable of producing both elastic and transfer processes with the same parameter will certainly have preference to others, those can only produce elastic but not the corresponding transfer processes. So, this study is motivated with a view to test how far, the two proposed alternative types of potentials capable of analyzing the ALAS effect in elastic scattering can account for the one, two and three nucleon transfer reactions.

The present study comprises basically of three steps:

(1) to generate parameters of three form of alpha-nucleus potentials by fitting α-elastic scattering data on the sd-shell targets.

(2) to analyze the single, two and three nucleon transfer reaction data on the targets using the corresponding potential parameters.

(3) to extract the spectroscopic information available in the study of the reaction processes.

1.3. *Methodology*

One nucleon transfer reactions probe the single particle structure of nuclear states [32]. The (α,t) reaction having large negative Q-value has the special criterion of populating selectively the states of high angular momentum.

In contrast, two nucleon transfer reactions probe the correlation that exists between nucleon pairs in the states produced. The nature of this correlation can be best understood if the structure of the light particles in the reaction is relatively well known. In that view, it has been shown as a well-known fact that the (α,d) reaction is a valuable spectroscopic tool for locating two-particle states [33–37]. Because of the large negative Q-value involved, the reaction favours the transitions to states coupled to the maximum allowed spin. Moreover, unlike the one-nucleon transfer reaction, the (α,d) reaction involving two nucleon transfer is dependent on the coherence property, e.g., the signs of the different components of the wave function. The (α,d) reactions enjoy another advantage in that they can be analyzed in terms of both the macroscopic (cluster transfer) and the microscopic approaches in the form factor calculations. The important feature of the (α,d) reactions lies in populating states with T=0 transfer. Moreover, since the spin transfer S=1 is unique, the *l*-transfer L=J is only allowed for the natural parity states (assuming the angular momentum in deuteron as *l*=0), two L-transfers $L = J \pm 1$ are permitted for exciting the unnatural parity states.

The three-nucleon transfer e.g., (α,p) reaction involves a complex process. In addition to contribution from compound nucleus and pre-compound processes, the direct

part of the reaction may comprise of triton stripping, knock-on and heavy particle stripping. Triton stripping has been found to be the dominant one [42]. Although the oscillations in the angular distribution can be reproduced reasonably by the DWBA calculation on the basis of triton-stripping, the absolute magnitude of cross-section are underestimated by two to three orders in such predictions [43]. However, the (α,p) reaction has shown to be a valuable spectroscopic tool for locating high-spin states at higher excitation of the final nucleus because of the 'high-spin selectivity' arising from a strong angular momentum mismatch between entrance and outgoing channels [150]

The experimental data for elastic and reaction processes has been chosen keeping conformity with the object of the present study. The ^{27}Al $(\alpha,\alpha)^{27}$Al and ^{28}Si$(\alpha,\alpha)^{28}$Si data are taken from the references Yasue *et al.* [44] and Jarczyk *et al.* [9] respectively. The source of ^{29,30}Si$(\alpha,\alpha)^{29,30}$Si data is the reference [45].

For single nucleon-transfer reaction, the present study includes the experimental data of Yasue *et al.* [44] for the ^{27}Al$(\alpha,t)^{28}$Si reaction at E_α= 64.5 MeV leading to 56 transitions with an energy resolution of about 35 keV. The DWBA analyses of the work of Yasue *et al.* [44] use only the normal optical potential. But they did not use the appropriate form factor as well as full finite-range calculations for the transitions to the states in the unbound region. In the present study, the scheme is to investigate the effect of FFR for particle transfer to bound as well as to unbound states using normal optical, Michel and molecular potentials within the formalism of resonance form factor formulated by Vincent and Fortune [46,47]. One point of discrepancy in relation to this experimental data is to be noted here that there are no cross-section data either of elastic or of reaction beyond the scattering angle greater than 60^0 (CM). Hence, lack of the data

at the large scattering angle may cause some limitation in shedding deeper insight in determining the details of the potentials.

For the two-nucleon transfer reaction, the present study is undertaken to examine the normal optical, molecular and Michel potentials in analyzing the two-nucleon transfer reactions $^{28}Si(\alpha,d)^{30}P$ from Jankowski *et al.* [18] at 26 MeV incident energy and $^{29,30}Si(\alpha,d)^{31,32}P$ [48] reactions at 25 MeV probe energy. In the first case, the target is an α-cluster nucleus and there is a substantial ALAS effect in the angular distributions. For the latter two non-alpha cluster nuclei, Davis and Nelson [48] could forge reasonable fits to the reaction data by adjusting the parameters of the normal optical potential obtained from the elastic fit. So, in the present study, in this case, the α-nucleus potential parameters for all form factors (normal optical, Michel and molecular) generated by fitting the elastic data have been used without any modification to analyze the reaction data both in macroscopic and microscopic calculations.

For three nucleon transfer reaction, the experimental data of $^{28}Si(\alpha,p)^{31}P$ from Jankowski *et al.* [18] has been chosen with the obvious purpose to examine to what extent, the molecular and Michel potential can account for the ALAS effect observed in this three nucleon transfer reaction on the nucleus ^{28}Si, which is well known for producing ALAS effect. The experimental data of the $^{28}Si(\alpha,p)^{31}P$ reaction from Janskowski *et al.* [18], provides the angular distribution at large scattering angles (θ_{cm}~170°), where the data is expected to be sensitive to the nature of α-nucleus potential.

The present study involves the methodology of Distorted Wave Born Approximation (DWBA) for all the cases of one, two and three-nucleon transfer reactions. In the three reactions resulting angular momentum mismatch due to large

magnitude of the reaction Q-value leads to the dominant contribution from the nuclear interior and hence to show the sensitivity of the α-potential. For analyzing two-nucleon transfer reaction data, both the macroscopic (cluster transfer) and microscopic form factors have been used. The three-nucleon transfer (α,p) reaction is treated with both the macroscopic DWBA method and CCBA formalism for analyses.

Consequently, the first few chapters present the theoretical formalism, in context to the present study. Chapter-two contains the theoretical background of the general formalism of the optical potential giving special attention to present different forms of alpha-nucleus potentials. Chapter-three is devoted to illustrate the theory of direct reaction process involving one, two, and three-nucleon transfer. The formalism of coupled-channels Born Approximation (CCBA) has been developed in chapter-four. Chapter-five is engaged in presenting the DWBA analyses of one, two, and three-nucleon transfer reactions. Chapter-six deals with results and discussion of the study and chapter-seven summarizes the conclusion.

Appendix presents the articles based on the present study, those are published in the Journal.

CHAPTER 2

OPTICAL MODEL

2.1. *Prologue to optical model analysis of elastic scattering*

In the theory of DWBA, one of the ingredients of the transition amplitude is the 'distorted waves' in the entrance and exit channels. Those are nothing but the elastic scattering wave functions of the mentioned channels, associated with the relative motions of the colliding pairs before and after the collision.

These distorted waves are generated from the Schrödinger equation in the optical model approximation

$$\left\{\nabla^2 + k^2 - \left(\frac{2\mu}{\hbar^2}\right)\left[U(r)+U_c(r)\right]\right\}\chi = 0 \qquad (2.1)$$

To solve the Schrödinger equation, it is necessary to have a complete knowledge of the forms of optical potential $[U(r)+U_c(r)]$ which includes the Coulomb potential in addition to nuclear one. The present study involves the α-nucleus potential in the entrance channel and triton, deuteron and proton-nucleus potential in the exit channels. So, this section will be devoted to underline the general formalism of the optical model potential as well as its different concrete forms for α-nucleus system.

The general formalism of optical model has been extensively dealt with for decades since from its first introduction and truly speaking it is now basically and mostly the subject matter of text-books. A brief and relevant theoretical aspect of the optical model has been presented here and the details follows from the references [49–53]

2.2. *General formalism of the optical potential*

An optical model is a model of the effective interaction. It attempts to replace the complicated many-body problem posed by the interaction of two nuclei by the much simpler problem of two particles interacting through a potential. Such a replacement is only feasible within a model space containing just one or a few channels. With a one-channel model, the most common case, only the elastic scattering can be described. Sometimes, a few particular inelastic channels are also included. This is often referred to as a 'generalized' optical model and leads to coupled-channels problems.

So, the optical model lies on the basis of the assumption that the scattering is determined by the bulk features of the nuclei and is insensitive to the details of nuclear structure, and hence it might be possible to describe it by a simple model of the effective interaction.

To do this , a simplifying assumption is made that all individual nucleon-nucleon interactions between the projectile and the target nucleus can be replaced by one effective interaction. The interaction can be replaced by a potential V(r), where r is the separation of the projectile and the nucleus. This is the same as the assumption underlying the shell-model.

Now, the question arises, what would be the overall feature and form of this potential. A general argument is usually accepted in this formalism that, inside the nucleus, the projectile is aware only of its nearest neighbors because of the short-range character of the nucleon-nucleon interaction. Since it is surrounded by nucleons, there is no net force and the potential V(r) is expected to be uniform inside the nucleus. As the

nucleon-nucleon force is of short range, it is also expected that the potential will follow the nuclear matter distribution. Hence the potential begins to fall from its interior value in the region of nuclear surface.

The potential, thus apprehended by itself will not suffice to account for the experimental data , because, it is only able to scatter the incident particles; in reality, they may also be absorbed by the compound nucleus and/or by the other non-elastic processes. So, the removal of these particle fluxes have a profound effect on the scattering process.

At this point, the *optical model* makes the use of an analogy between the scattering and absorption of particles by a nucleus and those of light by a cloudy-crystal ball. So, analogous to complex refractive index in the optical phenomena, the idea of complex potential has been introduced to explore the scattering problem in the nuclear case.

To show that the basic idea of a complex potential, namely , that its imaginary part has the effect of removing particle flux from elastic channel, we take the Schrödinger equation for scattering by a complex potential [53]

$$\nabla^2\psi + \frac{2\mu}{\hbar^2}(E + U + iW)\psi = 0 \qquad (2.2)$$

Multiplying by ψ^*, and subtracting the complex conjugate of this equation multiplied by ψ, we get,

$$\psi^*\nabla^2\psi - \psi\nabla^2\psi^* = -\frac{4i\mu W}{\hbar^2}\psi\psi^* \qquad (2.3)$$

Now the quantum mechanical expression for the density of current is

$$\vec{j} = \frac{i\hbar}{2\mu}\left(\psi^*\frac{\partial\psi}{\partial r} - \psi\frac{\partial\psi^*}{\partial r}\right) \qquad (2.4)$$

From Eq. (2.3)

$$\vec{\nabla}.\vec{j} = -\frac{2}{\hbar} W\psi\psi^* \qquad (2.5)$$

and $\psi^*\psi$ is the probability density, so this equation is equivalent to the classical continuity equation,

$$\frac{\partial\rho}{\partial t} + div\vec{j} = -kv\rho \qquad (2.6)$$

where v is the velocity of the particle inside the nucleus, a steady state has been attained so that the term $\frac{\partial\rho}{\partial t}$ in the above equation vanishes. This shows that providing W>0, the imaginary part of the complex potential has the effect of absorbing flux from the incident beam.

The total absorption cross-section from the total measured flux can be calculated, so that, [53]

$$\sigma_A = \int_0^{2\pi}\int_0^{\pi} \frac{i\hbar}{2\mu U}\left(\psi^* \frac{\partial\psi}{\partial r} - \psi\frac{\partial\psi^*}{\partial r}\right) r^2 \sin\theta \; d\theta \; d\varphi \qquad (2.7)$$

Now, the wave function,

$$\psi = -\sum_L \frac{(2L+1)}{2ikr} P_L(\cos\theta)\left(S_L e^{ikr} - e^{-ikr}\right) \qquad (2.8)$$

where $S_L = e^{2i\delta_L}$ is the partial scattering amplitude, δ_L being the phase shift.

Hence,

$$\sigma_A = \frac{\pi}{k^2}\sum_L (2L+1)\left(1 - |S_L|^2\right) \qquad (2.9)$$

and the total cross-section is given by,

$$\sigma_T = \frac{2\pi}{k^2}\sum(2L+1)\,(ReS_L) \qquad (2.10)$$

The differential cross-section for the elastic scattering of the nucleon or group of nucleons by nuclei can also be described by the optical model potential making use of the quantum mechanical scattering formalism.

Thus, the optical potential is the extension of the shell-model potential for bound nucleons to positive energies. It is essentially the same potential, representing the nuclear mean field, that acts on both bound and scattered particles, and it thus unifies the understanding of nuclear structure and nuclear reactions.

2.3. The standard forms of different part of the optical potential

2.3.1. *Real part of the potential*

The real part of the potential is due to the action of all the nucleons in the nucleus on the incident particle and it is usual to assume, at least for light ions that the interior of the real potential is flat and attractive (negative) and, because of short range of nuclear force, rises quickly and monotonically to zero in the surface region.

Many analytic forms have been used for real part of potential that embody the above assumption [49,50], but the most popular one has been the Woods-Saxon [54], a particular case of an Eckart [55] potential:

$$U(r) = -Vf(x_0), \qquad f(x_0) = \left(e^{x_0}+1\right)^{-1}, \quad x_0 = \left(r-R_0\right)/a_0 \qquad (2.11)$$

where V, R_0 and a_0 are known as the well-depth, radius and diffuseness, respectively.

2.3.2. *Imaginary part of the potential*

The imaginary or absorptive potential is assumed to have a 'volume' or 'surface' form or sometimes a sum of both types. The volume form is usually defined as, [52]

$$W(r) = W_V f(x_W), \qquad f(x_W) = \left(e^{x_W} + 1\right)^{-1}, \quad x_W = \left(r - R_W\right)/a_W \tag{2.12}$$

where the radius R_w and diffuseness a_w need not have the same values as in the real potential.

The surface absorption is most often taken to be proportional to the derivative of *f(x)* [52],

$$W_S(r) = 4W_D \frac{df(x_D)}{dx_D} = -4W_D \frac{e^{x_D}}{\left(e^{x_D} + 1\right)^2}, \quad x_D = \left(r - R_D\right)/a_D \tag{2.13}$$

This has a peak value of $-W_D$ at $\mathrm{r} = \mathrm{R_D}$ (hence the factor of 4 in the definition) and a FWHM of $\Delta \mathrm{x_D} = 3.525$. If both surface and volume terms are used, one frequently assumes $R_D = R_W$ and $a_D = a_W$.

2.3.3. *The spin-orbit coupling*

The simplest vector spin-orbit coupling has the form similar to predominantly a surface type of coupling; the phenomenological form that is commonly used [52] is,

$$U_{SO}(r) = V_{SO}\left(\frac{\hbar}{m_\pi c}\right)^2 \frac{1}{r}\frac{df(x_{SO})}{dr}\vec{L}.\vec{I}\ , \quad x_{SO} = \left(r - R_{SO}\right)/a_{SO} \tag{2.14}$$

where the Woods-Saxon function *f(x)* is defined as usual . The factor $\left(\frac{\hbar}{m_\pi c}\right)^2$, the square of the pion Compton wavelength is a relic of the derivation of this term from the meson theory of nuclear forces; its numerical value is close to 2 fm^2. It is also to be noted that when $I = \frac{1}{2}$, U_{SO} is frequently defined with I replaced by the Pauli vector $\sigma = 2I$; the corresponding coefficient V_{so} is then often only half as large. Sometimes it is usual to allow $R_{SO} \neq R_V$, $a_{SO} \neq a_V$.

2.3.4. *Coulomb potential*

Coulomb potential $V_C(r)$ is that of charged particle in the electrostatic field of the nucleus. This is calculable from the nuclear charge distribution but in practice, it is sufficiently accurate to use the potential due to a sphere of radius R_C with its charge uniformly spread throughout its volume,

$$V_C(r) = \begin{cases} \dfrac{Z_I Z_T e^2}{2R_C}\left(3 - \dfrac{r^2}{R_c^2}\right) & r \leq R_c \\ \dfrac{Z_I Z_T e^2}{r} & r > R_C \end{cases} \qquad (2.15)$$

where Z_I and Z_T are the charges of the incident particle and target nucleus. R_C is given by $R_C = r_C A_T^{1/3}$.

2.4. Alpha-nucleus potential

The present work investigates the effects of different forms of α-nucleus potential on transfer reactions. It has been already mentioned in the introduction that the

conventional form of optical potential for α-particle is inadequate in accounting for the ALAS effect. So, theoretical formulation for alternative proposals for α-nucleus potentials demanding the adequacy in accounting for ALAS is relevant. This section will be devoted for extracting the necessary aspects of the following forms of α-nucleus potentials:

1. Usual form of optical potential henceforth called 'Normal optical potential'.
2. Squared Woods-Saxon potential henceforth called 'Michel potential'.
3. Molecular type of potential henceforth called 'Molecular potential'.

2.4.1. Normal optical potential for α-nucleus system

The normal optical potential for the α-nucleus system including Coulomb term is given by,

$$V(r) = V_C(r) - Vf(x_0) - i\left[Wf(x_W) - 4W_D \frac{df(x_D)}{dx_D}\right] \qquad (2.16)$$

where $f(x_i) = \left(1 + e^{x_i}\right)^{-1}$ with $x_i = \left(r - r_i A^{1/3}\right)/a_i$ and the subscript i = 0, W and D.

The Coulomb radius is given by $R_C = r_c A^{1/3}$, A is target mass.

2.4.2. The Woods –Saxon Squared Potential (Michel Potential)

The squared Woods –Saxon potential (Michel potential) was first used for a successful description of the α-^{40}Ca scattering from 20 to 170 MeV [56]. With the introduction of an energy dependent Gaussian factor to the real part, it has since been applied to the α-^{16}O scattering between 20 and 150 MeV [57] and produced excellent fits with the experimental data. Using this potential, some works have been done in

describing successfully the alpha cluster structure in ^{44}Ti [58,59] and oscillations in the fusion excitation function [60]. Adding a slight angular momentum dependence and an increase in barrier height, it has also been possible to explain low energy data down to 3.5 MeV [61]. This phenomenological form of potential has been found to be very similar to the equivalent local potential obtained in microscopic analysis using the resonating group (RGM) [62,63].

The Michel potential form including Coulomb term $V_C(r)$ comprises of the following [57] real $V_M(r)$ and $W_M(r)$ parts:

$$V_M(r) = V_0\left\{1+\alpha\, exp\left[-\left(\frac{r}{\rho}\right)^2\right]\right\}\left\{1+exp\left(\frac{r-R_R}{2a_R}\right)\right\}^{-2} + V_C(r) \qquad (2.17)$$

$$W_M(r) = -W_0\left[1+exp\left(\frac{r-R_I}{2a_I}\right)\right]^{-2} \qquad (2.18)$$

with $V_C(r)$ and R_C being the same as standard optical potential. α and ρ are two parameters introduced to take care of the energy dependence of the real part.

2.4.3. *The molecular potential*

2.4.3.1. How it has been introduced

The basic theoretical foundation of the molecular potential is embedded in the early works of Block and Malik [25]. In this paper they proposed it in an one-dimensional fits. Subsequently, L. Rickertsen *et al.*[64] fitted ^{16}O-^{16}O data nicely with the proposed nuclear molecular potential. The parameters of this potential were estimated from the two-nucleon potential in a model of the transient nuclear matter.

On the other hand, K.A. Brueckner *et al.* [65] derived this more accurately from two-nucleon interaction using Energy Density Functional (EDF) formalism using sudden approximation. But, it had a numerical error. Reichstein and Malik [28] showed that both in sudden and in adiabatic approximation, non-monotonic potential is expected. The sudden approximation was close to the one used by Rickertsen *et al.* [64] to fit ^{16}O-^{16}O data. The fit was extended to higher energies [66]. That the potential should be really non-local is discussed in Workshop on High Resolution, Heavy-Ion physics [67]. Subsequently the ^{12}C-^{12}C elastic data were fitted with molecular potential [68]. That the ^{12}C-^{12}C potential is molecular is confirmed by N. Ohtsuka *et al.* [69], M.A. Hooshyar, B. Compani-Tabrizi and F.B. Malik [70] and Mangård *et al.* [29]. Tariq *et al.*[19] could fit α+^{28}Si elastic scattering data by a molecular potential which was close to the derived potential from the EDF approach and also the derived scaled potential from the EDF can explain α+ $^{30,32}S$ elastic data as discussed in the present work.

W.Scheid, R. Lingensa and W. Greiner [71] showed that the calculation using two-centered shell model also yields a molecular potential. Determination of the ^{12}C-^{12}C potential from an inverse scattering theory also reveals it to be molecular [72].

Calculation of the imaginary part of molecular potential from two-nucleon phase-shifts [73] led it to be volume like and energy dependent, as is used in the present work.

With an object, to follow and illustrate the methods of parametrization of the molecular potential, the relevant aspects of EDF is being furnished here in the following section.

2.4.3.2. Energy density functional (EDF) formalism

The EDF formalism has its root in the statistical theory of nuclear total energy, first proposed by P. Gombas [74], R.A. Berg and L. Wilets [75], and L.Wilets [76],. They used simple two-nucleon interaction. Brueckner and his collaborators [77–80] and Bethe [81], refined this to include realistic two-nucleon interaction having hard-core at short distance. However, they failed to obtain proper binding energy with the observed density distribution.

Following the paper of Hohenberg and Kohn [82] which shows that the energy of any finite system could be written as a functional of energy density, J. Lombard [83] could reproduce nuclear masses using a density distribution derived in the Hartree-Fock calculations. However, Malik and Reichstein [84] clearly showed that nuclear masses can be reproduced using observed density distribution and energy density functional derived from the realistic Gammel-Thaler two-nucleon potential [80,85]

In this formalism, the total energy of the system is described as a functional of the local density which comprises of a nuclear matter part along with Coulomb correction as well as corrections due to non-homogeneity of nuclear density in the form of a term involving the gradient of the density.

The starting point of this formalism is the energy-density functional

$$E(\rho) = \int \varepsilon[\rho(r)]d^3r \qquad (2.19)$$

where ρ is the density which is the function of the relative distance between two colliding nuclei. So, to calculate the total energy of the system, a consistent and tractable form of ε(ρ) has to be known. In the works of Brueckner and his collaborators [77–80], ε(ρ) has been reported in the form,

$$\varepsilon(\rho) = (K.E)_{TF} + \rho V(\rho,\alpha) + \left(\frac{e}{2}\right) \Phi_c \rho_p - 0.7386 e^2 \rho_p^{4/3} + \left(\frac{\hbar^2}{8M}\right)\eta(\nabla\rho)^2 \qquad (2.20)$$

The first term $(K.E)_{TF}$ is the kinetic energy of the particles in the Thomas- Fermi approximation, having the following form,

$$(K.E.)_{TF} = \frac{3}{5}\left(\frac{\hbar^2}{2M}\right)\left(\frac{3\pi^2}{2}\right)^{2/3}\frac{1}{2}\left[(1+\alpha)^{5/3} + (1-\alpha)^{5/3}\right]\rho^{5/3} \qquad (2.21)$$

where M is the nucleon mass and $\alpha = \frac{N-Z}{A}$ is the neutron excess.

The second term V(ρ,α) in Eq.(2.20) is the non-Coulomb and nuclear matter contribution to the functional. It has been calculated within the framework of Brueckner-Hartree-Fock theory using the Brueckner, Gammel and Thaler [80,85] two nucleon interaction, and is given by ,

$$V(\rho,\alpha) = b_1(1 + a_1\alpha^2)\rho + b_2(1 + a_2\alpha^2)\rho^{4/3} + b_3(1 + a_3\alpha^2)\rho^{5/3} \qquad (2.22)$$

The parameters a and b are obtained by nuclear matter calculations with variable neutron excess [80].

The third term in Eq.(2.20) is the Coulomb interaction among protons and Φ_e can be expressed in relation to proton charge distribution ρ_p as

$$\Phi_c = \int e \frac{\rho_p(\vec{r})}{|\vec{r} - \vec{r}'|} d^3\vec{r}' \qquad (2.23)$$

The fourth term in Eq.(2.20) is the Pauli correction to the third term in the local density approximation [87].

The last term is the non-homogeneity correction. The coefficient η in the density gradient term incorporates both (a) the Weizsäcker non-homogeneity correction to the kinetic energy due to variable density distribution, and (b) additional corrections originating from those correlation between nucleons which are not included in $V(\rho,\alpha)$.

Using observed density distribution, one can get observed nuclear masses with η=8. For example, the calculated binding energies and masses calculated for different nuclei by Malik *et al.*[27,88] are exhibited in Tables (2.1–2.3). Now the method can be extended to calculate the potential V(r) between two nuclei within the framework of the energy density formalism following the London-Heitler type of approximation as,

$$V(r) = E(\rho_1, \rho_2) - E\left(\rho_1 \quad at \quad r = \infty\right) - E\left(\rho_2 \quad at \quad r = \infty\right) \qquad (2.24)$$

$E(\rho_1,\rho_2)$ is the mean energy of the compound system computed using Eq. (2.19), where density of the system is composed of an overlap of two density distribution $\rho_1(r)$, and $\rho_2(r)$ each of which varies continuously as a function of the separation distance r. The quantities E(ρ_1 at r = ∞) and E(ρ_2 at r = ∞) are the energies of the colliding nuclei when they are far apart.

It is evident from Eq.(2.24) that the parametrization of the interaction potential depends on the consideration of how the energy density $E(\rho_1,\rho_2)$ is superimposed, when energy densities $\rho_1(r)$ and $\rho_2(r)$ are known.

Table-2.1. Calculated total binding energies (cols. 4 and 5) using EDF for $\gamma = 8$ and 9. Experimental values given in col. 3 are from [90]. 2pf and 3pf in col. 2 are two and three point Fermi distribution functions from [89]. The last column gives results of liquid drop [91].

ELEMENT	DENSITY FUNCTION	B.E. (MeV) EXPT.	B.E. (MeV) $\gamma = 8$	B. E. (MeV) $\gamma = 9$	B. E. (MeV) M+S
^{12}C	2pf	92.2	92.5	88.0	
^{14}N	3pf	104.7	111.0	106.9	
^{16}O	3pf	127.6	125.2	121.3	123.0
^{24}Mg	2pf	198.3	194.1	189.3	
	3pf		194.5	189.9	
^{28}Si	2pf	236.5	234.3	228.5	
	3pf		239.1	233.3	
^{40}Ca	3pf	342.1	340.6	333.8	340.0
^{51}V	2pf	445.8	461.5	451.5	
^{58}Ni	3pf	506.5	516.5	506.7	
^{70}Ge	2pf	610.5	609.1	599.1	
^{88}Sr	2pf	768.4	793.5	778.7	
^{114}Cd	2pf	972.6	984.1	969.3	
^{139}La	2pf	1164.8	1184.1	1166.1	
^{148}Sm	2pf	1225.4	1229.6	1212.6	
^{165}Ho	2pf	1344.2	1339.4	1321.9	
^{197}Au	2pf	1559.4	1592.8	1568.9	
^{206}Pb	2pf	1622.3	1630.1	1607.7	
^{208}Pb	2pf	1636.4	1667.8	1642.3	1627.0
^{238}U	2pf	1801.7	1808.6	1785.1	1805.0

Table-2.2. Parameters used by various groups in evaluating nuclear masses and binding energy per nucleon E/A, in MeV, Fermi wave length, K_F in fm^{-1} and compressibility K, BGT, MR, BBCL, L and NN refer, respectively, to refs. [a], [b], [c], [d], [e] [80, 88, 79, 83, 92].

Parameters	BGT[a]	MR[b]	BBCL[c]	L[d]	NN[e]
η_2	8.0	10.3	11.955	15.2	7.23
b_1	-717.6	-741.28	-741.28	-818.25	-588.75
b	1142.2	1179.89	1179.89	1371.06	563.56
b_3	-452.6	-467.54	-467.54	-556.55	160.92
a_1	-0.146	-0.1933	0.2	-0.316	-0.424
a_2	0.23	0.3128	0.316	0.2	-0.0973
a_3	1.2	1.725	1.646	-1.646	-2.25
E/A	-15.23	-16.59	-16.59	-16.0	-15.6
k_F	1.433	1.447	1.447	1.36	1.36
k	172.6	184.7	184.7	180.00	250.0

[a] K. A. Brueckner, S. Coon, and J. Dabrowski, Phys. Rev. 168, 1184 (1968) [80].
[b] I. Reichstein and F. B. Malik, Condensed Matter Theory, 1, 291 (1985) [88].
[c] K. A. Brueckner, J. R. Buchler, R. C. Clerk and R. J. Lombard, Phys. Rev. 181, 1543 (1969) [79].
[d] R. J. Lombard, Ann. Phys. (N. Y.) 77, 380 (1973) [83].
[e] H. Ngô and Ch. Ngô, Nucl. Phys. A348, 140 (1980) [92].

Table-2.3. Calculated masses by various groups in the energy density approximation are compared with the experimental ones, marked EXPT. and with those obtained from the standard mass formula of Myers and Swiatecki (MS) [e]., MR [a], L [b], BBCL [c], and NN [d] refer, respectively, to the calculations in Refs.

NUCLEI	EXPT	MR[a]	L[b]	BBCL[c]	NN[d]	MS[e]
^{16}O	127.6	123.3	128.8	127.6	121.2	123
^{32}S	271.8	270.1				
^{40}Ca	342.1	342.0	342	340	342.1	340
^{48}Ca	416.0	416.2	422	422	348.9	415
^{56}Fe	492.3	496.7				
^{60}Ni	526.9	532.1	524	524	530.8	524
^{90}Zr	783.9	793.4	780	780	792.3	782
^{118}Pd		998.4				
^{122}Cd		1033.3				
^{140}Ce	1172.7	1181.8	1169	1173	1185.1	1171
^{142}Ba	1180.3	1185.7				
^{165}Ho	1344.8	1356.1				
^{208}Pb	1636.5	1628.8	1627	1630	1639	1627
^{234}U	1776.0	1778.0				
^{238}U	1801.7	1798.5	1797	1812	1814	1805
^{240}Pu	1813.4	1811.0				
^{240}Cf		1804.8				

[a] I. Reichstein and F. B. Malik, Condensed Matter Theory, 1, 291 (1985) [88].
[b] R. J. Lombard, Ann. Phys. (N. Y.) 77, 380 (1973) [83].
[c] K. A. Brueckner, J. R. Buchler, R. C. Clerk and R. J. Lombard, Phys. Rev. 181, 1543 (1969)[77].
[d] H. Ngô and Ch. Ngô, Nucl. Phys. A348, 140 (1980) [92].
[e] W. D. Myers and W. J. Swiatecki, Nucl. Phys. 81. 1 (1966) [91].

There may be two considerations at this point [29],

(i) adiabatic approximation,

(ii) sudden approximation.

The adiabatic approximation incorporates the idea that the density function ρ of the compound system is generated in such a way that at no point of the compound system does the density exceed that of the central density of any of the colliding nuclei. That means , in this case, the densities as they interpenetrate, have enough time to reorient and readjust and hence the parameters of the density distribution can be obtained by minimizing the energy with respect to them at every point of separation [28,67,84,93].

In the case of the sudden approximation [78], it is considered that the collision time of the two nuclei is shorter than the characteristic time of the internal motion of a nucleon so that the nuclei remain as if, frozen during the collision. And hence one can generate density ρ of the composite system by simply adding the densities of the two colliding nuclei as,

$$E(\rho_1,\rho_2) \cong E(\rho_1+\rho_2) \qquad (2.25)$$

Thus, once $\rho_1(r)$ and $\rho_2(r)$ are specified, $E(\rho_1,\rho_2)$ at a separation distance r can be obtained from Eq.(2.25).

2.4.3.3. Parametrization of the Molecular Potential

The basic idea of the sudden approximation has been applied to parametrize the interaction potential in the scattering of two heavy ions [64,69]. The method has been extended to α-^{28}Si nucleus elastic scattering in the ALAS region [29]. In the early paper

[84] to make the calculation more tractable, instead of using usual Fermi distribution for nuclear density, a trapezoidal form of distribution has been approximated. The result obtained using Fermi-distribution and trapezoidal approximation are shown to be satisfactorily close [29], but trapezoidal approximation gives the favourable situation for calculation avoiding the complexity.

The trapezoidal density distribution can be described as, [84],

$$\rho(r)=\begin{cases}\rho_0 & 0\le r\le r_0\\ \rho_0\left(\dfrac{b-r}{b-r_0}\right) & r_0\le r\le b\\ 0 & b\le r\le\infty\end{cases} \qquad (2.26)$$

The parameter b determines the surface thickness and r_0 the range of the constant density zone. These two parameters are related to the half-density radius C and the 10%-90% surface thickness parameter t by the relation,

$$b=C+\left(\tfrac{5}{8}\right)t \quad \text{and} \quad r_0=C-\left(\tfrac{5}{8}\right)t \qquad (2.27)$$

For generating the alpha-^{28}Si potential a density distribution of α and ^{28}Si has been considered in a consistent way, using actual observed density distribution and the potential is found to be similar to that of trapezoidal approximation [29]. Based on the total consideration, the real part of the molecular potential is parametrized as,

$$V(R)=-V_0\left[1+exp(R-R_0)\right]^{-1}+V_1\,exp\left[-\left(\frac{R}{R_0}\right)^2\right]+V_c \qquad (2.28)$$

with

$$V_c(R)=\begin{cases}\left(\dfrac{z_1 z_2 e^2}{2R_c}\right)\left(3-\dfrac{R^2}{R_c^{\,2}}\right) & R \le R_c \\ \dfrac{z_1 z_2 e^2}{R}, & R \ge R_c\end{cases} \qquad (2.29)$$

The Coulomb radius (R_c) of the composite system can be written as the sum of the Coulomb radii of the two nuclei separately [69], i.e.,

$$R_c = R_{c1} + R_{c2} = r_c\left(A_1^{1/3} + A_2^{1/3}\right) \qquad (2.30)$$

where A_1 and A_2 are the atomic masses of the two nuclei and r_c is the proportionality constant.

The imaginary part of the potential, W(R), is of Gaussian type,

$$W(R) = -W_0(E)\exp\left[-\left(\frac{R}{R_w}\right)^2\right] \qquad (2.31)$$

A microscopic calculation of the imaginary part [73] indicates this to be of the volume type and energy dependent.

Such a potential has been successfully used in the description of the α-^{28}Si elastic scattering in the ALAS region of 21 to 28 MeV with an energy independent real potential [19,29].

2.4.3.4. Scaling of the Parameters

Many of the parameters are expected to scale smoothly with mass numbers.

Using the simple scaling procedure,

$$R_i = R_{oi} + r_i A^{1/3} \qquad \text{i = 0, 1, W and C} \qquad (2.32)$$

and

$$V_i = b_i\left[4^{1/3} + A_T^{1/3} - (4+A_T)^{1/3}\right] \qquad \text{i = 0 and 1} \qquad (2.33)$$

it could also describe reasonably the elastic scattering of alpha particles from ^{32}Si and ^{34}S isotopes [19,94]. Actually scaling is likely to work among adjacent nuclei only and where the sudden approximation holds.

2.5. Comparative presentation of real parts of different forms of alpha-nucleus potential

The real part of different forms of α-nucleus potentials excluding the Coulomb part are,

1) ***Normal optical potential*** (WS)

The real part of normal optical potential (WS) is given as,

$$U(r) = -Vf(x_0), \qquad f(x_0) = \left(e^{x_0}+1\right)^{-1}, \quad x_0 = \frac{(r-R_0)}{a_0}$$

where V, R_0 and a_0 are known as the well-depth, radius and diffuseness respectively.

2) ***Squared-Woods-Saxon (Michel) potential***

The real part of Michel one is,

$$V_M(r) = V_0\left\{1+\alpha\, exp\left[-\left(\frac{r}{\rho}\right)^2\right]\right\}\left\{1+exp\left(\frac{r-R_R}{2a_R}\right)\right\}^{-2}$$

α and ρ are two parameters introduced to take care of the energy dependence of the real part.

3) ***Molecular potential***

The real part of molecular potential is,

$$V(R) = -V_0\left[1 + exp(R - R_0)\right]^{-1} + V_1 exp\left[-\left(\frac{R}{R_0}\right)^2\right]$$

The schematic representation of the real parts of different forms of alpha-^{28}Si has been displayed in the Fig. 2.1.

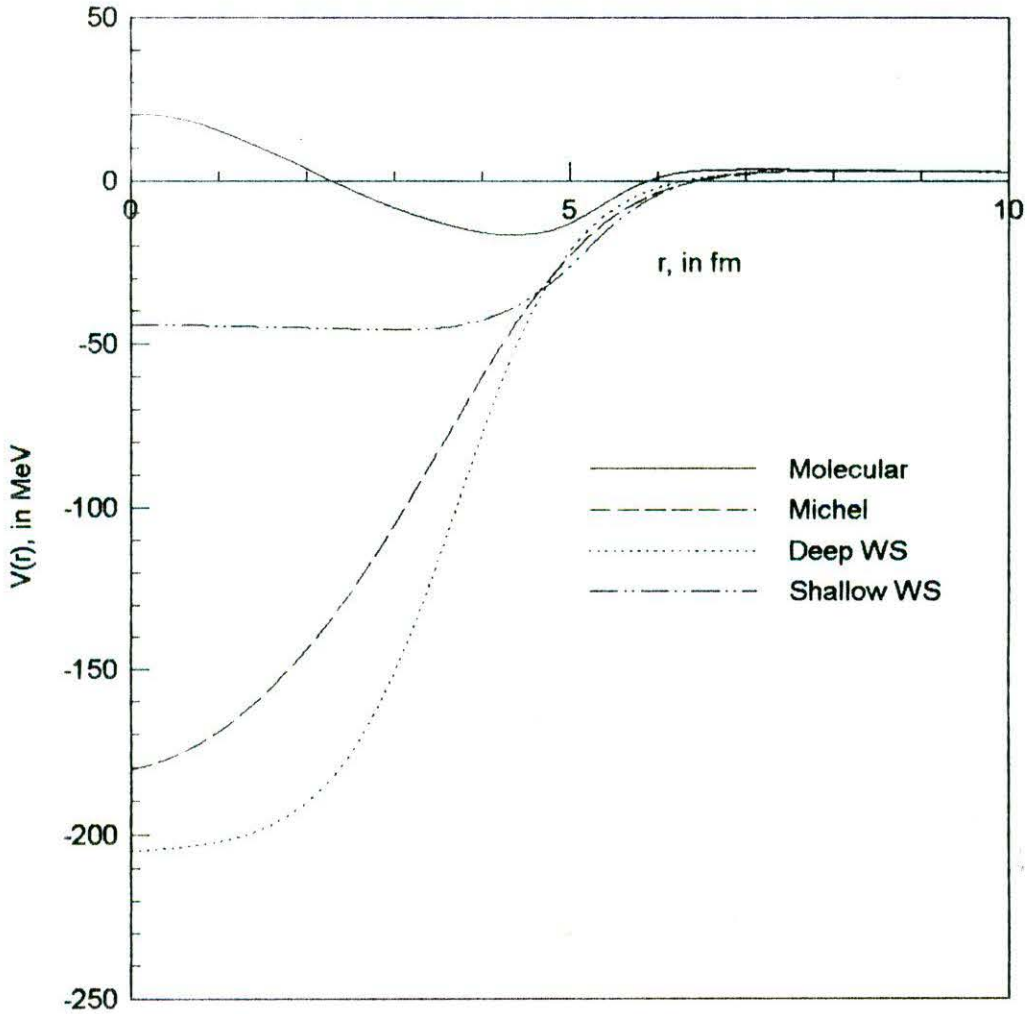

Fig.2.1. Schematic representation of real part of different alpha-^{28}Si potential.

CHAPTER 3

THEORY OF DIRECT NUCLEAR REACTION

3.1. *A prelude to direct reaction*

The goal of achieving an exact theory of nuclear reactions which would involve the solution of the nuclear many-body problem is yet to be reached. Immense efforts have been employed to analyze huge accumulation of experimental data related to nuclear reactions throughout the past decades and the process is on going. Amongst multifarious models to confront different phenomena, two models of the nuclear reactions have enjoyed particular success. Those are compound nucleus (CN) model and direct reactions (DR) models.

The study of direct nuclear reactions originated from the observation of some reactions characterized by the forward peaked angular distribution [95] and theories put forward to explain those observations [97,98]. The question of defining 'direct' reactions is one to which no all- embracing answer can be given. However, extensive review works have been done on it and it is usual to attribute the following characteristics to direction reactions:

(a) In direct reaction the transition from the incident channel to the reaction channel takes place in one step without the formation of an intermediate state.

(b) The interaction time for occurring direct-reaction is very short (~10^{-22} sec).

(c) The direct reaction is a surface process [101,102].

Qualitatively, it is assumed that in direct nuclear reaction, there is a good overlap between the wave function of the entrance and exit channels where the collision may occur with a minimum rearrangement of the constituent nucleons. As DR involves a

single step and only a few degrees of freedom, the reaction amplitudes depend on the overlap of the initial and final states; consequently direct reaction cross-sections represents the relations between two nuclear states. In addition, direct reactions are much more selective in the final states that they populate.

The direct reaction can be usually be classified into:

(i) The inelastic scattering where either one of the nucleons in the target makes a transition to a state or many nucleons coherently excited result in oscillation or rotations of the whole nucleus.

(ii) The transfer reactions comprising a transfer of a few nucleons either from the projectile to the target (stripping reactions) or from the target to the ejectile(pick-up reaction)

(iii) The knock-on reaction, where a nucleon or a light composite particle is ejected from the target by the projectile which itself continues to be the part of the residual final state. These reactions are also known as quasi-free scattering since here the collision takes place between the projectile and the ejectile, the rest portion of the target remaining as spectator.

3.2. *Basic principle of the theory of direct nuclear reaction*

The direct reaction theory of nuclear reactions can be regarded as an extension of the optical model [103]. According to the optical model, the elastic interaction between two nuclei can be described by a complex potential well. The direct reaction theory accepts the optical potentials as a first approximation, but introduces, as a perturbation an additional interaction which gives rise to non-elastic processes. This additional interaction affects some simple internal degree of freedom of one of the two nuclei involved in the collision. On the basis of this basic principle of perturbation different physical phenomena of direct nuclear interaction which includes inelastic, nuclear transfer (one or more) and the other rearrangement processes can be taken into account. Through the decades, starting from the models describing the simplest idea of one-nucleon transfer to more complicated processes of direct nuclear reactions have been successfully developed [52, 103–107].

The theory of direct nuclear reactions is concerned with calculating the transition amplitudes for various types of nuclear reactions on the basis of the models describing the physical situations. Since the direct interaction can be treated as a perturbation, the transition amplitude is given simply by the matrix element of the direct interaction with respect to the initial and final states of the wave functions. The physical content is essentially the extension of that carried by the formalism of Born approximation. Here, a few subsequent sections will be employed to develop this formalism step by step to tractable form to elucidate the realistic form of the nucleon transfer reactions.

3.3. The theory of distorted wave Born approximation (DWBA) for one-nucleon transfer

3.3.1. Transition amplitude

The DWBA theory of the reaction A(a, b)B is based upon a transition amplitude of the form [38,106]

$$T^{DW} = \left\langle \chi_b^{(-)} \Phi_B | V | \Phi_A \chi_a^{(+)} \right\rangle \qquad (3.1)$$

where, Φ_B and Φ_A denote respectively, the intrinsic states of the two nuclei in the initial and final channels. The functions χ_a and χ_b are the 'distorted waves'. They are elastic scattering wave functions which describe the relative motion of the pair a, A before collision and b, B after the collision respectively. In the optical model approximation the distorted waves are generated from a Schrödinger equation as mentioned in the previous chapter,

$$\left\{ \nabla^2 + k^2 - \left(\frac{2\mu}{\hbar^2} \right) \left[U(r) + U_c(r) \right] \right\} \chi = 0 \qquad (3.2)$$

where, $U(r)$ is the optical model potential, $U_c(r)$ the Coulomb potential and μ is the reduced mass of the pair. When the particle a and b have spin, and a spin-orbit coupling potential is included in the $U(r)$ in the Eq.(3.2), the functions χ become matrices in spin-space $\chi_{m'm}$, when m is the z-component of spin. Terms with $m' = m$ allow the possibility of spin-flip during the elastic scattering.

In application of the distorted-wave Born approximation to the transition amplitude Eq. (3.1), a certain pattern having to do with the angular momentum couplings will emerge each time. The particular factors that go into this, of course, depend on the

type of reaction under consideration. At this point, the general form has been anticipated and elucidated in the respective concrete cases subsequently. The brackets in Eq.(3.1) denotes an integration over the position coordinates of all nucleons and a sum over spin (and iso-spin if used) coordinates. There are (A+a) nucleons, so there are 3(A+a) spatial coordinates. Three of them will be chosen as c.m. coordinates in this system. The remainder are relative coordinates. For a rearrangement collision (a+A) → (a-x) + (A+x)≡ b+B, a convenient set of such relative coordinates consists of the 3(A-1), 3(x-1), and 3(b-1) intrinsic coordinates of A, x, and b together with $\vec{R}$ and $\vec{\rho}$, as shown in Fig.3. 1

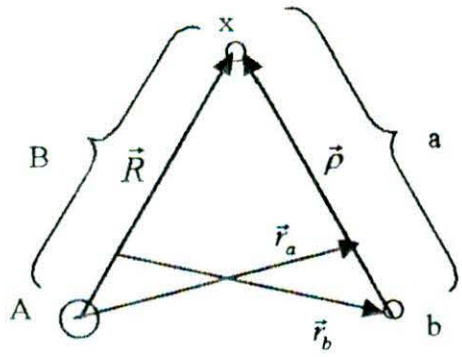

Fig.3.1. Schematic representation of the vector coordinates of the single-nucleon stripping reaction A(a,b)B, where (B = A+x) and (a = b+x; x=1)

which comprise of the correct number 3(A+a) – 3 of relative coordinates. A zero-range approximation is sometimes employed in nucleon-transfer reactions especially when **a** is a light nucleus like a deuteron, triton, or alpha etc. The interaction in this case is taken as a delta function on the coordinate $\vec{\rho}$. This is convenient because it reduces the number of

integration variables. Moreover, the distorted waves depend on the channel coordinates $\vec{r}_a$ and $\vec{r}_b$, which in terms of $\vec{R}$ and $\vec{\rho}$ are given by,

$$\vec{r}_a = \vec{R} - (b/a)\vec{\rho}, \qquad \vec{r}_b = (A/B)\vec{R} - \vec{\rho} \tag{3.3}$$

In the zero-range approximation,

$$\vec{r}_a \to \vec{R}, \qquad \vec{r}_b = (A/B)\vec{R}, \quad \vec{\rho} \to 0 \tag{3.4}$$

so that, the channel coordinates are conveniently proportional.

If the zero-range approximation is not made, then it is most convenient to transform $\vec{R}$ and $\vec{\rho}$ to $\vec{r}_a$ and $\vec{r}_b$, because the distorted waves are only known numerically as the solutions to the optical potential Schrödinger equation as shown in Eq.(3.2).

The transformation involves a non-unit Jacobian

$$d\vec{\rho}d\vec{R} = Jd\vec{r}_a d\vec{r}_b$$

Where, J is a matrix, indicated symbolically by,

$$J = \frac{\partial(\vec{\rho},\vec{R})}{(\vec{r}_a,\vec{r}_b)} = \begin{pmatrix} a & B \\ x & A+a \end{pmatrix}^3 \tag{3.5}$$

which relates the volume elements in the two coordinate systems.

After integrating over the intrinsic coordinates [104], the Eq. (3.1) can be written as

$$T^{DW} = J\int \chi_b^{(-)^*}\left(\vec{k}_b,\vec{r}_b\right) \left\langle \Psi_B\Psi_b|V|\Psi_A\Psi_a\right\rangle \chi_a^{(+)^*}\left(\vec{k}_a,\vec{r}_a\right) d\vec{r}_a d\vec{r}_b \tag{3.6}$$

$\vec{k}_a$ and $\vec{k}_b$ are the relative momenta before and after the collision respectively.

3.3.2. Multipole expansion of the interaction matrix

The matrix element of the interaction in Eq. (3.6) causing the non-elastic event, taken between the internal states of the colliding pairs is given by,

$$\langle \Psi_B \Psi_b | V | \Psi_A \Psi_a \rangle = \int \Psi_B^* \Psi_b^* V \Psi_A \Psi_a d\xi \qquad (3.7)$$

where, ξ represents all the coordinates independent of r_a and r_b. This factor is function of r_a and r_b and plays the role of a effective interaction for the transition between the elastic scattering states χ_a and χ_b. It contains all the information on nuclear structure, angular momentum selection rules and even the type of reaction (whether stripping, knock-on etc.) being considered.

The matrix element Eq. (3.7) can be expanded into terms which correspond to the transfer to the nucleus of a definite momentum *j*, which in turn is comprised of an orbital part *l* and spin part *s* [108]. If the particles **a** and **b** have spins $\vec{s}_a$ and $\vec{s}_b$, and the target and residual nuclear spins are $\vec{J}_A$ and $\vec{J}_B$, respectively, we define,

$$\vec{j} = \vec{J}_B - \vec{J}_A, \quad \vec{s} = \vec{s}_a - \vec{s}_b, \qquad \vec{l} = \vec{j} - \vec{s} \qquad (3.8)$$

The multipole series may be written with the Clebsch-Gordon coefficients [110] corresponding to the vector coupling in Eq. (3.8) as [38],

$$J\langle J_B M_B, s_b m_b | V | J_A M_A, s_a m_a \rangle = \sum_{lsJ} i^{-l} G_{lsJ,m}(\vec{r}_b, \vec{r}_a; bB, aA)$$

$$\times (-1)^{s_b - m_b} \langle J_A M_A, M_B - M_A | J_B M_B \rangle \langle s_a s_b m_a, -m_b | s m_a - m_b \rangle$$

$$\times \langle lsm, m_a - m_b | jM_B - M_A \rangle \qquad (3.9)$$

where $m = M_B - M_A + m_b - m_a$, the symbols bB, aA as arguments of G denotes the dependence on the various nuclear quantum numbers (other than z-components of spin). The function G may be defined by the inverted form of the expression (3.9) as

$$G_{lsj,m} = i^l J\left(\frac{2l+1}{2J_B+1}\right)\sum_{M_B M_A m_b m_a}\langle J_B M_B, s_b m_b|V|J_A M_A, s_a m_a\rangle$$

$$\times(-)^{s_b-m_b}\langle J_A jM_A, M_B - M_A|J_B M_B\rangle \times\langle s_a s_b m_a, -m_b|sm_a - m_b\rangle$$

$$\times\langle lsm, m_a - m_b|jM_B - M_A\rangle \qquad (3.10)$$

The factor i^l is included to ensure convenient time reversal properties [110].

It is helpful to write G as the product of two factors

$$G_{lsj,m}(\vec{r}_b, \vec{r}_a) = A_{lsj} f_{lsj,m}(\vec{r}_b, \vec{r}_a) \qquad (3.11)$$

A_{lsj} is the spectroscopic coefficient which includes fractional parentage coefficients for initial and final nuclear states and interaction strength. $f_{lsj,m}$ is the form factor.

It is evident from the Eq.(3.6) that the transition amplitude involves an integration over the space of both r_a and r_b. This six-dimensional integral is difficult in numerical calculation. Hence, the so called 'zero-range' approximation is often introduced , on two grounds, the interaction potential V has a short range and one or more of the internal wave functions has a small range. This zero-range assumption has the physical meaning that particle b is emitted at the same point at which particle a is absorbed, so that

$$\vec{r}_b = \left(A/B\right)\vec{r}_a .$$

The form factor of the Eq. (3.11) can then be written as

$$f^{(zero)}_{lsj,m}(\vec{r}_b,\vec{r}_a)=\delta\left(\vec{r}_b-\left(A/B\right)\vec{r}_a\right)\int f_{lsj,m}\left(\left(A/B\right)r_a-\rho,r_a\right)d\rho$$

$$=F_{lsj}(r_a)\;Y_l^{m}{}^{*}(\theta_a,\varphi_a)\;\delta\left(r_b-\left(A/B\right)r_a\right)\qquad(3.12)$$

Now, using the expressions (3.9) and (3.11), the transition amplitude (3.6) may be written [38],

$$T^{DW}=\left\langle\vec{k}_b,J_BM_B,s_bm_b\middle|V\middle|\vec{k}_a,J_AM_A,s_am_a\right\rangle$$

$$=\sum_{lsj}(2j+1)^{\frac{1}{2}}A_{lsj}\left\langle J_AjM_A,M_B-M_A\middle|J_BM_B\right\rangle\times\beta_{sj}^{lmm_bm_a}\left(\vec{k}_b,\vec{k}_a\right)\quad(3.13)$$

where $m=M_B-M_A+m_b-m_a$ and the 'reduced' amplitude $\beta_{sj}^{lmm_bm_a}$ is given by,

$$(2j+1)^{1/2}i^l\beta_{sj}^{lmm_bm_a}\left(\vec{k}_b,\vec{k}_a\right)=\sum_{m'_am'_bm'}\left\langle lsm',m'_a-m'_b\middle|jm-m_b+m_a\right\rangle$$

$$\times\left\langle s_as_bm'_a,-m'_b\middle|sm'_a-m'_b\right\rangle(-)^{s_b-m'_b}\int d\vec{r}_a\int d\vec{r}_b\,\chi^{(-)*}_{m'_bm_b}\left(\vec{k}_b,\vec{r}_b\right)$$

$$\times f_{lsj,m'}(\vec{r}_b,\vec{r}_a)\chi^{(+)}_{m'_am_a}\left(\vec{k}_a,\vec{r}_a\right)\qquad(3.14)$$

In the absence of spin-orbit coupling, the $\chi_{mm'}$ becomes diagonal and spin components $m=m'$. So, 'reduced' amplitude β_{sj} becomes,

$$(2j+1)\tfrac{1}{2}\beta_{sj}^{lmm_bm_a}(no.s.o.)=\left\langle lsm,m_a-m_b\middle|m-m_b+m_a\right\rangle$$

$$\times\left\langle s_as_bm_a,-m_b\middle|sm_a-m_b\right\rangle\times(-)^{s_b-m_b}(2l+1)^{\frac{1}{2}}\beta_{sj}^{lm}\qquad(3.15)$$

where,

$$(2l+1)^{1/2} i^l \beta_{sj}^{lm} = \int dr_a \int dr_b \chi_b^{(-1)^*}\left(\vec{k}_b, \vec{r}_b\right) f_{lsj,m}(\vec{r}_b, \vec{r}_a) \chi_a^{(+)}\left(\vec{k}_a, \vec{r}_a\right) \qquad (3.16)$$

This β_{sj} will still depend upon s and j, if the form factor f depends upon these quantum numbers.

3.3.3 Assumptions underlying DWBA formalism

The important assumptions underlying the formalism for making the calculations more tractable are:

(a) In DWBA theory, it is assumed that the transfer takes place directly from the target state to the final state by the simple deposit of the transfer particle to or from the target. Since the interaction potential (V_{bx}) does not depend on the A coordinates of the target, the reaction can take place only to the extent they are in the same state of the motion in the final nucleus; otherwise the matrix element would vanish.

(b) Another assumption concerns the distorted wave of the entrance and the exit channels. In practice, they are chosen to be wave functions of optical potentials whose parameters are chosen to reproduce the elastic cross-section. Any wave function which has the same phase shifts at large distances yields the same elastic cross-section. Since there are ambiguities and uncertainties in the optical model parameters, there are corresponding uncertainties in the wave functions in the nuclear region.

(c) The interaction potential (V_{bx}) is assumed to be central.

(d) The internal structure of the transferred particle is assumed to be unchanged during its transfer from target to the residual nucleus. And for single nucleon transfer, the parentage expansion may be described in shell-model terms.

(e) In DWBA, the transfer reaction is considered to be so weak that it may be treated in first order. This assumption may usually be valid, but Rawitscher and Mukherjee [109] have pointed out that in some reactions cross-sections are usually large. This implies that there may be other processes involved. Thus, the inelastic processes especially those involving collective states, are likely to be generally the more important of the higher order corrections to the DWBA.

(f) Sometimes it is usually assumed that the interaction potential V_{bx} (x is the transferred cluster or particle) has a short range and one or more of the internal wave functions has a small range. This assumption gives rise to 'zero-range approximation'.

Some of these assumptions may be elucidated in more concrete form involved in the following way:

1) It is mentioned earlier that in the reaction A(a,b)B, the projectile is assumed to be made up of the emitted particle b and another particle x which is captured by the targert, so that a= b+x and B=A+x.

The interaction responsible is taken to be V_{bx} , the potential binding b and x to form a.

For the present purpose, it is assumed that V_{bx} is central, that is, scalar in the separation distance r_{bx}, so that b and x are in a s state of relative motion within a.

The nuclear matrix element (3.9) is then explicitly written as [38],

$$\langle J_B M_B, s_b m_b | V | J_A M_A, s_a m_a \rangle$$

$$= \int \Psi^*_{J_B M_B}(r_{xA}, \xi_a \xi_A)\ \Psi^*_{s_b m_b}(\xi_b)\ V_{bx}(r_{bx} \xi_b \xi_x)\ \Psi_{J_A M_A}(\xi_A)\ \Psi_{s_a m_a}(r_{bx} \xi_b \xi_x) d\xi_A\ \ d\xi_b\ \ d\xi_x$$

(3.17)

Here ξ_A, ξ_x and ξ_b are the internal coordinates of the corresponding particle. The spin transfer s is now the spin of the transferred particle x. [Since, in general x may be a cluster of nucleons, s need not be unique].

The precise treatment of the amplitude (3.16) will depend upon the reaction model being considered.

However, for convenience, the wave function for the residual nucleus may be expanded in terms of the eigenstates of the target

$$\Psi_{J_B M_B}(r_{xA}, \xi_x \xi_A) = \sum_{j\mu J'_A M'_A} \Psi_{J'_A M'_A}(\xi_A) \Omega^{BA'}_{j\mu}(r_{xA} \xi_x) \langle J'_A j M'_A \mu | J_B M_B \rangle \qquad (3.18)$$

Since, it is assumed that the interaction V_{bx} does not depend on the coordinates r_{xA}, and hence cannot disturb the internal degrees of A only one term of the sum over J'_A, M'_A in Eq.(3.18) will contribute to the matrix element (3.17), namely that corresponding to the state of the target nucleus, $J'_A = J_A$ and $M'_A = M_A$.The Clebsch-Gordon co-efficient in Eq.(3.18) takes care of angular momentum coupling. The

remaining factor $\Omega_{j\mu}$ is associated with the wave function for the 'particle' x. The last factor $\Omega_{j\mu}$ may be expanded into spherical harmonics in r_{xA}, the coordinates of the centre of mass of x with respect to that of A, as,

$$\Omega^{BA}_{j\mu}(r_{xA},\xi_x)=\sum_{lsm} i^l Y_l^m(\theta_{xA},\varphi_{xA})\Phi^{BA}_{s,\mu-m}(r_{xA},\xi_x)\times\langle lsm,\mu-m|j\mu\rangle \quad (3.19)$$

In general, the function Φ that carries angular momentum s with component $(\mu-m)$ ***cannot be factored into functions depending on the radial coordinates*** r_{xA} ***and the 'internal' coordinates*** ξ_x ***separately. Simple factoring is only feasible if the internal structure of x does not change during its transfer from a to A and can be ignored. Strictly, it is only true for single-nucleon transfer.***

Even if Φ is not simply factorable, the integration over the internal co-ordinates ξ_b and ξ_x in Eq. (3.17) may be performed,

$$\iint \Psi^*_{s_b m_b}(\xi_b)\Phi^{BAlj}_{s,\mu-m}{}^*(r_{xA},\xi_x)V_{bx}(r_{bx},\xi_b\xi_x)\Psi_{s_a m_a}(r_{bx},\xi_b\xi_x)d\xi_b\xi_x$$

$$=\langle s_b s m_b,\mu-m|s_a m_a\rangle H_{lsj}(r_{xA},r_{bx}) \quad (3.20)$$

the scalar function H is defined by Eq. (3.20). Using Eq.(3.18), (3.19) and (3.20) in the matrix element (3.17), and comparing with Eq. (3.9), it may be immediately written as

$$G_{lsj,m}(\vec{r}_b,\vec{r}_a)=J\hat{s}_a\hat{s}^{-1}Y_l^m{}^*(\theta_{xA},\varphi_{xA})H_{lsj}(r_{xA},r_{bx}) \quad (3.21)$$

Here H is a scalar, the rotational property of G are clear. Further, G carries parity of $(-)^l$ even without use of zero-range approximation. *This is a consequence of the assumption that b and x are in an s state of relative motion when they form a.*

2) For a particular case of single-nucleon transfer, the parentage expansion (3.18) may be described in shell-model terms [111,112]. Hence, the function Ω can be

identified as the wave function Ψ for the nucleon orbital (l, j), times a spectroscopic amplitude

$$\Omega_{j\mu}^{BA}(r_{xA}, \xi_x) = \alpha_{lj}^{BA} \Psi_{lj,\mu}(r_{xA}, \xi_x) \qquad (3.22).$$

The usual spectroscopic factor [112] is then just $S_{lj} = n(\alpha_{lj})^2$ (n is the number nucleons in the orbit). The sum over l and s in Eq.(3.19) is now superfluous as $s = \frac{1}{2}$ only and $l = j \pm \frac{1}{2}$ according to parity change, and the function Φ is factorable,

$$\Phi_{s\alpha}^{BA,lj}(r_{xA}, \xi_x) = \alpha_{lj}^{BA} U_{lj}(r_{xA}) \Psi_{s\alpha}(\xi_x) \qquad (3.23)$$

where, U_{lj} is the radial function for the shell-model orbit and $\Psi_{s\sigma}$ is the nucleon spin function. Consequently, H_{lsj} in Eq. (3.20) is also factorable,

$$H_{lsj}(r_{xA}, r_{bx}) = \alpha_{lj}^{BA} U_{lj}(r_{xA}) D(r_{bx}) \qquad (3.24)$$

where,

$$\langle s_b s m_b \sigma | s_a m_a \rangle D(r_{bx})$$

$$= \iint \Psi_{s_b m_b}{}^*(\xi_b) \Psi_{s\sigma}{}^*(\xi_x) V_{bx}(r_{bx}, \xi_b \xi_x) \Psi_{s_a m_a}(r_{bx}, \xi_b \xi_x) d\xi_b \xi_x \qquad (3.25)$$

If the wave function for a is also factorable that is, if

$$\Psi_{s_a m_a}(r_{bx}, \xi_b \xi_x) = \Phi_a(r_{bx}) \Psi_{s_a m_a}(\xi_b \xi_x) \qquad (3.26)$$

then D in Eq. (3.25) becomes just

$$D(r_{bx}) = V_{bx}^{(s_a)}(r_{bx}) \Phi_a(r_{bx}) \qquad (3.27)$$

where $V^{(s_a)}$ is the value of V in the spin-state s_a.

The zero-range approximation is usually obtained by assuming that the function $D(r_{bx})$ is of short-range and may be replaced by a delta function as,

$$D(r_{bx}) \approx D_o \delta(r_{bx}) \tag{3.28}$$

Since,

$$r_{bx} = \left(r_b - \left(A/B \right) r_a \right) \left(aB/x(a+A) \right), \text{ then}$$

$$\delta(r_{bx}) = \delta\left(r_b - \left(A/B \right) r_a \right) \left(aB/x(a+A) \right)^{-3}$$

so that Jacobian in the expression cancels out from the amplitude.

3.3.4. Differential cross-section

The differential cross-section for unpolarised projectiles projectiles and unpolarized target nuclei is given [38] by,

$$\frac{d\sigma}{d\Omega} = \frac{\mu_a \mu_b}{\left(2\pi\hbar^2\right)^2} \frac{k_b}{k_a} \frac{\sum |T|^2}{(2J_A+1)(2s_a+1)} \tag{3.29}$$

Where, μ_a and μ_b are the reduced masses of the respective particles, and the sum is over M_A, m_a, M_B and m_b. In terms of the reduced amplitudes (3.14), Eq.(3.29) becomes,

$$\frac{d\sigma}{d\Omega} = \frac{\mu_a \mu_b}{\left(2\pi\hbar^2\right)^2} \frac{k_b}{k_a} \frac{2J_B+1}{(2J_A+1)(2s_a+1)} \sum_{jmm_b m_a} \left| \sum_{ls} A_{lsj} \beta_{sj}^{lmm_b m_a} \right|^2 \tag{3.30}$$

It is to be noted that sum over M_A and M_B has made different j values incoherent, but interference between different s and l remains. If only one value each of s and l are important or allowed, Eq. (3.30) may be written as,

$$\frac{d\sigma}{d\Omega} = \frac{2J_B+1}{2J_A+1} \sum_j \frac{|A_{lsj}|^2}{2s_a+1} \sigma_{lsj}(\theta) \tag{3.31}$$

where the 'reduced' cross-section is

$$\sigma_{lsj}(\theta) = \frac{\mu_a \mu_b}{(2\pi\hbar^2)^2} \frac{k_b}{k_a} \sum_{mm_b m_a} \left| \beta_{sj}^{lmm_b m_a} \right|^2 \qquad (3.32)$$

In order to compute the cross-section, it is necessary to have explicit expression for the 'reduced amplitude' β. It can be done with help of the partial wave expansion of the distorted wave χ. Restricting to the coupling like $\vec{L}.\vec{S}$ [108], the expansion of the distorted wave may be written as,

$$\chi_{m'm}^{(+)}(\vec{k},\vec{r}) = \left(\frac{4\pi}{kr}\right) \sum_{JLM} \langle LsMm | JM+m \rangle \langle LsM+m-m', m' | JM+m \rangle$$

$$\times i^L \chi_{LJ}(k,r) Y_L^M{}^*(\theta_k \varphi_k) Y_L^{M+m-m'}(\theta_r \varphi_r) \qquad (3.33)$$

The resultant angular momentum, $\vec{J} = \vec{L} + \vec{s}$, and its z-component $(M+m)$ are conserved during scattering by the spin-orbit potential, whereas the individual z-components of $\vec{L}$ and $\vec{s}$ are not. The partial waves are solutions of the Schrödinger equation

$$\left[\frac{d^2}{dr^2} + k^2 - \frac{L(L+1)}{r^2} - \left(\frac{2\mu}{\hbar^2}\right)\left(U + U_C + U_L^J\right)\right] \chi_{LJ}(k,r) = 0 \qquad (3.34)$$

with $\chi_{LJ}(0) = 0$. For large r, beyond the range of the nuclear potentials, these radial waves have the form,

$$\chi_{LJ}(k,r) = \tfrac{1}{2} i \left[H_L^*(kr) - \eta_L^J H_L(kr)\right] \exp(i\sigma_L) \qquad (3.35)$$

where, $H_L = G_L + iF_L$ is the outgoing-wave Coulomb function [113], and η_L^J is the reflection coefficient or scattering matrix element for the (L,J) wave. The η_L^J are computed by numerically integrating Eq. (3.34) and matching the function and its derivative to the form (3.35) at large r. In Eq. (3.34), $U(r)$ is the central optical, $U_C(r)$

the Coulomb potential and $U_L^J(r)$ the value of the spin-orbit coupling for the L and J wave.

For more general case, the form factor of Eq.(3.11) is expanded in spherical harmonics in r_a and r_b separately,

$$f_{lsj,m}(r_b,r_a) = \sum F^{sj}_{lL_1L_2}(r_b,r_a) Y^M_{L_1}{}^*(\theta_b\varphi_b) Y^{m-M}_{L_2}(\theta_a\varphi_a) \times \langle L_1 L_2 M m - M | lm \rangle \quad (3.36)$$

The Clebsch-Gordon coefficient ensures that f behaves like $Y_l^m{}^*$ under rotations. Using this in Eq.(3.13) with the partial wave expansion (3.19), only $L_1 = L_b$, $L_2 = L_a$ terms contributes, and we obtain for the 'finite range' case, if $m \geq 0$,

$$\beta^{lmm_bm_a}_{sj}(\theta, FR) = \pi_{ab}(-)^{m+j+s_b-s_a}\,\beta^{l-m-m_b-m_a}_{sj}(\theta, FR)$$

$$= \sum_{L_aL_bJ_aJ_b} i^{l-L_a-L_b}\hat{L}_a\hat{L}_b\hat{l}\hat{s}\langle J_b\, jm_b - m, m - m_b + m_a | J_a m_a\rangle$$

$$\times \langle L_a s_a 0 m_a | J_a m_a\rangle \langle L_b s_b - m, m_b | J_b m_b - m\rangle$$

$$\times \left[\frac{(L_b - m)!}{(L_b + m)!}\right]^{1/2} P^m_{L_b}(\theta) \begin{pmatrix} j & l & s \\ J_a & L_a & s_a \\ J_b & L_b & s_b \end{pmatrix} I^{lsj}_{L_aJ_bL_aJ_a} \quad (3.37)$$

where,

$I^{lsj}_{L_bJ_bL_aJ_a} = \frac{4\pi}{k_ak_b}\int r_a dr_a \int r_b dr_b \chi_{L_bJ_b}(k_b,r_b) F^{sj}_{lL_bL_a}(r_b,r_a)\chi_{L_aJ_a}(k_a,r_a)$, π_{ab} is the sign of parity change $(-)^{L_a+L_b}$; and $\hat{x} = (2x+1)^{1/2}$.

With this explicit form of 'reduced' amplitude β, the Eq. (3.16) and (3.17) gives the expression of differential cross-section.

3.4. Effect of non-locality of the optical potential

The effect of non-locality of the optical potential is usually considered in all DWBA treatment. A brief theoretical background has been outlined here. The illustration follows basically the references [99,106,114]. In most analysis of elastic scattering a phenomenological optical potential is sought which yields agreement with the data. This optical potential, $U_L(\vec{r})$, is usually taken to have a simple local form. By local, it is meant that at the point $\vec{r}$, the particle feels the potential only at that point. The Schödinger equation then reads,

$$\left(-\frac{\hbar^2}{2\mu}\nabla^2 + U_L(\vec{r}) - E\right)\Psi(\vec{r}) = 0 \qquad (3.38)$$

The situation in a real scattering problem, is always more complicated than encompassed by this equation. For example, the incident particle can excite the nucleus. The true state vector for the system has therefore, many components describing many things that can happen, and those are coupled to each other by virtue if the mutual interactions that can connect the various components or channels.

Nonetheless, fundamental theory shows that the complicated problem involving many channels can be reduced to a simpler one containing few , or only the elastic channels, provided that the interaction between the scattered particle and the nucleus is suitably modified. This modified, or effective, interaction is, however, a very complicated object. No really satisfactory calculation of it can be made, and certainly not an exact

one. It is usual to transmit the effect in the energy dependence and non-locality means that the term $U_L(\vec{r})\Psi(\vec{r})$ in Eq. (3.38) must be replaced by

$$\int U(\vec{r},\vec{r}')\Psi(\vec{r}')d\vec{r}' \tag{3.39}$$

where $U(\vec{r},\vec{r}')$ is the non-local potential. Thus the wave function at point $\vec{r}$ depends on conditions at all other points in the range of the non-local potential.

The consequences of a particular separable form of the non-locality have been explored by Perey and Buck [114]. Their result is

$$U(r,r') = U_0\left(\tfrac{1}{2}|\vec{r}+\vec{r}'|\right)H(\vec{r}-\vec{r}') \tag{3.40}$$

where, in numerical applications, the function H is taken to be Gaussian.

Two points to be noted here: first, that the equivalent local potential that yielded the same scattering as the non-local potential is weaker $|U_L| < |U_0|$; and, second, that in the interior region the wave function of the non-local potential, $\Psi_{NL}(\vec{r})$, smaller than the local potential $\Psi(\vec{r})$ which is known as 'Perey effect'. In fact, when the form of the non-locality, $H(\vec{r}-\vec{r}')$ is taken to be Gaussian of range β, a relationship between these two wave functions can be found such that

$$\Psi_{NL}(\vec{r}) = F(r)\psi(\vec{r}) \tag{3.41}$$

where $F(r)$ goes to unity in the exterior region but in the interior region F is less than unity and is [99]

$$F(r) = \left\{1 - \left(\frac{\mu\beta^2}{2\hbar^2}\right)U_L(r)\right\}^{\frac{1}{2}} \tag{3.42}$$

where, μ is the reduced mass. The value of β which Perey and Buck found for nucleons that yields a best fit to the data is $\beta(p) \approx 0.85 fm$, $\beta(\alpha) \approx 0.2 fm$, $\beta(d) \approx 0.54 fm$ and $\beta(t) \approx (0.2 - 0.3) fm$ [39].

3.5. Full finite-range DWBA computation

Charlton [149] developed a method to calculate full finite-range DWBA matrix element. This method is based on plane-wave expansions of the distorted waves, which allows a separation of coordinates and, in effect, replaces integrals with sums over plane-wave states.

The differential cross-section for a stripping reaction A(a,b)B is given by the Eq. (3.29) as,

$$\frac{d\sigma}{d\Omega} = \frac{\mu_a \mu_b}{(2\pi\hbar^2)^2} \frac{k_b}{k_a} \frac{1}{(2J_A + 1)(2s_a + 1)} \sum_{jmm_b m_a} \left| T^{DW} \right|^2 \tag{3.43}$$

where the transition amplitude (Eq. 3.6)

$$T^{DW} = J \int d\vec{r}_a d\vec{r}_b \chi_b^{(-)*}(\vec{k}_b, \vec{r}_b) \langle \psi_B \psi_b | V | \psi_A \psi_a \rangle \chi_a^{(+)}(\vec{k}_a, \vec{r}_a) \tag{3.44}$$

Now, the transition matrix can be written in terms of spectroscopic amplitude and reduced amplitude (Eq. 3.13) as,

$$T^{DW} = \sum_{lsj} (2j+1)^{1/2} A_{lsj} \langle J_A j M_A, M_B - M_A | J_B M_B \rangle \times \beta_{sj}^{jmm_b m_a}(\vec{k}_b, \vec{k}_a) \tag{3.45}$$

where $m = M_B - M_A + m_b + m_a$ and the 'reduced' amplitude $\beta_{sj}^{lmm_a m_b}$ is given by,

$$(2j+1)^{1/2} i^l \beta_{sj}^{lmm_a m_b}\left(\vec{k}_b, \vec{k}_a\right) = \sum_{m_a' m_b' m'} \left\langle lsm', m_a' - m_b' \middle| jm' - m_b' + m_a' \right\rangle$$

$$\times \left\langle s_a s_b m_a', -m_b' \middle| s m_a' - m_b' \right\rangle (-)^{s_b - s_a}$$

$$\int d\vec{r}_a d\vec{r}_b \chi_{m_b' m_b}^{(-)}\left(\vec{k}_b, \vec{r}_a\right)^* \times f_{lsm}(\vec{r}_b, \vec{r}_a) \chi_{m_a' m_a}^{(+)}\left(\vec{k}_a, \vec{r}_a\right) \qquad (3.46)$$

$f_{lsm}(\vec{r}_b, \vec{r}_a)$ is the form factor given by Eq. (3.36).

The coordinates $\vec{r}_a = \vec{R} - \left(\frac{b}{a}\right)\vec{\rho}$ and $\vec{r}_b = \left(\frac{A}{B}\right)\vec{R} - \vec{\rho}$ are shown in Fig. (3.1).

The distorted waves can be expanded using spherical harmonic as (Eq. 3.33)

$$\chi_{m'm}^{(\pm)}\left(\vec{k}, \vec{r}\right) = \left(\frac{4\pi}{kr}\right) \sum_{JLM} \left\langle LsMm \middle| JM + m \right\rangle \left\langle LsM + m - m', m' \middle| JM + m \right\rangle$$

$$\times i^L \chi_{LJ}^{(\pm)}(k, r) \mathcal{Y}_L^M(\theta_k \varphi_k) \mathcal{Y}_L^{M+m+m'}(\theta_r, \varphi_r) \qquad (3.47)$$

By using the method proposed by Charlton [149], the radial part of the distorted wave can be written as,

$$\chi_{LJ}^{(\pm)}(k, r) = (kr) \sum_{n=1}^{N(L)} a_{nLJ}^{(\pm)} j_L(k_n r) \qquad (3.48)$$

where j_L is a spherical Bessel function, and the expansion is applied over a limited region of space (for values of the radial coordinate up to R_L =20 to 25 fm.) and $N(L)$ is the number of plane-wave states at the partial wave quantum number state L. The coefficients $a_{nLJ}^{(\pm)}$ may be found as overlaps of χ_{LJ} and j_L, if the k_n's are chosen in such a way as to allow the functions to form a complete orthonormal set. This can be

accomplished, by choosing k_n such that $j_L(k_nR_L)=0$ or $j_L(k_nR_L)'=0$, where prime denotes derivative with respect to the argument evaluated at R_L.

But, Charlton [149] expanded the coefficients $a_{nLJ}^{(\pm)}$ to calculate numerically as,

$$a_{nLJ}^{(\pm)} = \sum_{n'=1}^{N(L)} N_{nn'}^{L} b_{n'LJ}^{(\pm)} \tag{3.49}$$

where

$$b_{n'LJ}^{(\pm)} = k^{-1} \int_0^{R_L} r dr \chi_{LJ}^{(\pm)}(kr) j_L(k_n r), \tag{3.50}$$

and

$$N_{nn'}^{L} = \left(\vec{O}^{L} \right)^{-1}_{nn'} \tag{3.51}$$

where $\vec{O}^{L}$ is a matrix and its elements are

$$O_{nn'}^{L} = \int_0^{R_L} r^2 dr \;\; j_L(k_n r) j_L(k_{n'} r) \tag{3.52}$$

Using the technique of Eq. (7–10), the radial part of Eq. (3.48) can be written as,

$$\chi_{LJ}^{(\pm)}(k,r) = (kr) \sum_{n=1}^{N(L)} \sum_{n'=1}^{N(L)} N_{nn'}^{L} b_{nLJ}^{(\pm)} j(k_n r) \tag{3.53}$$

With the use of

$$4\pi (i)^L j_L(kr) Y_L^M(\hat{r}) = \int d\hat{k}_n e^{i\vec{k}_n \cdot \vec{r}} Y_L^M(\hat{k}_n) \tag{3.54}$$

the expansion of the radial part of the distorted wave may be expressed as

$$4\pi (i)^L j_L(kr) Y_L^M(\hat{r}) = (kr) \sum_{n=1}^{N(L)} \sum_{n'=1}^{N(L)} N_{nn'}^{L} b_{n'LJ}^{(\pm)} \int d\hat{k}_n e^{i\vec{k}_n \cdot \vec{r}} Y_L^M(\hat{k}_n) \tag{3.55}$$

This form is used in a full finite-range (FFR) expression of transition matrix element. The computer code DWUCK5 [39] calculates the differential cross-section using this method.

3.6. The DWBA theory for two-nucleon transfer

3.6.1. Contrast between one and two-nucleon transfer reaction

As described in the previous sections, one-nucleon transfer reactions probe the single-particle structure of nuclear states. The angular distribution is sensitive to the orbital angular momentum of the state into which the nucleon is transferred to or transferred from. For two-nucleon transfer reactions, the angular distribution again is sensitive to the angular momentum transferred in the reaction. However, here the angular momentum is carried by a pair of nucleons, so that it does not directly reflect the angular momenta of the single-particle states into which the nucleons are transferred. Only to the extent that the two single-particle angular momenta must sum to the transferred angular momentum is there a constraint. The angular momentum of the pair generally can be shared between them in many different ways, and nothing in the measurement of the transferred angular momentum distinguishes between these. Therefore, all such ways that the angular momentum can be shared, consistent with the structure of the nuclear states connected by the reaction, must contribute *coherently* to the reaction. These coherence can produce large cross-sections in states for which it is constructive and very small ones in states for which it is destructive. The coherence depends on the correlation between the two nucleons – the degree to which they are transferred.

Correlation in the motion of a pair of nucleons inside a nucleus depends on two factors, one, the conservation of the angular momentum and parity and two, the nucleon-nucleon interaction. The angular momentum and parity of the nuclear state impose a certain minimum correlation because the motion of the nucleons must be consistent with

these conserved quantities. It is usually referred as static correlation and the nucleon-nucleon interaction induces spatial and spin correlation, known as dynamical correlation. In the language of shell-model, it is the interaction that is responsible for configuration mixing in the nuclear wave functions.

Consequently, the two-nucleon transfer reactions provide a means of testing nuclear wave functions in details not accessible to single-particle transfer reactions.

3.6.2. DWBA formalism for two nucleon transfer

It is sensible to develop DWBA formalism for two-nucleon transfer reactions analogous to that of one-nucleon transfer. We shall consider the two-nucleon transfer stripping reaction A(a,b)B represented diagrammatically in Fig.3.2a.

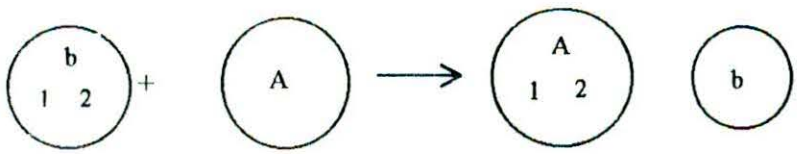

Fig.3.2a.Schematic diagram of two-nucleon transfer.

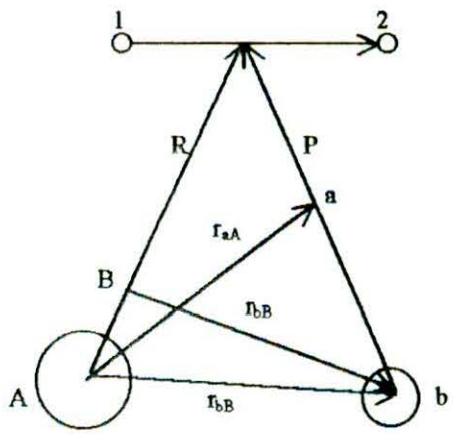

Fig.3.2b. Schematic representation of the vector coordinates used in the stripping reaction A(a,b)B of two-nucleon transfer. The point labeled B and a correspond to the c.m. of B(=A +1+2) and a(=b+1+2).

The DWBA expression for the transition amplitude for two-nucleon transfer can be written [105,115,116] as,

$$T_{fi} = J\sum_{\sigma_{a'},\sigma_{b'}} \int \chi^{(-)*}_{\sigma_{b'},\sigma_b}\left(\vec{k}_b,\vec{r}_{bB}\right)\left\langle \psi_{b',B}\middle| V_{aA}-\bar{U}_{aA}\middle|\psi_{a',A}\right\rangle$$

$$\times \chi^{(+)}_{\sigma_{a'},\sigma_a}\left(\vec{k}_a,\vec{r}_{aA}\right)d\vec{r}_{aA}d\vec{r}_{bB} \qquad (3.56)$$

Here J is the Jacobian of transformation to the relative coordinates $\vec{r}_{aA}$ and $\vec{r}_{bB}$, V_{aA} is the sum of all two-body interaction potentials between each nucleon in the projectile **a** and those in the target nucleus A; $\bar{U}_{aA}$ is the optical potential describing elastic scattering in the incident channel; $\chi^{(+)}_{\sigma_{a'},\sigma_a}$ and $\chi^{(-)}_{\sigma_{b'},\sigma_b}$ are the distorted waves in the entrance and exit channels respectively; $\psi_{a',A}$ and $\psi_{b',B}$ are respectively the totally antisymmetrized wave functions of the (a+A) and (b+B) systems. The primes on a and b in $\psi_{a',A}$, $\psi_{b',B}$, $\chi_{\sigma_{a'},\sigma_a}$ and $\chi_{\sigma_{b'},\sigma_b}$ are written to indicate that the corresponding z component of spin should carry a prime.

Similar to single nucleon transfer reactions, the matrix element $\left\langle \psi_{b',B}\middle| V_{aA}-\bar{U}_{aA}\middle|\psi_{a',A}\right\rangle$ contained the details of the actual interaction, while the distorted waves characterize the dynamics of the reaction

3.6.3. Exchange Effect on Transition Matrix

The totally antisymmetrized wave function $\psi_{a,A}$ can be expanded [105] as a linear combination of products of separately antisymmetrized wave functions ψ_a and ψ_A, i.e.,

$$\psi_{a,A} = \binom{a+A}{a}^{-\frac{1}{2}} \sum_{m=0}^{a} (-)^m \binom{a}{m}\binom{A}{m} P_{aA}\psi_a\psi_A \qquad (3.57)$$

where $P_{aA}\psi_a\psi_A$ makes m interchanges of particles between the groups a and A. $\binom{a+A}{a}^{-½}$ is the normalization factor. Similarly, $\psi_{b,B}$ can be expanded as

$$\psi_{b,B} = \binom{b+B}{b}^{-½} \sum_{n=0}^{b} (-)^n \binom{B}{n}\binom{b}{n} P_{bB}\psi_b\psi_B \qquad (3.58)$$

The interaction potential which appears in the transition amplitude can be written more explicitly as,

$$V_{aA} - \bar{U}_{aA} = \sum_{k=3}^{a}(V_{1k} + V_{2k}) + \left[\sum_{j=1}^{B}\sum_{k=3}^{a} V_{jk} - \bar{U}_{aA}\right] \qquad (3.59)$$

where V_{jk} is the two-body potential between nucleons j and k ; the sum k is over all nucleons in the projectile a, and the sum j over those in the core nucleus A. Assuming the 'core-independent' transition, the second term of the Eq.(3.59) becomes zero. So, with the foregoing assumption, the nuclear matrix element in (Eq.3.56) becomes,

$$\left\langle \psi_{b',B} \middle| V_{aA} - \bar{U}_{aA} \middle| \psi_{a',A} \right\rangle \approx \binom{a}{2}^{½}\binom{A+2}{2}^{½}$$

$$\times \left\langle \psi_{b'}\psi_B \middle| \sum_{k=3}^{b}(V_{1k} + V_{2k}) \middle| \psi_{a'}\psi_A \right\rangle \qquad (3.60)$$

3.6.4. Angular momentum expansion of the nuclear matrix element

Equation (3.60) can be evaluated with the help of nuclear shell model description of the wave functions of ψ_A and ψ_B. For stripping reaction, the first step is to expand the

final nucleus wave function $\psi_B(\xi_A, \vec{r}_1, \vec{r}_2)$ into a core wave function $\psi_A(\xi_A)$ and a pair wave function $\psi(\vec{r}_1, \vec{r}_2)$ using *jj* coupling. Integrating over the core coordinates ξ_A, the following result [105,106] is obtained :

$$\left\langle \psi_{b',B} \left| V_{aA} - \bar{U}_{aA} \right| \psi_{a',A} \right\rangle = \binom{a}{2}^{1/2} \binom{A+2}{2}^{1/2} \sum_{MN}^{[n_1 l_1 j_1]\,[n_2 l_2 j_2]\,LSJT} I_{AB}\left([n_1 l_1 j_1]\,[n_2 l_2 j_2]; JT \right)$$

$$\times \left(J_A M_A JM | J_B M_B \right) \left(T_A N_A TN | T_B N_B \right) \begin{bmatrix} l_1 & l_2 & L \\ \frac{1}{2} & \frac{1}{2} & S \\ j_1 & j_2 & J \end{bmatrix}$$

$$\times \left\langle \psi_{b'} \psi^{l_1 l_2\, LSJT}_{MN} \left| \sum \left(V_{1k} + V_{2k} \right) \right| \psi_{a'} \right\rangle \qquad (3.61)$$

The expansion coefficients known essentially as fractional parentage coefficients (cfp) are given by,

$$I_{AB}\left([n_1 l_1 j_1]\,[n_2 l_2 j_2]; JT \right) = \int \left[\psi^{*J_A T_A}(\xi_A)\ \psi^{*j_1 j_2 JT}(\vec{r}_1, \vec{r}_2) \right]^{J_B T_B}_{M_B N_B}$$

$$\times \psi^{J_B T_B}_{M_B N_B}(\xi_A, \vec{r}_1, \vec{r}_2)\ d\xi_A d\vec{r}_1 d\vec{r}_2 \qquad (3.62)$$

where the square brackets denote vector coupling, i.e.,

$$\left[\psi^{J_A T_A} \psi^{JT} \right]^{J_B T_B}_{M_B N_B} = \sum_{M_A N_A MN} \left(J_A M_A JM | J_B M_B \right) \left(T_A N_A TN | T_B N_B \right)$$

$$\times \psi^{J_A T_A}_{M_A N_A} \psi^{JT}_{MN} \qquad (3.63)$$

The *LS-jj* transformation bracket [104] in Eq.(3.61) is related to 9*j* symbol [110].

Now, the integral in Eq.(3.61) can be written in a form which separates the orbital and spin-isospin wave functions as

$$\left\langle \psi_{b'}\psi^{l_1 l_2 LSJT}_{MN} \middle| \sum (V_{1k}+V_{2k}) \middle| \psi_{a'} \right\rangle = \sum_{\Lambda\Sigma} (L\Lambda S\Sigma | JM)$$

$$\times \sum_{j=1}^{2}\sum_{k=3}^{a} \Sigma^{FG} X^{FG}_{jk} \left\langle \chi^{s_b t_b}_{\sigma_{b'} v_b} \chi^{ST}_{\Sigma N} \middle| Q^{F}_{jk} R^{G}_{jk} \middle| \chi^{s_a t_a}_{\sigma_{a'} v_a} \right\rangle \delta_{S+T,1} \qquad (3.64)$$

Here X^{FG}_{jk} contains only spatial integrals; that is,

$$X^{FG}_{jk} = \left\langle \varphi^{l_b=0}_{0} \varphi^{l_1 l_2 L}_{\Lambda} \middle| U^{FG}(r_{jk}) \middle| \varphi^{l_a=0}_{0} \right\rangle \qquad (3.65)$$

and the general form of the two-body interaction potential is given as

$$V_{jk} = \Sigma^{FG} U^{FG}(r_{jk})\ Q^{F}_{jk} R^{G}_{jk} \qquad (3.66)$$

Here $Q^{0}_{jk}(Q^{1}_{jk})$ and $R^{0}_{jk}(R^{1}_{jk})$ are spin and isospin singlet (triplet) projection operators for the pair *jk* and $U^{FG}(r_{jk})$ are radial wave functions; the pair wave function is

$$\psi^{l_1 l_2 LSJT}_{MN} = \sum_{\Lambda\Sigma} (L\Lambda S\Sigma | JM)\ \varphi^{l_1 l_2 L}_{\Lambda} \chi^{ST}_{\Sigma N} \delta_{S+T,1} \qquad (3.67)$$

where φ and χ are orbital and spin-isospin wave functions respectively.

For the case of (α,d) reaction a=4, b=2; $s_a = 0$, $t_a = 0$ and $s_b = 1$, $t_b = 0$, so the expansion of χ_a, is

$$\chi^{s_a=0,t_a=0}_{0,0}(1,2,3,4) = \Sigma^{S'T'} \left\langle \tfrac{1}{2}^{4}(00) \middle\{ \middle| \tfrac{1}{2}^{2}(S'T'); \tfrac{2}{1/2}(S'T') \right\rangle$$

$$\times \left[\chi^{S'T'}(1,2) \chi^{S'T'}(3,4) \right]^{00}_{00} \qquad (3.68)$$

The two-particle fractional parentage co-efficient has the value

$$(-)^{S'+1} \frac{1}{\sqrt{2}} \delta_{S'+T',1}$$

Evaluating the spin integration as displayed in Eq.(3.64) with the method of Racah algebra [105], the nuclear matrix element can be written as:

$$\left\langle \psi_{b'B} \middle| V_{aA} - \bar{U}_{aA} \middle| \psi_{a'A} \right\rangle = \binom{a}{2}^{\frac{1}{2}} \binom{A+2}{2}^{\frac{1}{2}} \sum_{\Lambda\Sigma MN}^{[n_1 l_1 j_1][n_2 l_2 j_2] LSJT} (-)^{b+1} \frac{1}{\sqrt{2}} \delta_{S+T,1}$$

$$\times I_{AB}\left([n_1 l_1 j_1]\ [n_2 l_2 j_2]; JT \right) \left(J_A M_A JM | J_B M_B \right) \left(T_A N_A TN | T_B N_B \right)$$

$$\times \left(s_b \sigma_{b'} S\Sigma | s_a \sigma_{a'} \right) \left(t_b \nu_b TN | t_a \nu_a \right) \left(L\Lambda S\Sigma | JM \right)$$

$$\times \begin{bmatrix} l_1 & l_2 & L \\ \frac{1}{2} & \frac{1}{2} & S \\ j_1 & j_2 & J \end{bmatrix} i^L f_{\Lambda}^{l_1 l_2 LST}(\vec{r}_{aA}, \vec{r}_{bB}) \tag{3.69}$$

where

$$f_{\Lambda}^{l_1 l_2 LST}(\vec{r}_{aA}, \vec{r}_{bB}) = i^{-L} \sum^{FG} (-)^G U\left(\tfrac{1}{2}\tfrac{1}{2}\tfrac{1}{2}\tfrac{1}{2}; FS\right) U\left(\tfrac{1}{2}\tfrac{1}{2}\tfrac{1}{2}\tfrac{1}{2}; GT\right)$$

$$\times \delta_{F+G,1} \left\langle \varphi_0^{l_b=0} \varphi_{\Lambda}^{l_1 l_2 L} \left| \sum_{j=1}^{2} \sum_{k=3}^{a} U^{FG}(r_{jk}) \right| \varphi_0^{l_a=0} \right\rangle \tag{3.70}$$

3.6.5. Differential cross-section

Using Eq.(3.69) for nuclear matrix element the transition amplitude can be written [104,105,112] as

$$T_{fi} = \sum_{M}^{[n_1 l_1 j_1][n_2 l_2 j_2] LSJT} b_{ST} \Im_{AB}^{\frac{1}{2}} \left([n_1 l_1 j_1]\ [n_2 l_2 j_2] \right) \left[(2s_b + 1)\ (2J+1) \right]^{\frac{1}{2}} \left(J_A M_A JM | J_B M_B \right)$$

$$\times \begin{bmatrix} l_1 & l_2 & L \\ \frac{1}{2} & \frac{1}{2} & S \\ j_1 & j_2 & J \end{bmatrix} \beta^{LSJT}_{M\ \sigma_a \sigma_b}(\theta) \tag{3.71}$$

The 'spectroscopic amplitude' $\Im^{\frac{1}{2}}_{AB}$ is analogous to that used in single stripping theory [112] namely,

$$\Im^{\frac{1}{2}}_{AB}\left(\left[n_1 l_1 j_1\right]\left[n_2 l_2 j_2\right];JT\right)=\binom{A+2}{2}^{\frac{1}{2}} I_{AB}\left(\left[n_1 l_1 j_1\right]\left[n_1 l_2 j_2\right];JT\right) \qquad (3.72)$$

Also, b_{ST} is defined by:

$$b_{ST}=(-)^{b+1}\binom{a}{2}^{\frac{1}{2}}\left[2(2S+1)\right]^{-\frac{1}{2}}\left(t_b \nu_b TN\middle| t_a \nu_a\right)\ \delta_{S+T,1} \qquad (3.73)$$

$b_{ST}{}^2$ is essentially the spectroscopic factor for the light particles [104].

$\beta^{LSJT}_{M\ \sigma_a\sigma_b}$ in Eq.(3.71) is given by,

$$\beta^{LSJT}_{M\ \sigma_a\sigma_b}(\theta)=\sum i^{l_b-l_a-L}(-)^{\sigma_a-s_a+L+S-J}\left[\frac{(2l_a+1)\ (2l_b+1)}{(2J+1)}\right]$$

$$\times\left[\frac{(l_b-\lambda_b)\ !}{(l_b+\lambda_b)\ !}\right]^{\frac{1}{2}}\left(l_a 0 s_a \sigma_a\middle| j_a \sigma_a\right)\left(l_b \lambda_b s_b-\sigma_b\middle| j_b, \lambda_b-\sigma_b\right)$$

$$\times\left(j_a \sigma_a j_b, \lambda_b-\sigma_b\middle| J-M\right)\begin{bmatrix} l_a & l_b & L \\ s_a & s_b & S \\ j_a & j_b & J \end{bmatrix}$$

$$\times P_{l_b\lambda_b}(\cos\theta) I^{l_1 l_2 l l_a j_a l_b j_b ST} \qquad (3.74)$$

where, $\lambda_b=\sigma_b-\sigma_a-M$,

$$I^{l_1 l_2 U_a j_a l_b j_b ST} = \frac{4\pi}{k_a k_b} J \int u_{l_b j_b}(k_b, r_{bB}) F^{l_1 l_2 U_a l_b ST}(r_{aA}, r_{bB})\ u_{l_a j_a}(k_a, r_{aA})\ r_{aA}\ \ r_{bB} dr_{aA}\ \ dr_{bB}$$

(3.75)

and

$$F^{l_1 l_2 U_a l_b ST}(r_{aA}, r_{bB}) = \sum_{\Lambda_a \Lambda_b} \left(L_a \Lambda_a L_b \Lambda_b | L\Lambda\right)$$

$$\times \int f^{l_1 l_2 LST}_{\Lambda}(\vec{r}_{aA}, \vec{r}_{bB})\ Y^*_{L_a \Lambda_a}(\hat{r}_{aA})\ Y^*_{L_b \Lambda_b}(\hat{r}_{bB})\ d\hat{r}_{aA}\ \ d\hat{r}_{bB} \qquad (3.76)$$

Using Eq.3.71 the expression for the differential cross-section for two-nucleon transfer reaction can be written as [105,106],

$$\left(\frac{d\sigma}{d\Omega}\right)_{stripping} = \frac{\mu_a \mu_b}{\left(2\pi\hbar^2\right)^2} \frac{k_b}{k_a} \frac{(2J_B+1)}{(2J_A+1)} \left| \sum_{M \varsigma_a \sigma_b}^{J} \ \sum^{[n_1 l_1 j_1]\ [n_1 l_1 j_1] LST} \right.$$

$$\times b_{ST}\ \ \Im^{\frac{1}{2}}_{AB}\ \left([n_1 l_1 j_1]\ [n_2 l_2 j_2]\ ; JT \right) \left(T_A N_A TN \middle| T_B N_B \right)$$

$$\left. \times \begin{bmatrix} l_1 & l_2 & L \\ \frac{1}{2} & \frac{1}{2} & S \\ j_1 & j_2 & J \end{bmatrix}\ \beta^{LSJT}_{M\ \ \sigma_a \sigma_b} \right|^2 \qquad (3.77)$$

3.6.6. Numerical evaluation of the radial integral

To evaluate $I^{l_1 l_2 U_a j_a l_b j_b}$ one must specify the detail of the coordinates with reference to Fig. (3.3). Defining $r_{jk} = \vec{r}_j - \vec{r}_k$ as position vector of the center of mass of the particle j relative to the center of mass of k, where r_j (with one subscript) is the position vector of j relative to an (arbitrary) origin, one can write,

$$\vec{R} = \tfrac{1}{2}(\vec{r}_{1A} + \vec{r}_{2A})$$

$$\vec{P} = \tfrac{1}{2}(\vec{r}_{1b} + \vec{r}_{2b}).$$

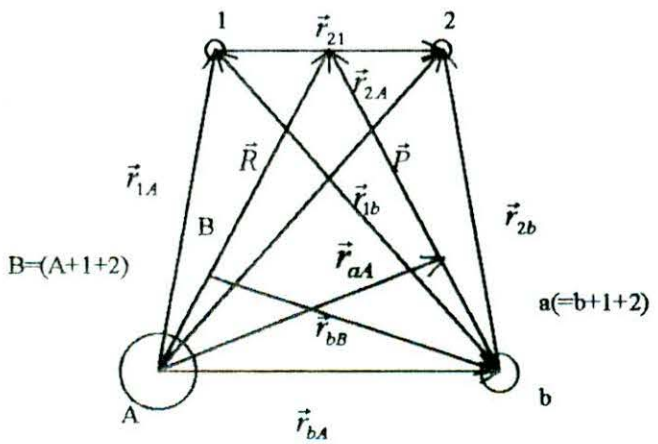

Fig. 3.3. Schematic representation of vector coordinates used in the description of the direct stripping reaction A(a,b)B. The points labeled A and b correspond to the center of mass of B(=A+1+2) and a(=b+1+2).

Denoting all internal coordinates of the nucleide by ξ, the equation for $f^{l_1 l_2 L}_{\Lambda}$ may now be written in the form:

$$f^{l_1 l_2 L}_{\Lambda}(\vec{r}_{aA}, \vec{r}_{bB}) = i^{-L} \int \varphi^{*l_b=0}_{0}(\xi_b)\ \varphi^{l_1 l_2 L}_{\Lambda}(\vec{P}, \vec{r}_{21}, \vec{R})$$

$$\times \left[\sum_{j=1}^{2} \sum_{k=3}^{a} U(r_{jk}) \right]\ \varphi^{l_a=0}_{0}(\xi_b, \vec{P}, \vec{r}_{21})\ d\xi_b\ \ d\vec{r}_{21} \qquad (3.78)$$

where the coordinates ξ_b and $\vec{r}_{21}$ are independent of $\vec{r}_{bB}$ and $\vec{r}_{bA}$. However, the functional form of the internal wave functions of the transferred pair and the outgoing ejectile, and that of the interaction potential , are most conveniently expressed using the relative coordinate and the center of mass coordinates of the respective pair. The Jacobian of transformation between these coordinates is

$$J = \frac{\partial(\vec{R}, \vec{P})}{\partial(\vec{r}_{bB}, \vec{r}_{aA})} = \left[\frac{Ba}{2(a+A)} \right]^3 \qquad (3.79)$$

So, the expansion coefficients in Eq.(3.76) are given by

$$F^{l_1 l_2 U_a l_b}(\vec{r}_{bB}, \vec{r}_{aA}) = \sum \left(l_a \lambda_a l_b \lambda_b | L\Lambda \right)$$

$$\times \int f^{l_1 l_2 L}_{\Lambda}(\vec{r}_{bB}, \vec{r}_{aA}) Y^{*}_{l_b \lambda_b}(\hat{r}_{bB}) Y^{*}_{l_a \lambda_a}\, d\hat{r}_{aA} d\hat{r}_{bB} \qquad (3.80)$$

and hence the Eq. (3.75) can be written as

$$I^{l_1 l_2 U_a j_a l_b j_b} = \frac{4\pi}{k_a k_b} J \int u_{l_a j_b}(k_a, r_{aA}) F^{l_1 l_2 U_a l_b}(r_{aA}, r_{bB})$$

$$\times u_{l_b j_b}(k_b, r_{bB}) r_{aA} r_{bB}\, dr_{aA} dr_{bB} \qquad (3.81)$$

For reaction (α,d) integration must be made over four coordinates ξ_a and $\vec{r}_{21}$ in Eq. (3.78), r_{aA} and r_{bB} in Eq. (3.81).

Now, the differential cross-section then can be numerically evaluated in terms of these radial integrals involving the coefficients.

3.6.7. Approximation for simplifying the calculation

1) ***Zero-range Approximation***

Because of the complexity of the problem, a zero-range approximation is usually made. It essentially reduces $f^{l_1 l_2 L}_{\Lambda}$ to a function of one argument and reduces $I^{l_1 l_2 U_a j_a l_b j_b}$ to a single integral . The equation (3.78) is replaced by [105]

$$f^{l_1 l_2 L}_{\Lambda}(\vec{r}_{aA},\vec{r}_{bB}) = \delta(\vec{P}) F_0^{l_1 l_2 L}(\vec{r}_{aA}) Y_{L\Lambda}(\vec{r}_{aA}) \qquad (3.82)$$

The implication of this assumption is that either the internal wave function of the incoming projectile **a**, or the interaction potential has a range short enough that it may be replaced by a delta function. Referring to the Fig. 3.3 the vector $\vec{P}$ can be written in terms of $\vec{r}_{bB}$ and $\vec{r}_{aA}$:

$$\vec{P} = \frac{Ba}{2(a+A)}[\gamma\vec{r}_{aA} - \vec{r}_{bB}] \qquad (3.83)$$

where $\gamma = \frac{A}{B}$. Using the expansion the delta function in terms of spherical harmonics the final expression for zero-range form factor $F_0^{l_1 l_2 L}(\vec{r}_{aA})$ can be written as,

$$F_0^{l_1 l_2 L}(\vec{r}_{aA}) = i^{-L} \int \varphi_0^{*l_b}(\xi_b)\ \varphi_\Lambda^{l_1 l_2 L}(\vec{P}, \vec{r}_{21}, \vec{r}_{aA}) \left[\sum\sum U(r_{jk}) \right] \varphi_0^{l_a}(\xi_b, \vec{P}, r_{21})$$

$$\times Y_{LA}^{*}(\hat{r}_{aA})\ d\xi_b\ \ d\hat{r}_{21} d\vec{P}\ \ d\hat{r}_{aA} \qquad (3.84)$$

This equation is only valid in the zero-range approximation; that is, either the wave function of a or the interaction potential must be considered sufficiently short range that a delta function $\delta(\vec{P})$ can be introduced into the Eq. (3.84).

3.6.8. Wave function of the transferred pair of nucleons

The pair wave function $\varphi_\Lambda^{l_1 l_2 L}$ can be written as a product of single-particle wave functions as:

$$\varphi_\Lambda^{l_1 l_2 L}(\vec{r}_{1A}, \vec{r}_{2A}) = N \sum_{\lambda_1 \lambda_2} (l_1 \lambda_1 l_2 \lambda_2 | L\Lambda) \sum (-)^m P_{12}^m \varphi_{\lambda_1}^{[n_1 l_1 j_1]}(\vec{r}_{1A}) \varphi_{\lambda_2}^{[n_2 l_2 j_2]}(\vec{r}_{2A}) \qquad (3.85)$$

where P_{12}^m is an operator which makes m interchanges between the particles 1 and 2. If $[n_1 l_1 j_1] \equiv [n_2 l_2 j_2]$ the normalization factor $N = \frac{1}{2}$; otherwise $N = \frac{1}{\sqrt{2}}$ [117].

Using the wave function, the radial integral $f_\Lambda^{l_1 l_2 L}$ may be written as:

$$f_\Lambda^{l_1 l_2 L} = i^{-L} 2N \sum \left(l_1 \lambda_1 l_2 \lambda_2 \middle| L\Lambda \right) \left\langle \varphi_0^{l_a=0} \varphi_{\lambda_1}^{[n_1 l_1 j_1]} \varphi_{\lambda_2}^{[n_2 l_2 j_2]} \middle| \sum_{j=1}^{2} \sum_{k=3}^{a} U(r_{jk}) \middle| \varphi_0^{l_a=0} \right\rangle \qquad (3.86)$$

Following Glendenning [104], g is defined as $g = 2N$, where

$$g = 1, \text{ if } [n_1 l_1 j_1] \equiv [n_2 l_2 j_2]$$

$$= \sqrt{2}\ , \text{otherwise.} \qquad (3.87)$$

The radial integral of the form factor for two-nucleon transfer reaction contains wave function generated from the product of the single particle shell-model wave functions of the variables of the separate particles. However, the calculation can be usually be performed more simply if the wave function is expressed in terms of the relative and center-of-mass variables of the two particles.

The wave function of the products of the functions of the variables of the separate particles can be calculated in the following methods:

a) A Method has been developed by Talmi [118] and Moshinsky [119] where the single particle wave functions are assumed to be the infinite harmonic oscillator wave functions. This method associates Brody and Moshinsky [120] brackets with the calculation. Glendenning prescribed this method for the two-nucleon transfer form factor [104,115,121].

b) Another method of performing the transformation to relative and c.m. coordinates with the single-particle wave functions of a finite well has been treated by first expanding the finite well wave functions in terms of harmonic oscillator wave functions of varying numbers of nodes, and then performing the Talmi-Moshinsky transformation components [122,123].

c) The third method introduced by Bayman and Kallio [107], where transformation has been performed directly with the finite well wave functions and does not involve the harmonic oscillator expansion. The condition is this that it is limited to that part of the wave function in which the two-particles have relative angular momentum zero. The computer code DWUCK uses the Bayman-Kallio form factor.

d) Another prescription for the two-nucleon form factor is that of Rook and Mitra [124] which also does not use any transformation to relative and c.m. coordinates. The Rook-Mitra form factor treats the transferred pair wave function as a product of two Woods-Saxon wave functions. In the zero-range approach the relative motion of the two nucleons is ignored so that the two wave functions have the same radial argument. A finite range correction can be made using the local energy approximation; in this case, the wave functions of the two transferred nucleons have different radial arguments. The Rook-Mitra form factor is incorporated in the distorted wave computer program NELMAC [125]. Lewis *et al.* [126] have compared the Bayman-Kallio and Rook-Mitra form factors, but have not been able to identify either prescription as being superior to the other.

Drisko and Rybicki [122] have emphasized that the proper treatment of transfer process requires wave functions with the asymptotic behaviour of a finite well as because the process is sensitive to the nuclear wave functions in the vicinity of the nuclear surface and beyond. Here the methods due to Glendenning and Bayman-Kallio will be presented in a brief form and in the present study Bayman-Kallio's method has been followed in computer computation [DWUCK4].

3.6.8.1. Glendenning method for two nucleon wave function

The essential steps for the method for evaluation of $F_0^{l_1 l_2 L}$ using pure two-nucleon wave function suggested by Glendenning [104,115] is being outlined here.

First, the wave functions $\varphi^{[n_1 l_1 j_1]}_{\lambda_1}(\vec{r}_{1A})$ and $\varphi^{[n_2 l_2 j_2]}_{\lambda_2}(\vec{r}_{2A})$ in Eq. (3.86) in the previous section are transformed into functions of relative and center-of-mass coordinates:

$$\sum_{\lambda_1\lambda_2}\left(l_1\lambda_1 l_2\lambda_2\middle|L\Lambda\right)\ \varphi^{[n_1 l_1 j_1]}_{\lambda_1}(\vec{r}_{1A})\ \varphi^{[n_2 l_2 j_2]}_{\lambda_2}(\vec{r}_{2A})$$

$$=\sum\left\langle \bar{n}l,\bar{N}L' : L\middle|\bar{n}_1 l_1,\bar{n}_2 l_2\right\rangle\ \left(l\lambda L'\Lambda'\middle|L\Lambda\right)$$

$$\times\varphi^{nl}_{\lambda}(\vec{r}_{21})\ \varphi^{NL'}_{\Lambda'}(\vec{R}) \qquad (3.88)$$

where $nl\lambda$, $NL'\Lambda'$ are the quantum numbers describing the relative and center-of-mass motion of the transferred pair. It is to be noted that the notation n is used as the number of radial nodes in the wave functions including the origin, but in Eq. (3.88) $\bar{n}=n-1$ has been used according to the definition used by Moshinsky [120,147]. If the single-particle wave functions are chosen to normalized oscillator functions with the parameter $\nu=\frac{m\varpi}{\hbar}$:

$$\varphi^{[n_1 l_1 j_1]}_{\lambda_1}(\vec{r}_{1A})=R_{n_1 l_1}\left(\nu r_{1A}^2\right)\ \left[i^{l_1}Y_{l_1\lambda_1}(\hat{r}_{1A})\right] \qquad (3.89a)$$

$$\varphi^{[n_2 l_2 j_2]}_{\lambda_2}(\vec{r}_{2A})=R_{n_2 l_2}\left(\nu r_{2A}{}^2\right)\ \left[i^{l_2}Y_{l_2\lambda_2}(\hat{r}_{2A})\right] \qquad (3.89b)$$

then,

$$\varphi^{nl}_{\lambda}(\vec{r}_{21})=R_{nl}\left(\tfrac{1}{2}\nu r_{21}{}^2\right)\ \left[i^{l}Y_{l\lambda}(\hat{r}_{21})\right] \qquad (3.90a)$$

$$\varphi^{NL'}_{\Lambda'}(\vec{R})=R_{NL'}\left(2\nu R^2\right)\ \left[i^{L'}Y_{L'\Lambda'}(\hat{R})\right] \qquad (3.90b)$$

and the transformation coefficients are well known [118–120] and have been tabulated by Brody and Moshinsky [120].

Here the oscillator radial function is defined as:

$$R_{nl}(\nu r^2)=\left[\frac{2\bar{n}!\,\nu^{3/2}}{\Gamma(\bar{n}+l+3/2)}\right]^{1/2}(\nu r^2)^{l/2}\exp\left(-\tfrac{1}{2}\nu r^2\right)\,L_{\bar{n}}^{l+\frac{1}{2}}(\nu r^2) \qquad (3.91)$$

where

$$L_{\bar{n}}^{l+\frac{1}{2}}(\nu r^2)=\sum_{k=0}^{\bar{n}}\binom{\bar{n}+l+\frac{1}{2}}{\bar{n}-k}\frac{(-\nu r^2)^k}{k!};$$

$$\nu=\frac{m\omega}{\hbar};\qquad \bar{n}=n-1$$

and the harmonic oscillator potential is $\frac{1}{2}m\omega^2 r^2$. In this case, the sum in Eq. (3.88) is restricted according to:

$$\left.\begin{aligned}2n_1+l_1+2n_2+l_2&=2n+l+2N+L'\\ l_1+l_2+l+L'&=even\end{aligned}\right\} \qquad (3.92)$$

Following the pure relative s-states for the light particles, l is taken to be zero. Incorporating Eq. (3.88) and Eq.(3.86), $F_0^{l_1 l_2 L}$ can be written as:

$$F_0^{l_1 l_2 L}(\vec{r}_{aA})=i^{-L}g\sum\left\langle \bar{n}0,\bar{N}L:L\middle|\bar{n}_1 l_1,\bar{n}_2 l_2:L\right\rangle$$

$$\times\int\varphi^{l_a=0^*}_{0}(\xi_b)\,\varphi^{n0^*}(\vec{r}_{21})\left[\sum\sum U(r_{jk})\right]\,\varphi^{l_a=0}_{0}(\xi_a)\,\varphi^{NL}_{\Lambda}(\vec{R})\,Y^*_{L\Lambda}(\hat{r}_{aA})\,d\xi_b\;d\vec{r}_{21}\;d\vec{P}\;d\hat{r}_{aA}$$

(3.93)

Finally, performing the integration over ξ_b and $\vec{r}_{21}$ and assuming a Gaussian form for potential and for the wave function of nucleide **a**, the differential cross-section in the absence of the spin-orbit forces, in the zero interaction approximation can be written as [105,121]:

$$\left(\frac{d\sigma}{d\Omega}\right)_{stripping} = \frac{\mu_a\mu_b}{\left(2\pi\hbar^2\right)^2}\frac{k_b}{k_a}\frac{(2J_B+1)}{(2J_A+1)}\sum_{\Lambda}^{LSJT} b_{ST}{}^2\left(T_A N_A TN\middle|T_B N_B\right)^2[D(S,T)]^2$$

$$\times\left|\sum^N G_N(LSJT)\sum^{l_a l_b} \Gamma_{\Lambda}^{l_a l_b L} P_{l_b\Lambda}(\cos\theta) J^{l_a l_b L}\right|^2 \qquad (3.94)$$

where,

$$G_N(LSJT) = \Omega_d\Omega_n\sum^{[n_1l_1j_1]\ [n_2l_2j_2]} gS_{AB}^{1/2}\left([n_1l_1j_1]\ [n_2l_2j_2]:JT\right)\begin{bmatrix} l_1 & l_2 & L \\ \frac{1}{2} & \frac{1}{2} & S \\ j_1 & j_2 & J\end{bmatrix}$$

$$\times\left\langle \bar{n}0,\bar{N}L:L\middle|\bar{n}_1l_1,\bar{n}_2l_2:L\right\rangle,$$

$$\Gamma_{\Lambda}^{l_a l_b L} = i^{l_b-l_a-L}\left[\frac{(2l_a+1)\ (2l_b+1)}{(2L+1)}\right]\left[\frac{(l_a-\Lambda)}{(l_a+\Lambda)}\right]^{1/2}\left(l_b0l_a\Lambda\middle|L\Lambda\right)\ \left(l_b0l_a0|L0\right),$$

$$J^{l_a l_b L} = \frac{(4\pi)^{\frac{1}{2}}C_0}{\gamma k_a k_b}\int u_{l_a}(k_a,r)\ R_{NL}\left(2\nu r^2\right)\ u_{l_b}(k_b,\gamma r)\ dr,$$

Ω_d and Ω_n are integrals of the products of the oscillator wave functions over ξ_b and $\vec{r}_{21}$ respectively.

The wave function $R_{NL}\left(2\nu r^2\right)$ in the radial integral is essentially describing the motion of the center-of-mass of the transferred pair of particles. The energy of this pair of particles is given by the experimental separation energy. Consequently, the asymptotic behaviour of the wave function $R_{NL}\left(2\nu r^2\right)$ should be exponential in form, $exp(-\alpha r)$, with the constant α, determined by the separation energy. However, in the treatment given here, the wave function $R_{NL}\left(2\nu r^2\right)$ was chosen to an oscillator function. To correct for

this, Glendenning [104] recommends matching a Hankel function onto $R_{NL}\left(2\nu r^2\right)$ at some suitably large radius.

3.6.8.2. Bayman- Kallio's method of two-nucleon wave function

Bayman and Kallio [107] started deriving two-nucleon wave function from normalized two-particle shell-model wave function as,

$$\Psi_M^{n_1 l_1 j_1; n_2 l_2 j_2; I,T}\left(\vec{r}_1\sigma_1, \vec{r}_2\sigma_2\right) =$$

$$\frac{\left[\psi_{m_1}^{n_1 l_1 j_1}\left(\vec{r}_1,\sigma_1\right)\ \psi_{m_2}^{n_1 l_2 j_2}\left(\vec{r}_2,\sigma_2\right)\right]_M^I + (-)^T\left[\psi_{m_1}^{n_1 l_1 j_1}\left(\vec{r}_2,\sigma_2\right)\ \psi_{m_2}^{n_2 l_2 j_2}\left(\vec{r}_1,\sigma_1\right)\right]_M^I}{\left[2\left(1+\delta_{n_1 n_2}\delta_{l_1 l_2}\delta_{j_1 j_2}\right)\right]^{1/2}} \qquad (3.95)$$

T is the isobaric spin, zero, if the state is symmetric in the two-particles and unity if the it is antisymmetric. The bracket notation indicates vector coupling to total angular momentum I and its z component M. The single particle states $\psi_m^{nlj}\left(\vec{r},\sigma\right)$ have the form

$$\psi_m^{nlj}\left(\vec{r},\sigma\right) \equiv \left[\varphi^l\left(\vec{r}\right)\chi^{1/2}(\sigma)\right]_m^j \qquad (3.96a)$$

$$\varphi_m^l\left(\vec{r}\right) \equiv u_{nlj}(r)Y_m^l\left(\hat{r}\right) \qquad (3.96b)$$

The radial function $u_{nlj}(r)$ are normalized solutions of the radial Schrödinger equation with the chosen single-particle potential.

To find the part of the wave function (3.95) in which the two-particles have zero-angular momentum, it is expanded in an LS coupling representation with the help of normalized 9*j* symbol [107] as,

$$\Psi_M^{n_1 l_1 j_1; n_2 l_2 j_2; i, T}(\vec{r}_1\sigma_1, \vec{r}_2\sigma_2) = \sum \begin{bmatrix} l_1 & \frac{1}{2} & j_1 \\ l_2 & \frac{1}{2} & j_2 \\ L & S & I \end{bmatrix}$$

$$\times \frac{\left\{ \left(\left[\varphi^{l_1}(\vec{r}_1)\ \varphi^{l_2}(\vec{r}_2) \right]^L + (-)^{1+S+T} \left[\varphi^{l_1}(\vec{r}_2) \varphi^{l_2}(\vec{r}_1) \right]^L \right) \left[\chi^{1/2}(\sigma_1) \chi^{1/2}(\sigma_2) \right]^S \right\}_M^I}{\left[2\left(1 + \delta_{n_1 n_2}\ \delta_{l_1 l_2} \delta_{j_1 j_2} \right) \right]^{1/2}} \qquad (3.97)$$

The part of this wave function in which the two-particles have zero relative angular momentum is permutation symmetric in $\vec{r}_1$ and $\vec{r}_2$. Thus, if T=1, then S=0 term and if T=0, only the S=1 term is taken.

The relative and center-of-mass coordinates in a symmetric form are defined as

$$\vec{r} \equiv (\vec{r}_2 - \vec{r}_1)/\sqrt{2} \qquad (3.98a)$$

$$\vec{R} \equiv (\vec{r}_2 + \vec{r}_1)/\sqrt{2} \qquad (3.98b)$$

and an expansion of the form

$$\frac{\left[\varphi_{m_1}^{l_1}(\vec{r}_1)\ \varphi_{m_2}^{l_2}(\vec{r}_2) \right]_M^L + \left[\varphi_{m_1}^{l_1}(\vec{r}_2)\ \varphi_{m_2}^{l_2}(\vec{r}_1) \right]_M^L}{\left[2\left(1 + \delta_{n_1 n_2} \delta_{l_1 l_2} \delta_{j_1 j_2} \right) \right]^{1/2}}$$

$$= \sum_{\lambda, \Lambda} \frac{f_{\lambda,\Lambda}^{L}(r,R)}{rR} \left[Y^{\lambda}(\hat{r}) Y^{\Lambda}(\hat{R}) \right]_M^L \qquad (3.99)$$

are envisaged.

Setting $\hat{R} = \hat{z}$ and integrating Eq. (3.99), $f_{o,L}^{L}(r,R)$ is obtained as

$$f_{0,L}^{L}(r,R)=\frac{rR}{(2L+1)^{1/2}}$$

$$\times\int_{(\hat{R}=\hat{z})}\frac{\left[\varphi_{m_1}^{l_1}(\vec{r}_1)\ \varphi_{m_2}^{l_2}(\vec{r}_2)\right]_M^L+\left[\varphi_{m_1}^{l_1}(\vec{r}_2)\ \varphi_{m_2}^{l_2}(\vec{r}_1)\right]_M^L}{\left[2\left(1+\delta_{n_1n_2}\delta_{l_1l_2}\delta_{j_1j_2}\right)\right]^{1/2}}d\hat{r} \qquad (3.100)$$

as, $$Y_M^A(\hat{z})=\delta_{M,0}\left(\frac{2A+1}{4\pi}\right)^{1/2}$$ and

$$Y_0^0(\hat{r})=\frac{1}{(4\pi)^{1/2}}.$$

The "distribution function" $f_{0,L}^{L}(r,R)$ obtained by performing the integral in Eq. (3.100) contains all the information about the relative angular momentum zero part of the two particle wave function.

In zero-range DWBA treatment of stripping into the two-particle state, one need to evaluate the form factors using this radial part of the wave function in Eq.(3.100) transformed into a function of relative and center-of-mass coordinates generated from a finite well single particle wave function.

3.6.9. Selection rules for two-nucleon transfer

A number of general rules known as selection rules arise from the formalism adopted in the processes of two-nucleon transfer reaction. They come into being from the properties of the wave functions used to describe

(a) the initial and final states,

(b) the incoming and outgoing particles, and

(c) orbitals of the transferred particles.

Let the initial and final nuclei are described by the quantum numbers J_A, T_A and J_B, T_B respectively; and the two transferred nucleons by the single-particle orbitals $[n_1 l_1 j_1]$ and $[n_2 l_2 j_2]$; then,

(1) $T_B - T_A = 0, \pm 1$

$$|j_1 - j_2| \le |J_B - J_A| \le j_1 + j_2 .$$

(2) If both the initial and final nuclei are considered to be states of good seniority and reduced isospin, then

$$v_B - v_a = 0, \pm 2$$

$$t_B - t_A = 0, \pm 1$$

where v's and t's are seniority and reduced isospin quantum numbers respectively.

(3) Let L, S, J and T be the possible quantum numbers of the transferred pair (i.e., l_1+l_2=L etc.) ; then

$$|T_B - T_A| \le T \le T_B + T_A$$

$$|J_B - J_A| \le J \le J_B + J_A$$

also

$$|l_1 - l_2| \le L \le l_1 + l_2$$

$$|j_1 - j_2| \le J \le j_1 + j_2 .$$

(4)The parity change between the initial and final states is given by

$$\Delta\pi = (-)^{l_1 + l_2}$$

If the transferred particles are in a relative s-state, then $l_1 + l_2 + L = \text{even}$ and $\Delta\pi = (-)^L$.

(5) The restriction on L, S, J and T are derived requiring that the transferred pair should be anti-symmetric that is,

when, S=0, T=1

S=1, T=0.

3.7. *The DWBA theory for three-nucleon transfer*

3.7.1. Transition amplitude with a microscopic form factor

Analogous to single and two-nucleon transfer, the transition amplitude for three-nucleon transfer reaction in DWBA is given by [127]

$$T_{(\alpha,p)}^{DW} = \iint d\vec{R}d\vec{r}\,\chi^{(-)*}\left(\vec{k}_p,\vec{r}_{pB}\right)\left\langle\psi_p\psi_B\left|V\right|\psi\psi_A\right\rangle^{\alpha}\chi^{(+)}\left(\vec{k}_\alpha,\vec{r}_{\alpha A}\right) \qquad (3.101)$$

In the expression for the transition amplitude the integration is carried out over the center of mass coordinate $\vec{R} = \frac{1}{3}\left(\vec{r}_1 + \vec{r}_2 + \vec{r}_3\right)$ and the relative coordinate $\vec{r} = \frac{1}{3}\left(\vec{r}_1 + \vec{r}_2 + \vec{r}_3\right) - \vec{r}_4$ between the ejectile nucleon labeled 4 and the three transferred nucleons labeled 1, 2, and 3. The distorted wave functions $\chi^{(+)}\left(\vec{k}_\alpha,\vec{r}_{\alpha A}\right)$ and $\chi^{(-)}\left(\vec{k}_p,\vec{r}_{pB}\right)$ in the entrance and exit channels are functions of the relative coordinates $\vec{r}_{pB} = \left(\frac{m_A}{m_B}\right)\vec{R} - \vec{r}$ and $\vec{r}_{\alpha A} = \vec{R} - \left(\frac{m_p}{m_\alpha}\right)\vec{r}$ in these channels (Fig. 3.4.), where m's are the masses of the particle indicated in the subscripts.

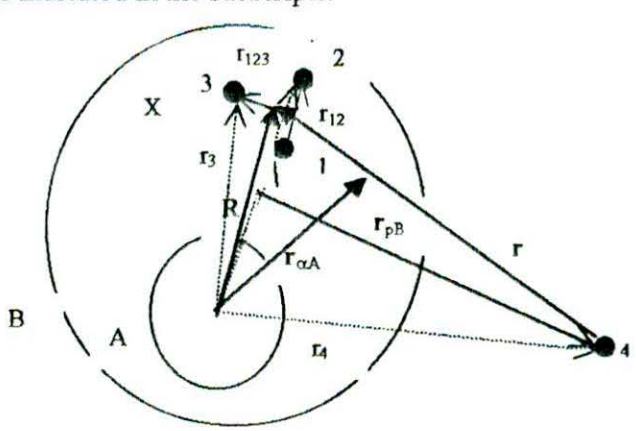

Fig. 3.4. Coordinates used in the three-nucleon reaction.

3.7.2. Nuclear matrix element

The antisymmetrized nuclear matrix element with the superscript a

$$\left\langle \psi_p \psi_B | V | \psi_\alpha \psi_A \right\rangle^a = \binom{4}{3}^{\frac{1}{2}} \binom{A+3}{3}^{\frac{1}{2}} \left\langle \psi^a{}_p \psi_B{}^a | V | \psi_\alpha{}^a \psi_A^a \right\rangle \qquad (3.102)$$

depends on the internal wave functions of the projectile ψ_α^a, the ejectile ψ_p, the target nucleus ψ_A^a, and the residual nucleus ψ_B^a. The binomial coefficients $\binom{4}{3}^{\frac{1}{2}}$ and $\binom{A+3}{3}^{\frac{1}{2}}$ stem as usual from the antisymmetrization procedure [105]. In order to calculate the nuclear matrix element (3.102) we need the interaction potential responsible for the three-nucleon transfer

$$V = \sum_{i=1}^{3} V_{i4}(\vec{r}_{i4}) \qquad (3.103)$$

which is a sum over the effective nucleon-nucleon potentials $V_{i4}(\vec{r}_{i4})$ between ejectile nucleon 4 and the three-transferred nucleons 1,2, and 3. The antisymmetrized wave function for the alpha-particle is also needed, which can be split up into a space and spin-isospin part

$$\psi_\alpha^a(\xi_1,\xi_2,\xi_3,\xi_4) = \varphi_\alpha(\vec{r}_1,\vec{r}_2,\vec{r}_3,\vec{r}_4)^{L_\alpha=0}_{M_{L_\alpha}=0} \times \chi_\alpha^a(1,2,3,4)^{S_\alpha=T_\alpha=0}_{M_{s_\alpha}=N_\alpha=0} \qquad (3.104)$$

The wave function for the residual nucleus ψ_B^a can be expanded in the JT representation with the wave functions of the target nucleus and the three transferred nucleons as

$$\psi_B^a(\xi_B)^{J_BT_B}_{M_BN_B} = \binom{A+3}{3}^{-\frac{1}{2}} \sum_{JJ_ATT_A} \sum_{\rho} \mathbf{S}^{\frac{1}{2}}_{AB}(\rho JT)$$

$$\times \left[\psi_A^a(\xi_A)^{J_AT_A} \times \psi_x^a(\xi_1,\xi_2,\xi_3)^{\rho JT}\right]^{J_BT_B}_{M_BN_B} \qquad (3.105)$$

where the cross-product is defined as

$$\left[\psi_A^a(\xi_A)^{J_AT_A} \times \psi_x^a(\xi_1,\xi_2,\xi_3)\right]^{J_BT_B}_{M_BN_B} \equiv \sum_{M_AM} \sum_{N_AN} \left\langle J_AM_AJM \middle| J_BM_B \right\rangle$$

$$\times \left\langle T_AN_ATN \middle| T_BN_B \right\rangle \psi_A^a(\xi_A)^{J_AT_A}_{M_AN_A} \psi_x^a(\xi_1,\xi_2,\xi_3)^{\rho JT}_{MN} \qquad (3.106)$$

Here ρ represents all quantum numbers necessary to characterize the three transferred nucleons. ξ_A and ξ_B are the internal coordinates of the target nucleus A and the residual nucleus B. The $\xi_i = (r_i, \sigma_i, \tau_i)$ with $i = 1,\ 2$ and 3 are the space, spin, and isospin with $\vec{r}_i$ with respect to the center of mass of the core A. The expansion coefficients $\mathbf{S}^{\frac{1}{2}}_{AB}(\rho JT)$ are the spectroscopic amplitudes.

The antisymmetrized three-particle wave function can be written as

$$\psi_x^a(\xi_1,\xi_2,\xi_3)^{\rho JT}_{MN} = N(\rho)Z(\rho)\psi_x(\xi_1,\xi_2,\xi_3)^{\rho JT}_{MN} \qquad (3.107)$$

$N(\rho)$ and $Z(\rho)$ are the normalization and antisymmetrization factors [128]. The three-particle wave function can be split up into a space and spin-isospin dependent part by transforming from *jj* to *LS* representation using 9*j* symbols

$$\psi_x(\xi_1,\xi_2,\xi_3)^{\rho JT}_{MN} = \sum_{LS}\sum_{L_{12}S_{12}} \begin{bmatrix} l_1 & \frac{1}{2} & j_1 \\ l_2 & \frac{1}{2} & j_2 \\ L_{12} & S_{12} & J_{12} \end{bmatrix} \begin{bmatrix} L_{12} & S_{12} & J_{12} \\ l_3 & \frac{1}{2} & j_3 \\ L & S & J \end{bmatrix}$$

$$\times \left[\varphi_x(\vec{r}_1,\vec{r}_2,\vec{r}_3)^{\rho L} \times \chi_x(1,2,3)^{\rho ST} \right]^{JT}_{MN} \qquad (3.108)$$

where $S = \frac{1}{2}$ is taken for the spin transfer.

By inserting Eqs.(3.105 –3.108) into the expression for the nuclear matrix element (3.102), this matrix element can be spit up into a space and a spin-isospin part. Hence the transition amplitude can be reduced to form [127],

$$T^{DW}_{(\alpha,p)}(A,B) = \binom{4}{3}^{\frac{1}{2}} \sum_{JM} \langle J_A M_A JM | J_B M_B \rangle \left\langle T_A N_A \tfrac{1}{2}\left(\tfrac{1}{2}\right) \;\middle|\; T_B N_B \right\rangle$$

$$\times \sum_L \left\langle L(M+M_p)\tfrac{1}{2}(-M_p) \,|JM\right\rangle \left\langle \tfrac{1}{2}M_p\,\tfrac{1}{2}(-M_p)\,|00\right\rangle$$

$$\times \left\langle \tfrac{1}{2}\tfrac{1}{2}\tfrac{1}{2}(-\tfrac{1}{2})\,|00\right\rangle$$

$$\times \sum_{\rho}\sum_{L_{12}S_{12}} (-1)^{T_{12}} \tfrac{1}{\sqrt{2}} \delta_{S_{12}+T_{12},1} g(\rho) \begin{bmatrix} l_1 & \frac{1}{2} & j_1 \\ l_2 & \frac{1}{2} & j_2 \\ L_{12} & S_{12} & J_{12} \end{bmatrix} \begin{bmatrix} L_{12} & S_{12} & J_{12} \\ l_3 & \frac{1}{2} & j_3 \\ L & \frac{1}{2} & J \end{bmatrix}$$

$$\times \mathbf{S}^{\frac{1}{2}}_{AB}(\rho JT) \int d\vec{R}\; d\vec{r}\, \chi^{(-)^*}\left(\vec{k}_p,\vec{r}_{pB}\right) F^{\rho L}_{M_L}(\vec{R},\vec{r})\; \chi^{(+)}\left(\vec{k}_\alpha,\vec{r}_{\alpha A}\right) \qquad (3.109)$$

The configuration factor $g(\rho)$ comes from the antisymmetrization and normalization procedure [128].

3.7.3. Microscopic form factor for alpha-projectile

The form factor $F^{\rho L}_{M_L}(\vec{R},\vec{r})$ is defined as the space part of the nuclear matrix element in Eq. (3.109)

$$F^{\rho L}_{M_L}(\vec{R},\vec{r}) = \left\langle \varphi_\alpha(\vec{r}_1,\vec{r}_2,\vec{r}_3,\vec{r}_4)^0_0 \middle| \sum_{i=1}^{3} V_{i4}(\vec{r}_{i4}) \middle| \varphi_x(\vec{r}_1,\vec{r}_2,\vec{r}_3)^{\rho L}_{M_L} \right\rangle \qquad (3.110)$$

In order to calculate this form factor the coordinates $(\vec{r}_1,\vec{r}_2,\vec{r}_3,\vec{r}_4)$ are to be transformed to new coordinates $\vec{R}$, $\vec{r}$, $\vec{r}_{12} = \vec{r}_2 - \vec{r}_1$ and $\vec{r}_{123} = \vec{r}_3 - \frac{1}{2}(\vec{r}_1 + \vec{r}_2)$ (Fig. 3.4).

If the alpha-particle wave function is assumed to have a Gaussian form [127]

$$\varphi_\alpha(\vec{r}_1,\vec{r}_2,\vec{r}_3,\vec{r}_4)^0_0 = \left[\frac{128\eta^6}{\pi^3}\right] exp\left[-\eta^2 \sum_{i<j}(r_i - r_j)^2\right] \qquad (3.111)$$

with the size parameter $\eta = 0.233\,\text{fm}^{-1}$, which is correlated to the equivalent harmonic oscillator constant $\nu_\alpha = 0.434\,\text{fm}^{-2}$ by $\eta^2 = \frac{1}{8}\nu_\alpha$ and to the rms radius of the alpha particle by $\langle r^2 \rangle^{\frac{1}{2}} = \frac{3}{8\eta}$ =1.61 fm. Performing the coordinate transformation [129],

$$\varphi_\alpha(\vec{r}_1,\vec{r}_2,\vec{r}_3,\vec{r}_4)^0_0 = \varphi^{(1)}_\alpha(\vec{r})\ \varphi^{(2)}_\alpha(\vec{r}_{12},\vec{r}_{123})$$

$$= \left[\frac{3\nu_\alpha}{4\pi}\right]^{\frac{3}{4}} exp\ \left[-\nu_\alpha\left(\tfrac{3}{8}r^2\right)\right] \left[\frac{\nu_\alpha{}^2}{3\pi^2}\right]^{\frac{3}{4}} exp\ \left[-\nu_\alpha\left(\tfrac{1}{4}r_{12}^2 + \tfrac{1}{3}r_{123}^2\right)\right] \qquad (3.112)$$

The interacting potential is also assumed to have a Gaussian form

$$\sum_{i=1}^{3} V_{i4}(\vec{r}_{i4}) = U_0 \sum_{i=1}^{3} exp\left[-\beta^2(\vec{r}_4 - \vec{r}_i)^2\right] \qquad (3.113)$$

with $U_0 = 70\,\mathrm{MeV}$ and $\beta = 0.632\ \mathrm{fm}^{-1}$[130]. In terms of the coordinates $(\vec{r}, \vec{r}_{12}, \vec{r}_{123})$, $(i4)$ can be written after applying the Chant-Mangelson approximation [130],

$$V(\vec{r}, \vec{r}_{12}, \vec{r}_{123}) \approx V^{(1)}(\vec{r})\ V^{(2)}(\vec{r}_{12}, \vec{r}_{123})$$

$$= 3U_0\, exp\ \left(-\beta^2 r^2\right) \left\{ \tfrac{2}{3} exp\ \left[-\beta^2\ \left(\tfrac{1}{4} r_{12}^2 + \tfrac{1}{9} r_{123}^2\right)\right] + \tfrac{1}{3} exp\ \left[-\beta^2\ \left(\tfrac{4}{9} r_{123}^2\right)\right] \right\} \qquad (3.114)$$

With Glendenning approximation, the potential can be written as,

$$V(\vec{r}, \vec{r}_{12}, \vec{r}_{123}) \approx V^{(1)}(r) = 3U_0\, exp\left(-\beta^2 r^2\right) \qquad (3.115)$$

The space-part of the three-nucleon wave function is given as

$$\varphi_x(\vec{r}_1, \vec{r}_2, \vec{r}_3)^{\rho L}_{M_L} = \left\{ \left[\varphi(\vec{r}_1)^{\rho_1} \times \varphi(\vec{r}_2)^{\rho_2} \right]^{\rho_{12} L_{12}} \times \varphi(\vec{r}_3)^{\rho_3} \right\}^{\rho L}_{M_L} \qquad (3.116)$$

with single-particle wave function,

$$\varphi(\vec{r}_i)^{\rho_i} = \frac{1}{r_i} u(r_i)_{n_i l_i j_i} Y^{l_i}_{m_i}(\hat{r}_i) \quad \text{where} \quad (i = 1,2,3),$$

which are calculated in a Woods-Saxon potential.

In order to transform this wave function (3.116) to the new coordinates, the single-particle wave functions $\varphi(\vec{r}_i)^{\rho_i}$ are expanded in terms of the harmonic oscillator wave functions with the harmonic oscillator constant ν. The expansion coefficients are denoted by a_{p_i}, where p_i is the radial quantum number of the corresponding harmonic oscillator wave functions to the above mentioned coordinates using the generalized

Talmi-Moshinsky [131] bracket $\langle n_1 l_1 n_2 l_2 : \lambda | \mu_1 \mu_2 | NLnl : \lambda \rangle$ for particles with different masses μ_1 and μ_2.

Inserting $\varphi_x(\vec{R}, \vec{r}_{12}, \vec{r}_{123})$, $V(\vec{r}, \vec{r}_{12}, \vec{r}_{123})$ and $\varphi_\alpha(\vec{r}, \vec{r}_{12}, \vec{r}_{123})$ into Eq.(3.110), the form factor split up into three terms, each depending on $\vec{R}$, $\vec{r}$, and $(\vec{r}_{12}, \vec{r}_{123})$ respectively. Integrating over the internal coordinates $\vec{r}_{12}$ and $\vec{r}_{123}$ the form factor reduces to

$$F^{\rho L}_{M_L}(\vec{R}, \vec{r}) = D^{(\alpha,p)}(\vec{r}) \sum_{N' N'_{12} n' n''} \sum_{p_1 p_2 p_3} a_{p_1} a_{p_2} a_{p_3} \langle p_1 l_1 p_2 l_2 : L_{12} | \mu\mu | N'_{12} L_{12} n' 0 : L_{12} \rangle$$

$$\times \langle N'_{12} L_{12} p_3 L_3 : L | 2\mu\mu | N' L n'' 0 : L \rangle I_{n'n} \varphi^{N'L}_M(\vec{R}) \qquad (3.117)$$

where μ is the mass of a nucleon.

The r-dependent finite range normalization factor $D^{(\beta,p)}(\vec{r})$ is given by

$$D^{(\alpha,p)}(\vec{r}) = V^{(1)}(\vec{r}) \varphi^{(1)}_\alpha(\vec{r})$$

$$= 3U_0 \left[\frac{3\nu_\alpha}{4\pi}\right]^{\frac{3}{4}} exp\left[-r^2\left(\beta^2 + \tfrac{3}{4}\nu_\alpha\right)\right] \qquad (3.118)$$

The radial form factor $\varphi^{N'L}_m(\vec{R})$ is the spherical harmonic oscillator function

$$\varphi^{N'L}_M(\vec{R}) = \frac{1}{R} H_{N'L}(3\nu R^2) Y^L_M(\hat{R}) \qquad (3.119)$$

The overlap $I_{n'n''}$ is the integral over the internal coordinates $\vec{r}_{12}$ and $\vec{r}_{123}$.

In the case of Glendenning approximation (3.115) the overlap integral reduces to

$$I_{n'n} = (4\nu_\alpha \nu)^{3/2} \left[\frac{(2n'+1)!!(2n''+1)!!}{n'! n''! 2^{n'} 2^n}\right]^{\frac{1}{2}}$$

$$\times\left(\nu_\alpha+\nu\right)^{-3}\left[\frac{\nu_\alpha-\nu}{\nu_\alpha+\nu}\right]^{n'+n^*} \tag{3.120}$$

3.7.4. Zero-range approximation

In the zero-range approximation the normalization factor (3.118) is given as [127],

$$D^{(\alpha,p)}(\vec{r})=V^{(1)}\varphi_\alpha^{(1)}\approx D_0^{(\alpha,p)}\delta(\vec{r}) \tag{3.121}$$

$D_0^{(\alpha,p)}$ can be calculated by the integral

$$D_0^{(\alpha,p)}=\int d\vec{r}\,V^{(1)}(\vec{r})\varphi_\alpha^{(1)}(\vec{r}) \tag{3.122}$$

3.7.5. Transition amplitude with a cluster form-factor

In the cluster approximation the interaction potential, projectile wave function, and residual nucleus wave function in the expressions (3.103–3.105) are replaced respectively by

$$\hat{V}=V_{tp}^{(1)}(\vec{r}) \tag{3.123}$$

$$\hat{\psi}_\alpha^a(\xi_t,\xi_p)=\varphi_\alpha^{(1)}(\vec{r})_{M_a=0}^{L_a=0}\chi_\alpha^a(t,p)_{M_{s_a}=N_a=0}^{S_a=T_a=0} \tag{3.124}$$

$$\psi_B^a(\xi_B)_{M_BN_B}^{J_BT_B}=\begin{pmatrix}A+3\\3\end{pmatrix}^{-\frac{1}{2}}\sum_{JJ_ATT_A}\sum_{LS}\sum\hat{\mathbf{S}}_{\mathbf{AB}}^{\frac{1}{2}}(LSJT)$$

$$\times\left[\psi_A^a(\xi_A)^{J_aT_A}\times\psi_t(\xi_t)^{LSJT}\right]_{M_BN_B}^{J_BT_B} \tag{3.125}$$

The wave functions are given in the LSJT representation and the cluster space, spin, and isospin coordinates $\xi_t = \left(\vec{R}, \sigma_t, \tau_t\right)$. After performing the spin algebra the transition amplitude is reduced as [127]

$$T^{DW}_{(\alpha,p)}(A,B) = \binom{4}{3}^{\frac{1}{2}} \sum_{JM} \left\langle J_A M_A JM | J_B M_B \right\rangle \left\langle T_A N_A \tfrac{1}{2}\left(\tfrac{1}{2}\right) | T_B N_B \right\rangle$$

$$\times \sum_{L} \left\langle L\left(M + M_p\right) \tfrac{1}{2}\left(-M_p\right) | JM \right\rangle \left\langle \tfrac{1}{2} M_p \tfrac{1}{2}\left(-M_p\right) | 00 \right\rangle$$

$$\times \left\langle \tfrac{1}{2}\tfrac{1}{2}\tfrac{1}{2}\left(-\tfrac{1}{2}\right) | 00 \right\rangle$$

$$\times \hat{\mathbf{S}}^{\frac{1}{2}}_{\mathrm{AB}} \left(L \tfrac{1}{2} J \tfrac{1}{2}\right) \iint d\vec{R} \; d\vec{r}\, \chi^{(-)*}\left(\vec{k}_p, \vec{r}_{pB}\right) \hat{F}^{LJ}_{M_L}\left(\vec{R}, \vec{r}\right) \chi^{(+)}\left(\vec{k}_\alpha, \vec{r}_{\alpha A}\right) \quad (3.126)$$

where the form factor $\hat{F}^{LJ}_{M_L}\left(\vec{R}, \vec{r}\right)$ is given as

$$\hat{F}^{LJ}_{M_L}\left(\vec{R}, \vec{r}\right) = \left\langle \varphi^{(1)}_{\alpha}(\vec{r})^{0}_{0} \; \left| V^{(1)}_{t,p}(\vec{r}) \right| \; \varphi_t\left(\vec{R}\right)^{LJ}_{M_L} \right\rangle$$

$$= D(\vec{r}) \; \varphi_t\left(\vec{R}\right)^{LJ}_{M_L} \quad (3.127)$$

with the radial wave function $\varphi_t\left(\vec{R}\right)^{LJ}_{M_L}$ of triton t calculated in a Woods-Saxon potential between t and the target nucleus A. Here the radial quantum number is restricted to its maximum value N, which is given by the conservation of the oscillator quanta in the Talmi-Moshinsky [118,119] transformation,

$$Q \equiv 2N + L = \sum_{i=1}^{3} \left(2n_i + l_i\right) \quad (3.128)$$

3.7.6. Differential cross-section

The differential cross-section for three-nucleon transfer A(α,p)B can be written as [127]

$$\left(\frac{d\sigma}{d\Omega}\right) = \frac{\mu_{\alpha A}\mu_{pB}}{(2\pi\hbar)^2}\frac{k_p}{k_\alpha}\frac{1}{(2J_A+1)}\sum_{M_\alpha M_A M_B}\left| T^{DW}_{(\alpha,p)}(A,B)\right|^2 \qquad (3.129)$$

The quantities $\mu_{\alpha A}$ and μ_{pB} are the reduced masses and $\vec{k}_\alpha$ and $\vec{k}_p$ are the relative momenta in the entrance and exit channels respectively. M_A and M_B are the magnetic quantum numbers of the target and residual nuclei.

CHAPTER 4

CCBA AND CRC FORMALISM

4.1. Introduction to CCBA and CRC

An alternative approach often used to interpret and analyze the experimental data of direct reaction is 'coupled-channels' (CC) method. The method usually considered as the extension of the distorted wave method confronting more complicated situations.

By coupled-channels method it is meant that these are the solutions that include a relatively small set of coupled equations that results from considering a model wave functions with a small number of terms. The truncation to a small basis states implies the use of an effective Hamiltonian and interaction.

When rearrangement is being considered, so that the states from more than one partition enter, the name 'coupled-reaction channels' (CRC) has come into use.

There may be situation of rearrangement collision in which a role is played by inelastic transitions before and after the rearrangement event. When the two sets of coupled equations are solved for the inelastic transitions before and after the rearrangement and the rearrangement itself is treated to the first order, the method is usually known as coupled-channels Born approximation (CCBA).

This chapter will deal with the basic formalism of (CC) necessary and relevant to the present study. The illustration will basically follow the references [52,132,133].

The Fig. 4.1 illustrate schematically some standard model processes:

(a) Fig. 4.1(a) shows some possible transitions for inelastic scattering; in particular, it indicates no direct coupling from the ground state A to the

excited state A**, but this state may be excited via A* as an intermediate state. It also indicates a 'self-coupling' term for the A* as an intermediate state. Solving the coupled equations of the CC method for this system would correspond to the infinite sum of all possible combinations of the arrows.

(b) Fig. 4.1(b) illustrates an analogous situation for a rearrangement collision; solving the corresponding CRC equations is equivalent to summing all possible combinations of arrows.

(c) Fig 4.1(c). represents similar situation to the case of Fig. 4.1(b), but one in which a third partition has been considered which may supply the intermediate states. This may also be solved by the first-order (direct) plus second order ('two-step') solution.

(d) Fig. 4.1(d) represents a rearrangement collision in which inelastic transitions before and after the rearrangement event plays an important role. This feature is accounted for by the CCBA method as mentioned before.

All the formalism in relation to the basis of the DWBA method applies to the coupled-channels Born approximation (CCBA), since the latter is simply an extension of the former.

The CCBA was proposed by Penny and Satchler and also developed by Iano and Austern [133]

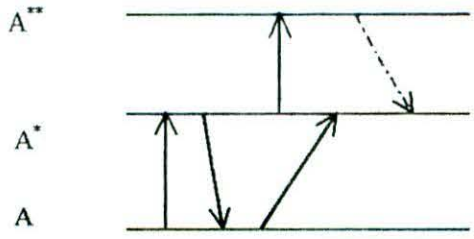

(a). Inelastic $A(a,a')A^{*}(a',a'')A^{**}$

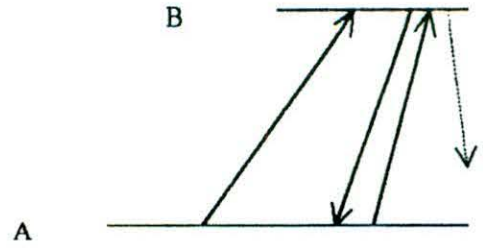

(b). Rearrangement $A(a,b)B$

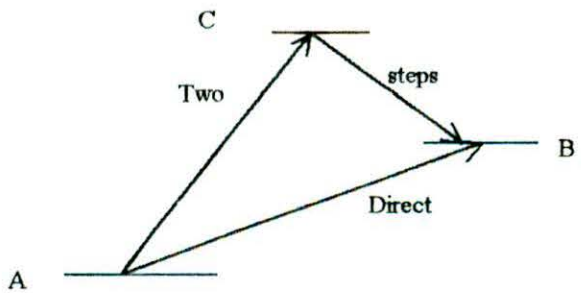

(c). Two-step Rearrangement, e.g. $A(a,c)C(c,b)B$

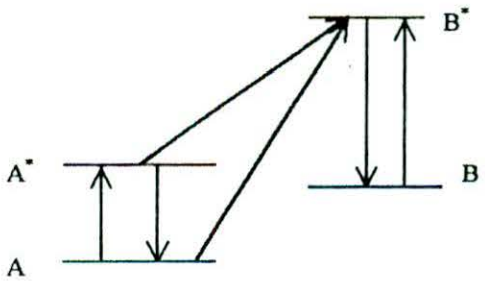

(d). Inelastic + Rearrangement, e.g. $A(a,a')A^{*}(a',b)B$

Fig. 4.1. A schematic representation of some multi-step processes.
Each arrow represents a matrix element of the interaction.

4.2. Basis of the CC method for inelastic scattering

The total wave function Ψ for a system may be expanded in a complete (and infinite) set of internal states ψ_α for one particular partition $\alpha \equiv a + A$, as

$$\Psi = \sum_\alpha \chi_\alpha(\vec{r}_\alpha)\ \psi_\alpha(\xi_\alpha) \qquad (4.1)$$

where $\vec{r}_\alpha$ is the channel coordinate for the α–partition and ξ_α represents the corresponding internal coordinates. In the usual scattering situation, a boundary condition is imposed that the function χ_α for the entrance channel has the asymptotic form of a plane plus outgoing spherical waves while all the other $\chi_{\alpha'}$ have outgoing waves only.

If the form (4.1) is inserted into the Schrödinger equation for the system,

$$(E - H)\ \Psi = 0 \qquad (4.2)$$

H may be expressed in a form appropriate for the α partition as,

$$H = H_\alpha + k_\alpha + V_\alpha \qquad (4.3)$$

Multiplying from the left by one of the Ψ_α^*, integrating over the internal ξ_α coordinates and using the orthogonality relation, we get the (infinite) set of coupled equations for the channel functions $\chi_\alpha(\vec{r}_\alpha)$, of which a representative one is

$$\left[E - \varepsilon_\alpha - k_\alpha - \left(\alpha \ |V_\alpha|\ \alpha' \right) \right] \chi_\alpha(\vec{r}_\alpha) = \sum_{\alpha' \neq \alpha} \left(\alpha \ |V_\alpha|\ \alpha' \right) \chi_{\alpha'}(\vec{r}_\alpha) \qquad (4.4)$$

The interaction matrix elements are integrals over the ξ_α alone, so they remain functions of $\vec{r}_\alpha$:

$$\left(\alpha \left| V_\alpha \right| \alpha'\right) \equiv \int \psi_\alpha^*(\xi_\alpha)\ V_\alpha(\vec{r}_\alpha, \xi_\alpha)\ \psi_{\alpha'}(\xi_{\alpha'})\ d\xi_\alpha \qquad (4.5a)$$

$$= V_{\alpha\alpha'}(\vec{r}_\alpha) \quad \text{(say)} \qquad (4.5b)$$

4.3. CCBA formalism with spinless target, projectile and ejectile

The CCBA formalism with a simple case in which the target, projectile and emitted particles all have zero-spin and even parity is being considered first. Let us consider a rearrangement collision A(a,b)B (Fig.4.2).

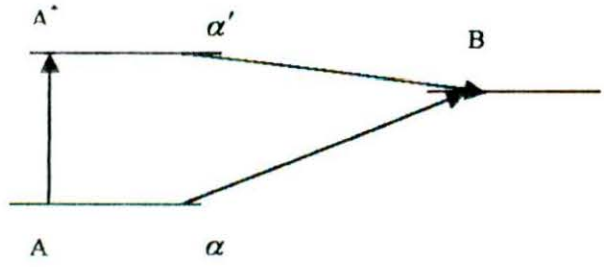

Fig. 4.2. Schematic diagram for A(a,b)B rearrangement collision.

Inelastic scattering to a single excited state of the target with spin I_A is included, but it is assumed that there is no inelastic effect in the exit channel as shown schematically in Fig.4.2. So, the distorted wave in the exit channel is standard one. For the general case, the distorted wave will be similar to that in the entrance channel. In the entrance channel coupling between the ground state and one excited state is being considered. So, the CC wave may be written as,

$$\Psi_\alpha^{(+)} = \psi_{\alpha 00}(x)\chi_{\alpha 0,\alpha 0}(\vec{k},\vec{r}) + \sum_{M_A} \psi_{\alpha I_A M_A}(x)\chi^{(+)}_{\alpha I_A M_A,\alpha 0}(\vec{k},\vec{r}) \qquad (4.6)$$

Where the first term describes purely elastic scattering from the target ground state $\psi_{\alpha 00}$, while the second term describes inelastic transitions to the excited state $\psi_{\alpha' I_A M_A}$ with spin I_A and projection M_A. The elastic wave $\chi^{(+)}_{\alpha 0,\alpha 0}$ contains both incoming and while the inelastic wave $\chi^{(+)}_{\alpha' M_A,\alpha 0}$ contains outgoing waves only [52].

4.4. The transition amplitude

The CCBA transition amplitude for the transition $\alpha \to \beta$ [52,132,133,], in a form analogous to DWBA can be written as:

$$T^{CCBA}_{\beta\alpha} = \sum_{\alpha'\beta'} \left\langle \chi^{(-)}_{\beta'\beta} \ \psi_{\beta'} \right| (H-E) \left| \ \chi^{(+)}_{\alpha'\alpha} \ \psi_{\alpha'} \right\rangle \qquad (4.7)$$

The generalized distorted waves are the solutions of the finite sets of the coupled equations with generalized auxiliary potential U_α and U_β, which now have non-vanishing, off-diagonal matrix elements within their chosen sets of closely coupled states. When the waves from Eq. (4.6) are inserted into Eq. (4.7) for the transition amplitude, there will have two terms corresponding to the two parts of the wave Eq.(4.6) as follows:

$$\begin{aligned} T^{CCBA}_{M_B}\left(\vec{k}_\beta,\vec{k}_\alpha\right) &= \iint d\vec{r}_\beta d\vec{r}_\alpha \chi^{(-)^*}_\beta\left(\vec{k}_\beta,\vec{r}_\beta\right) I_{\beta I_B M_B,\alpha 00}\left(\vec{r}_\beta,\vec{r}_\alpha\right)\chi^{(+)}_{\alpha 0,\alpha 0} \\ &+ \sum_{M_A}\iint d\vec{r}_\beta dr_\alpha \chi^{(-)^*}_\beta\left(\vec{k}_\beta,\vec{r}_\beta\right) I_{\beta I_\beta M_\beta,\alpha' I_A M_A}\left(\vec{r}_\beta,\vec{r}_\alpha\right)\chi^{(+)}_{\alpha' M_A,\alpha 0}\left(\vec{k}_\alpha,\vec{r}_\alpha\right) \quad (4.8) \\ &= T^{CCBA}_{M_\beta}(direct) + T^{CCBA}_{M_\beta}(indirect) \quad (say). \end{aligned}$$

where I_B and M_B are respectively the spin and its projection of the final nucleus in the channel β and its projection.

The first term describes the usual type of DW amplitude except that the elastic wave $\chi_{\alpha 0,\alpha 0}$ is generated by the coupled equations instead of by a one-channel equation with a simple optical potential.

The second term describes transitions in which the target is excited before transfer takes place.

For the present purpose, we use the zero-range form for the interaction kernel I_B, the $\alpha \to \beta$ transfer from the target ground-state (assumed to be zero-spin) is associated with a unique angular momentum transfer $l = I_B$ (and $m = M_B$). The corresponding interaction kernel in Eq. (4.8) has the form [52]:

$$I_{\beta\alpha} \equiv I_{\beta I_B M_B;\alpha 00}(\vec{r}_\beta, \vec{r}_\alpha) = (S_l^\alpha)^{1/2} f_l^\alpha(\vec{r}_\alpha)[i^l Y_l^m(\vec{r}_\alpha)]^* \delta(\vec{r}_\beta - \gamma \vec{r}_\alpha)\delta_{I_B l}\delta_{M_B m} \qquad (4.9)$$

where $\gamma = A/B$.

Here a factor $(S_l^\alpha)^{1/2}$ have been separated explicitly that is usually called a spectroscopic amplitude, so that the radial form factor may be chosen to have a simple normalization:

$$\int f_l^\alpha(r)^2 r^2 dr = 1 \qquad (4.10)$$

Transfer from the excited state of the target allows more than one angular momentum transfer l' (unless $I_A = 0$):

$$|I_A - I_B| \le l' \le I_A + I_B \qquad (4.11)$$

The interaction kernel for this $\alpha' \to \beta$ transfer is,

$$I_{\beta\alpha'} \equiv I_{\beta I_B M_B, \alpha' I_A M_A}\left(\vec{r}_\beta, \vec{r}_\alpha\right) = \sum \left(S^{\alpha'}\right)^{1/2} f_{l'}^{\alpha'}(r_\alpha) \left[i^{l'} Y_{l'}^{m'}(\hat{r}_\alpha)\right]^* \delta\left(\vec{r}_\beta - \gamma \vec{r}_\alpha\right)$$

$$\times (-)^{I_A - M_A} \left\langle I_B I_A M_B, -M_A \middle| l'm' \right\rangle \qquad (4.12)$$

where the $\left(S_{l'}^{\alpha}\right)^{1/2}$ are the corresponding spectroscopic amplitudes using the same normalization as in Eq.(4.10).

With the kernels (4.9) and (4.12) in the amplitude (4.8) with axes chosen with z along $\vec{k}_\alpha$ and y along $\vec{k}_\alpha \times \vec{k}_\beta$, and for $m \geq 0$, the transition amplitude reduces to,

$$T_m^{CCBA}\left(\vec{k}_\beta, \vec{k}_\alpha\right) = \delta_{I_B I'} \delta_{M_M m} \sum_{L_\alpha L_\beta} \hat{L}_\alpha{}^2 \hat{L}_\beta^2 \hat{l}^{-1} \left[\frac{\left(L_\beta - m\right)!}{\left(L_B + m\right)!}\right]^{1/2} \left\langle L_\beta L_\alpha m 0 \middle| l m \right\rangle$$

$$\times P_{L_\beta}^m(\theta) \left\{A_l^{L_\beta L_\alpha}(direct) + A_l^{L_\beta L_\alpha}(indirect)\right\} \qquad (4.13a)$$

$$= (-)^m T_{-m}^{CCBA}\left(\vec{k}_\beta, \vec{k}_\alpha\right) \qquad (4.13b)$$

where

$$A_l^{L_\beta L_\alpha}(direct) = i^{L_\alpha - L_\beta - l} \left\langle L_\beta L_\alpha 00 \middle| l0 \right\rangle \left(S_l^\alpha\right)^{1/2} X_l^{L_\beta L_\alpha}(direct) \qquad (4.14a)$$

$$A_l^{L_\beta L_\alpha}(indirect) = \sum_{l' L'_\alpha} i^{L'_\alpha - L_\beta - l'} \left\langle L_\beta L'_\alpha 00 \middle| l'0 \right\rangle \hat{L}'_\alpha \hat{l}' W\left(L_\alpha L'_\alpha l l'; I_A L_\beta\right)$$

$$\times \left(S_{l'}^{\alpha'}\right)^{1/2} X_{l'}^{L'_\beta L_\alpha}(indirect) \qquad (4.14b)$$

and $\hat{x} = (2x+1)^{1/2}$, L_α and L_β's are orbital angular momenta of the respective channels.

The radial integrals are given by,

$$X_l^{L_\beta L_\alpha}(direct) = \frac{(4\pi)^{1/2}}{\gamma k_\beta k_\alpha} \int dr \chi_{L_\beta}(k_\beta, \lambda r) f_l^\alpha(r) \chi_{L_\alpha}(k_\alpha, r) \qquad (4.15a)$$

$$X_l^{L_\beta, L'_\alpha L_\alpha}(indirect) = \frac{(4\pi)^{1/2}}{\gamma k_\beta k_\alpha} \int dr \chi_{L_\beta}(k_\beta, \lambda r) f_{l'}^{\alpha'}(r) \chi_{L'_\alpha, L_\alpha}(k_\alpha, r) \quad (4.15b)$$

The first (direct) term is the same as the DWBA expression except the χ_{L_α} partial waves are here generated from the coupled equations. The second (indirect) describes the contributions going through the excited state $\alpha \to \alpha' \to \beta$.

4.5. The differential cross-section

The expression for the differential cross-section has the usual form:

$$\frac{d\sigma_{\beta\alpha}}{d\Omega} = \frac{\mu_\alpha \mu_\beta}{(2\pi\hbar^2)^2} \frac{k_\beta}{k_\alpha} \sum \left| T_m^{CCBA}(\vec{k}_\beta, \vec{k}_\alpha) \right|^2 \qquad (4.16)$$

It is evident from Eq.(4.13) for T that there occurs interference between the direct and indirect amplitudes, which may be destructive or constructive. This may be of great importance in the identification of these processes.

The relative importance of the indirect process depends on, among other things, the magnitude of the inelastic waves $\chi_{L'_\alpha L_\alpha}$ in the vicinity of the nuclei relative to the elastic waves. This is determined by the strength of the inelastic excitation. The

importance of the indirect term also depends on the relative sizes of the spectroscopic amplitudes $\left(S_l^{\alpha}\right)^{\frac{1}{2}}$ and $\left(S_l^{\alpha'}\right)^{\frac{1}{2}}$. If the direct transition is inhibited because $\left(S_l^{\alpha}\right)^{\frac{1}{2}}$ is small for some reason of nuclear structure but $\left(S_l^{\alpha'}\right)^{\frac{1}{2}}$ is not so inhibited , this may allow the indirect process to compete successfully or even dominate.

4.6. General case including mutual excitation

Using the generalized coupled-channels (CC) wave in channel spin representation and generalized transfer of interaction kernels, general form of the CCBA transition amplitude [132,134] can be written in more explicit form as:

$$
\begin{aligned}
T^{(CCBA)}_{\beta I_B M_B I_b M_b, \alpha I_A M_A I_a M_a}\left(\vec{k}_\beta, \vec{k}_\alpha\right) = & \sum_{m_\alpha L_\alpha L_\beta} A^{m_\beta m_\alpha}_{L_\beta L_\alpha}\left(\hat{k}_\beta, \hat{k}_\alpha\right) \sum_{S_\alpha S_\beta J} \left\langle I_A I_\alpha M_A M_\alpha \middle| S_\alpha M_\alpha \right\rangle \\
& \times \left\langle I_B I_b M_B M_b \middle| S_\beta M_\beta \right\rangle \\
& \times \left\langle L_\alpha S_\alpha m_\alpha M_\alpha \middle| J M_J \right\rangle \sum (-)^{J - S'_\beta - L'_\beta - l} (-)^{I'_B + I'_b - I'_A - I'_a} \\
& \times \hat{l}^2 \hat{J}_{b\alpha} \hat{J}_{BA} \hat{S}'_\alpha \hat{S}'_\beta W\left(L'_\alpha L'_\beta S'_\alpha S'_\beta; lJ\right) \\
& \times \begin{Bmatrix} l & J_{b\alpha} & J_{BA} \\ S'_\beta & I'_b & I'_B \\ S'_\alpha & I'_a & I'_A \end{Bmatrix} X^{J; L'_\beta S'_\beta I'_B I'_b, L_\beta S_\beta I_B I_b; L'_\alpha S'_\alpha I'_A I'_a, L_\alpha S_\alpha I_A I_a}_{l J_{b\alpha} J_{BA}}
\end{aligned} \tag{4.17}
$$

where,

$$\vec{J}_{BA} = I_B - I_A \ , \ \vec{J}_{ab} = I_b - I_a ,$$

$$\vec{I}_A + \vec{I}_\alpha = \vec{S}_\alpha , \qquad \vec{L}_\varepsilon + \vec{S}_\alpha = \vec{J} = \vec{L}'_\alpha + \vec{S}'_\alpha , \qquad \vec{S}'_\alpha = \vec{I}'_A + \vec{I}'_a$$

and $m_\beta = m_a + M_a + M_A - M_b - M_B$.

I_a and I_b are the spins of light particles, M_a and M_b are their respective projections.

The second sum in Eq. (4.17) is over

$$L'_\alpha,\ I'_\alpha,\ I'_A,\ S'_\alpha,\ L'_\beta\ \ I'_b,\ I'_B,\ S'_\beta,\ l,\ J_{b\alpha}\ \text{ and }\ J_{BA}$$

The radial integral X is given by [52],

$$X^{J;\beta',\beta;\alpha',\alpha}_{lJ_{b\alpha}J_{BA}} = \frac{4\pi}{k_\beta k_\alpha}\int r_\alpha dr_\alpha \int r_\beta dr_\beta \chi^J_{\beta',\beta}(k_\beta, r_\beta) g^{L'_\beta L'_\alpha}_{lJ_{b\alpha}(I'_b I'_A)J_{BA}(I'_B I'_A)}(r_\beta, r_\alpha)\chi^J_{\alpha',\alpha}(k_\alpha, r_\alpha)$$

where, $g^{L'_\beta L'_\alpha}_l(r_\beta, r_\alpha)$ is partial wave form factor for the lth wave and $A^{m_\beta m_\alpha}_{L_\beta L_\alpha} = 4\pi(-)^{m_\beta}\left[Y^{-m_\beta}_{L_\beta}(\hat{k}_\beta)Y^{m_\alpha}_{L_\alpha}(\hat{k}_\alpha)\right]$ is the angle factor

Using the above transition amplitude the differential cross-section for general case becomes,

$$\frac{d\sigma_{\beta\alpha}}{d\Omega} = \frac{\mu_\alpha\mu_\beta}{(2\pi\hbar^2)^2}\frac{k_\beta}{k_\alpha}\frac{1}{(2I_A+1)(2I_a+1)}\sigma_{\beta\alpha}(\theta) \qquad (4.18)$$

where, $\sigma_{\beta\alpha}(\theta) = \sum_{M_B M_b M_A M_a}\left|T^{CCBA}_{\beta I_B M_B I_b M_b,\alpha I'_A M_A l_a M_a}(\vec{k}_\beta, \vec{k}_\alpha)\right|^2$ and θ is the angle between $\vec{k}_\beta$ and $\vec{k}_\alpha$.

The computer computation has been performed using the code CHUCK3 [39].

CHAPTER 5
STUDY OF α-INDUCED TRANSFER REACTIONS

5.1. Study of (a,t) Reaction

5.1.1. Formalism for DWBA computation

The differential cross-section (Eq. 3.29) for a transfer reaction with a particular j-transfer in the DWBA theory [38,52] is given by,

$$\frac{d\sigma}{d\Omega} = \frac{\mu_i \mu_f}{(2\pi\hbar^2)^2} \frac{k_f}{k_i} \frac{1}{(2J_i+1)(2s_a+1)} \sum |T_{fi}|^2 \qquad (5.1)$$

Where, J_i and s_a are the spins of the target and the projectile respectively. μ's and k's are, respectively, the reduced masses and wave numbers. The subscripts i and f refer to the incident and outgoing channels, respectively. Σ denotes the sum over all magnetic sub-states. T_{fi} is the transition amplitude given in Eq. (3.13).

In the iso-spin representation, the experimental cross-section of the stripping reaction in full finite-range (FFR) calculations [39] is given by

$$\left(\frac{d\sigma}{d\Omega}\right)_{\exp} = \frac{2J_f+1}{2J_i+1} C^2 Ss \left(\frac{d\sigma}{d\Omega}\right)_{DWUCK5} \qquad (5.2)$$

$\left(\frac{d\sigma}{d\Omega}\right)_{DWUCK5}$ means cross-section calculated with the computer code DWUCK5, C^2 is the iso-spin Clebsch-Gordon co-efficient, S and s are respectively the heavy and light particle spectroscopic factors. J_f and J_i are the total spins of the final and initial nuclei respectively. The corresponding expression [39] for zero-range (ZR) approximation is:

$$\left(\frac{d\sigma}{d\Omega}\right)_{exp} = \frac{\left(2J_f+1\right)}{\left(2J_i+1\right)\left(2j+1\right)} D_0^{\,2} C^2 S \left(\frac{d\sigma}{d\Omega}\right)_{DWUCK4} \qquad (5.3)$$

D_0^2 is the normalization constant and $\left(\frac{d\sigma}{d\Omega}\right)_{DWUCK4}$ is the cross-section calculated with DWUCK4.

For the analyses of the data for the unbound states of the final nucleus, the resonance form factor formulated by Vincent and Fortune [46,47] has been applied. It is assumed that the resonance has a Breit-Wigner shape and in such a case the differential cross-section is given [47] by

$$\frac{d\sigma}{d\Omega} = \frac{\Gamma \mu k}{\hbar} \frac{d\sigma^F}{d\Omega} \qquad (5.4)$$

Here $\frac{d\sigma^F}{d\Omega}$ is the cross-section predicted at the energy of resonance (the positive energy of transferred proton relative to the core). Γ is the width of the resonance; μ is the reduced mass of the transferred proton and the target nucleus; and k is the wave-number of the proton at the resonance energy. Γ is estimated from the relation [47]

$$\frac{2}{\Gamma} = \frac{2\mu}{\hbar^2 k}\left[\int_0^{R_{max}} |u(r)|^2 dr + \frac{G}{2k}\frac{d}{dk}\left(\frac{G'}{G}\right)\right]. \qquad (5.5)$$

Here u(r) is the radial wave function of proton in the field of target core and $r = R_{max}$ is the distance beyond which nuclear potentials are assumed to be zero. G and G' are the irregular Coulomb function and its derivative at $r = R_{max}$, respectively.

5.1.2. DWBA Analysis of $^{27}Al(a,t)^{28}Si$ Reaction

The ZR and FFR DWBA calculations for the angular distributions have been performed using the computer codes DWUCK4 and DWUCK5 [39], respectively. Both the codes are modified to include Michel and molecular potentials. For the ZR calculations, a Gaussian form of finite range correction in the local energy approximation [32,39] with the correction parameter R=0.7 fm., has been used. Corrections due to non-locality [39] of potentials in the conventional form have been applied using the non-locality parameters $\beta(\alpha)$=0.2, $\beta(t)$=0.2 and $\beta(p)$=0.85 fm. The FFR analyses have been performed for both bound and unbound regions using each of the Michel, molecular and normal optical model types of potentials.

5.1.2.1. Choice of Potential Parameters

For entrance channel, the parameters of the molecular and Michel types of potential are generated by fitting the angular distributions of elastic data [44] using the Chi-squared minimization code MINUIT [41] in conjunction with the optical model code SCAT2 [135] modified to incorporate the Michel and molecular potentials. The fits to the elastic data are shown in Fig.5.1. The normal optical-potential-parameter set used in the present analysis is taken from [136]. The parameters of all three types of potentials are given in Table 5.1. The parameters of the bound state geometry are also noted in Table 5.1. For a bound state of ^{28}Si in both the FFR and ZR calculations as well as for the

bound state of alpha in the FFR calculations, the single proton transfer wave function has been computed adjusting the WS potential well depth so that its eigenvalue equals the separation energy [32].

For the triton potential in the exit channel, different sets of triton potential have been employed. Two sets of triton potentials, labeled set-1 and set-2 in Table 5.1, have been found to fit the data reasonably well with the molecular, normal optical or Michel potential in the entrance channel as can be seen in Figs. 5.2a–5.2c. The set-2 of triton potential produces a slightly better fit at the larger scattering angle region when the molecular potential has been used in the α-channel (Fig.5.2a). On the other hand, the normal optical or the Michel potential in the α-channel produces good fit to the data for the set-1 of triton potential in the exit channel Fig. 5.2b. We have, therefore, finally chosen the set-2 of triton potential with molecular potential and the set-1 of the triton potential with the Michel or normal optical potential in the α-channel for the analyses of the data. It is to be noted that, the sensitivity of the predicted cross-sections to the triton potential seems to be much stronger in the case of the normal optical potential in the entrance (Fig.5.2b) than for cases with the other two potentials.

5.1.2.2. Angular distributions

The FFR DWBA calculations for angular distributions for the best fits to the data using all three types of α-nucleus potentials for various *l*-transfers are compared to the experimental data in Figs. 5.4–5.9 for all levels.

The comparison of the ZR and FFR DWBA calculations of the angular distributions for the ground state (g.s.) and the 11.58 MeV state, using the molecular, Michel and normal optical potentials with the experimental data are shown in Figs. 5.3a–5.3c.

The levels in Figs. 5.4–5.9 are grouped according to the associated *l*-transfers. The levels populated through the *l*=2, 3, and 4 transfers are shown in Figs. 5.4–5.6, respectively. On the other hand, the levels which have been obtained through the incoherent sum of more than one *l*-transfers such as *l* = 0+2, 1+3 and 2+4 are shown, respectively, in Figs. 5.7–5.9. The DWBA fit to the unresolved group at E_x=6.88 MeV has also been shown in Fig. 5.8 with the total incoherent contribution from *l*=2+3. In the previous study, Yasue *et al.* [44]. associated *l*=3 transfer for fitting 15.02, 15.85 and 16.11 MeV transitions, but, in the present study, it seems to be *l*=4. The predicted angular distributions using each of the molecular, Michel and normal optical potentials for both *l*-transfers (*l*=3 and *l*=4) are compared to the data in Fig. 5.10. Clearly the *l*=4 transfer is preferred in all three cases.

5.1.2.3. Spectroscopic strengths

The spectroscopic strengths of a reaction for a transition to a final state (J_f;T_f) with the transferred configuration (lj) is related to the spectroscopic factor S_{lj} [139] by

$$G_{lj} = \frac{\left(2J_f + 1\right)}{\left(2J_i + 1\right)} C^2 S_{lj} \qquad (5.6)$$

where C is the Clebsch-Gordon coefficient involving iso-spins of the target and the final nucleus.

The sum rule for the spectroscopic strength in case of the $^{27}Al(\alpha,t)^{28}Si$ reaction can then be expressed [139] by

$$\sum_{J_f} G_{lj} = \tfrac{1}{2}\langle n-\text{holes}\rangle \quad \text{for } T_f = 1,$$

$$= \tfrac{1}{2}\langle p-\text{holes}\rangle - \tfrac{1}{2}\langle n-\text{holes}\rangle \text{ for } T_f = 0,$$

where <p-holes> and <n-holes> are, respectively, the effective number of proton-holes and neutron-holes in the orbit (lj).

The total strength comprising transitions with T_f =0 and 1 is then

$$\sum_{J_f,,T_f} G_{lj} = \langle p-\text{holes}\rangle. \qquad (5.7)$$

The deduced sum of strengths for all l=2 transitions with j=3/2,5/2 transfers and T_f=0,1 is $\sum G = 2.33$. This is almost half of the sum rule strength 5.0, the number of proton holes in the $1d_{5/2}$ and $1d_{3/2}$ orbits. Similarly, the sum of all l=0 transition strengths for both T_f=0 and 1 has been found to be $\sum G = 0.96$ which is again 50% of the expected sum of 2.0.

The extracted transition strengths for the $(6^-;0)$ state at E_x=11.58 MeV and $(6^-;1)$ state at E_x=14.36 MeV; which, have stretched configuration $(1d_{5/2}^{-1},1f_{7/2})$ in the shell model, are 0.14 and 0.23 respectively, which is small compared to the expected full strength of 1.08 for each. One may, however, consider the fragmentation of 6^- strengths is due to the deformed structure of ^{28}Si-core, using the following assumptions,

(i) the vibrational state of the core does not change in the transition, (ii) the core has negative deformation and (iii) the proton-hole configuration in the target is $|\, j_i=5/2, \Omega_I=1/2 >$ i.e. the target has $J_i=5/2$ and $K_i=1/2$,

one may calculate the spectroscopic strength due to deformation, can then be calculated, using the expression [140,141]

$$G = \frac{(2J_f+1)}{(2J_i+1)} C^2S = g^2 C^2 \langle J_i K_i j\Omega | J_f K_f \rangle^2 C_{Nlj}(\Omega\omega\alpha)^2, \qquad (5.8)$$

where $C_{Nlj}(\Omega\omega\alpha)$ as defined in [140,141] are the coefficients connecting a deformed single particle state to spherical eigen-states, g^2 is unity as $K_i \neq 0$. The values of these coefficients have been taken from [142]. Eq. (5.8) with $K_f=4$ results in a strength of G=0.083 for each of the $(6^-;0)$ and $(6^-;1)$ states, which is, indeed, small.

Table 5.1. Potential parameters used in the DWBA calculations for $^{27}Al(\alpha,t)^{28}Si$.

Channel →	$\alpha+^{27}Al$			$t+^{28}Si$		$p+^{27}Al$	$t+p$
Potential type →	Optical	Michel	Molecular	Optical		Bound state	Bound state
				set-1	set-2		
V_o(MeV)	218.0	80.20	52.81	143.82	56.30	V)	V)
r_o(fm)	1.24	1. 617	1.55	1.19	1.40	1.25	1.25
a_o(fm)	0.68	0.60	0.57	0.682	0.72	0.70	0.65
V_1(MeV)			68.46				
R_1(fm)			2.84				
α		7.40					
ρ(fm)		2.90					
W_o(MeV)	25.6	55.20	58.13	31.30	50.10		
r_I(fm)	1.24	1.53		1.28	1.40		
a_I(fm)	0.68	0.52		0.999	0.72		
R_w(fm)			3.35				
W_D(MeV)							
r_D(fm)							
a_D(fm)							
$V_{s.o}$(MeV)				4.65		$\lambda = 25$	$\lambda = 25$
$r_{s.o}$(fm)				0.996			
$a_{s.o.}$(fm)				0.280			
r_c(fm)						1.25	1.25
R_c (fm)	5.10	3.90	9.30	3.94	3.94		
Ref. →	a)			b)	c)	d)	d)

V) adjusted to give the separation energy; [a] Ref. [136]; [b] Ref. [137] ; [c] Ref.[138]; [d] Ref. [51]

Table 5.2. States of ^{28}Si observed in the ^{27}Al(α,t)^{28}Si reaction at E_α=64.5 MeV and the deduced spectroscopic factors using different potentials.

Ex (MeV)	J^π; T a)	l(nlj)	$(2J_f+1)C^2S$ present work b)	c)	d)	e)†
g.s.	0^+; 0	$2(0d_{5/2})$	4.8	4.5	4.5	4.6
1.78	2^+; 0	(0 + 2)	0.7, 1.08	0.84, 1.26	0.672, 1.008	1.7, 1.2
4.62	4^+; 0	(2 + 4)	2.13, .022	2.90, 0.396	2.22, 0.117	2.5, 0.04
4.98	0^+; 0	$2(0d_{5/2})$	0.42	0.6	0.75	0.48
6.28	3^+; 0	(0 + 2)	0.138, 1.24	0.36, 2.04	0.63, 1.47	0.39, 1.4
6.69	0^+; 0	$2(0d_{5/2})$	0.03	0.048	0.048	0.04
6.88 6.89	3^-;0 4^+;0	(2+3)	0.27, 0.03	0.57, 0.03	0.456, 0.024	0.65, 1.1, 2.6
7.38 7.42	2^+;0 2^+;0	(0+2)	0.06, 0.86	0.3, 1.2	0.276, 1.104	0.15, 0.90
7.80	3^+; 0	(0 + 2)	0.26, 0.396	0.357, 0.663	0.315, 0.585	0.22, 0.35
7.93	2^+; 0	(0 + 2)	0.27, 0.672	0.63, 1.17	0.441, 0.819	0.7, 0.65, 0.06
8.26	2^+; 0	(0 + 2)	0.30, 1.20	0.15, 1.65	0.38, 1.5	0.13, 1.1
8.41	4^-; 0	(1 + 3)	0.48, 0.72	0.9, 0.9	0.9, 0.9	0.45, 1.0
8.54	6^+; 0	4	0.48	0.78	0.9	0.13
8.59	3^+; 0	(0 + 2)	1.0, 1.51	2.85, 2.85	1.8, 1.8	0.8, 1.9
8.90	1^-; 0	(1 + 3)	0.048, 0.072	0.076, 0.032	0.055, 0.023	0.018, 0.048
8.94	4^+; 0	(2+4)	0.054,0.023	0.022, 0.086	0.022, 0.086	0.11, 0.06
	5^-; 0	or 3	0.054	0.066	0.036	0.06
9.16	4^+; 0	4	0.02	0.03	.03	0.06
9.32	3^+;1	(0 + 2)	1.176, 0.50	1.95, 1.05	1.365, 0.735	1.5, 0.49
9.38	2^+;1	(0 + 2)	1.33, 0.88	3.36, 1.44	3.84, 0.96	1.6, 1.0
9.48	2^+; 0	(0 + 2)	0.52, 0.90	1.5, 1.5	1.026, 0.054	0.2, 0.24
9.70	5^-; 0	3	1.20	1.8	1.8	1.8
9.76	$(2, 3)^-$; 0	(1 + 3)	0.038, 0.113	0.576, 0.144	0.385, .096	0.06, 0.17
9.93	$(1, 2)^-$; 0	3	0.60	1.17	0.99	0.11
10.21	$(2- 4)^+$; 0	4	.096	0.126	0.126	0.17
10.38	3^+; 1	(0 + 2)	0.66, 1.98	1.13, 3.38	0.75, 2.25	0.65, 2.3
10.72	1^+;0+1	(2 + 4)	0.113, 0.038	1.92, 0.48	0.144, 0.036	0.11, 0.009
10.94	+	(2 + 4)	0.70, 0.08	1.37, 0.072	1.083, 0.057	0.32
11.10		(2+4)	0.105, 0.045	0.108, 0.072	0.072, 0.048	0.1, 0.04,
11.14	2^+	(2 + 4)	0.363, 0.297	0.274, 0.068	0.168, 0.042	0.02, 0.06
11.44 11.45	$2^+,3^+,4^+$; (0,1) 1^+;1	$(2+4)$	2.96, 0.16	5.99, 0.315	3.99, 0.21	3.8, 0.39
11.58	6^-; 0	3	1.41	1.86	1.68	2.1

[continued..]

Table 5.2. [continued..]

Ex (MeV)	J^{π}, T a)	l(nlj)	$(2J_f+1)C^2Ss^*$ present work b)	c)	d)	e)†
11.80	+	2+4	0.19, 0.157	0.36, 0.36	0.5, 0.22	0.13, 0.12
11.90	3^-; 0	(1+3)	0.4, 0.08	0.126,0.294	0.099, 0.231	0.49, 0.17
11.93	–	1 + 3	3.70, 0.195	5.67, 0.63	4.28, 0.23	4.7
11.97	$(2^+,4^+)$; 0	2+4	0.59, 0.066	0.972, 0.108	0.11, 0.066	0.5, 0.09
	or 3^-; 0	or 1+3	0.41, 0.221	0.655, 0.353	0.43, 0.23	0.4, 0.3
12.07	(2^+); 0	2+4	0.21, 0.09	0.315, 0.135	0.252, 0.108	0.3, 0.09
		or 3	0.21	0.36	0.24	0.2
12.24	$3^+ + 4^+$;0	2 + 4	0.1, 0.06	0.144, 0.216	0.144, 0.216	0.27, 0.12
12.30	2^+; 0	4	0.39	0.51	0.51	0.06
12.33	1^+; 1	2	0.72	1.32	0.9	0.55
12.49	3^-; 0	3	0.84	1.2	1.14	1.0
12.66	4^-; 1	3	3.00	5.4	4.2	3.8
12.82	1^-; 0	1+3	0.14, 0.32	0.20, 0.46	0.15, 0.36	0.03, 0.32
13.25	5^-; 1	3	3.30	5.4	4.2	3.6
13.99	–	3	0.63	1.02	0.78	1.6
14.36	6^-; 1	3	2.40	2.88	2.7	3.7
14.69	–	3	0.24	0.51	0.33	0.39
15.02	–	4	0.15	0.21	0.21	0.70
15.38	–	3	0.45	0.78	0.57	0.55
15.55	+	4	0.12	0.21	0.15	0.09
15.85	–	4	0.11	0..222	0.156	0.36
16.11	–	4	0.48	0.24	0.48	0.41
16.50	+	4	0.14	0.24	0.18	0.07

* s = 2.0 is the light particle spectroscopic factor.

† light particle spectroscopic factor is not mentioned in [44].

a) Ref. [151]; b) Optical; c) Michel; d) Molecular; e). Ref. [44].

Table 5.3. Comparison of the deduced spectroscopic strengths to the shell model predictions.

Ex (MeV)	J^{π}; T a)	l(nlj)	$G = \frac{(2J_f+1)}{(2J_i+1)} C^2S$ present work [b]	$G = \frac{(2J_f+1)}{(2J_i+1)} C^2S$ shell-model [c]
g.s.	0^+; 0	$2(0d_{5/2})$	0.375	0.53
1.78	2^+; 0	(0 + 2)	0.06, 0.08	0.38, 0.06
4.62	4^+; 0	(2 + 4)	0.19, 0.01	0.33, 0.00
4.98	0^+; 0	$2(0d_{5/2})$	0.06	0.05
6.28	3^+; 0	(0 + 2)	0.05, 0.12	0.34, 0.14
6.69	0^+; 0	$2(0d_{5/2})$	0.004	0.005
6.88	3^-; 0	3	0.002	0.0
6.89	4^+; 0	2	0.038	0.27
7.38	2^+; 0	(0+2)	0.02, 0.09	0.02, 0.17
7.42	2^+; 0			
7.80	3^+; 0	(0 + 2)	0.03, 0.05	0.357, 0.663
7.93	2^+; 0	(0 + 2)	0.04, 0.07	0.00, 0.13
8.59	3^+; 0	(0 + 2)	0.15, 0.15	0.035, 0.21
9.32	3^+;1	(0 + 2)	0.11, 0.06	0.38, 0.06
9.38	2^+;1	(0 + 2)	0.32, 0.08	0.23, 0.05
10.38	3^+; 1	(0 + 2)	0.06, 0.19	0.01, 0.20
10.72	1^+;0+1	(2 + 4)	0.012, 0.006	0.015, 0.00
11.58	6^-; 0	3	0.14	0.083 [d]
14.36	6^-; 1	3	0.23	0.083 [d]

[a] Ref.[151]; [b] Molecular potential; [c] Ref. [143]; [d] Deformed shell-model [140,141].

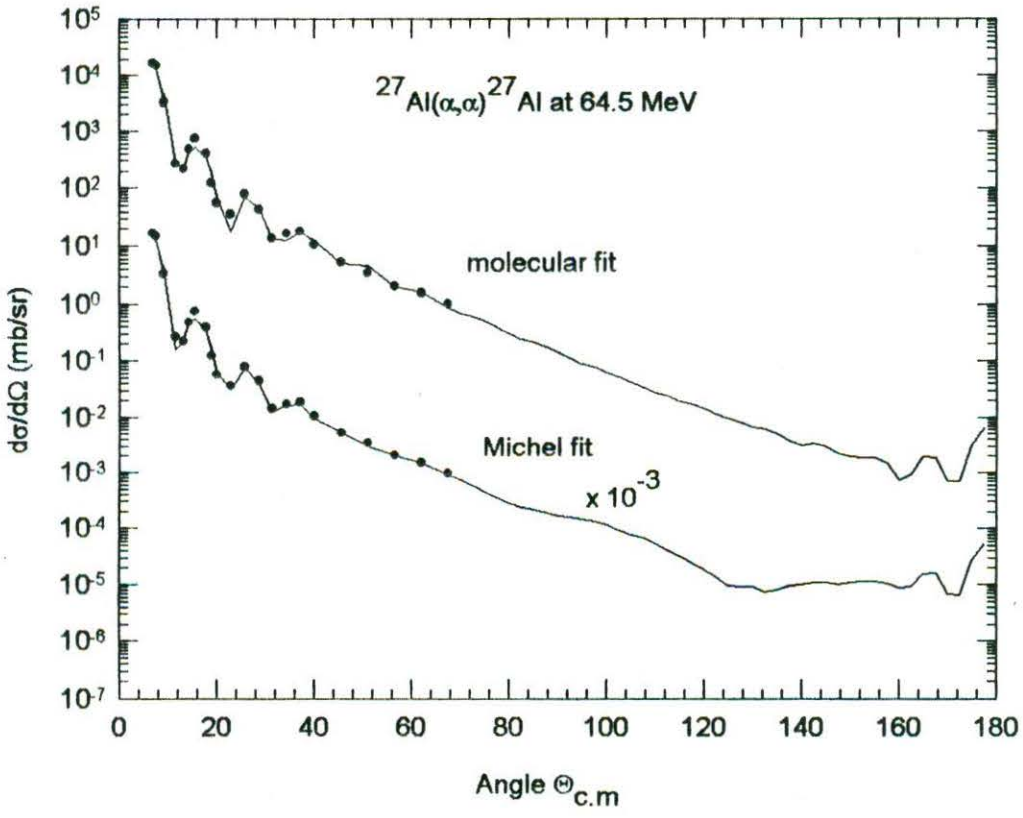

Fig.5.1. Fits to the α-^{27}Al elastic scattering data at 64.5 MeV with molecular and Michel potentials. Data are from Yasue *at al.* [44]

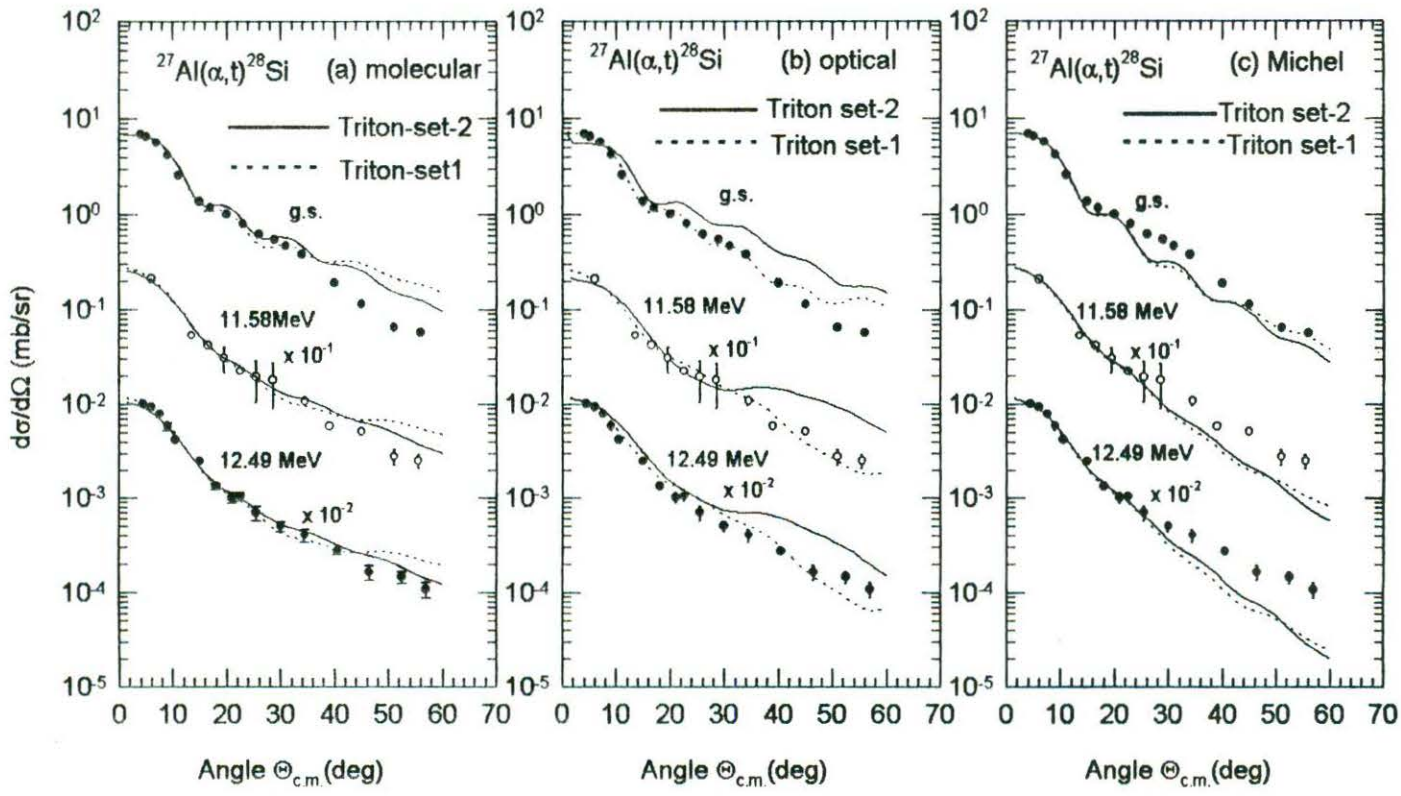

Fig.5.2. Full finite-range DWBA predictions compared to data [44] for three transitions using (a) molecular, (b) normal optical, and (c) Michel potentials with set-1 and set-2 (Table 5.1) of triton potentials in the exitchannel.

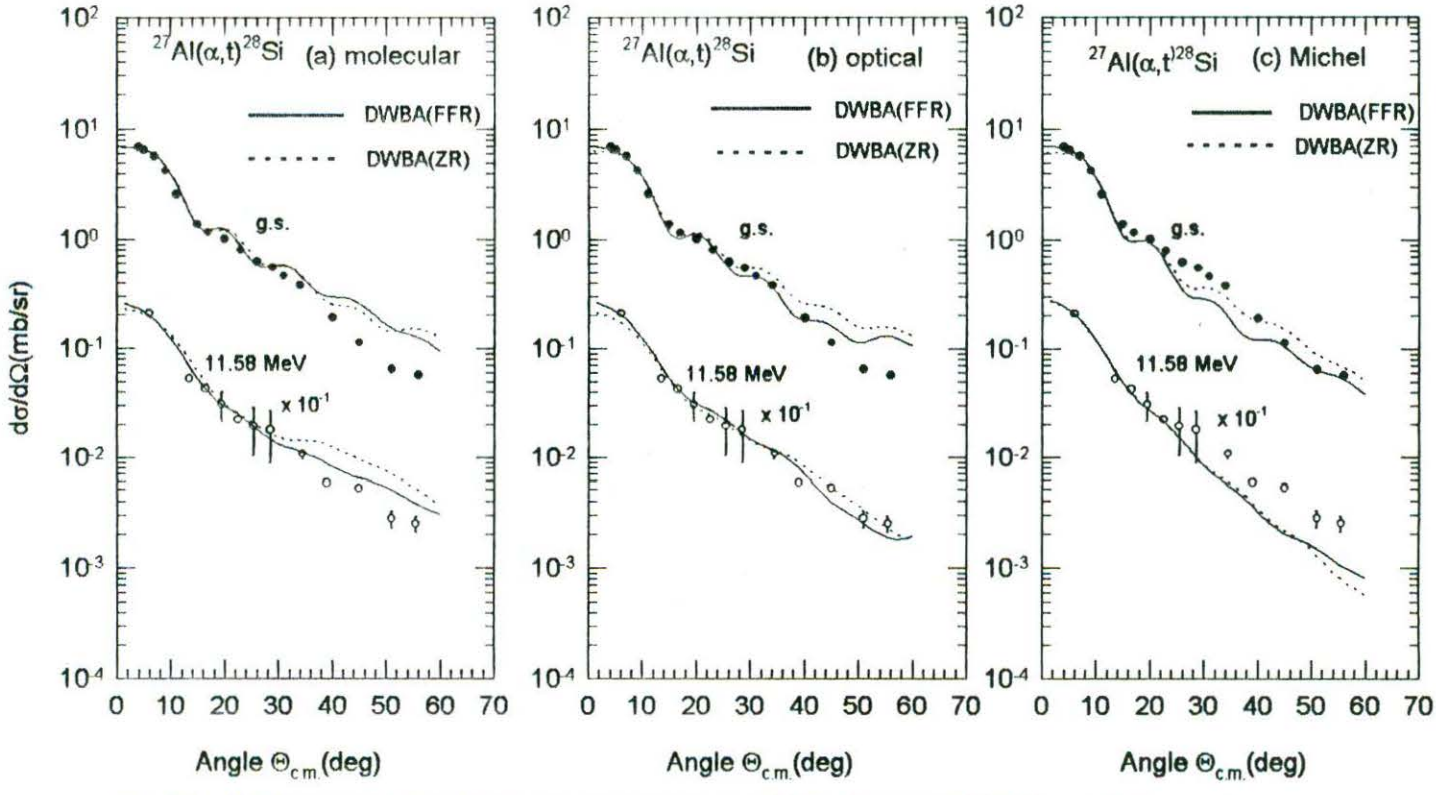

Fig. 5.3. Full finite-range (solid curves) and zero-range (dotted curves) DWBA predictions using (a) molecular,(b) normal optical, and (c) Michel potentials for the g.s. and E_x=11.58 MeV transitions are comprared to data. Data are from Yasue *et al.*[44]

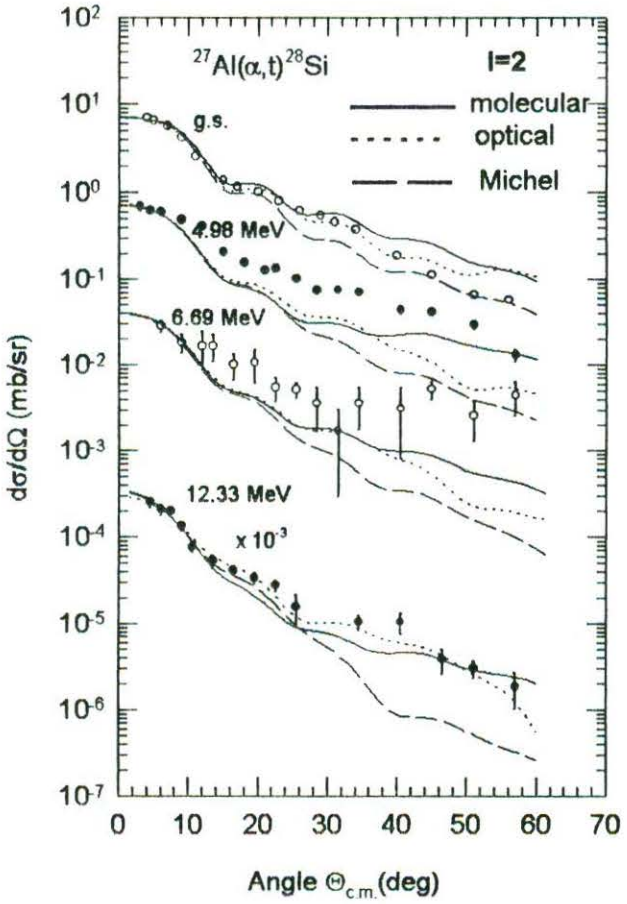

Fig.5.4. Full finite-range DWBA predictions using molecular (solid curves), normal optical (dotted curves), and Michel (dashed curves) potentials for the transitions with *l* values indicated are compared to data (solid or open circles). The triton potential of set-1 has been used with the normal optical and Michel potentials, and that of set-2 with the molecular potential in the α–channes.Data are from Yasue *et al.* [44]

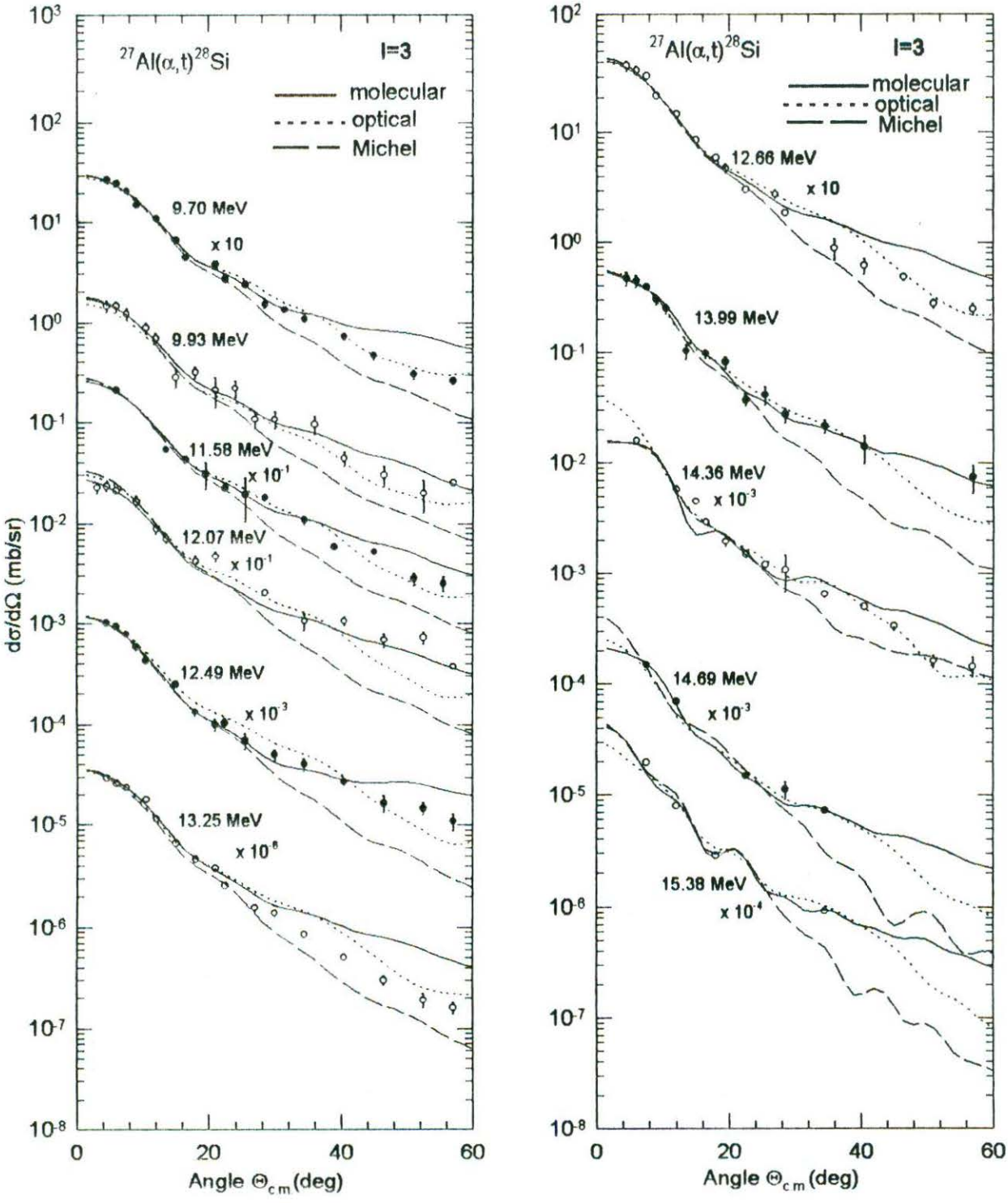

Fig. 5.5. Same as in Fig. 5.4. Data are from [44]

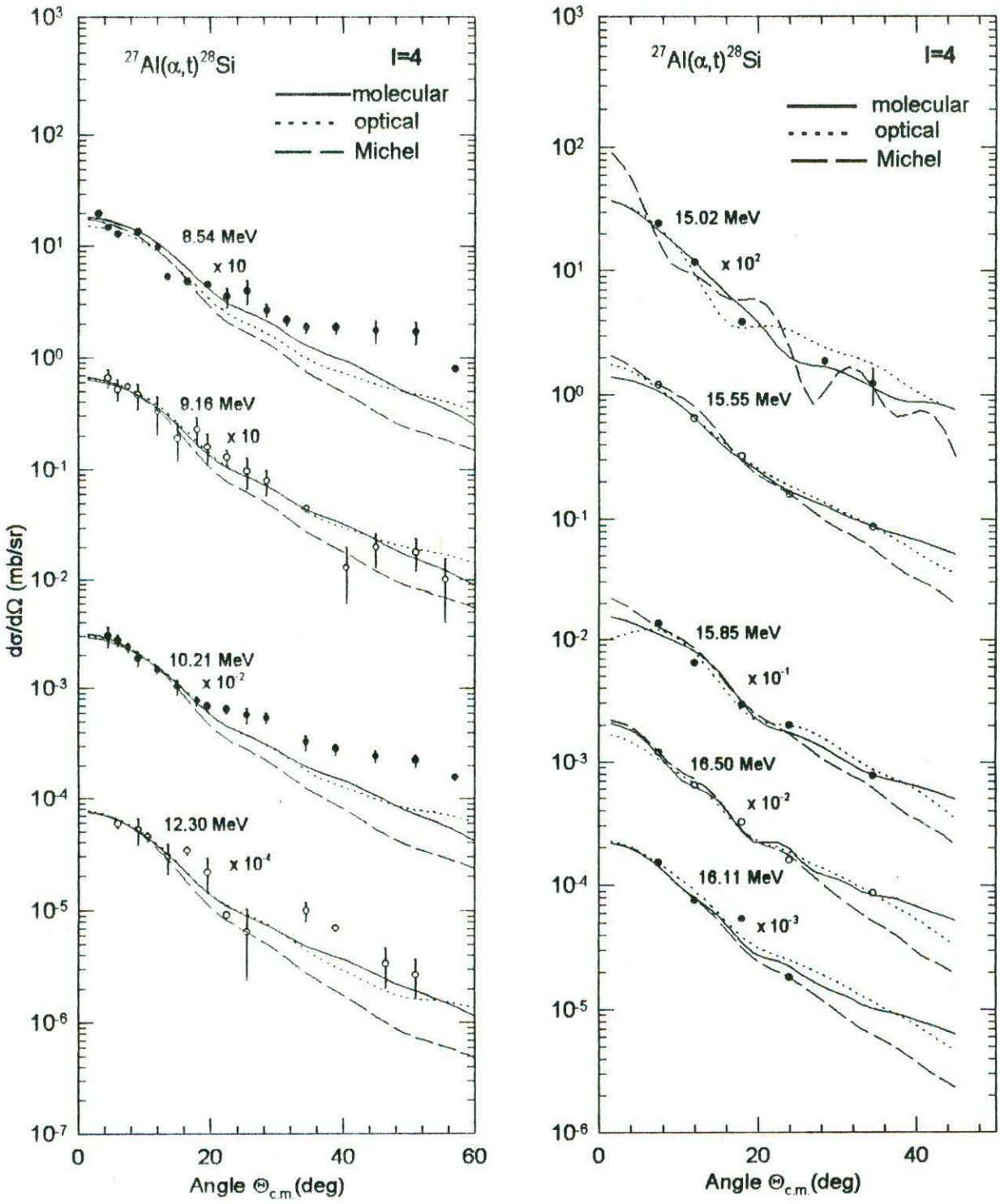

Fig. 5.6. Same as in Fig. 5.4. Data are from [44]

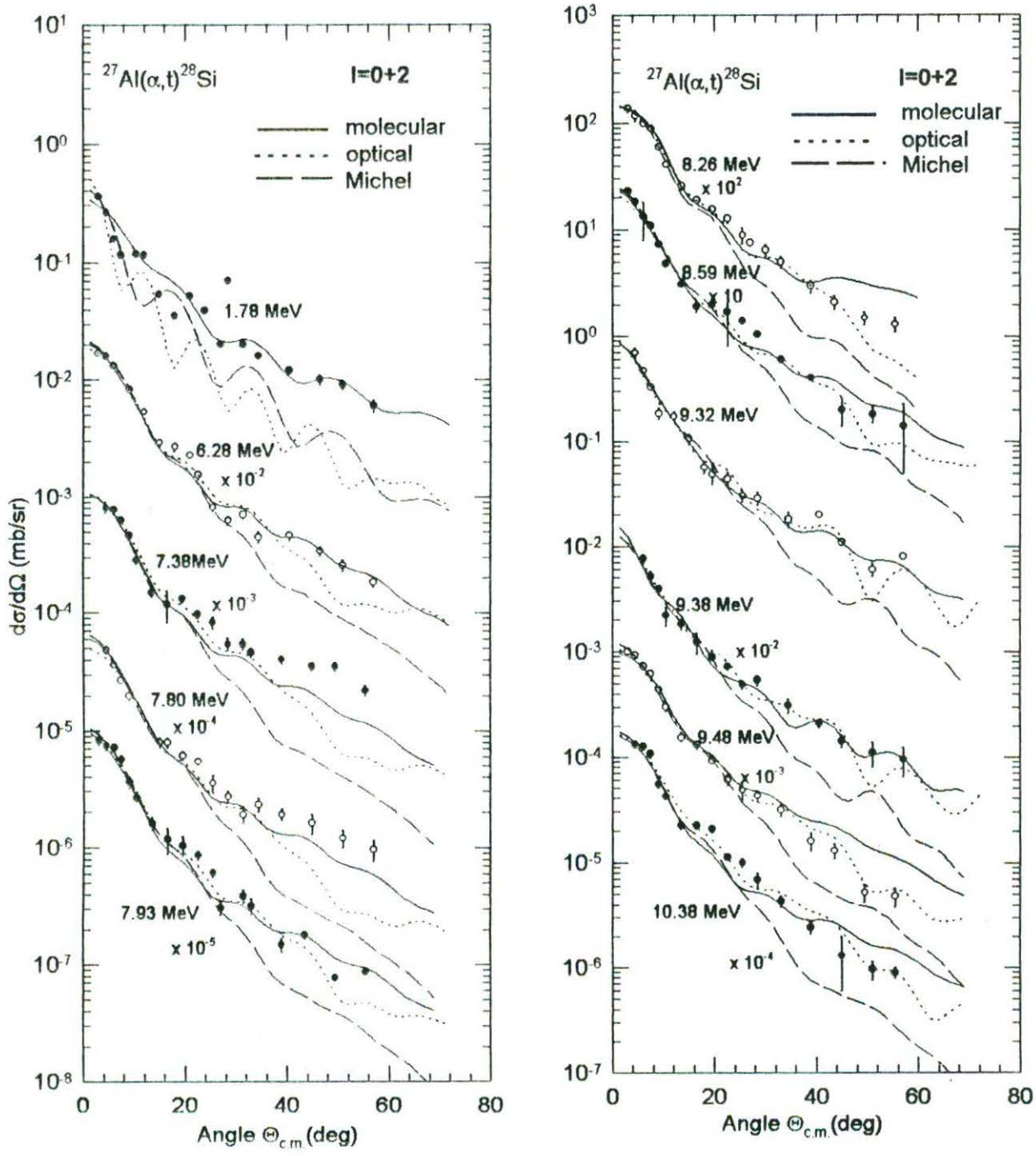

Fig. 5.7. Incoherent sums of full finite-range DWBA predictions using molecular (solid curves), normal optical (dotted curves), and Michel (dashed curves) potentials for the transitions with *l* values indicated are compared to data (filled or open circles). Data are from Yasue *et al.* [44].

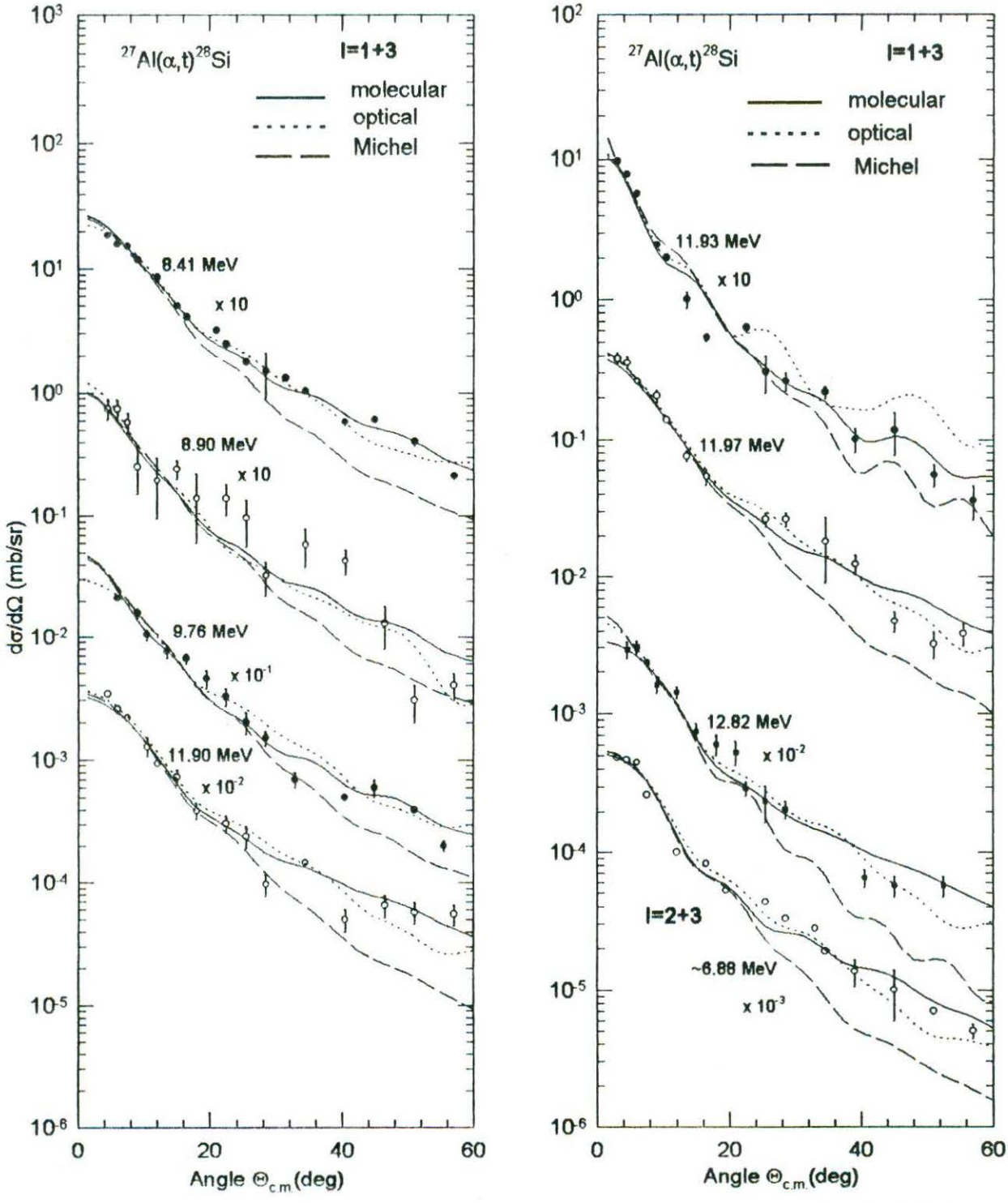

Fig.5.8. Same as in Fig. 5.7. The data of the 6.88 MeV transition are compared to the *l*=2+3 DWBA predictions.

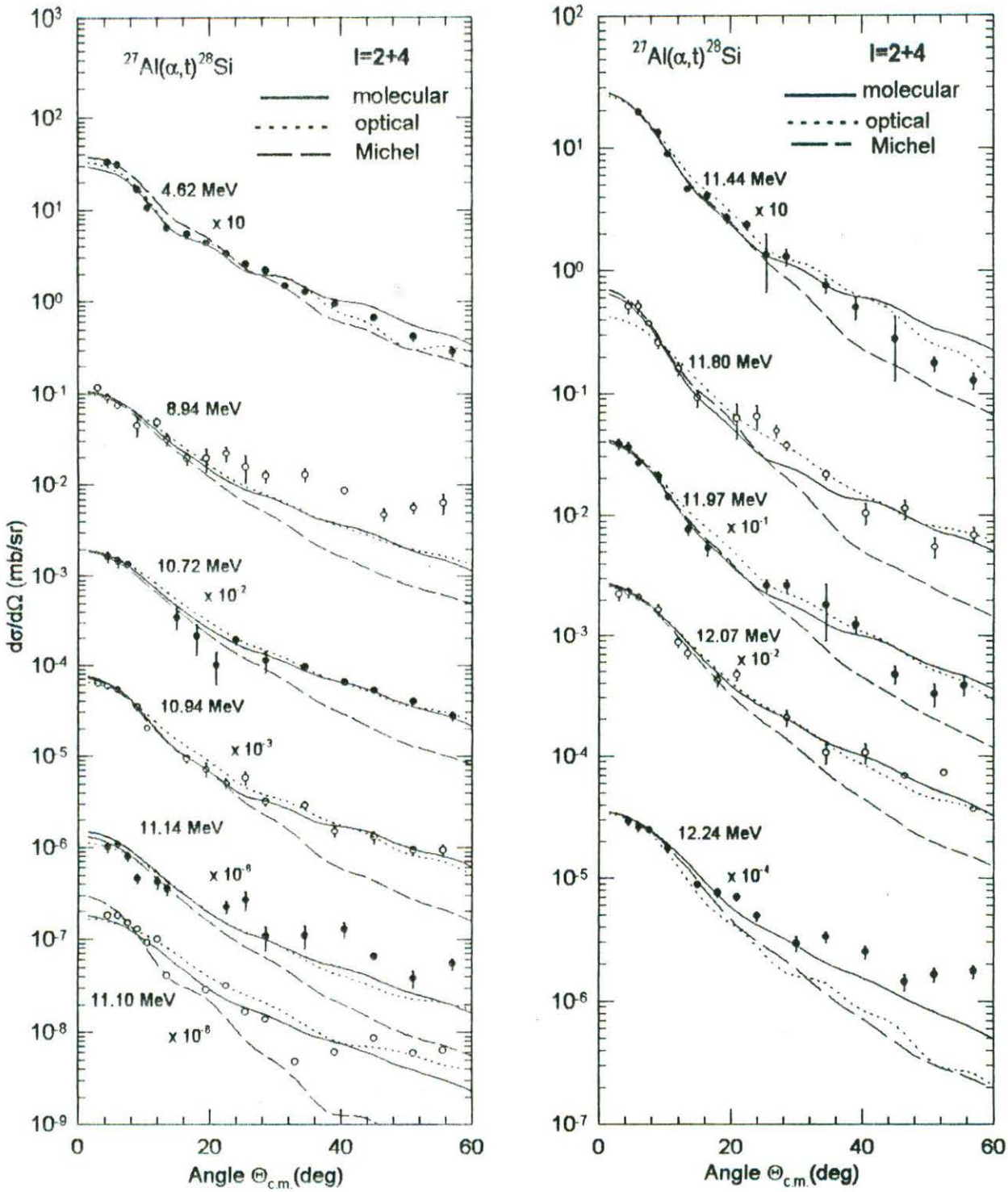

Fig. 5.9. Same as in Fig. 5.7. Data are from [44].

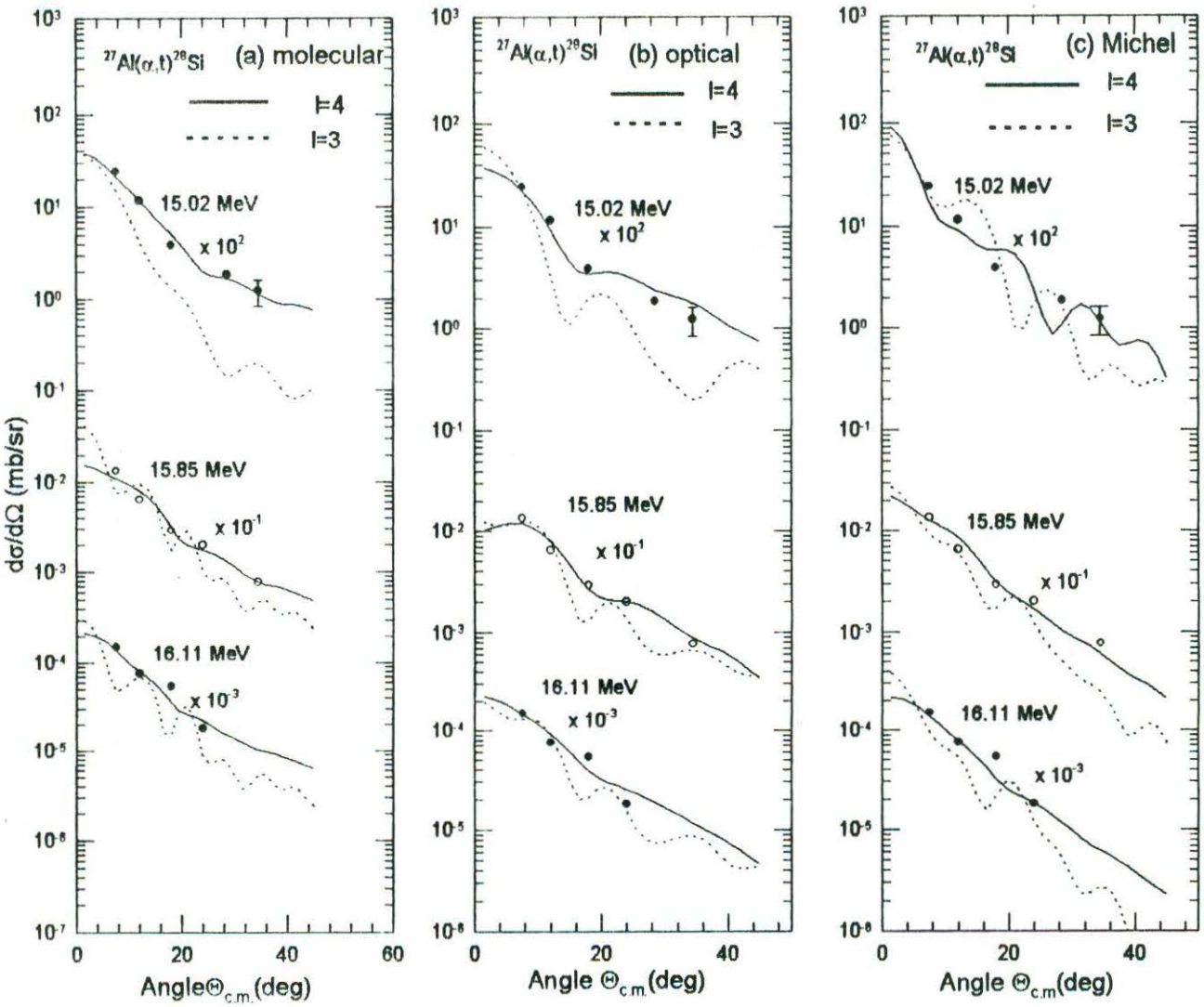

Fig. 5.10. Full finite-range DWBA predictions for transitions with *l*=4 (solid curves) and l=3 (dotted curves) values are compared to data for three transitions using (a) molecular, (b) normal optical, and (c) Michel potentials. Data are from Yasue *et al.* [44]

5.2. Study of (α,d) Reaction

5.2.1. Formalism for DWBA computation

In absence of spin-orbit interactions, the differential cross-section for a (α,d) reaction with a particular J-transfer in the DWBA theory [105] is given by,

$$\frac{d\sigma}{d\Omega} = \frac{\mu_i \mu_f}{(2\pi\hbar^2)^2} \frac{k_f}{k_i} \frac{(2J_f+1)}{(2J_i+1)} \sum_{LM} \left| \sum_{\rho_1\rho_2} \beta^{1/2}[\rho_1\rho_2; J0] \begin{bmatrix} l_1 & l_2 & L \\ \frac{1}{2} & \frac{1}{2} & 1 \\ j_1 & j_2 & J \end{bmatrix} B_M^L \right|^2 \quad \ldots \quad (5.9)$$

Where, μ's and k's are, respectively, the reduced masses and wave numbers. The subscripts i and f refer to the incident and outgoing channels, respectively. $\rho_1 = [n_1 l_1 j_1]$ and $\rho_2 = [n_2 l_2 j_2]$ denote the orbital quantum numbers for the transferred nucleons in the final nucleus. $\beta^{1/2}[\rho_1\rho_2; J0]$ are the spectroscopic amplitudes in the jj-coupling for an angular momentum transfer J and an isospin transfer T=0. [ ] refers to the normalized 9-j symbol, the LS-jj transformation factor [104]. B_M^L describes the kinematic aspects of the reaction. In Eq.(5.9) the light particle spectroscopic factor $c^2 s = 1.0$ for (α,d) reactions has been used.

In the macroscopic DWBA calculations, no information on the structure of the cluster is required except the quantum numbers (N, L) as defined by

$$2(n_1 + n_2) + l_1 + l_2 = 2N + L \qquad \ldots\ldots \quad (5.10)$$

where the quantum numbers $\nu = 0$ and $\lambda = 0$ are assumed for the relative 0s-state internal motion of the transferred cluster.

In Eq.(5.10), only one N – value is considered to contribute, the two nucleons in the cluster being in the relative 0s-state.

The structure amplitude G_{LJ} for two nucleon transfer, as defined by Glendenning [104] is expressed as

$$G_{LJ} = \sum_{\rho_1\rho_2} \left(2 - \delta_{\rho_1\rho_2}\right)^{1/2} \beta^{1/2}\left[\rho_1\rho_2; J0\right] \begin{bmatrix} l_1 & l_2 & L \\ \frac{1}{2} & \frac{1}{2} & 1 \\ j_1 & j_2 & J \end{bmatrix} \Omega_{00} \left\langle 00, NL{:}\, L \middle| n_1 l_1, n_2 l_2 {:}\, L \right\rangle \qquad \ldots.(5.11)$$

In Eq.(5.11), Ω_{00} denotes the overlap of the spatial wave function of relative motion of the two particles in the transferred cluster with the corresponding part in the incident α particle. $\langle \ | \ \rangle$ represents the Brody-Moshinsky bracket [104,105,147].

The expression for cross section in terms of the cluster quantum numbers (N,L) parallel to Eq.(5.9) can be written in the notation of Glendenning [104] as an incoherent sum over L and M as:

$$\frac{d\sigma}{d\Omega} = \frac{\mu_i \mu_f}{\left(2\pi\hbar^2\right)^2} \frac{k_f}{k_i} \frac{\left(2J_f + 1\right)}{\left(2J_i + 1\right)} \sum_{LM} \left| G_{LJ} \Re_M^L \right|^2 \qquad (5.12)$$

Denoting the cross sections calculated for an L-transfer and a J-transfer with the FFR code DWUCK5 [39] by $\left(\frac{d\sigma}{d\Omega}\right)_{DW5}^{LJ}$ and taking advantage of the incoherent sum over the L-transfer(s), one can write the experimental cross section as,

$$\left(\frac{d\sigma}{d\Omega}\right)_{exp} = \frac{(2J_f+1)}{(2J_i+1)}\sum_{LJ} A_{LJ}\left(\frac{d\sigma}{d\Omega}\right)^{LJ}_{DW5} \qquad (5.13)$$

In the cases of ^{28,30}Si $J_i = 0$, so the transferred total angular momentum J is unique, but for ^{29}Si, $J_i = \frac{1}{2}$, the transferred total angular momentum are restricted to two values $J=J_1$ and J_2 . The spin transfer being unity in the (α,d) reaction, one of the J-transfers, say J_1 involves two orbital angular momentum transfers $L=L_1$ and L_2. On the other hand, J_2 associates only one $L=L_3$ which is equal to one of L_1 and L_2, say L_1, such that $L_3=L_1$.

Thus, the above equation can be written explicitly as,

$$\left(\frac{d\sigma}{d\Omega}\right)_{exp} = \frac{(2J_f+1)}{(2J_i+1)}\left[\left(A_{L_1}\right)_{J_1}\left(\frac{d\sigma}{d\Omega}\right)^{L_1J_1}_{DW5} + \left(A_{L_2}\right)_{J_2}\left(\frac{d\sigma}{d\Omega}\right)^{L_2J_1}_{DW5} + \left(A_{L_1}\right)_{J_2}\left(\frac{d\sigma}{d\Omega}\right)^{L_1J_2}_{DW5}\right] \qquad (5.14)$$

Now, assuming $\left(\frac{d\sigma}{d\Omega}\right)^{L_1J_1}_{DW5} \approx \left(\frac{d\sigma}{d\Omega}\right)^{L_1J_2}_{DW5}$ which is valid in absence of any spin-orbit interaction and denoting $A_{L_1} = \left(A_{L1}\right)_{J_1} + \left(A_{L_2}\right)_{J_2}$, $A_{L_2} = \left(A_{L_2}\right)_{J_1}$ and taking off superscript J_2 on $\left(\frac{d\sigma}{d\Omega}\right)^{L_1J_2}_{DW5}$, Eq. (5.14) can be written as,

$$\left(\frac{d\sigma}{d\Omega}\right)_{exp} = \frac{(2J_f+1)}{(2J_i+1)}\left[A_{L1}\left(\frac{d\sigma}{d\Omega}\right)^{L1}_{DW5} + A_{L2}\left(\frac{d\sigma}{d\Omega}\right)^{L2}_{DW5}\right] \qquad (5.15)$$

On the other hand, the experimental cross-sections related to the microscopic cross-sections $\left(\frac{d\sigma}{d\Omega}\right)^{L}_{DW4}$ which has been calculated by the ZR code DWUCK4 [39] are given by,

$$\left(\frac{d\sigma}{d\Omega}\right)_{exp} = \aleph \frac{(2J_f+1)}{(2J_i+1)} \sum_J \frac{1}{(2J+1)} \left(\frac{d\sigma}{d\Omega}\right)^J_{DW4} \qquad (5.16)$$

$\aleph$ in Eq. (5.16) is the normalization constant for the (α,d) reactions. The form of Eq.(5.15) shows that A_{L1} and A_{L2} are the spectroscopic factors [37,150] for the L_1 and L_2 transfers, respectively. The cross sections in Eq. (5.15) being incoherent sum of the contributions from the two L-values (for natural parity transitions only one L-transfer L=J permitted) $L = J \pm 1$, the spectroscopic factor [150] A_L for each of the L-transfers and the normalization constant $\aleph$ can be extracted from Eq.(5.15) and Eq.(5.16) respectively by fitting the experimental cross sections.

5.2.2. DWBA analysis of $^{28}Si(\alpha,d)^{30}P$ reaction

The microscopic zero-range and macroscopic full finite-range (FFR) DWBA calculations for the angular distributions have been performed using the computer codes DWUCK4 and DWUCK5 [39], respectively. Both the codes are modified to include the Michel potential. Corrections due to non-locality [32,39] of potentials in the conventional form have been applied using the non-locality parameters β(α)=0.2, β(d)=0.54 and β(p)=0.85 fm. In both the microscopic ZR and macroscopic FFR calculations, the molecular, Michel, and normal optical types of α-^{28}Si potential and the optical d-^{30}P potential have been employed. The parameters of the molecular and Michel potentials are taken from the work of Tariq *et al.* [19]. The α-^{28}Si elastic fits are furnished in Fig. 5.11.The parameters of the normal shallow optical potentials for the incident channel are

from Jankowski *et al.* [18]. Several sets of the d-^{30}P optical potentials including that from [18] have been tried, but only the one from the work of Fitz *et al.*[148] produces the best fit. All the potential parameters employed in the present analyses are displayed in Table.5.4.

5.2.2.1. Macroscopic DWBA calculations

The macroscopic analyses have been performed using the full finite-range DWBA code DWUCK5 [39]. The parameters for the bound-state geometry of the d-d and d-^{28}Si Woods-Saxon (WS) potentials, shown in Table 5.4 are taken from [18]. The bound state wave functions for the transferred deuteron-cluster in alpha as well as the final nucleus have been generated by adjusting the deuteron separation energies. At the start of calculations, the accuracy parameters used in the code DWUCK5 have been assigned appropriate values, to define effective width of wave numbers [39,149] in the expansion of the distorted waves in terms of plane waves for making the zero-range calculations identical to those from the code DWUCK4 [39]. This ensures the necessary "convergence" for the integral for the zero-range form-factor, defined in Eq.(3.9) of Charlton [149].

The cluster configurations of the transferred deuteron for the different states of excitation are shown in Table 5.5. For the final states with natural parity, populated by one L-transfer, the DWBA predictions are normalized to the data to yield the relevant spectroscopic factor A_L as defined in Eq. (5.15). On the other hand, for the transitions involving two L-transfers, leading to the final states with unnatural parity, the spectroscopic factors are obtained by minimizing the χ^2 defined by

$$\chi^2 = \sum_i \left[\frac{\sigma_{exp}(\theta_i) - \sigma_{DW}(\theta_i)}{\Delta\sigma_{exp}(\theta_i)} \right]^2 \qquad (5.17)$$

where $\sigma_{exp}(\theta_i) = \left(\frac{d\sigma}{d\Omega}(\theta_i) \right)_{exp}$ and $\Delta\sigma_{exp}(\theta_i)$ are, respectively, the experimental cross section, as defined in Eq. (5.15), and its error at the scattering angle θ_i. $\sigma_{DW}(\theta_i)$ is the cross section predicted by the DWBA theory.

The DWBA predictions with the molecular (solid curves), normal optical (broken curves), and Michel (dotted curves) potentials are compared to the data of the ground (1^+), 0.709 (1^+), 1.454 (2^+), 2.72 (2^+) and 3.02 MeV (2^+) states in Fig. 5.12; to the data of the 1.974 (3^+), 2.538 (3^+), and 2.84 MeV (3^+) states in Fig. 5.13; and to the data of the 3.93 (2^-), 4.63 (3^+) and 5.42 MeV (2^+) states of ^{30}P in Fig. 5.14. It is amply clear from Figs. 5.12–5.14 that the calculations with the molecular potential produces the best fits to data for all the transitions. Furthermore, the Michel potential generates cross sections, which are lower by 1 to 2 orders of magnitude than those predicted by either the normal optical or the molecular potential. Table 5.6 gives the comparison of the total spectroscopic factors for the cluster transfer for the three types of potentials.

The compiled work of Endt and van der Leun [151] suggests alternative spin-parity for the 3.93 MeV state as $J^\pi = 1^+, 2^-$ or 3^+. While de Meijer *et al.* [37] assigned $J^\pi = 3^+$ for the state, Jankowski *et al.* [18] suggested 2^-. The DWBA calculations with the molecular potential for both $J^\pi = 2^-$ and 3^+, are compared to the experimental cross section in Fig.5.15. The $J^\pi = 2^-$ assignment is clearly favored, confirming the observation of Jankowski *et al.* [18].

5.2.2.2 Microscopic DWBA calculations

The microscopic ZR DWBA calculations have been performed using the zero-range code DWUCK4 for the positive parity states with the transferred particles stripped to the sd-shell. The present analyses make use of three sets of spectroscopic amplitudes $\beta^{1/2}$, two sets based on the FPSDI and MSDI Hamiltonians as defined in Wildenthal *et al.* [144] and the shell-model wave functions of the ^{28}Si and ^{30}P nuclei given by Wildenthal *et al.* [144,145] and the third one, labeled by CW [37], derived from the wave functions of Chung and Wildenthal referred to in [37]. The FPSDI and CW amplitudes are taken from de Meijer *et al.* [37], while the MSDI amplitudes are from Jankowski *et al.* [18]. All the three sets of spectroscopic amplitudes are calculated in the model space of $0d_{5/2}$-$1s_{1/2}$-$0d_{3/2}$. The spectroscopic amplitudes are presented in the Table (5.8–5.10). Since the codes DWUCK4 and DWUCK5 assume that the spherical harmonics carry a time reversal phase of i^l, a factor not used in the phase conventions adopted in the calculations of the spectroscopic amplitudes [37], the amplitudes have been multiplied by an extra phase of $i^{l_1+l_2-L}$ before feeding these to the codes.

The bound state wave functions for each of the transferred nucleons have been generated by assuming a real Woods-Saxon well with the geometry parameters r_0=1.25 fm. and a_0= 0.65 fm. and the depth adjusted to produce the binding energy equal to half the separation energy of the transferred deuteron. A Thomas-Fermi spin-orbit term with λ=25 has also been used for the bound state wave functions.

A Gaussian form of finite range correction in the local energy approximation [39] has been investigated. Fig. 5.16 compares the microscopic DWBA calculations for the molecular type of α-^{28}Si potential using R=0.0 fm. (broken curves), 0.7 fm. (solid curves) and 0.85 fm. (dotted curves) to the experimental data for the ground (1^+), 2.53 (3^+), 2.84 (3^+) and 3.02 MeV (2^+) states. The finite-range correction with R=0.7 fm improves the fits to the data.

The effect of the three types of the α-^{28}Si potential on the microscopic DWBA calculations has also been examined using the spectroscopic amplitudes $\beta^{1/2}$ calculated from the FPSDI interaction. Fig. 5.17 displays the DWBA predictions for the molecular (solid curves), normal optical (broken curves) and Michel (dotted curves) potentials, compare to the data for the ground (1^+), 0.71 (1^+), 1.45 (2^+) and 1.97 MeV (3^+) states of ^{30}P. As in the case of the macroscopic analyses, the molecular potential provides the best description of the data and the Michel gives the worst. Moreover, the predicted cross sections with the Michel potential are so small that they need normalization factors (Table 5.6), larger by orders of magnitude compared to those for the molecular and normal optical potentials.

Figs. 5.18 and 5.19 display the comparison of the microscopic DWBA calculations with finite-range parameter R=0.7 fm. and the molecular α-^{28}Si potential, for the FPSDI (solid curves), CW (broken curves) and MSDI (dotted curves) interactions. The calculations with the three interactions produce more or less the same quality fits to the data for the ground (1^+), 0.709 (1^+), 1.454 MeV (2^+) states (Fig.5.18). The FPSDI and CW amplitudes produce identical predictions for the 2.72 MeV (2^+) state (Fig. 5.18) and

2.84 MeV (3^+) state (Fig. 5.19) and the same quality fits to the 1.97 (3^+) and 2.538 (3^+) MeV states (Fig. 5.17). For the 3.02 MeV state, FPSDI gives a better description at large scattering angles than CW does (Fig. 5.18). Nonetheless, the spectroscopic amplitudes from the three interactions produce completely different spectroscopic factors S_L^a, as listed in Table 5.5. Moreover, the experimental cross sections for the reaction leading to the ground (1^+), 0.709 (1^+), 1.454 (2^+), 1.974 (3^+), 2.538 (3^+), 2.72 (2^+), 2.84 (3^+) and 3.02 MeV (1^+) states of ^{30}P, need normalization constants as listed in Table 5.7, which are widely different and inconsistent .

The 7.20 MeV (7^+) state is considered to have a pure stretched $(0f_{7/2})^2$ configuration leading to the spectroscopic amplitude for the (α,d) reaction as $\beta^{1/2}=1.0$ [35,37]. This model independent value of $\beta^{1/2}$ has been used to deduce the normalization constant for the reaction as $\aleph=722 \pm 25$, which compares closely with $\aleph=870\pm 20$ and 650 ± 20 obtained, following two methods for calculating the form-factors, by de Meijer *et al.* [37]. But only a few of the extracted $\aleph$-values for other states given in Table 5.7 are close to the model independent-value, deduced from the reaction data for the 7.20 MeV state. All the normalization constants extracted using molecular, normal optical and Michel potentials are exhibited in Tables (5.8–5.10) along with the corresponding spectroscopic amplitudes for three interactions. None of the FPSDI, CW and MSDI interactions produce a consistent set of values for the normalization constant.

5.2.2.3. Calculation of the spectroscopic factors

The model dependent spectroscopic factors are calculated from the FPSDI, CW and MSDI spectroscopic amplitudes $\beta^{1/2}$ by the method outlined in [37]. Since the

spectroscopic factor for the 7.20 MeV state is unity, the spectroscopic factor for other transitions can be given by

$$S_L^a = \left|G_{LJ}\right|^2 \Big/ \left|G_{67}(7.20)\right|^2 \qquad (5.18)$$

where the structure factor G_{LJ} is expressed through Eq. (5.11) and $G_{67}(7.20) = 0.56\Omega_{00}$ denotes the value of the structure factor for the 7.20 MeV state.

The total spectroscopic factor S^a for a transition is then given by

$$S^a = \sum_L S_L^a \qquad (5.19)$$

The S_L^a values, which are listed in Table 5.5, are calculated using the FPSDI and CW spectroscopic amplitudes taken from de Meijer *et al.* [37]. For the MSDI interaction, the S_L values are calculated using Eq. (5.18) from the MSDI spectroscopic amplitudes from Jankowski *et al.* [18]. The predicted spectroscopic factors S_L^a and S^a are compared in Tables 5.5 and 5.6. to the experimental spectroscopic factors A_L and $\sum A_L$ respectively, deduced from the macroscopic analyses.

Table 5.4.. Potential parameters used in the DWBA calculations for $^{28}Si(\alpha,d)^{30}P$ reaction. V is adjusted to give the separation energy.

Channel		$\alpha+^{30}Si$		$d+^{30}P$	d+d	$d+^{30}Si$
Type	Molecular[a]	Michel[a]	Optical[b]	Optical[c]	Bound state[b]	
V_0 (MeV)	27.0	25.0	50.42	102.7	V	V
R_0 (fm)	5.52	5.20	-	-	-	-
r_0 (fm)	-	-	1.699	1.07	1.05	0.935
a_0 (fm)	0.34	0.46	0.505	0.852	0.50	0.997
V_1 (MeV)	42.5	-	-	-		
R_1 (fm)	2.90	-	-	-		
α	-	7.12	-	-		
ρ (fm)	-	6.45	-	-		
W_0 (MeV)	17.0	34.0	10.34	-		
R_W (fm)	4.1	4.05	-	-		
r_I (fm)	-	-	1.699	-		
a_I (fm)	-	0.65	0.505	-		
W_D (MeV)	-	-	-	16.10		
r_D (fm)	-	-	-	1.53		
a_D (fm)	-	-	-	0.574		
V_{so}(MeV)	-	-	-	6.0		
r_{so} (fm)	-	-	-	1.07		
a_{so} (fm)	-	-	-	0.852		
r_C (fm)	-	1.30	1.30	1.15	1.25	1.3
R_C (fm)	9.35	-	-	-	-	-

[a] Ref. [19].
[b] Ref. [18].
[c] Ref. [148].

Table 5.5. Cluster spectroscopic factors of the $^{28}Si(\alpha,d)^{30}P$ reaction are compared to the theoretical shell-model factors for the FPSDI, CW and MSDI interactions. FPSDI and CW spectroscopic factors are taken from Ref.[37]. MSDI factors are calculated from the spectrocopic amplitudes $\beta^{1/2}$ of Ref.[18] by the method outlined in [37]. S_L^{σ} values are normalized to the value of $\left|G_{67}^{7.20}\right|^2$ for the 7.20 MeV state.

E_x	J^{π}	Cluster Config.	Cluster Spectroscopic Factor			Shell-model Spectroscopic Factor $S_L^{\sigma} = \left\|G_{LJ}\right\|^2 / \left\|G_{67}^{7.20}\right\|^2$		
(MeV)		N,L	A_L [a]	A_L [b]	A_L [c]	FPSDI	CW	MSDI
0.0	1^+	2,0	0.23±0.07	1.76±0.20	0.28	0.448	0.043	0.168
		1,2	0.23±0.07	[d]	0.56	0.237	0.121	0.031
0.709	1^+	2,0	0.16±0.07	1.45±0.20	-	0.029	0.030	0.020
		1,2	0.24±0.08	[d]	0.85	0.617	0.274	0.038
1.454	2^+	1,2	0.25±0.05	0.20±0.04	0.32	0.372 [a]	0.081	7.8×10^{-4}
1.974	3^+	1,2	0.11±0.04	0.72±0.13	-	0.041	0.078	0.004
		0,4	0.09±0.03	0.47±0.20	-	6.1×10^{-4}	0.134	1.5×10^{-3}
2.538	3^+	1,2	0.16±0.04	0.67±0.14	-	0.015	0.165	-
		0,4	0.07±0.03	< 0.25	-	0.426	0.076	-
2.72	2^+	1,2	0.28±0.05	0.12±0.02	0.34	0.058	0.045	-
2.84	3^+	1,2	0.08±0.02	0.16±0.07	-	0.007	0.007	-
		0,4	0.09±0.02	0.33±0.11	-	0.334	0.254	-
3.02	1^+	2,0	0.03±0.02	0.51±0.15	0.27	9.7×10^{-4}	0.319	-
		1,2	0.32±0.05	0.06±0.10	0.35	1.4×10^{-3}	0.021	-
3.93	2^-	2,1	0.11±0.04	-	0.32	-	-	-
		1,3	0.18±0.04	-	-	-	-	-
	(3^+)	(1,2)	(0.06±0.05)	(0.14±0.05)	-	-	-	-
		(0,4)	(0.08±0.05)	(0.05±0.06)	-	-	-	-
4.62	3^-	2,1	0.15±0.04	0.17±0.02	0.30	-	-	-
5.42	2^-	2,1	0.54±0.09	-	-	-	-	-
		1,3	0.06±0.03	-	0.86	-	-	-

[a] Present work.
[b] Ref. [37].
[c] Ref. [18].
[d] Too small a value to quote.

Table 5.6. Comparison of deduced total spectroscopic factors of the $^{28}Si(\alpha,d)^{30}P$ reaction from the macroscopic and the normalization factors for the microscopic FPSDI calculations using the molecular, normal optical and Michel potentials. Total spectroscopic factor is the sum of the spectroscopic factors for the two L-transfers for the unnatural parity states.

E_x (MeV)	J^π	L	Total spectroscopic factors $\sum A_L$			Normalization constant ℵ		
			Macroscopic calculations			Microscopic calculations		
			Molecular	Optical	Michel	Molecular	Optical	Michel
0.0	1^+	0+2	0.46	0.74	23.4	280	480	7000
0.709	1^+	0+2	0.40	1.33	30.0	70	85	8000
1.454	2^+	2	0.25	0.50	11.0	270	950	1800
1.974	3^+	2+4	0.20	0.57	20.0	1500	2000	35000

Table 5.7. Normalization constant ℵ for the microscopic zero-range calculations of $^{28}Si(\alpha,d)^{30}P$ for different shell-model interactions. $\aleph_{rel}$ is the relative normalization constant to the model independent ℵ=722 for the 7.20 MeV state.

E_x (MeV)	J^π	L	Normalization constant ℵ			Relative normalization constant $\aleph_{rel}$		
			Interaction			Interaction		
			FPSDI	CW	MSDI	FPSDI	CW	MSDI
0.0	1^+	0+2	280	4000	800	0.388	5.540	1.108
0.709	1^+	0+2	70	180	1500	0.096	0.249	2.08
1.454	2^+	2	270	850	5500	0.374	1.177	7.618
1.974	3^+	2+4	1500	500	7000	2.077	0.692	9.965
2.538	3^+	2+4	220	900	-	0.304	1.246	-
2.72	2^+	2	550	4500	-	0.762	6.233	-
2.84	3^+	2+4	350	450	-	0.484	0.623	-
3.02	1^+	0+2	14000	450	-	19.39	0.623	-

Table 5.8. Spectroscopic amplitudes and normalization constant for transitions in the $^{28}Si(\alpha,d)^{30}P$ reaction using molecular potential

E_x [a] (MeV)	J^π	Interaction	Spectroscopic amplitudes						Normalization constants **			
			$d_{5/2}d_{5/2}$	$d_{5/2}s_{5/2}$	$d_{5/2}d_{3/2}$	$s_{1/2}s_{1/2}$	$s_{1/2}d_{3/2}$	$d_{3/2}d_{3/2}$	N_{FPSDI}	N_{MSDI}	N_{CW}	N^{rel}
0	1^+	FPSDI [b]	-0.1291	-	-0.0576	-0.7264	-0.3659	+0.2000	280.0	-	-	0.350
		MSDI [c]	-0.09593	-	+0.03974	-0.40482	-0.13899	+0.08527	-	800	-	1.000
		CW [b]	-0.1071	-	-0.2557	-0.3346	-0.1859	+0.1727	-	-	4000.0	6.00
0.71	1^+	FPSDI	+0.0130	-	-0.0737	-0.3089	+0.7348	-0.1835	70.0	-	-	0.087
		MSDI	-0.03825	-	+0.04540	-0.14308	+0.16475	-0.07733	-	1500.0	-	1.88
		CW	-0.0054	-	-0.0070	-0.2429	+0.4729	-0.1418	-	-	180.0	0.225
1.45	2^+	FPSDI	-	+0.0556	+0.0044	-	+0.7385	-	270	-	-	0.340
		MSDI	-	-0.15183	-0.00501	-	+0.16456	-	-	5500	-	6.874
		CW	-	+0.0173	-0.1422	-	+0.4527	-	-	-	850	1.06

[Continued..]

Table 5.8. [continued..]

Spectroscopic amplitudes and normalization constant for transitions in the $^{28}Si(\alpha,d)^{30}P$ reaction using molecular potential

E_x [a] (MeV)	J^+	Interaction	Spectroscopic amplitude						Normalization constants**			
			$d_{5/2}d_{5/2}$	$d_{5/2}s_{5/2}$	$d_{5/2}d_{3/2}$	$s_{1/2}s_{1/2}$	$s_{1/2}d_{3/2}$	$d_{3/2}d_{3/2}$	N_{FPSDI}	N_{MSDI}	N_{CW}	N^{rel}
1.97	3^+	FPSDI	-0.0001	-0.2131	-0.0329	-	-	+0.0098	1500.0	-	-	1.875
		MSDI	+0.08666	-0.08176	+0.05548	-	-	-	-	7000.0	-	8.750
		CW	+0.0700	+0.2618	-0.0445	-	-	+0.3502	-	-	500	6.00
2.54	3^+	FPSDI	-0.0105	-0.0458	+0.0829	-	-	+0.6726	220.0	-	-	0.274
		CW	+0.1005	+0.3200	-0.0807	-	-	-0.2881	-	-	900.0	1.124
2.72	2^+	FPSDI	-	-0.0723	+0.1274	-	-0.3415	-	550.0	-	-	0.686
		CW	-	+0.0506	-0.3035	-	-01072	-	-	-	4500	5.624

[Continued...]

Table 5.8. [continued..]

Spectroscopic amplitudes and normalization constants for transitions in the $^{28}Si(\alpha,d)^{30}P$ reaction using molecular potential

E_x [a] (MeV)	J^π	Interaction	Spectroscopic amplitude						Normalization Constants **			
			$d_{5/2}d_{5/2}$	$d_{5/2}s_{5/2}$	$d_{5/2}d_{3/2}$	$s_{1/2}s_{1/2}$	$s_{1/2}d_{3/2}$	$d_{3/2}d_{3/2}$	N_{FPSDI}	N_{MSDI}	N_{CW}	N_{rel}
2.84	3^+	FPSDI	-0.0081	+0.0914	-0.1004	-	-	+0.5200	350.0	-	-	0.438
		CW	+0.0174	-0.0506	+0.2130	-	-	-0.3979	-	-	450.0	0.562
3.02	1^+	FPSDI	+0.0004	-	-0.0499	-0.0392	-0.0121	-0.1595	1.40×10^4	-	-	17.51
		CW	+0.2574	-	-0.3648	+0.2212	+0.0859	-0.2665	-	-	450.0	0.562

a) P. M. Endt and C. van der Leun, Nucl. Phys. **A310**(1978)1.[151]
b) R. J. de Meijer, L. W. Put, J. J. Akerman, J. C. Vermenlen, and C. R. Bingham, Nucl. Phys. **A386**(1982)200.[37]
c) K. Jankowski, A. Grzeszuk, M. Siemaszko, A. Surowiec, W. Zipper, A. Budzanowski, and E. Kozik, Nucl. Phys. **A426**(1984)1-19.[18]

**N_{FPSDI} = Normalization Constant using molecular potential and Spectroscopic amplitudes extracted from FPSDI interaction;
N_{MSDI}= Normalization Constant using molecular potential and Spectroscopic amplitudes extracted from MSDI interaction;
N_{CW}= Normalization Constant using molecular potential and Spectroscopic amplitudes extracted from CW interaction
$N_{rel.}$= Normalization Constants relative to the Normalization Constant= 800.0 obtained for the Ex=7.20 MeV; $J^\pi=7^+$ state assuming a $1.000(1f_{7/2})^2$ spectroscopic amplitude.

Table-5.9. Spectroscopic amplitudes and normalization constants for transitions in the $^{28}Si(\alpha,d)^{30}P$ reaction using optical potential

E_x [a] (MeV)	J^π	Interaction	Spectroscopic amplitudes						Normalization constants **			
			$d_{5/2}d_{5/2}$	$d_{5/2}s_{5/2}$	$d_{5/2}d_{3/2}$	$s_{1/2}s_{1/2}$	$s_{1/2}d_{3/2}$	$d_{3/2}d_{3/2}$	N_{FPSDI}	N_{MSDI}	N_{CW}	N^{rel}
0	1^+	FPSDI [b]	-0.1291	-	-0.0576	-0.7264	-0.3659	+0.2000	480.0	-	-	0.80
		MSDI [c]	-0.09593	-	+0.03974	-0.40482	-0.13899	+0.08527	-	1000-		1.25
		CW [b]	-0.1071	-	-0.2557	-0.3346	-0.1859	+0.1727	-	-	5000.0	6.25
0.71	1^+	FPSDI	+0.0130	-	-0.0737	-0.3089	+0.7348	-0.1835	85.0	-	-	0.100
		MSDI	-0.03825	-	+0.04540	-0.14308	+0.16475	-0.07733	-	1800.0	-	2.25
		CW	-0.0054	-	-0.0070	-0.2429	+0.4729	-0.1418	-	-	180.0	0.263
1.45	2^+	FPSDI	-	+0.0556	+0.0044	-	+0.7385	-	280	-	-	0.352
		MSDI	-	-0.15183	-0.00501	-	+0.16456	-	-	9000	-	11.25
		CW	-	+0.0173	-0.1422	-	+0.4527	-	-	-	950	1.188

[Continued...]

Table 5.9. [continued..]

Spectroscopic amplitudes and normalization constant for transitions in the $^{28}Si(\alpha,d)^{30}P$ reaction using optical potential

E_x [a] (MeV)	J^π	Interaction	Spectroscopic amplitude						Normalization constants**			
			$d_{5/2}d_{5/2}$	$d_{5/2}s_{5/2}$	$d_{5/2}d_{3/2}$	$s_{1/2}s_{1/2}$	$s_{1/2}d_{3/2}$	$d_{3/2}d_{3/2}$	N_{FPSDI}	N_{MSDI}	N_{CW}	N^{rel}
1.97	3^+	FPSDI	-0.0001	-0.2131	-0.0329	-	-	+0.0098	2000.0	-	-	2.5
		MSDI	+0.08666	-0.08176	+0.05548	-	-	-	-	8000.0	-	10.0
		CW	+0.0700	+0.2618	-0.0445	-	-	+0.3502	-	-	800	1.0
2.54	3^+	FPSDI	-0.0105	-0.0458	+0.0829	-	-	+0.6726	10.0	-	-	0.125
		CW	+0.1005	+0.3200	-0.0807	-	-	-0.2881	-	-	1100.0	1.375
2.72	2^+	FPSDI	-	-0.0723	+0.1274	-	-0.3415	-	600.0	-	-	0.75
		CW	-	+0.0506	-0.3035	-	-01072	-	-	-	5500	6.88

[Continued...]

Table 5.9. [continued..]

Spectroscopic amplitudes and normalization constant for transitions in the $^{28}Si(\alpha,d)^{30}P$ reaction using optical potential

E_x [a] (MeV)	J^π	Interaction	Spectroscopic amplitude						Normalization Constants **			
			$d_{5/2}d_{5/2}$	$d_{5/2}s_{5/2}$	$d_{5/2}d_{3/2}$	$s_{1/2}s_{1/2}$	$s_{1/2}d_{3/2}$	$d_{3/2}d_{3/2}$	N_{FPSDI}	N_{MSDI}	N_{CW}	N_{rel}
2.84	3^+	FPSDI	-0.0081	+0.0914	-0.1004	-	-	+0.5200	9200	-	-	11.5
		CW	+0.0174	-0.0506	+0.2130	-	-	-0.3979	-	-	12000	15.0
3.02	1^+	FPSDI	+0.0004	-	-0.0499	-0.0392	-0.0121	-0.1595	-	-	-	
		CW	+0.2574	-	-0.3648	+0.2212	+0.0859	-0.2665	-	-	-	

a) P. M. Endt and C. van der Leun, Nucl. Phys. **A310**(1978)1 [151].
b) R. J. de Meijer, L. W. Put, J. J. Akerman, J. C. Vermenlen, and C. R. Bingham, Nucl. Phys. **A386**(1982)200 [37].
c) K. Jankowski, A. Grzeszuk, M. Siemaszko, A. Surowiec, W. Zipper, A. Budzanowski, and E. Kozik, Nucl. Phys. **A426**(1984)1-19 [18].

**N_{FPSDI} = Normalization Constant using optical potential and Spectroscopic amplitudes extracted from FPSDI interaction;
N_{MSDI}= Normalization Constant using optical potential and Spectroscopic amplitudes extracted from MSDI interaction;
N_{CW}= Normalization Constant using optical potential and Spectroscopic amplitudes extracted from CW interaction
$N_{rel.}$= Normalization Constants relative to the Normalization Constant= 800.0 obtained for the Ex=7.20 MeV; $J^\pi=7^+$ state assuming a $1.000(1f_{7/2})^2$ spectroscopic amplitude.

Table 5.10. Spectroscopic amplitudes and normalization constant for transitions in the $^{28}Si(\alpha,d)^{30}P$ reaction using Michel potential

E_x [a] (MeV)	J^π	Interaction	Spectroscopic amplitudes						Normalization constants [**]			
			$d_{5/2}d_{5/2}$	$d_{5/2}s_{5/2}$	$d_{5/2}d_{3/2}$	$s_{1/2}s_{1/2}$	$s_{1/2}d_{3/2}$	$d_{3/2}d_{3/2}$	N_{FPSDI}	N_{MSDI}	N_{CW}	N^{rel}
0	1^+	FPSDI [b]	-0.1291	-	-0.0576	-0.7264	-0.3659	+0.2000	7000	-	-	8.75
		MSDI [c]	-0.09593	-	+0.03974	-0.40482	-0.13899	+0.08527	-	-	-	-
		CW [b]	-0.1071	-	-0.2557	-0.3346	-0.1859	+0.1727	-	-	70000.0	87.5
0.71	1^+	FPSDI	+0.0130	-	-0.0737	-0.3089	+0.7348	-0.1835	8000.0	-	-	10.0
		MSDI	-0.03825	-	+0.04540	-0.14308	+0.16475	-0.07733	-	-	-	-
		CW	-0.0054	-	-0.0070	-0.2429	+0.4729	-0.1418	-	-	6000	7.5
1.45	2^+	FPSDI	-	+0.0556	+0.0044	-	+0.7385	-	1800	-	-	2.25
		MSDI	-	-0.15183	-0.00501	-	+0.16456	-	-	-	-	-
		CW	-	+0.0173	-0.1422	-	+0.4527	-	-	-	18000	22.5

[Continued...]

Table 5.10. [continued..]

Spectroscopic amplitudes and normalization constant for transitions in the $^{28}Si(\alpha,d)^{30}P$ reaction using Michel potential

E_x [a] (MeV)	J^π	Interaction	Spectroscopic amplitude						Normalization constants**			
			$d_{5/2}d_{5/2}$	$d_{5/2}s_{5/2}$	$d_{5/2}d_{3/2}$	$s_{1/2}s_{1/2}$	$s_{1/2}d_{3/2}$	$d_{3/2}d_{3/2}$	N_{FPSDI}	N_{MSDI}	N_{CW}	N^{rel}
1.97	3^+	FPSDI	-0.0001	-0.2131	-0.0329	-	-	+0.0098	35000	-	-	43.75
		MSDI	+0.08666	-0.08176	+0.05548	-	-	-	-	-	-	-
		CW	+0.0700	+0.2618	-0.0445	-	-	+0.3502	-	-	1500018.75	
2.54	3^+	FPSDI	-0.0105	-0.0458	+0.0829	-	-	+0.6726	7000	-	-	8.75
		CW	+0.1005	+0.3200	-0.0807	-	-	-0.2881	-	-	17000	21.25
2.72	2^+	FPSDI	-	-0.0723	+0.1274	-	-0.3415	-	300.0	-	-	0.375
		CW	-	+0.0506	-0.3035	-	-01072	-	-	-	90000	11.25

[Continued...]

Table 5.10. [continued..]

Spectroscopic amplitudes and normalization constant for transitions in the $^{28}Si(\alpha,d)^{30}P$ reaction using Michel potential

E_x [a] (MeV)	J^π	Interaction	Spectroscopic amplitude						Normalization Constants **			
			$d_{5/2}d_{5/2}$	$d_{5/2}s_{5/2}$	$d_{5/2}d_{3/2}$	$s_{1/2}s_{1/2}$	$s_{1/2}d_{3/2}$	$d_{3/2}d_{3/2}$	N_{FPSDI}	N_{MSDI}	N_{CW}	N_{rel}
2.84	3^+	FPSDI	-0.0081	+0.0914	-0.1004	-	-	+0.5200	2.9×10^4	-	-	36.25
		CW	+0.0174	-0.0506	+0.2130	-	-	-0.3979	-	-	1.9×10^5	237.5
3.02	1^+	FPSDI	+0.0004	-	-0.0499	-0.0392	-0.0121	-0.1595	-	-	-	-
		CW	+0.2574	-	-0.3648	+0.2212	+0.0859	-0.2665	-	-	-	-

a) P. M. Endt and C. van der Leun, Nucl. Phys. **A310**(1978)1 [151].
b) R. J. de Meijer, L. W. Put, J. J. Akerman, J. C. Vermenlen, and C. R. Bingham, Nucl. Phys. **A386**(1982)200 [37].
c) K. Jankowski, A. Grzeszuk, M. Siemaszko, A. Surowiec, W. Zipper, A. Budzanowski, and E. Kozik, Nucl. Phys. **A426**(1984)1-19[18].

**N_{FPSDI} = Normalization Constant using Michel potential and Spectroscopic amplitudes extracted from FPSDI interaction;
N_{MSDI}= Normalization Constant using Michel potential and Spectroscopic amplitudes extracted from MSDI interaction;
N_{CW}= Normalization Constant using Michel potential and Spectroscopic amplitudes extracted from CW interaction
N_{rel}= Normalization Constants relative to the Normalization Constant= 800.0 obtained for the Ex=7.20 MeV; $J^\pi=7^+$ state assuming a $1.000(1f_{7/2})^2$ spectroscopic amplitude.

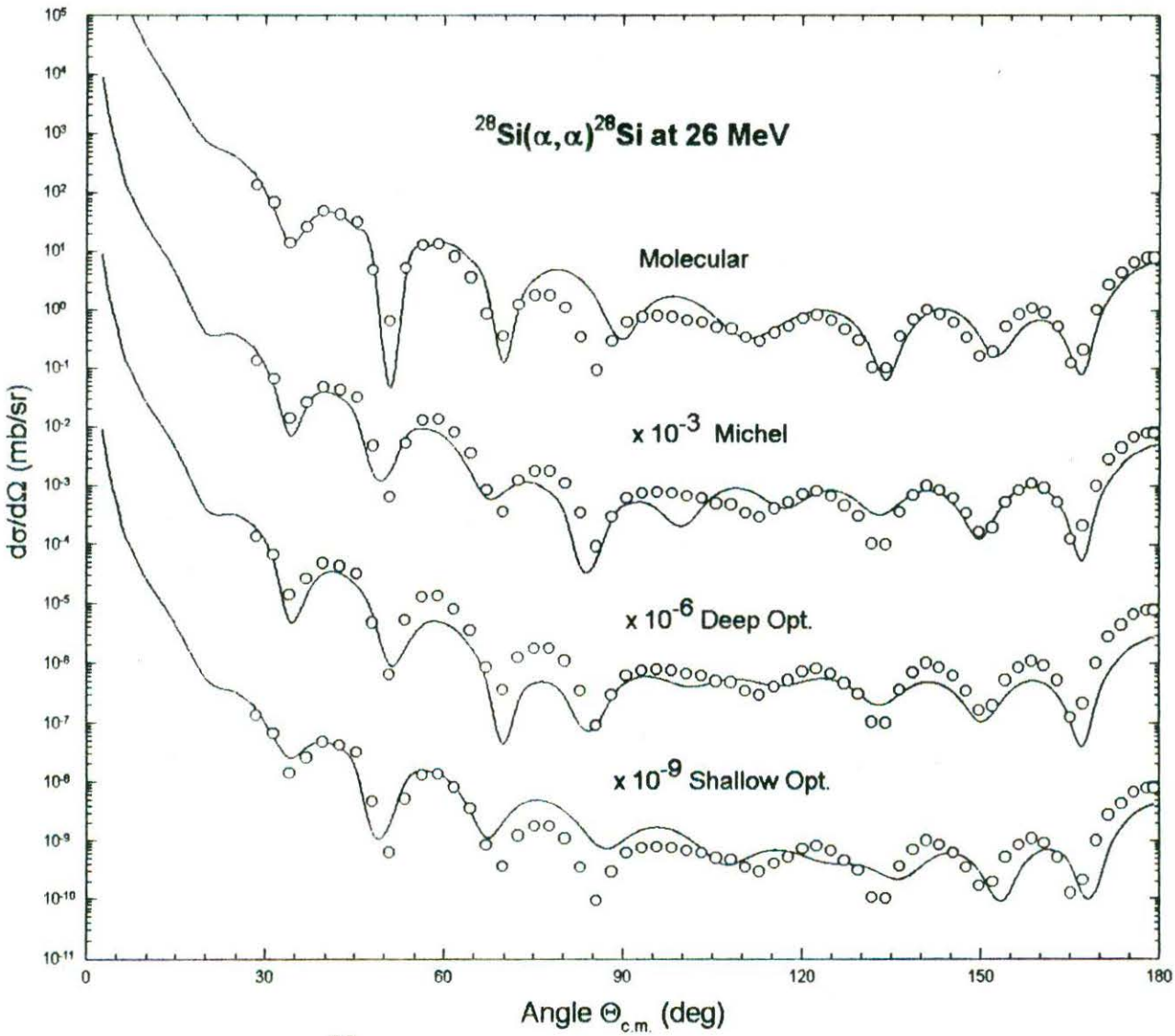

Fig.5.11. Fits to the α-^{28}Si elastic scattering data at 26 MeV (lab.) with the molecular, Michel, deep and shallow normal optical potentials. Data are from [9]

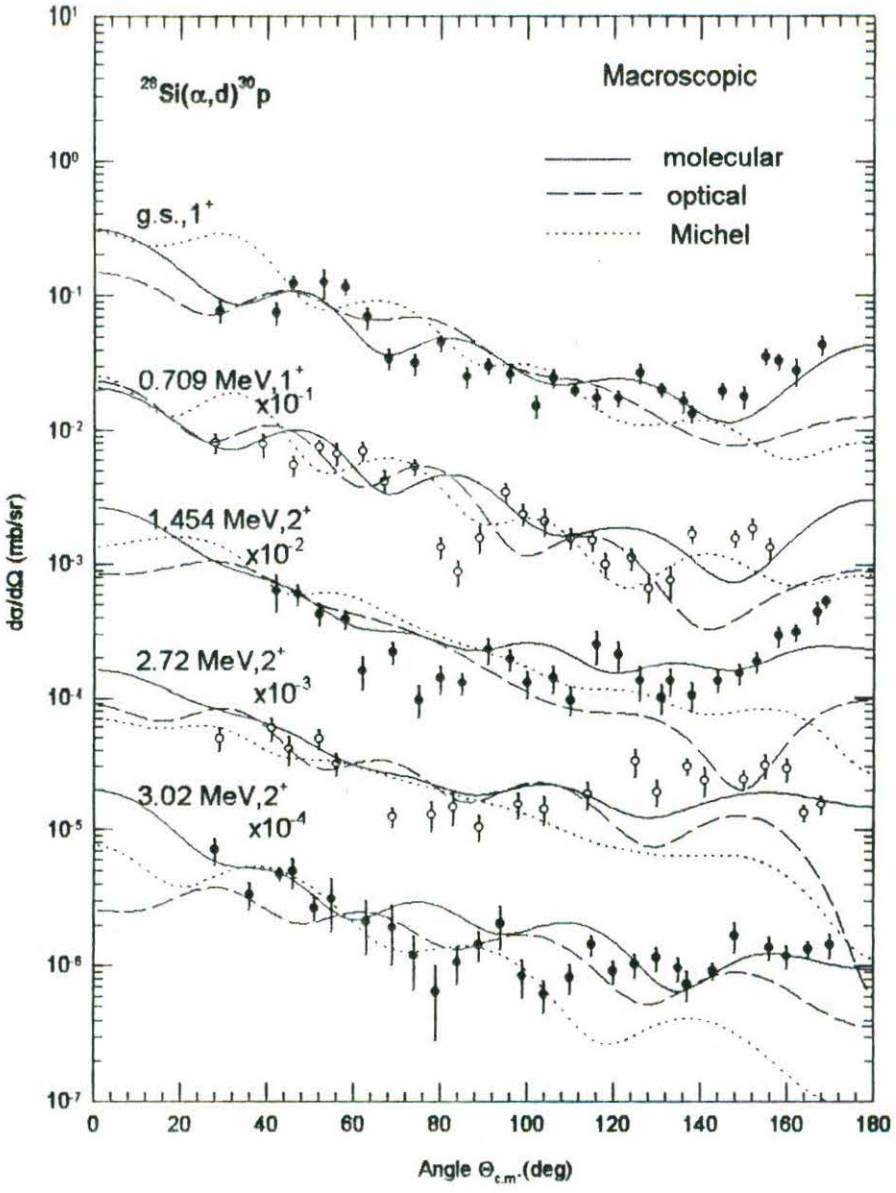

Fig.5.12. Comparison of the full finite-range macroscopic DWBA calculations for the ^{28}Si(α,d)^{30}P reactionat 26 MeV leading to the 1^+ and 2^+ states of ^{30}P to the differential cross-section data.The solid, brokenand dotted curves are the predictions using the molecular, normal optical, and Michel α-^{28}Si potentials, respectively. Data are from [18].

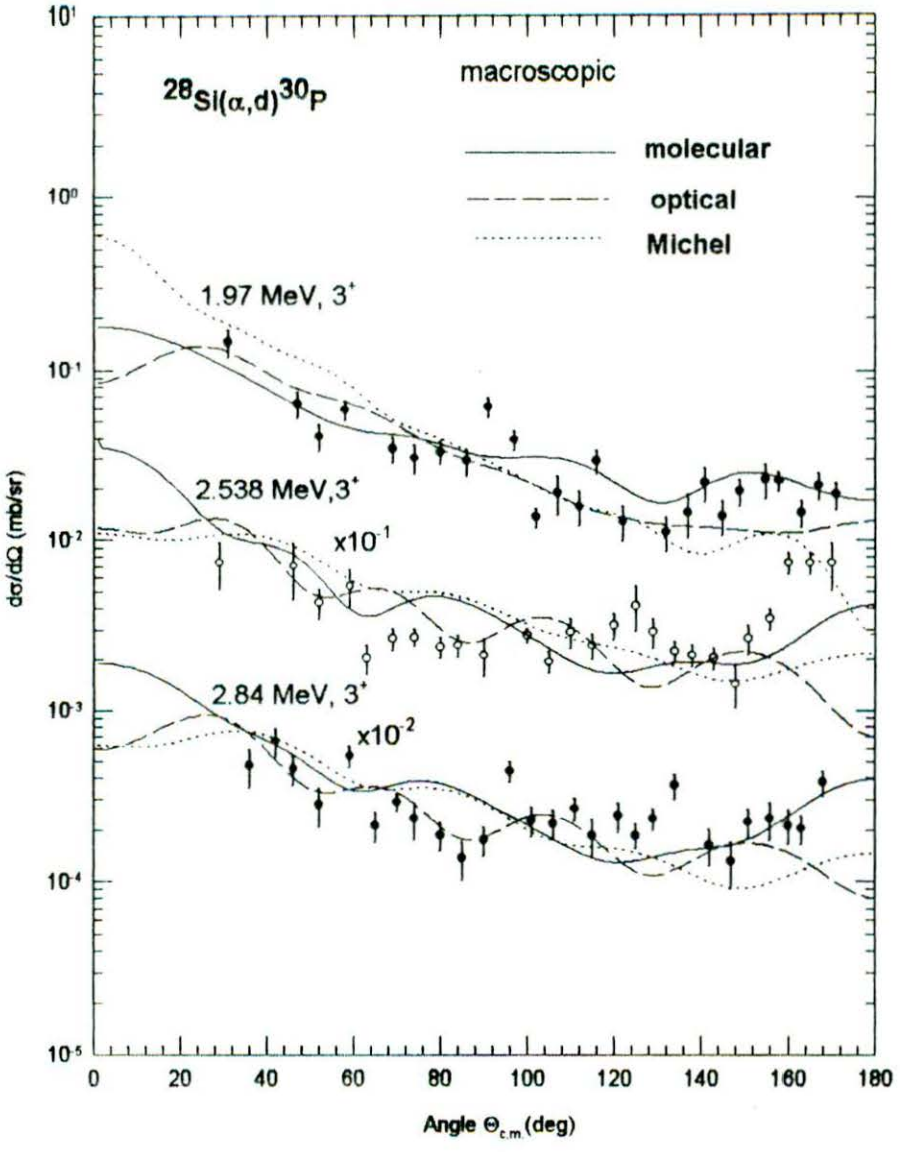

Fig. 5.13. Same as in Fig.5.12 for the transition to the 3^+ states of ^{30}P. Data are from [18].

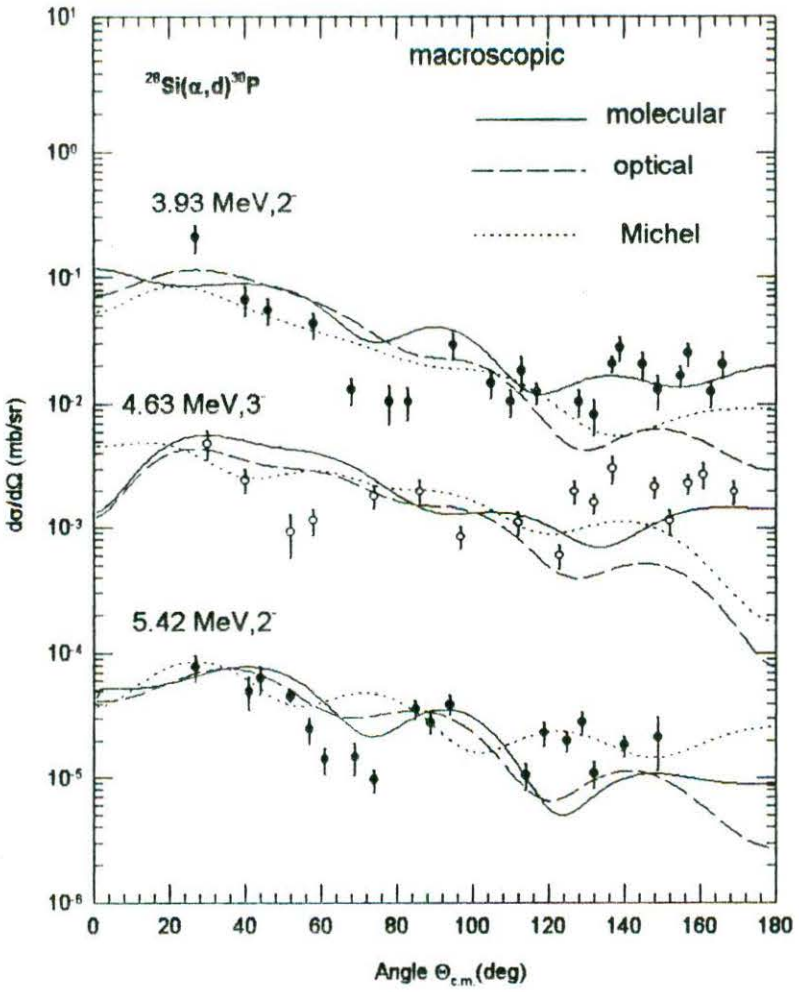

Fig. 5.14. Same as in Fig.5.12 for the transition to the 2^- and 3^- states of ^{30}P. Data are from [18].

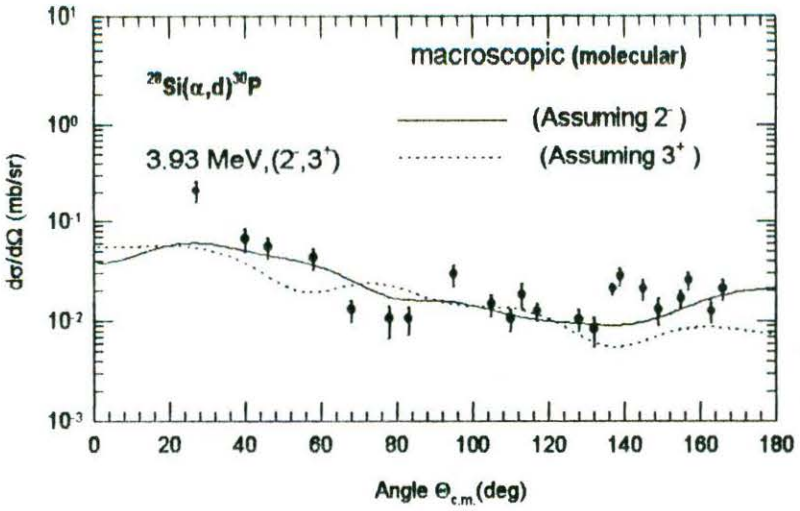

Fig.5.15. Full finite-range macroscopic DWBA calculations using the molecular α-^{28}Si potential for the 3.93 MeV state assuming the spin-parity $J^{\pi}=2^-$ (solid curve) and 3^+ (dotted curves) are compared to the data. Data are from [18]

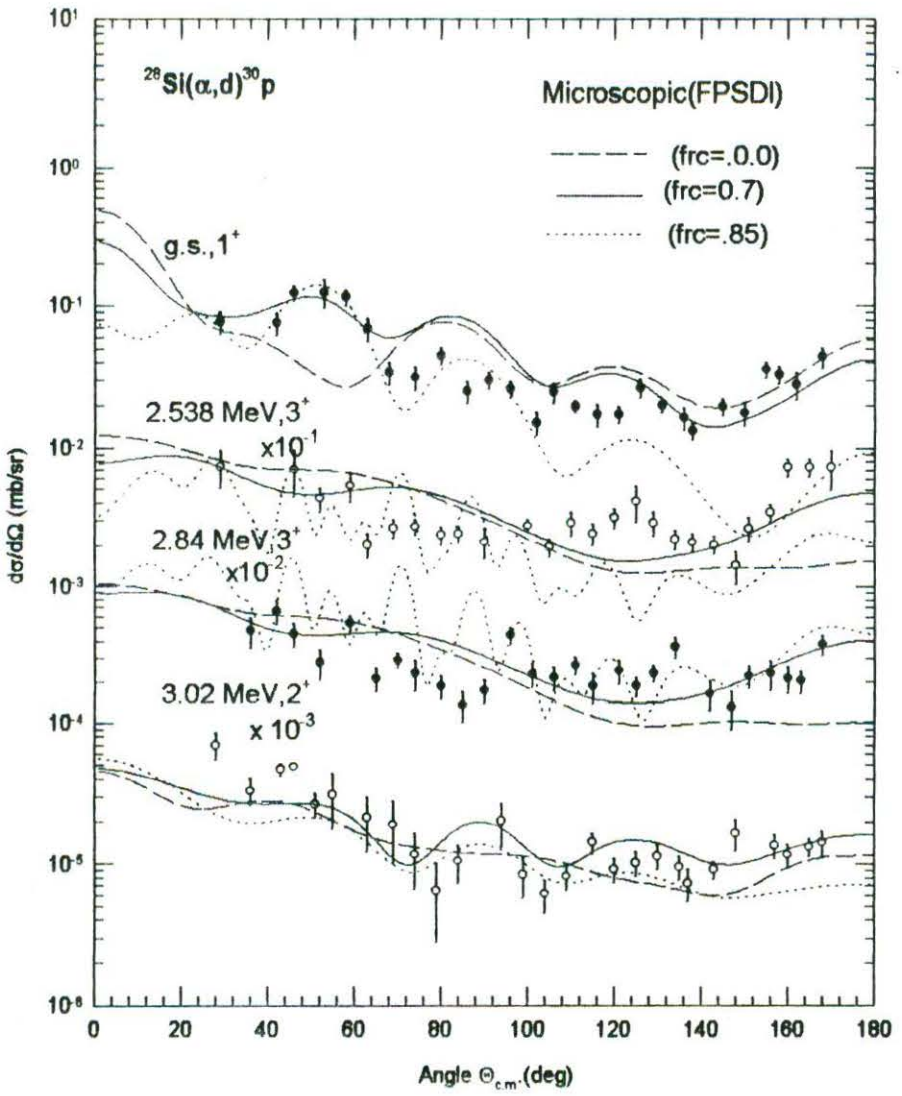

Fig. 5.16. Comparison of the zero-range microscopic DWBA calculations using the FPSDI spectroscopic amplitudes and the molecular potential in the α-channel for the ^{28}Si(α,d)^{30}P reaction at 26 MeV leading to the ground (1^+), 2.538(3^+), 2.84(3^+) and 3.02 (2^+) MeV states of ^{30}P to the differential cross-section data. The solid curves are the predictions using the finite-range (FR) correction with FR parameter R=0.7 fm. The broken and dotted curves are the predictions with R=0.0 and 0.85 fm., respectively. Data are from [18].

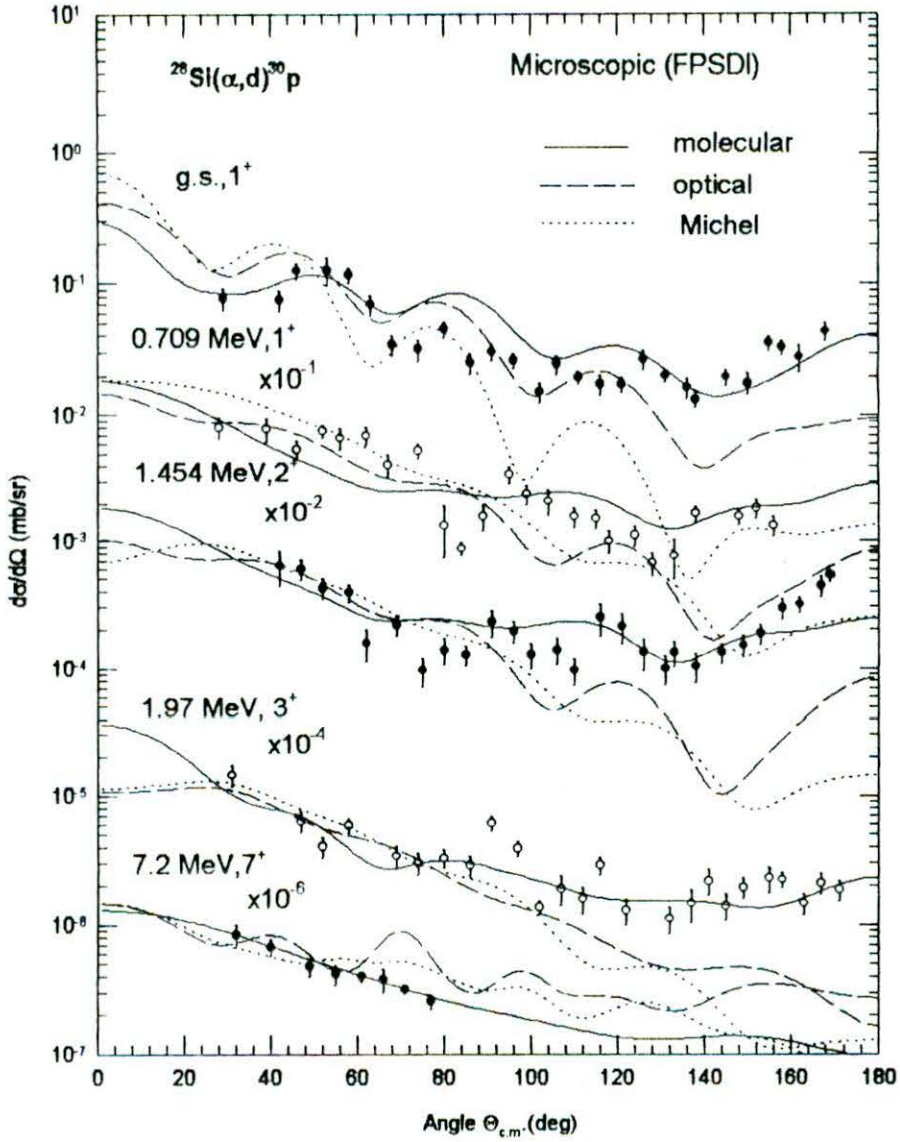

Fig. 5.17. Comparison of zero-range microscopic DWBA calculations with FR correction for the ^{28}Si(α,d)^{30}P reaction at 26 MeV leading to the ground (1^+), 0.709(1^+), 1.454(2^+), 1.93(3^+), and 7.20 (7^+) MeV states of ^{30}P to the differential cross-section data. The solid, broken and dotted curves are the predictions using the molecular, optical and Michel α-^{28}Si potentials, respectively. Data are from [18]

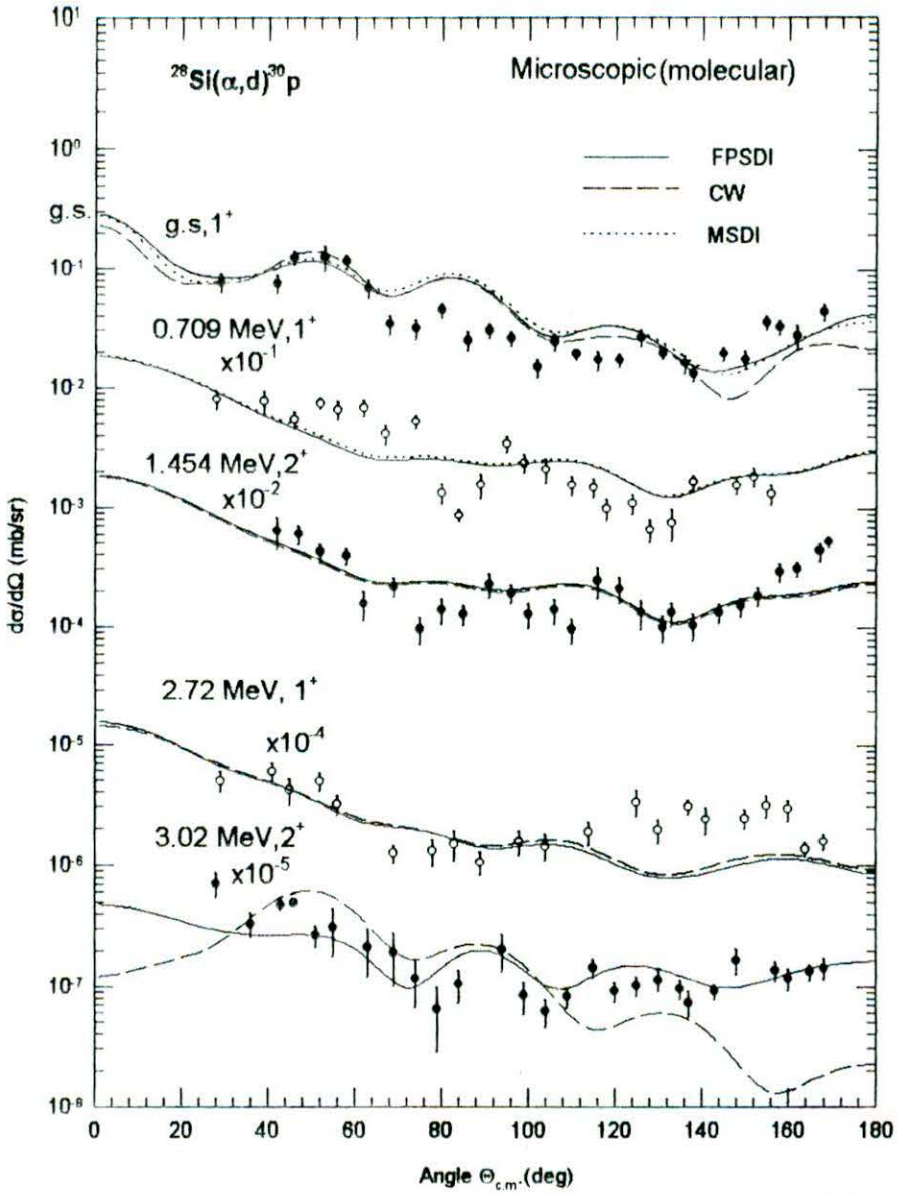

Fig. 5.18. Comparison of zero-range microscopic DWBA calculations with FR correction and the molecular potential for the ^{28}Si(α,d)^{30}P reaction at 26 MeV, leading to the 1^+ and 2^+ states of ^{30}P to the differential cross-section data. The solid, broken and dotted curves are the predictions using the FPSDI, CW, and MSDI spectroscopic amplitudes. Data are from [18].

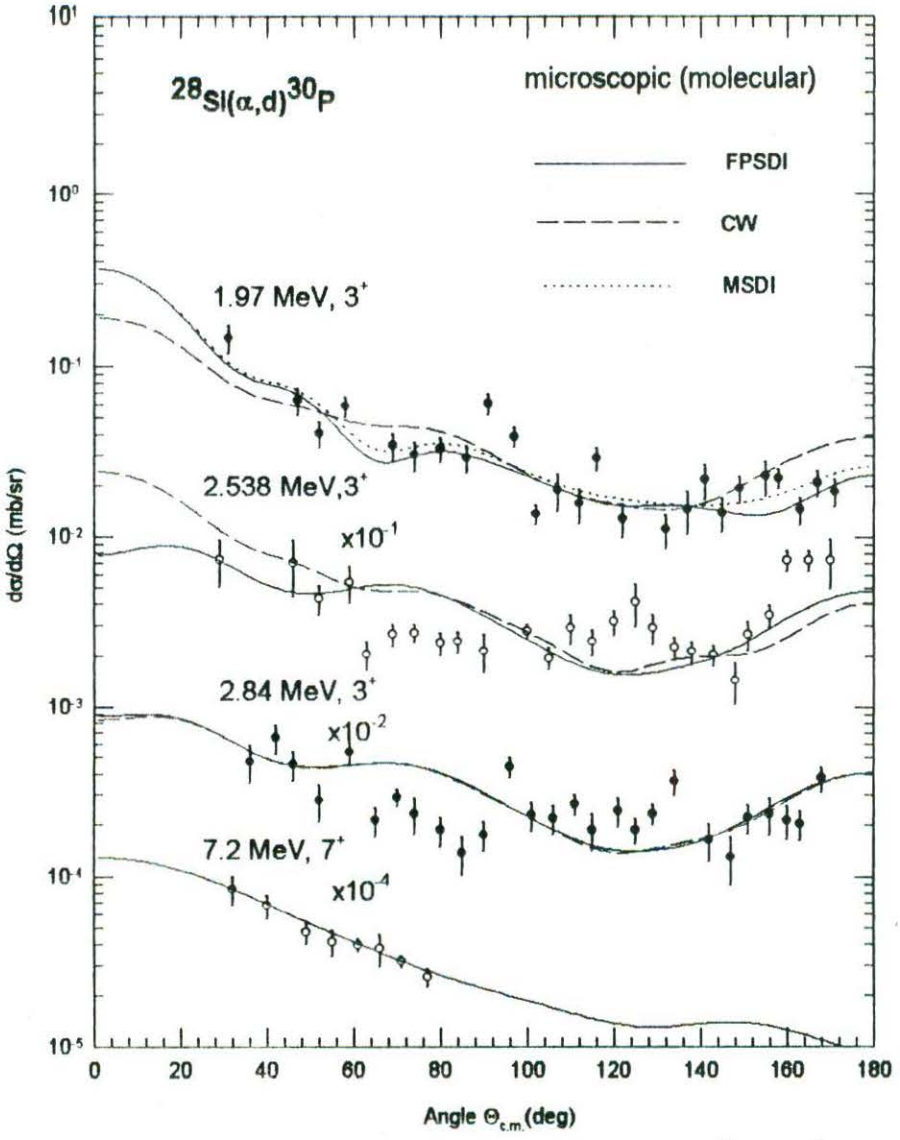

Fig.5.19. Same as in Fig. 5.18. for transitions to the 3^+ and 7^+ states of ^{30}P. Data are from [18].

5.2.3. *DWBA analysis of the $^{29}Si(\alpha,d)^{31}P$ reaction.*

Both the macroscopic full finite-range DWBA and microscopic zero-range DWBA calculations have been performed in the case of the $^{29}Si(\alpha,d)^{31}P$ using the computer code DWUCK5 and DWUCK4 [39] respectively. Corrections due to the non-locality [32,39] of potentials have been applied using the non-locality parameters $\beta(\alpha)$=0.2, $\beta(d)$=0.54 and $\beta(p)$=0.85 fm. In both the macroscopic FFR and the microscopic ZR calculations, the molecular, Michel and normal optical types of α-^{29}Si potential used, have been generated in the present work by fitting the elastic data [45], as shown in Fig 5.20. The d-^{31}P optical potential parameters are taken from the work of Fitz *et al.* [148]. All the potential parameters used are displayed in Table 5.11.

5.2.3.1. Macroscopic DWBA Calculations

The macroscopic analyses have been performed using full finite-range DWBA. The parameters of bound-state geometry for the d-d and d-^{29}Si Woods-Saxon (WS) potential, shown in the Table 5.11 are taken from [18]. The bound-state wave functions for the transferred deuterons in alpha as well as in the final nucleus have been generated by adjusting the deuteron separation energies. The accuracy parameters used in the computer code DWUCK5 have been assigned in the same way as performed in the study of the $^{28}Si(\alpha,d)^{30}P$ reaction.

The cluster configurations of the transferred deuteron for the different states of excitation are shown in Table 5.12. It is to be noted that for the (α,d) reaction on ^{29}Si, there are two possible values of the total transferred angular momentum J for odd J and even parity or an even J and odd parity. For the final states populated by more than one

L-transfers for a single J transfer, the cross-sections are added incoherently and the spectroscopic factors A_L are deduced from Eq. (5.15) coupled with the minimization of χ^2 defined in Eq. (5.17). On the other hand, for the transitions, involving more than one J transfer , use of Eq. (5.15) along with the minimization of χ^2 leads to the extraction of the total spectroscopic factor for the same L, but different J transfers. The deduced spectroscopic factors are listed in Table 5.12.

The DWBA predictions with the molecular (solid curves), standard optical (broken curves) and Michel (dotted carves) potentials are compared to the data of the ground ($1/2^+$), 1.27 ($3/2^+$), and 2.23 ($5/2^+$) MeV states in Fig. 5.21; to the data of 3.13 ($1/2^+$), 3.30 ($5/2^+$) and 3.41 ($7/2^+$) MeV states in Fig. 5.22 and to the data of 3.51 ($3/2^+$), 4.19 ($5/2^+$), and 4.26 ($3/2^+$) MeV states of ^{31}P in Fig.5.23.

5.2.3.2. Microscopic DWBA calculations

The microscopic calculations have been performed using the zero-range code DWUCK4. The present analyses make use of three sets of spectroscopic amplitudes $\beta^{1/2}$, based on MSDI, RIP, and KB hamiltonians [48]. These three sets of amplitudes are obtained from Ref. [45] and are furnished in Tables (5.14–5.16) along with the respective normalization constants deduced from fitting the experimental data from Ref [48]. The phase conventions used are similar to that used in the analyses of the ^{28}Si(α,d)^{30}P reaction.

The bound state wave functions for each of the transferred nucleons have been generated by assuming a real Woods-Saxon well with the geometry parameters r_0=1.25 fm. and a_0=0.65 fm and the depth adjusted to produce the binding energy equal to half

the separation energy of the transferred deuteron. A Thomas-Fermi spin-orbit term with λ=25 has also been used for the bound state wave function.

A Gaussian form of the finite-range correction in the LEA [39] has been investigated. Fig. 5.24 compares the microscopic DWBA calculations for the molecular type of α-^{29}Si potential using R=0.0 fm. (broken lines), 0.7 fm. (solid lines) and 0.8 fm. (dotted lines) to the experimental data for ground ($1/2^+$), 1.27($3/2^+$), and 2.23 ($5/2^+$) MeV states of ^{31}P. The finite range parameter R= 0.7 fm. seems to give the best fit to the data.

The effect of three types of the α-^{29}Si potential on the microscopic DWBA calculations has been examined using the spectroscopic amplitudes $\beta^{1/2}$ calculated from MSDI, RIP and KB interactions. Figs. 5.25–5.27 display the DWBA predictions for the molecular potential using spectroscopic amplitudes $\beta^{1/2}$ from MSDI (solid curves), RIP (broken curves) and KB (dotted curves) interactions compared to the data for the ground state ($1/2^+$) , 1.27 ($3/2^+$), 2.23 ($5/2^+$), 3.13($1/2^+$), 3.30 ($5/2^+$), 3.41 ($7/2^+$), 3.51($3/2^+$), 4.19($5/2^+$) and 4.26 ($3/2^+$) MeV states. Similarly, Figs. 5.28–5.30 show the same for normal optical and Figs. 5.31–5.33 for Michel potentials. Figs. 5.34 –5.36 display in a comparative manner, the DWBA predictions compared to the data using molecular, normal optical and Michel potentials and spectroscopic amplitudes $\beta^{1/2}$ of MSDI.

5.2.3.3. Calculations of theoretical spectroscopic factors

Skwirczynska *et al.* [150], calculated the spectroscopic factor from the expression

$$S_L^C = \sum \left| \sum \beta^{1/2}[\rho_1 \rho_2; J\,0] \begin{bmatrix} l_1 & l_2 & L \\ \frac{1}{2} & \frac{1}{2} & 1 \\ j_1 & j_2 & J \end{bmatrix} \right|^2 \qquad (5.20)$$

Comparison of Eq. (5.20), which occurs in Eq. (5.9), with the expression (Eq. 5.11) for structure factor G_{LJ}, which is associated with the expression for the macroscopic cross-section in Eq. (5.12), suggests that the kinematic part B_M^L in Eq. (5.9) is still not free of microscopic quantum numbers. Hence, Eq. (5.20) does not represent in total the macroscopic spectroscopic factor, although it may give the right order. On the other hand, the spectroscopic factor defined [37] in Eq. 5.18 in terms of the structure factor G_{LJ} (Eq. 5.11) is complete in itself. Therefore, the value of $|G_{LJ}|^2$ relative to that for any state with spectroscopic amplitude $\beta^{1/2} = 1$ and with a stretched configuration, can yield a real measure of spectroscopic strength of a state populated through the transfer (L,J). Thus, if it is assumed that there exists a state in the final nucleus populated *via* $J^\pi = 7^+$ through the transfer configuration $(f_{7/2})^2$ and the target configuration does not involve the orbital $f_{7/2}$, then one can deduce the spectroscopic factors relative to the $|G_{67}|^2$ as done in the analysis of the $^{28}Si(\alpha,d)^{30}P$ reaction with the observed state at E_x = 7.20 MeV using Eq. 5.18. Thus, the spectroscopic factors are estimated using the expression

$$S_L^\sigma = \sum_J |G_{LJ}|^2 \Big/ |0.56\Omega_{00}|^2 \qquad (5.21)$$

where $G_{67} = 0.56\Omega_{00}$ represents the structure factor for an unobserved state populated with the $J^\pi = 7^+$ transfer $\beta^{1/2} = 1.0$. The sum over J encompasses the cases where the target spin is non-zero.

The total spectroscopic factors S^{σ} for a transition is then obtained by the Eq. (5.19)

The spectroscopic factors S_L^{σ} and S^{σ}, using three sets of spectroscopic amplitudes $\beta^{\frac{1}{2}}$ from the MSDI, RIP and KB interactions [45] have been calculated and noted in Tables 5.12 and 5.13. These theoretically predicted spectroscopic factors are also compared to experimentally deduced values using three (molecular, normal optical and Michel) types of potentials in Tables 5.12 and 5.13.

Table 5.11. Potential parameters used in the DWBA calculations for $^{29}Si(\alpha,d)^{31}P$. V is adjusted to give the separation energy.

Channel		$\alpha+^{29}Si$		$d+^{31}P$	d+d	$d+^{29}Si$
Type	Molecular[a]	Michel[a]	Optical[a]	Optical[b]	Bound state[c]	
V_0 (MeV)	26.3	31.41	182.45	102.7	V	V
R_0 (fm)	5.45	4.83	-	-	-	-
r_0 (fm)	-	-	1.15	1.07	1.05	0.935
a_0 (fm)	0.34	0.55	0.76	0.852	0.50	0.997
V_1 (MeV)	42.5	-	-	-		
R_1 (fm)	2.90	-	-	-		
α	-	7.39	-	-		
ρ (fm)	-	6.45	-	-		
W_0 (MeV)	17.92	34.91	13.5	-		
R_W (fm)	4.1	4.06	-	-		
r_I (fm)	-	-	1.51	-		
a_I (fm)	-	0.64	0.70	-		
W_D (MeV)	-	-	-	16.10		
r_D (fm)	-	-	-	1.53		
a_D (fm)	-	-	-	0.574		
V_{so} (MeV)	-	-	-	6.0		
r_{so} (fm)	-	-	-	1.07		
a_{so} (fm)	-	-	-	0.852		
r_C (fm)	-	1.30	1.30	1.15	1.25	1.3
R_C (fm)	9.45	-	-	-	-	-

[a] Present work.
[b] Ref. [48].
[c] Ref. [18].

Table 5.12. Cluster spectroscopic factors for the $^{29}Si(\alpha,d)^{31}P$ extracted by molecular, normal optical and Michel potentials are compared to the theoretical shell-model factors for the MSDI, RIP and KB interactions. Factors are calculated from the spectroscopic amplitudes $\beta^{1/2}$ of Ref.[45] by the method outlined in [37].

E_x	J^π	J_f	Cluster Config.	Cluster Spectroscopic Factor			Shell-model Spectroscopic Factor S_L^σ		
(MeV)			N,L	A_L (molecular)	A_L (optical)	A_L (Michel)	MSDI	RIP	KB
0.0	$1/2^+$	1	2,0	0.18±0.06	12.6±2.62	7.2±1.44	0.611	0.027	0.024
			1,2	0.12±0.04	8.4±1.68	4.8±0.96	0.006	0.053	0.011
1.27	$3/2^+$	1	2,0	0.0525±0.01	3.0±0.6	1.8±0.36	0.007	0.009	0.006
			1,2	0.298±0.09	4.5±0.9	2.7±0.54	0.597	0.176	0.060
		2	1,2						
2.23	$5/2^+$	2	1,2	0.1425±0.04	5.03±1.05	1.58±0.32	0.112	0.220	0.013
		3	1,2						
			0,4	0.0075±0.002	0.265±0.07	0.084±.02	0.000	0.004	0.003
3.13	$1/2^+$	1	2,0	0.052±0.02	0.90±0.27	0.76±0.15	0.021	0.009	0.171
			1,2	0.078±0.02	1.50±0.30	1.14±0.23	0.229	0.036	0.026
3.30	$5/2^+$	2	1,2	0.0855±0.03	4.08±0.81	3.8±0.80	0.084	0.006	0.002
		3	1,2						
			0,4	0.0045±0.001	0.215±0.05	0.2±0.05	0.000	0.011	0.067
3.41	$7/2^+$	3	1,2	0.260±0.08	13.0±3.9	5.2±1.3	0.005	0.031	0.002
			0,4	0.0325±0.01	3.25±0.65	1.3±0.33	0.143	0.020	0.101
		4	0,4						
3.51	$3/2^+$	1	2,0	0.0585±0.02	1.8±0.36	1.5±0.38	0.001	0.060	0.002
			1,2						
		2	1,2	0.1365±0.04	4.2±0.84	3.5±0.88	0.169	0.012	0.200
4.19	$5/2^+$	2	1,2	0.088±0.03	4.0±0.80	4.4±1.1	0.058	0.077	0.010
		3	1,2						
			0,4	0.022±0.006	1.0±0.25	1.1±0.26	0.014	0.029	0.061
4.26	$3/2^+$	1	2,0	0.070±0.02	2.8±0.70	2.2±0.55	0.002	0.004	0.002
			1,2	0.135±0.04	4.2±1.05	3.3±0.83	0.005	0.052	0.011
		2	1,2						

Table 5.13. Total spectroscopic factors of $^{29}Si(\alpha,d)^{31}P$ reaction deduced from the macroscopic calculation using the molecular, normal optical and Michel potentials are compared to the corresponding total spectroscopic factors calculated with the spectroscopic amplitudes $\beta^{1/2}$ of three interactions (MSDI, RIP and KB) taken from Ref.[45] by the method outlined in Ref. [37].

E_x (MeV)	J^π	L	Total spectroscopic factors $\sum A_L$			Total spectroscopic factors S^σ		
			Macroscopic calculations			Microscopic calculations		
			Molecular	Optical	Michel	MSDI	RIP	KB
0.0	$1/2^+$	0+2	0.40	21.0	12.0	0.617	0.080	0.35
1.27	$3/2^+$	0+2	0.35	7.5	4.5	0.604	0.185	0.066
2.23	$5/2^+$	2+4	0.15	5.04	16.64	0.112	0.224	0.016
3.13	$1/2^+$	0+2	0.13	2.4	1.90	0.250	0.045	0.197
3.30	$5/2^+$	2+4	0.09	4.30	4.00	0.084	0.017	0.069
3.41	$7/2^+$	2+4	0.29	16.25	6.50	0.148	0.051	0.103
3.51	$3/2^+$	0+2	0.20	6.00	5.00	0.170	0.072	0.202
4.19	$5/2^+$	2+4	0.11	5.00	5.50	0.072	0.106	0.071
4.26	3/2	0+2	0.21	7.00	5.50	0.007	0.056	0.013

Table 5.14. Spectroscopic amplitudes and normalization constant for transitions in the $^{29}Si(\alpha,d)^{31}P$ reaction using molecular potential

E_x [a] (MeV)	J^π	J_{tra}	Interaction	Spectroscopic amplitudes [a] $d_{5/2}d_{5/2}$	$d_{5/2}s_{1/2}$	$d_{5/2}d_{3/2}$	$s_{1/2}s_{1/2}$	$s_{1/2}d_{3/2}$	Normalization constants [**] $d_{3/2}d_{3/2}$	N_{MSDI}	N_{RIP}	N_{KB}
0	$1/2^+$	1	MSDI	+0.220	-	-0.128	+0.725	+0.013	-0.144	55	-	-
			RIP	-0.385	-	-0.242	-0.168	-0.048	+0.097	-	100	
			KB	-0.011	-	-0.111	-0.239	-0.037	+0.093	-	-	2200
1.27	$3/2^+$	1	MSDI	-0.122	-	-0.046	-0.016	-0.562	+0.236	500	-	-
			RIP	-0.093	-	+0.044	-0.013	-0.265	+0.105	-	1700	-
			KB	+0.091	-	-0.021	+0.002	+0.151	-0.122	-	-	8000
		2	MSDI	-	0.012	0.055	-	+0462	-			
			RIP	-	0.047	-0.013	-	+0357	-			
			KB	-	-0.015	0.010	-	-0.171	-			
2.23	$5/2^+$	2	MSDI	-	-0.089	+0.063	-	-0.276	-	400	-	-
			RIP	-	-0.133	+0.063	-	+0.053	-	-	460	
			KB	-	-0.055	+0.170	-	+0.020	-	-	-	3000
		3	MSDI	+0.088	-0.305	-0.040	-	-	-0.008			
			RIP	-0.289	-0.374	-0.032	-	-	+0.005			
			KB	-0.050	-0.089	-0.029	-	-	-0.073			

[Continued...]

Table 5.14 (Continued..)

Spectroscopic amplitudes and normalization constant for transitions in the $^{29}Si(\alpha,d)^{31}P$ reaction using molecular potential

E_x (MeV)	J^+	J_{tra}	Interaction	Spectroscopic amplitudes					Normalization constants **			
				$d_{5/2}d_{5/2}$	$d_{5/2}s_{1/2}$	$d_{5/2}d_{3/2}$	$s_{1/2}s_{1/2}$	$s_{1/2}d_{3/2}$	$d_{3/2}d_{3/2}$	N_{MSDI}	N_{RIP}	N_{KB}
3.13	$1/2^+$	1	MSDI	-0.151	-	-0.122	-0.163	-0.380	+0.120	80	-	-
			RIP	-0.161	-	+0.057	+0.026	-0.136	+0.102	-	610	-
			KB	+0.094	-	-0.070	+0.464	-0.086	+0.204	-	-	50
3.30	$5/2^+$	2	MSDI	-	+0.063	-0.144	-	-0.324	-	180	-	-
			RIP	-	-0.028	-0.218	-	+0.129	-	-	270	-
			KB	-	+0.002	+0.087	-	-0.027	-	-	-	2300
		3	MSDI	-0.036	-0.035	0.102	-	-	+0.039			
			RIP	-0.038	-0.025	0.102	-	-	-0.066			
			KB	-0.040	-0.010	-0.051	-	-	+0.231			
3.41	$7/2^+$	3	MSDI	-0.047	+0.064	-0.151	-	-	+0.258	800	-	-
			RIP	+0.023	+0.087	-0.253	-	-	-0.045	-	18000	
			KB	+0.021	+0.006	-0.036	-	-	-0.311	-	-	1100
		4	MSDI	-	-	+0.121	-	-	-			
			RIP	-	-	+0.086	-	-	-			
			KB	-	-	+0.215	-	-	-			

[Continued...]

Table 5.14 (Continued..)

Spectroscopic amplitudes and normalization constants for transitions in the $^{29}Si(\alpha,d)^{31}P$ reaction using molecular potential

E_x (MeV)	J^π	J_{tra}	Interaction	Spectroscopic amplitudes [a]						Normalization constants **		
				$d_{5/2}d_{5/2}$	$d_{5/2}s_{1/2}$	$d_{5/2}d_{3/2}$	$s_{1/2}s_{1/2}$	$s_{1/2}d_{3/2}$	$d_{3/2}d_{3/2}$	N_{MSDI}	N_{RIP}	N_{KB}
3.51	$3/2^+$	1	MSDI	+0.055	-	+0.037	+0.020	+0.112	-0.107	11000	-	-
			RIP	-0.186	-	+0.180	-0.061	-0.079	+0.092	-	700	
			KB	-0.088	-	-0.050	+0.011	-0.301	+0.215	-	-	1300
		2	MSDI	-	-0.083	+0.070	-	+0.519	-			
			RIP	-	+0.032	+0.003	-	-0.088	-			
			KB	-	+0.010	-0.061	-	+0.285	-			
4.19	$5/2^+$	2	MSDI	-	+0.058	-0.038	-	-0.116	-	38000	-	-
			RIP	-	-0.050	+0.022	-	-0.051	-	-	4500	-
			KB	-	-0.027	+0.052	-	-0.132	-	-	-	1500
		3	MSDI	-0.030	+0.183	-0.169	-	-	-0.196			
			RIP	-0.071	-0.169	+0.269	-	-	-0.068			
			KB	-0.038	+0.082	-0.005	-	-	+0.239			
4.26	$3/2^+$	1	MSDI	+0.075	-	+0.120	+0.023	-0.100	-0.309	590	-	-
			RIP	-0.017	-	+0.088	-0.002	+0.137	+0.015	-	2500	
			KB	+0.037	-	-0.051	+0.005	+0.087	+0.022	-	-	3400
		2	MSDI	-	+0.058	-0.109	-	+0.033	-			
			RIP	-	-0.001	-0.264	-	-0.050	-			
			KB	-	-0.019	-0.105	-	-0.019	-			

a) Ref. [45]. ** Normalization constants using molecular potential.

Table 5.15. Spectroscopic amplitudes and normalization constants for transitions in the $^{29}Si(\alpha,d)^{31}P$ reaction using normal optical potential

E_x (MeV)	J^π	J_{tra}	Interaction	Spectroscopic amplitudes [a] $d_{5/2}d_{5/2}$	$d_{5/2}s_{1/2}$	$d_{5/2}d_{3/2}$	$s_{1/2}s_{1/2}$	$s_{1/2}d_{3/2}$	Normalization constants [b] $d_{3/2}d_{3/2}$	N_{MSDI}	N_{RIP}	N_{KB}
0	$1/2^+$	1	MSDI	+0.220	-	-0.128	+0.725	+0.013	-0.144	9.0×10^2	-	-
			RIP	-0.385	-	-0.242	-0.168	-0.048	+0.097	-	9.5×10^3	-
			KB	-0.011	-	-0.111	-0.239	-0.037	+0.093	-	1.5×10^3	
1.27	$3/2^+$	1	MSDI	-0.122	-	-0.046	-0.016	-0.562	+0.236	6.0×10^3	-	-
			RIP	-0.093	-	+0.044	-0.013	-0.265	+0.105	-	2.2×10^3	-
			KB	+0.091	-	-0.021	+0.002	+0.151	-0.122	-	-	8.9×10^3
		2	MSDI	-	0.012	0.055	-	+0462	-	-	-	-
			RIP	-	0.047	-0.013	-	+0357	-	-	-	-
			KB	-	-0.015	0.010	-	-0.171	-	-	-	-
2.23	$5/2^+$	2	MSDI	-	-0.089	+0.063	-	-0.276	-	6.5×10^3	-	-
			RIP	-	-0.133	+0.063	-	+0.053	-	-	7.3×10^3	-
			KB	-	-0.055	+0.170	-	+0.020	-	-	-	5.0×10^4
		3	MSDI	+0.088	-0.305	-0.040	-	-	-0.008	-	-	-
			RIP	-0.289	-0.374	-0.032	-	-	+0.005	-	-	-
			KB	-0.050	-0.089	-0.029	-	-	-0.073	-	-	-

[Continued...]

Table 5.15. (Continued..)

Spectroscopic amplitudes and normalization constants for transitions in the $^{29}Si(\alpha,d)^{31}P$ reaction using normal optical potential

E_x (MeV)	J^+	J_{tra}	Interaction	Spectroscopic amplitudes [a] $d_{5/2}d_{5/2}$	$d_{5/2}s_{1/2}$	$d_{5/2}d_{3/2}$	$s_{1/2}s_{1/2}$	$s_{1/2}d_{3/2}$	Normalization constants [a] $d_{3/2}d_{3/2}$	N_{MSDI}	N_{RIP}	N_{KB}
3.13	$1/2^+$	1	MSDI	-0.151	-	-0.122	-0.163	-0.380	+0.120	$1.2x10^3$	-	-
			RIP	-0.161	-	+0.057	+0.026	-0.136	+0.102	-	$1.5x10^4$-	
			KB	+0.094	-	-0.070	+0.464	-0.086	+0.204	-	-	$5.0x10^2$
3.30	$5/2^+$	2	MSDI	-	+0.063	-0.144	-	-0.324	-	$4.0x10^3$	-	-
			RIP	-	-0.028	-0.218	-	+0.129	-	-	$9.0x10^4$	-
			KB	-	+0.002	+0.087	-	-0.027	-	-	-	$8.0x10^4$
		3	MSDI	-0.036	-0.035	0.102	-	-	+0.039			
			RIP	-0.038	-0.025	0.102	-	-	-0.066			
			KB	-0.040	-0.010	-0.051	-	-	+0.231			
3.41	$7/2^+$	3	MSDI	-0.047	+0.064	-0.151	-	-	+0.258	$1.4x10^4$	-	-
			RIP	+0.023	+0.087	-0.253	-	-	-0.045	-	$2.8x10^5$	
			KB	+0.021	+0.006	-0.036	-	-	-0.311	-	-	$2.0x10^4$
		4	MSDI	-	-	+0.121	-	-	-			
			RIP	-	-	+0.086	-	-	-			
			KB	-	-	+0.215	-	-	-			

[Continued...]

Table 5.15 (Continued..)

Spectroscopic amplitudes and normalization constants for transitions in the $^{29}Si(\alpha,d)^{31}P$ reaction using normal optical potential

E_x (MeV)	J^+	J_{tra}	Interaction	Spectroscopic amplitudes [a] $d_{5/2}d_{5/2}$	$d_{5/2}s_{1/2}$	$d_{5/2}d_{3/2}$	$s_{1/2}s_{1/2}$	$s_{1/2}d_{3/2}$	$d_{3/2}d_{3/2}$	Normalization constants ** N_{MSDI}	N_{RIP}	N_{KB}
3.51	$3/2^+$	1	MSDI	+0.055	-	+0.037	+0.020	+0.112	-0.107	1.5×10^4	-	-
			RIP	-0.186	-	+0.180	-0.061	-0.079	+0.092	-	1.1×10^4	-
			KB	-0.088	-	-0.050	+0.011	-0.301	+0.215	-	-	1.6×10^4
		2	MSDI	-	-0.083	+0.070	-	+0.519	-			
			RIP	-	+0.032	+0.003	-	-0.088	-			
			KB	-	+0.010	-0.061	-	+0.285	-			
4.19	$5/2^+$	2	MSDI	-	+0.058	-0.038	-	-0.116	-	5.0×10^5	-	-
			RIP	-	-0.050	+0.022	-	-0.051	-	-	5.0×10^5	
			KB	-	-0.027	+0.052	-	-0.132	-	-	-	1.8×10^4
		3	MSDI	-0.030	+0.183	-0.169	-	-	-0.196			
			RIP	-0.071	-0.169	+0.269	-	-	-0.068			
			KB	-0.038	+0.082	-0.005	-	-	+0.239			
4.26	$3/2^+$	1	MSDI	+0.075	-	+0.120	+0.023	-0.100	-0.309	1.1×10^4	-	-
			RIP	-0.017	-	+0.088	-0.002	+0.137	+0.015	-		4.0×10^4
			KB	+0.037	-	-0.051	+0.005	+0.087	+0.022	-	-	5.8×10^4
		2	MSDI	-	+0.058	-0.109	-	+0.033	-	-	-	-
			RIP	-	-0.001	-0.264	-	-0.050	-	-	-	-
			KB	-	-0.019	-0.105	-	-0.019	-			

a) Ref. [45]. ** Normalization constants using optical potential.

Table 5.16. Spectroscopic amplitudes and normalization constant for transitions in the $^{29}Si(\alpha,d)^{31}P$ reaction using Michel potential

E_x (MeV)	J^+	J_{tra}	Interaction	Spectroscopic amplitudes [a] $d_{5/2}d_{5/2}$	$d_{5/2}s_{1/2}$	$d_{5/2}d_{3/2}$	$s_{1/2}s_{1/2}$	$s_{1/2}d_{3/2}$	$d_{3/2}d_{3/2}$	Normalization constants [**] N_{MSDI}	N_{RIP}	N_{KB}
0	$1/2^+$	1	MSDI	+0.220	-	-0.128	+0.725	+0.013	-0.144	$5.5x10^2$	-	-
			RIP	-0.385	-	-0.242	-0.168	-0.048	+0.097	-	$7.0x10^3$	-
			KB	-0.011	-	-0.111	-0.239	-0.037	+0.093	-	-	$1.2x10^4$
1.27	$3/2^+$	1	MSDI	-0.122	-	-0.046	-0.016	-0.562	+0.236	$3.2x10^3$	-	-
			RIP	-0.093	-	+0.044	-0.013	-0.265	+0.105	-	$1.1x10^3$	-
			KB	+0.091	-	-0.021	+0.002	+0.151	-0.122	-	-	$4.0x10^4$
		2	MSDI	-	0.012	0.055	-	+0462	-	-	-	-
			RIP	-	0.047	-0.013	-	+0357	-	-	-	-
			KB	-	-0.015	0.010	-	-0.171	-	-	-	-
2.23	$5/2^+$	2	MSDI	-	-0.089	+0.063	-	-0.276	-	$1.9x10^3$	-	-
			RIP	-	-0.133	+0.063	-	+0.053	-	-	$2.1x10^3$	
			KB	-	-0.055	+0.170	-	+0.02	-	-	-	$1.7x10^4$
		3	MSDI	+0.088	-0.305	-0.040	-	-	-0.008	-	-	-
			RIP	-0.289	-0.374	-0.032	-	-	+0.005	-	-	-
			KB	-0.050	-0.089	-0.029	-	-	-0.073	-	-	-

[Continued...]

Table 5.16 (Continued..)

Spectroscopic amplitudes and normalization constants for transitions in the $^{29}Si(\alpha,d)^{31}P$ reaction using Michel potential

E_x (MeV)	J^+	J_{tra}	Interaction	Spectroscopic amplitudes [a]					Normalization constants **			
				$d_{5/2}d_{5/2}$	$d_{5/2}s_{1/2}$	$d_{5/2}d_{3/2}$	$s_{1/2}s_{1/2}$	$s_{1/2}d_{3/2}$	$d_{3/2}d_{3/2}$	N_{MSDI}	N_{RIP}	N_{KB}
3.13	$1/2^+$	1	MSDI	-0.151	-	-0.122	-0.163	-0.380	+0.120	$5.5x10^2$	-	-
			RIP	-0.161	-	+0.057	+0.026	-0.136	+0.102	-	$1.9x10^4$	-
			KB	+0.094	-	-0.070	+0.464	-0.086	+0.204	-	-	$3.0x10^2$
3.30	$5/2^+$	2	MSDI	-	+0.063	-0.144	-	-0.324	-	$2.2x10^3$	-	-
			RIP	-	-0.028	-0.218	-	+0.129	-	-	$4.4x10^3$	-
			KB	-	+0.002	+0.087	-	-0.027	-	-	-	$4.3x10^4$
		3	MSDI	-0.036	-0.035	0.102	-	-	+0.039	-	-	-
			RIP	-0.038	-0.025	0.102	-	-	-0.066	-	-	-
			KB	-0.040	-0.010	-0.051	-	-	+0.231	-	-	-
3.41	$7/2^+$	3	MSDI	-0.047	+0.064	-0.151	-	-	+0.258	$8.0x10^2$	-	-
			RIP	+0.023	+0.087	-0.253	-	-	-0.045	-	$4.0x10^4$	-
			KB	+0.021	+0.006	-0.036	-	-	-0.311	-	-	$1.0x10^3$
		4	MSDI	-	-	+0.121	-	-	-	-	-	-
			RIP	-	-	+0.086	-	-	-	-	-	-
			KB	-	-	+0.215	-	-	-	-	-	-

[Continued...]

Table 5.16. (Continued..)

Spectroscopic amplitudes and normalization constant for transitions in the $^{29}Si(\alpha,d)^{31}P$ reaction using Michel potential

E_x (MeV)	J^+	J_{tra}	Interaction	Spectroscopic amplitudes [a]						Normalization constants **		
				$d_{5/2}d_{5/2}$	$d_{5/2}s_{1/2}$	$d_{5/2}d_{3/2}$	$s_{1/2}s_{1/2}$	$s_{1/2}d_{3/2}$	$d_{3/2}d_{3/2}$	N_{MSDI}	N_{RIP}	N_{KB}
3.51	$3/2^+$	1	MSDI	+0.055	-	+0.037	+0.020	+0.112	-0.107	$8.0x10^4$	-	-
			RIP	-0.186	-	+0.180	-0.061	-0.079	+0.092	-	$7.0x10^3$	-
			KB	-0.088	-	-0.050	+0.011	-0.301	+0.215	-	-	$8.0x10^3$
		2	MSDI	-	-0.083	+0.070	-	+0.519	-	-	-	-
			RIP	-	+0.032	+0.003	-	-0.088	-	-	-	-
			KB	-	+0.010	-0.061	-	+0.285	-	-	-	-
4.19	$5/2^+$	2	MSDI	-	+0.058	-0.038	-	-0.116	-	$2.2x10^4$	-	-
			RIP	-	-0.050	+0.022	-	-0.051	-	-	$3.0x10^4$	-
			KB	-	-0.027	+0.052	-	-0.132	-	-	-	$1.0x10^4$
		3	MSDI	-0.030	+0.183	-0.169	-	-	-0.196	-	-	-
			RIP	-0.071	-0.169	+0.269	-	-	-0.068	-	-	-
			KB	-0.038	+0.082	-0.005	-	-	+0.239	-	-	-
4.26	$3/2^+$	1	MSDI	+0.075	-	+0.120	+0.023	-0.100	-0.309	$5.9x10^3$	-	-
			RIP	-0.017	-	+0.088	-0.002	+0.137	+0.015	-	$2.5x10^4$	
			KB	+0.037	-	-0.051	+0.005	+0.087	+0.022	-	-	$3.4x10^4$
		2	MSDI	-	+0.058	-0.109	-	+0.033	-	-	-	-
			RIP	-	-0.001	-0.264	-	-0.050	-	-	-	-
			KB	-	-0.019	-0.105	-	-0.019	-	-	-	-

a) Ref. [45]. ** Normalization constants using Michel potential.

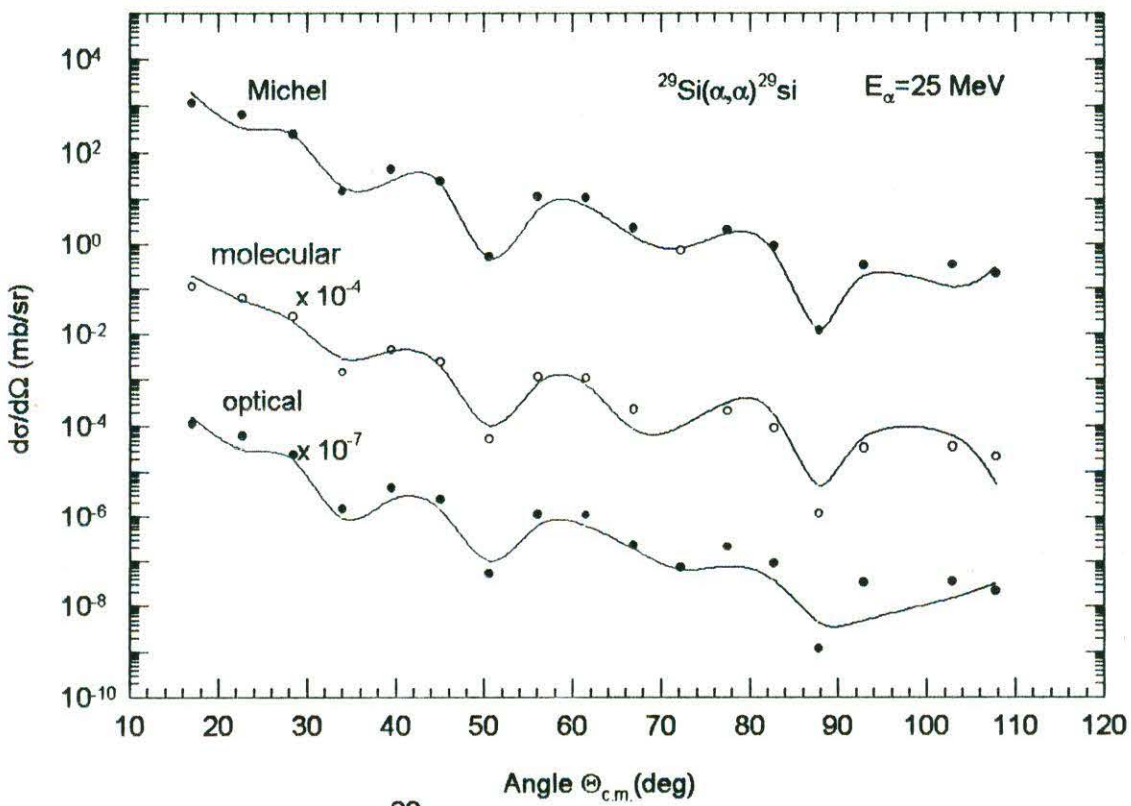

Fig. 5. 20. Fits to the α-^{29}Si elastic scattering data at 25 MeV (lab) with the Michel, molecular and normal optical potentials. Data are from [45]

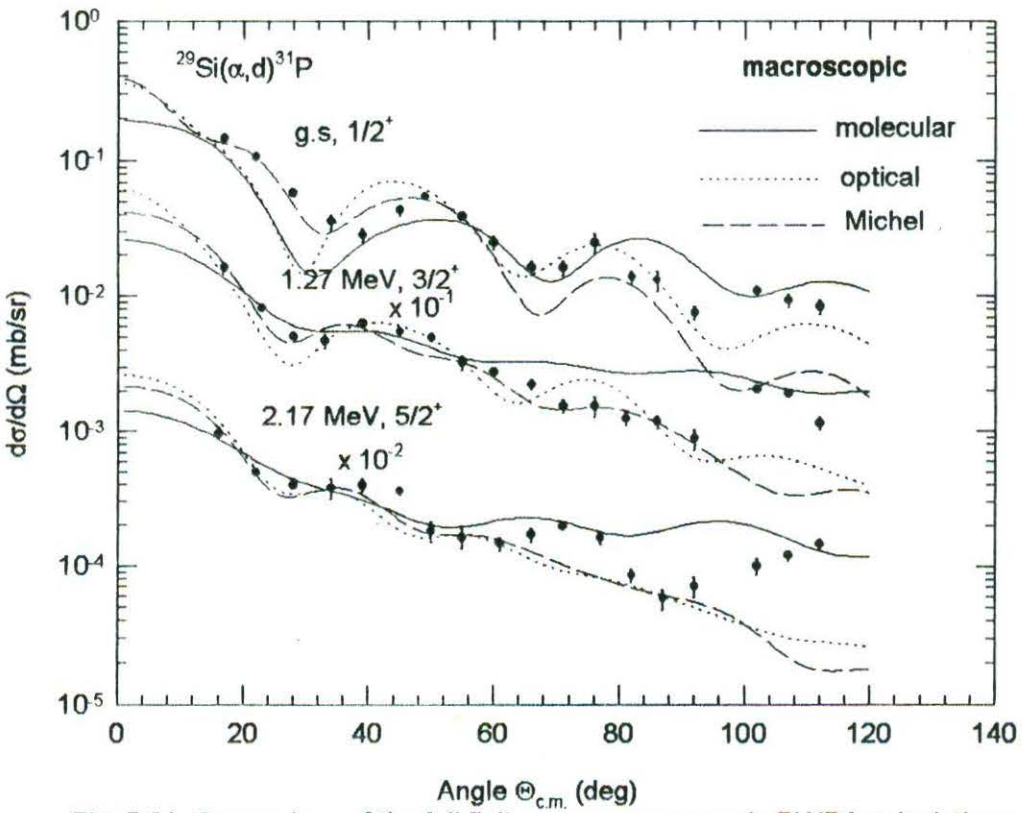

Fig. 5.21. Comparison of the full finite-range macroscopic DWBA calculations for the ^{29}Si(α,d)^{31}P reaction at 25 MeV leading to ground ($1/2^+$), 1.27($3/2^+$) and 2.23 ($5/2^+$) MeV states of ^{31}P to the differential cross-section data. The solid, dotted and broken curves are the predictions using the molecular, normal optical and Michel α-^{29}Si, Michel a-29Si potentials.Data are from [48].

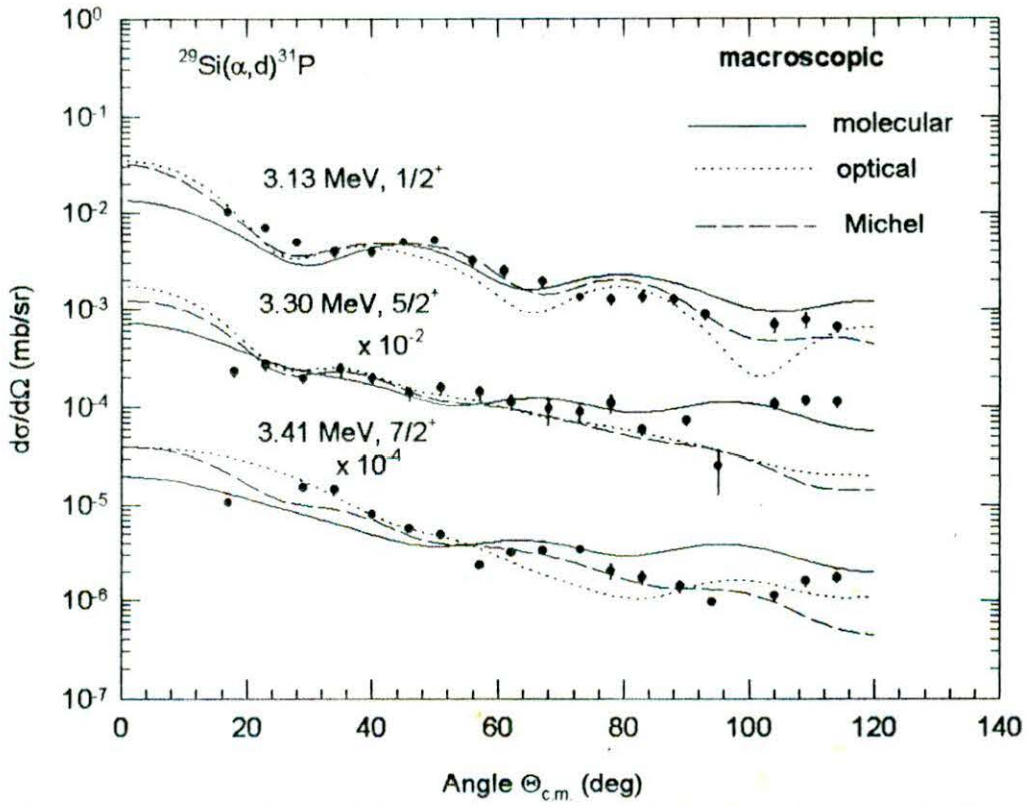

Fig. 5.22. Comparison of the full finite-range macroscopic DWBA calculations for the ^{29}Si(α,d)^{31}P reaction at reaction at 25 MeV leading to the 3.13(1/2$^+$), 3.30(5/2$^+$), 3.41(7/2$^+$) MeV states of ^{31}P to the differential cross-section data. The solid, dotted and broken curves are the predictions using the molecular, normal optical and Michel α-^{29}Si potentials respectively.Data are from [48].

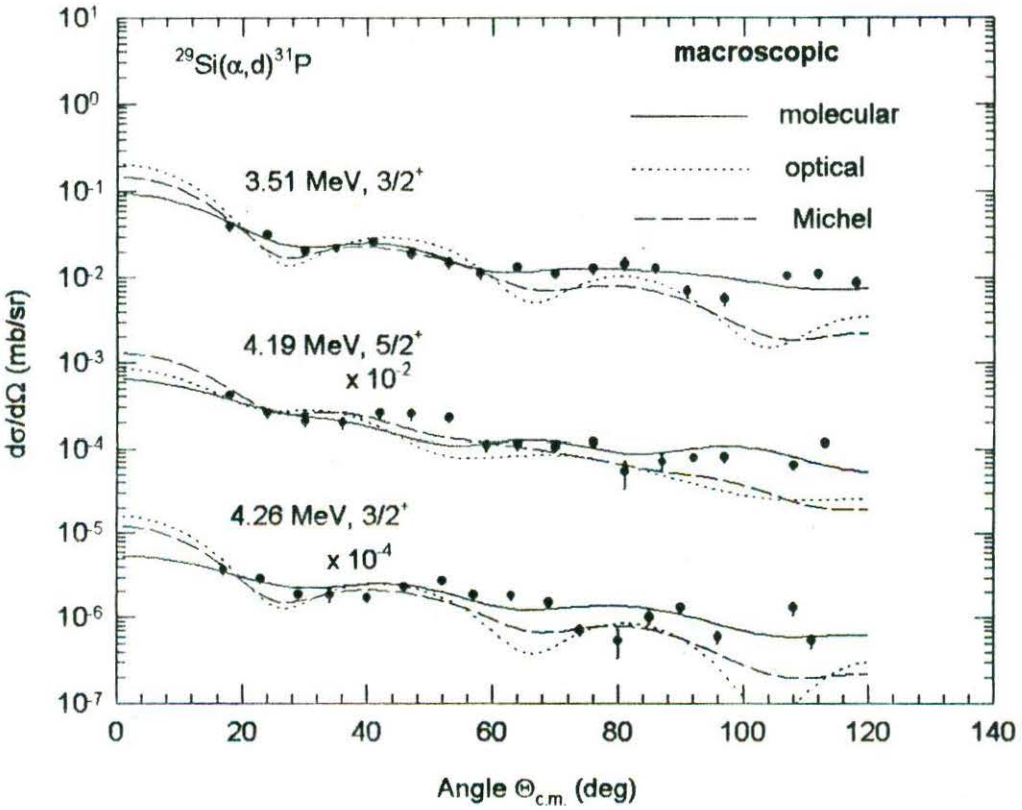

Fig. 5.23. Same as in Fig.5.21 for 3.51($3/2^+$), 4.19($5/2^+$) and 4.26($3/2^+$)MeV states of ^{31}P. Data are from [48].

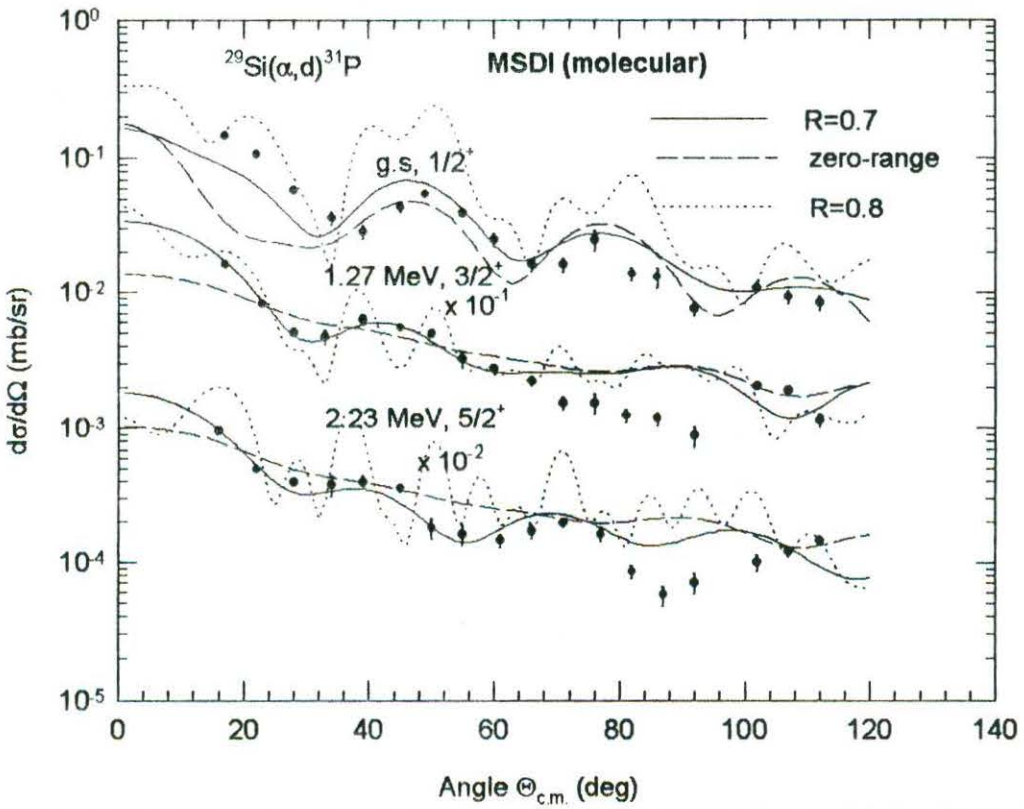

Fig.5. 24. Comparison of the zero-range microscopic DWBA calculations using the MSDI spectroscopic amplitudes and the molecular potential in the α–channel for the ^{29}Si(α,d)^{31}P reaction at 25 MeV leading to the ground ($1/2^+$), 1.27($3/2^+$), and 2.23($5/2^+$) MeV states of ^{31}P to the differential cross-section data. The solid curves are the predictions using the finite-range (FR) correction with R=0.7 fm. The broken and the dotted curves are the predictions with R=0.0 and 0.85 fm, respectively. Data are from [48]

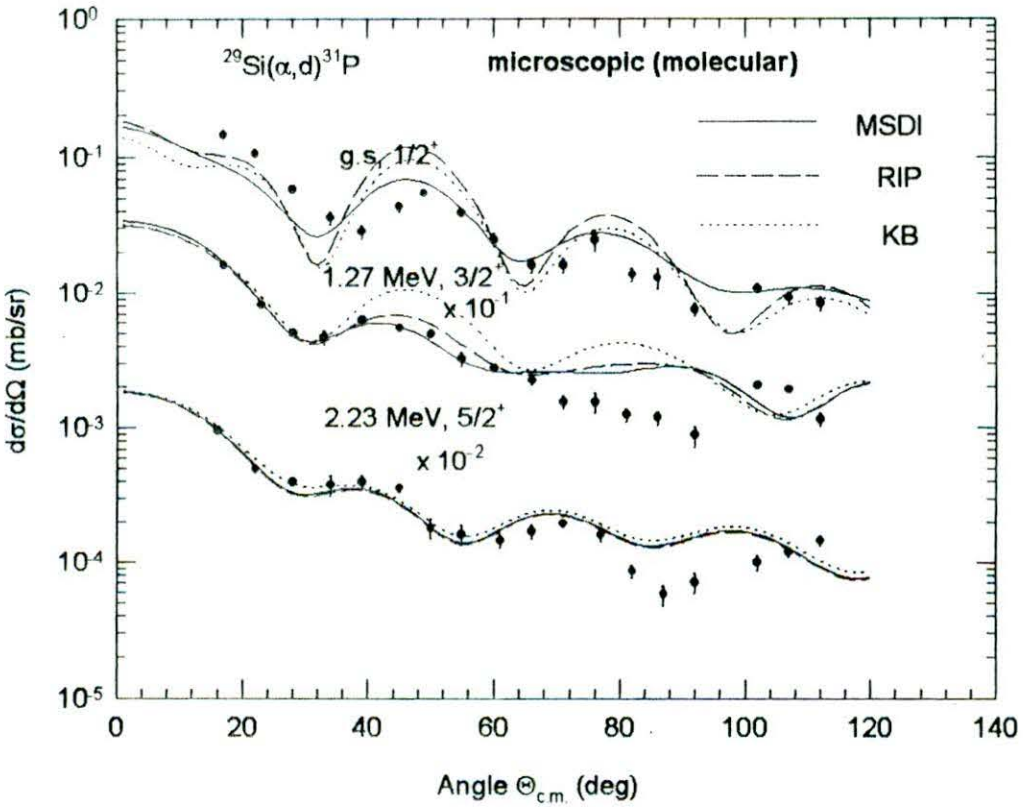

Fig. 5.25. Comparison of the zero-range microcopic DWBA calculations with FR correction (R=0.7 fm.) and the molecular potential in the α-channel for ^{29}Si(α,d)^{31}P reaction leading to the g.s. ($1/2^+$), 1.27 ($3/2^+$) and 2.23($5/2^+$) MeV states of ^{31}P to the differential cross-section data. The solid, broken and dotted curves are the predictions using the MSDI, RIP, and KB interactions respectively. Data are from [48].

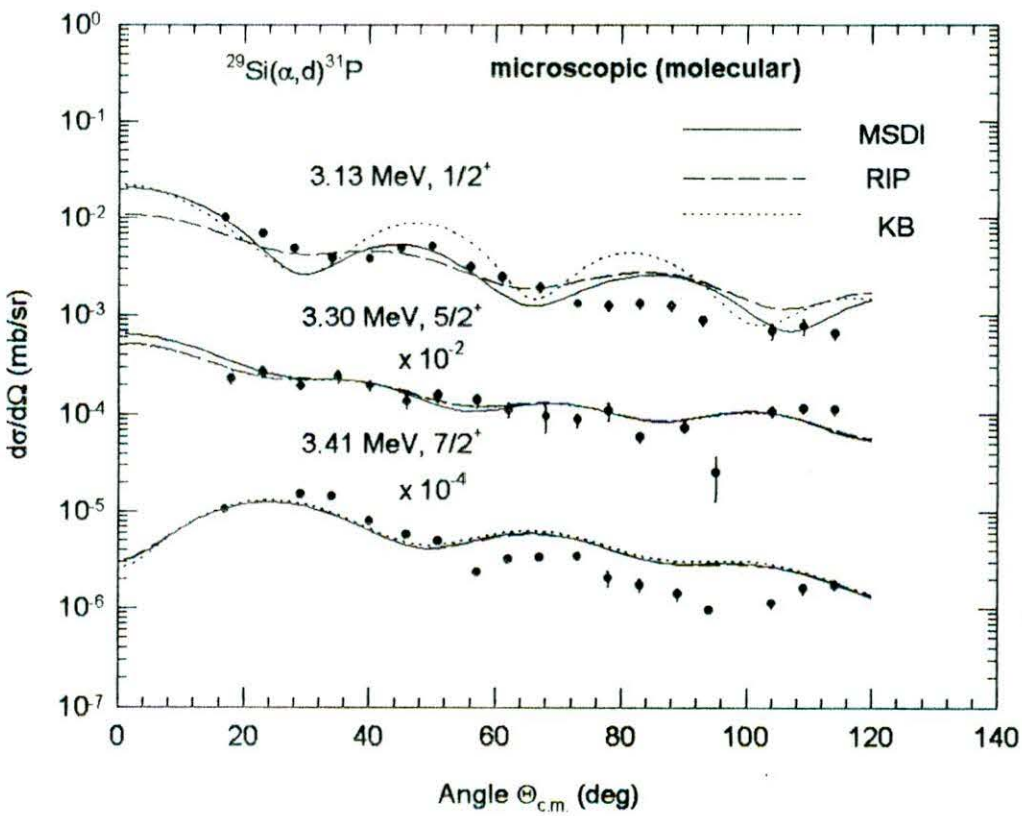

Fig. 5.26. Same as in Fig. 5.25 for 3.13($1/2^+$), 3.30($1/2^+$) and 3.41($5/2^+$) MeV states of ^{31}P. Data are from [48].

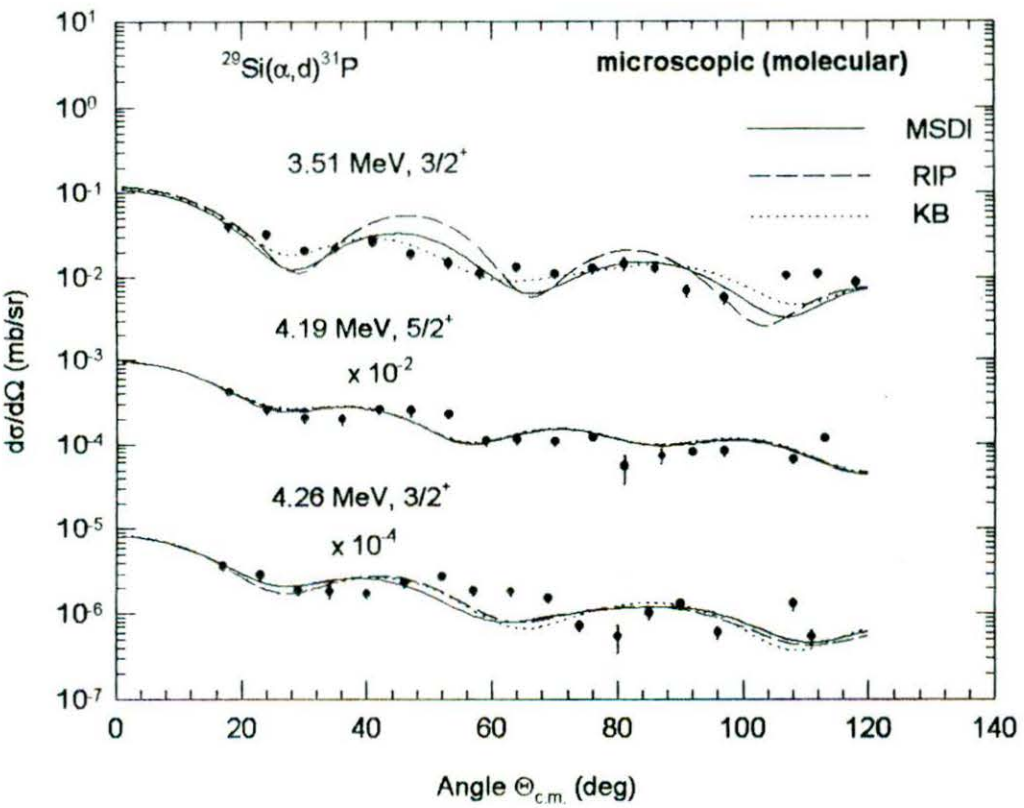

Fig. 5.27. Same as in Fig. 5.25 for 3.51($3/2^+$), 4.19($5/2^+$) and 4.26 ($3/2^+$) MeV states of ^{31}P. Data are from [48].

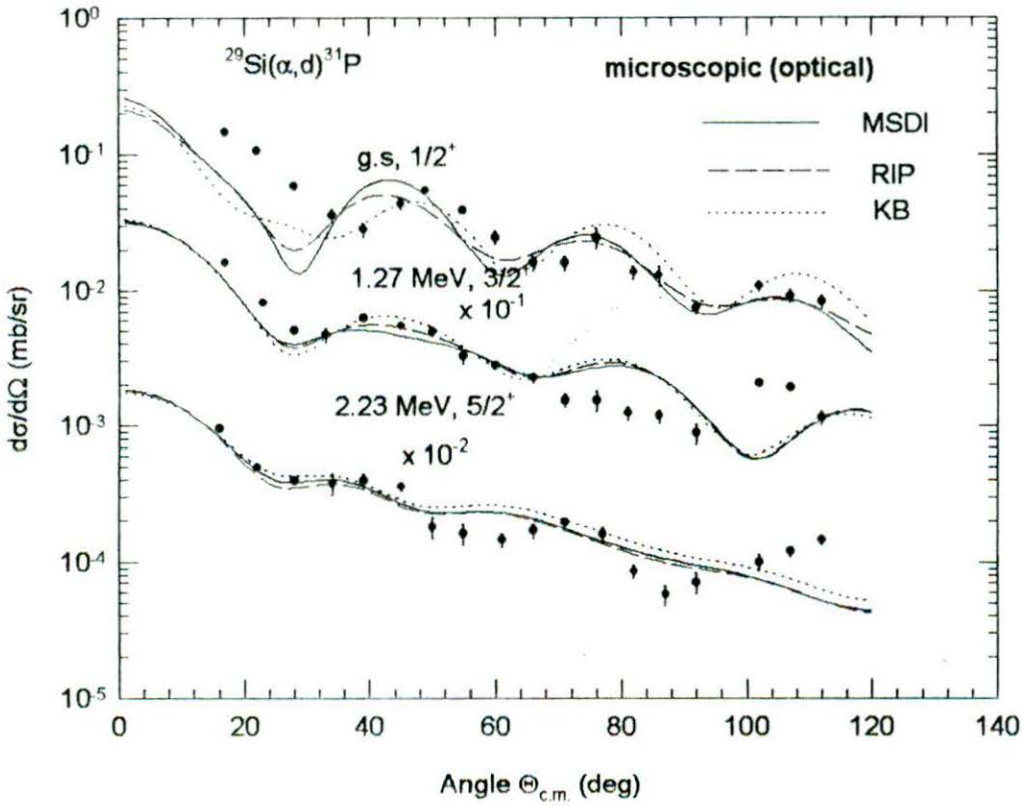

Fig. 5.28. Same as Fig. 5.25 using normal optical potential.
Data are from [48].

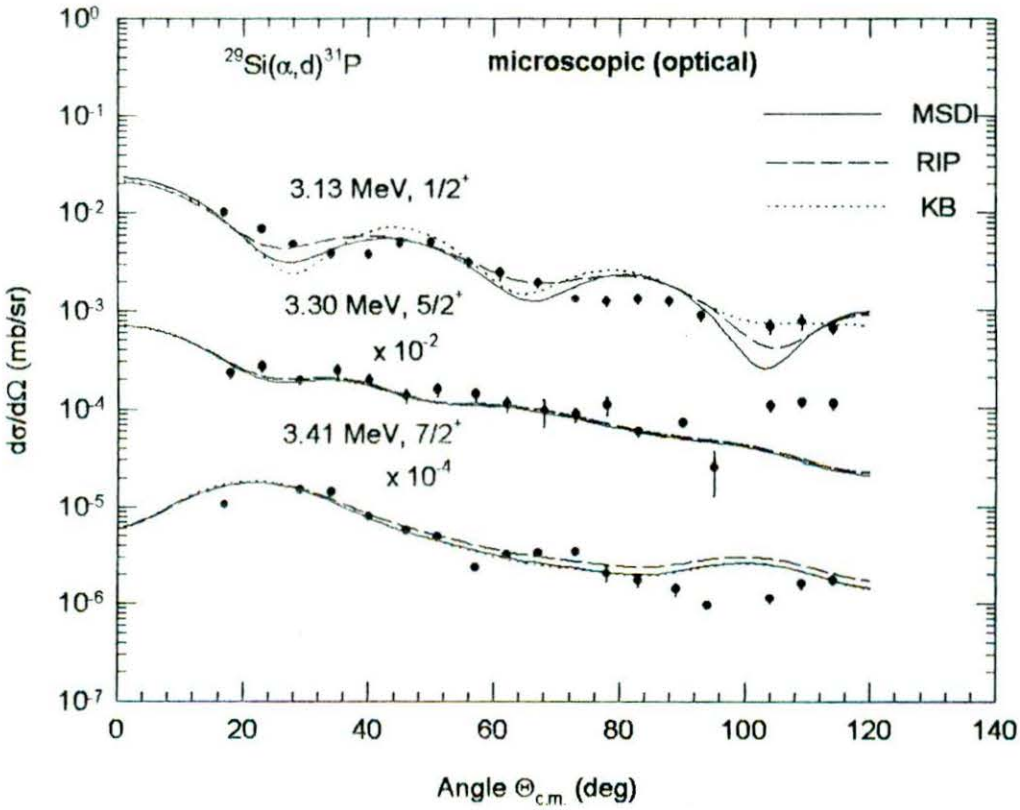

Fig. 5.29. Same as in Fig. 5.26 using normal optical potential.

Data are from [48].

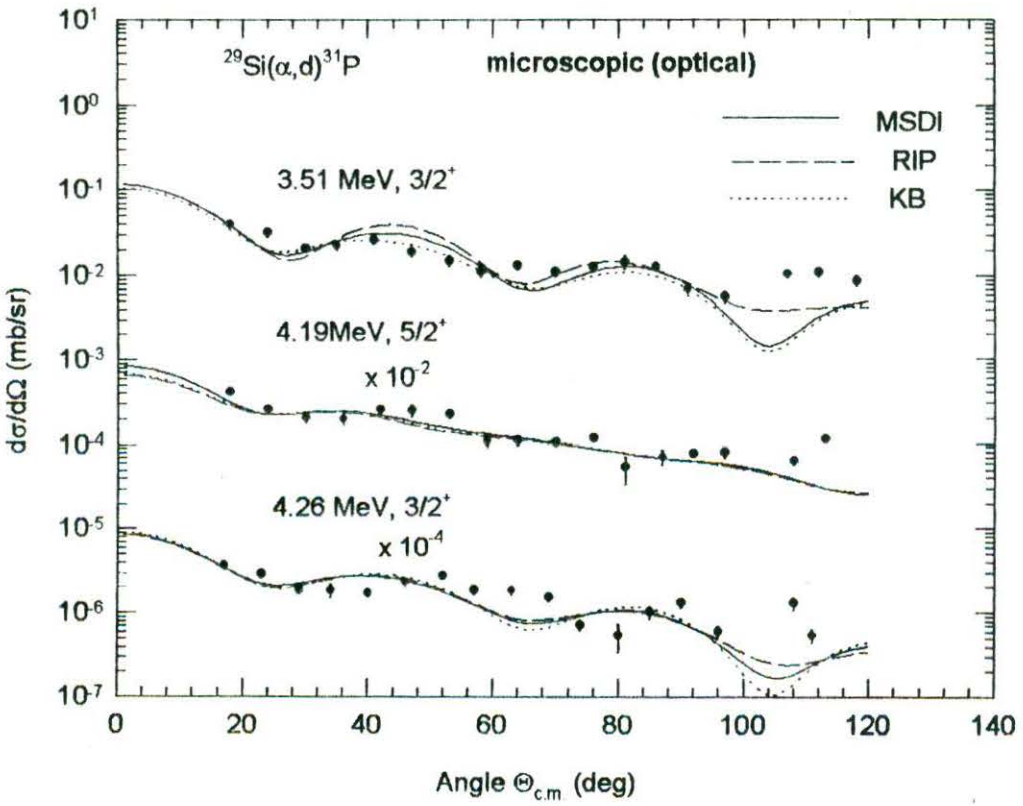

Fig. 5.30. Same as in Fig.5. 27 using normal optical potential. Data are from [48].

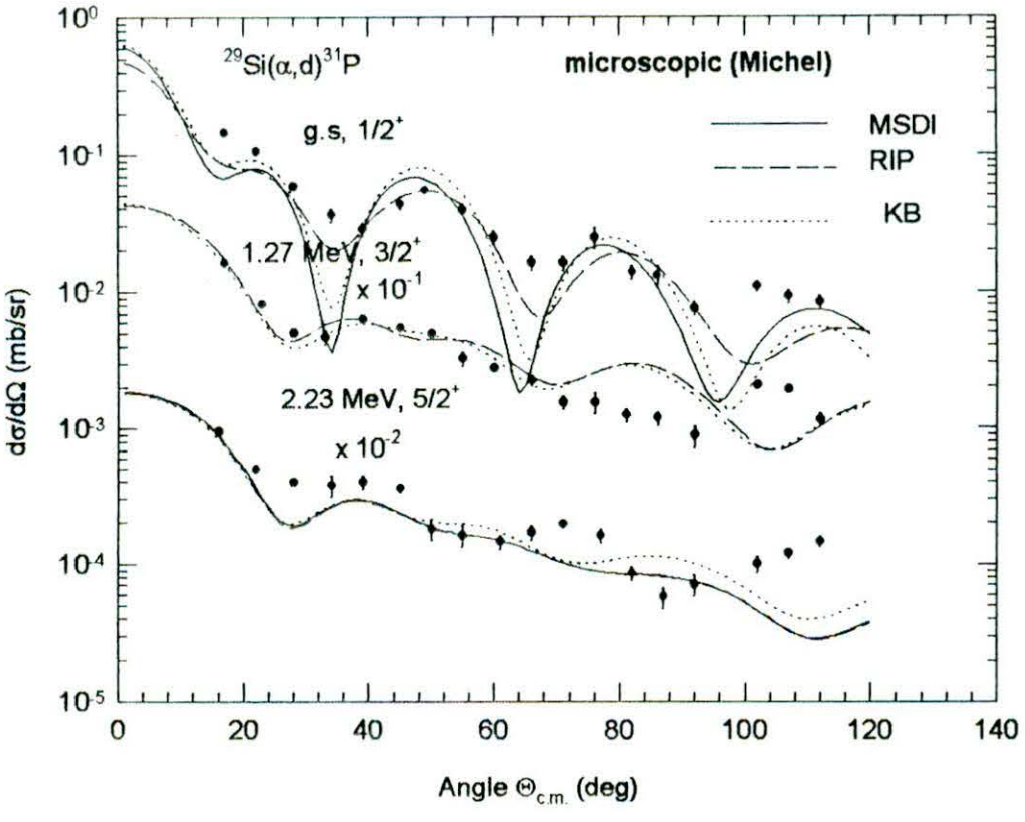

Fig. 5. 31. Same as in Fig.5.25 using Michel potential. Data are from [48].

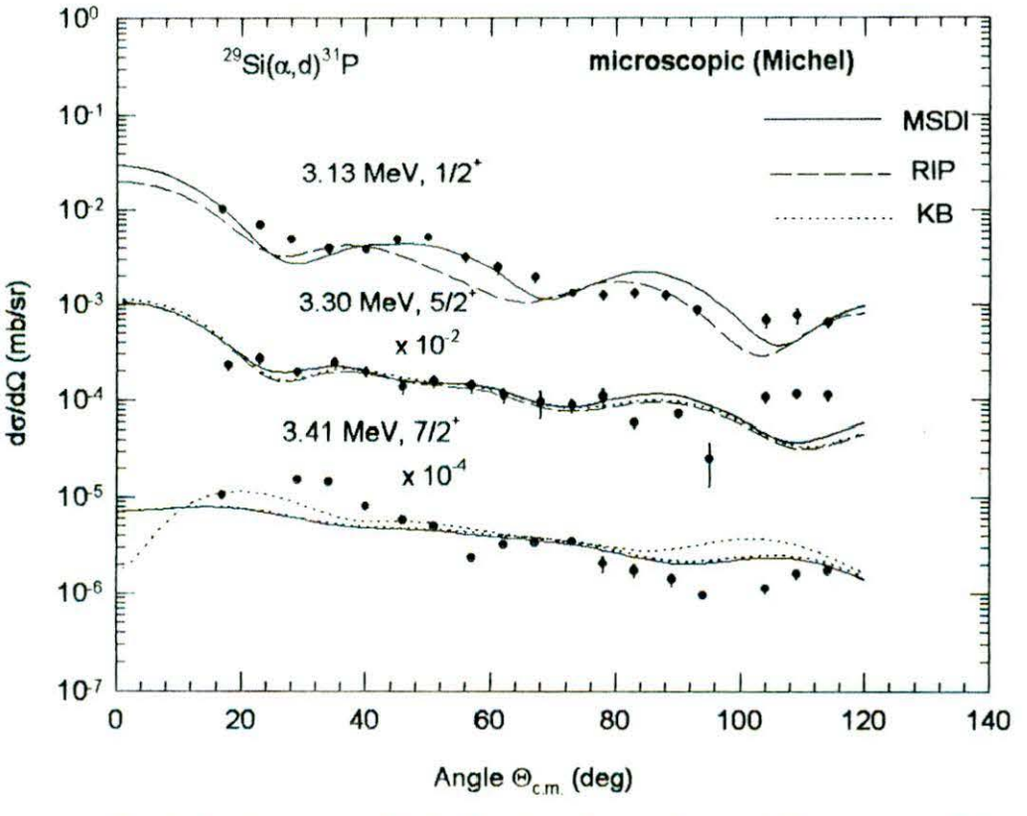

Fig. 5. 32. Same as in Fig.5.26 using Michel potential. Data are from [48].

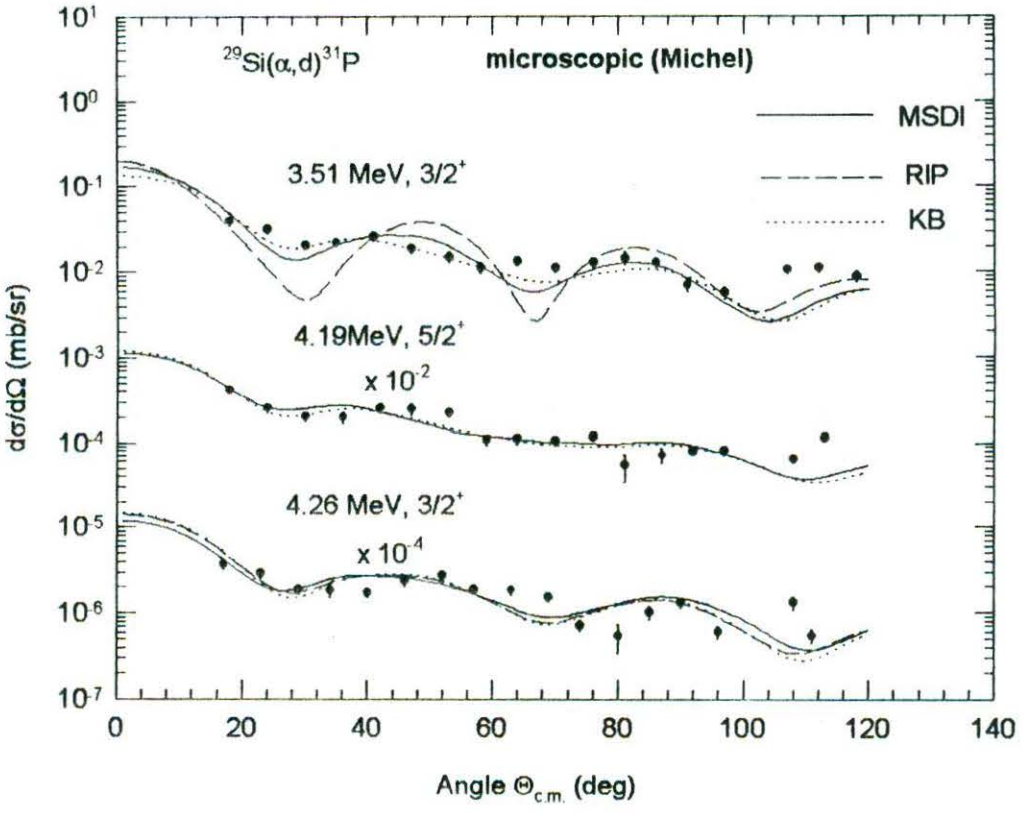

Fig. 5. 33. Same as in Fig.5.27 using Michel potential.Data are from [48].

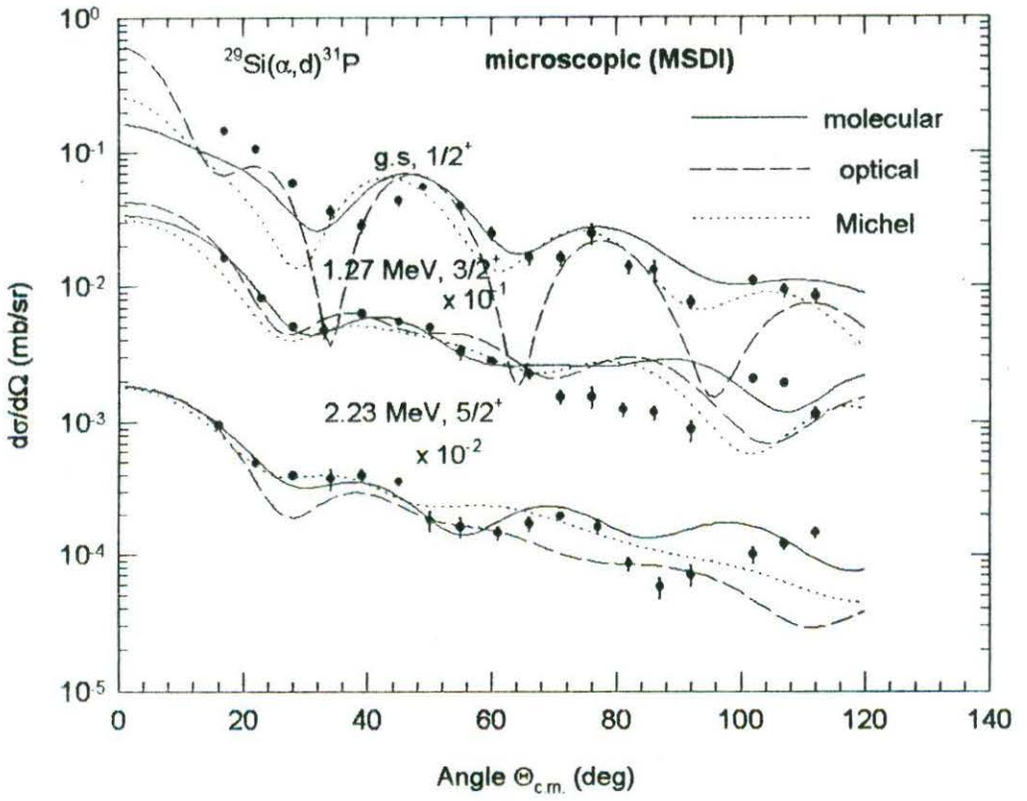

Fig. 5.34. Comparison of the zero-range microscopic DWBA calculations using the MSDI spectroscopic amplitudes and the molecular, normal optical and Michel potentials in the α-channel for the ^{29}Si(α,d)^{31}P reactions at 25 MeV leading to the ground (1/2$^+$), 1.27(3/2$^+$), and 2.23(5/2$^+$) MeV states of ^{31}P to the differential cross-section data. The solid, broken and dotted curves are the predictions using the molecular, normal optical and Michel potentials respectively.Data are from [48].

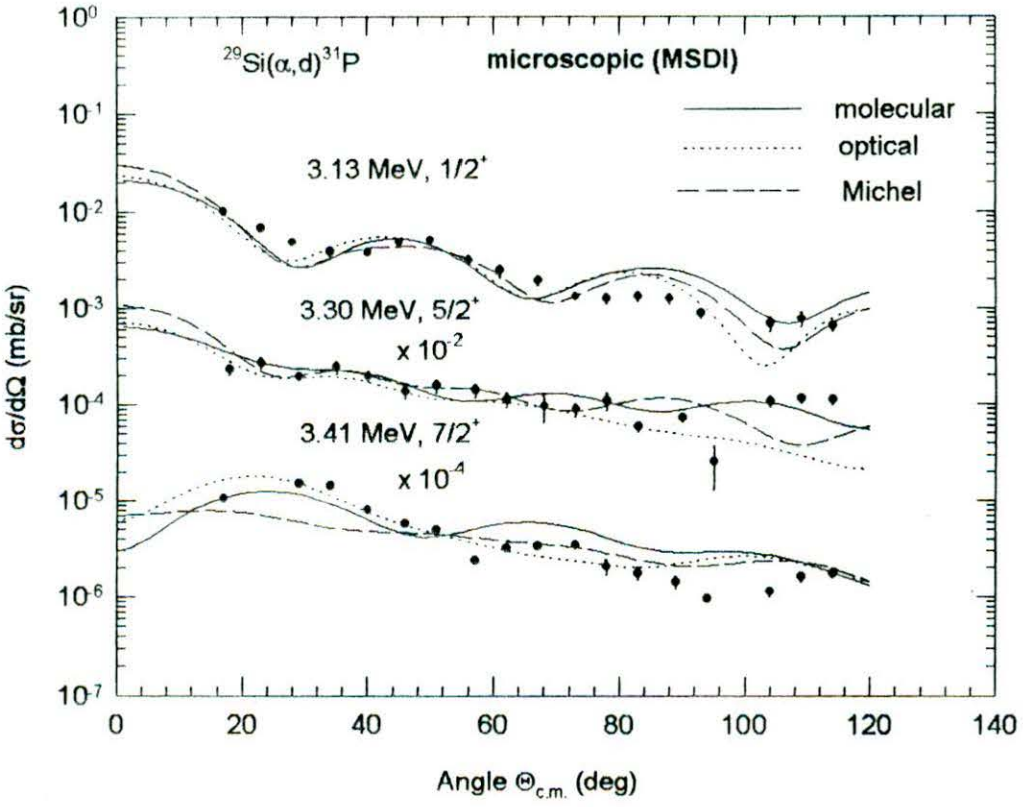

Fig. 5.35. Same as in Fig. 5.34. for 3.13($1/2^+$), 3.30($5/2^+$) and 3.41($7/2^+$) MeV states. Data are from [48].

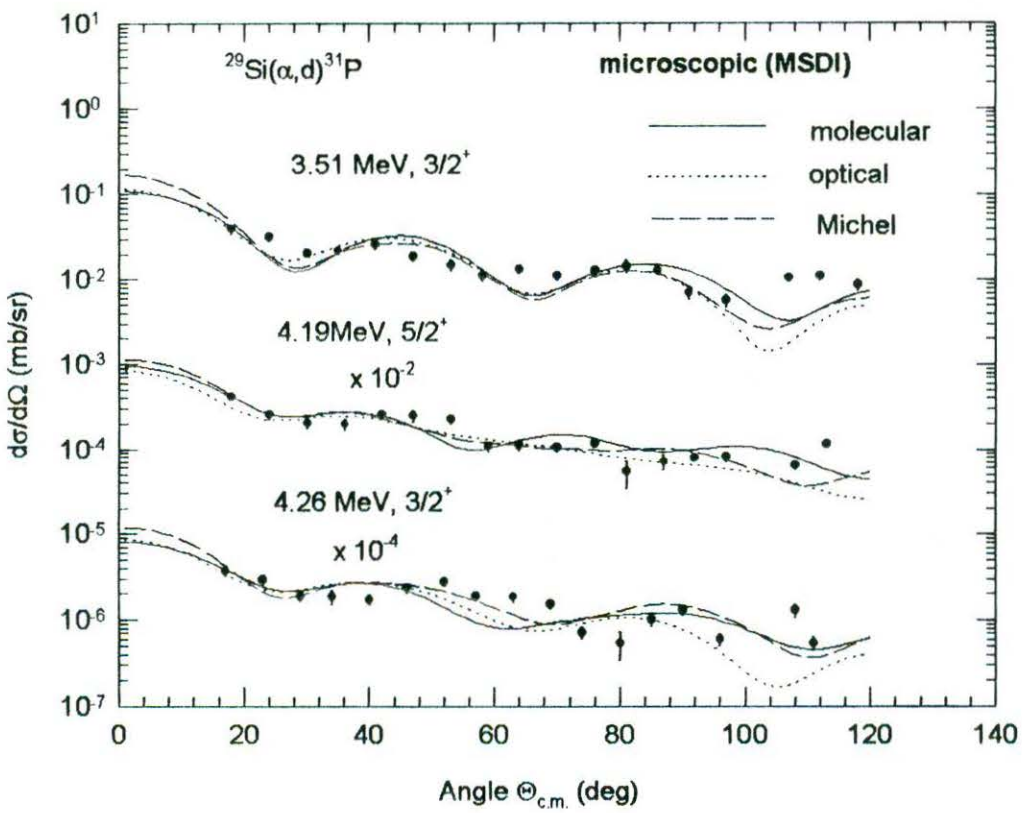

Fig. 5.36. Same as in Fig. 5.34. for 3.13($1/2^+$), 3.30($5/2^+$) and 3.41($7/2^+$) MeV states. Data are from [48].

5.2.4. DWBA analysis of the $^{30}Si(\alpha,d)^{32}P$ reaction

The microscopic zero-range (ZR) DWBA and macroscopic full finite-range (FFR) calculations for analyzing the $^{30}Si(\alpha,d)^{32}P$ reaction data have been performed using DWUCK4 and DWUCK5 [39] respectively.

As before, corrections due to non-locality [32,39] of potentials in the conventional form have been applied using the non-locality parameters $\beta(\alpha)$=0.2, $\beta(d)$=0.54 and $\beta(p)$=0.85 fm. In both the microscopic ZR and macroscopic FFR calculations, the molecular, standard and Michel types of α-^{30}Si potential in the entrance channel and the standard optical d-^{32}P in the exit channel have been employed. The parameters of the molecular , standard, and Michel potentials are generated by fitting the elastic data [45] of α-^{30}Si as shown in the Fig.5.37. The d-^{32}P standard optical potentials used has been procured from the work of Fitz *et al.* [148]. All the potential parameters used are displayed in Table 5.17.

5.2.4.1. Macroscopic DWBA calculations

The bound state geometry for d-d and d-^{30}Si Woods Saxon (WS) potential shown in Table 5.17 are taken from [18]. As usual, the bound-state wave functions for the transferred deuteron in alpha as well as in the final nucleus have been generated by adjusting the deuteron separation energy. The accuracy parameters used in the code has been assigned using the method as mentioned before (Sec. 5.2.2.1) in the analysis of the reaction on ^{28}Si.

The cluster configuration of the transferred deuteron for the different states of excitations are shown in Table 5.18. For the final states with natural parity states populated by one *L*-transfer, the DWBA predictions are compared to the data to yield the relevant spectroscopic factors A_L, as defined in Eq. 5.15. On the other hand, for the transitions involving two *L*-transfers leading to final states with unnatural parity spectroscopic factors A_L are extracted by using Eq. (5.15) and minimizing χ^2 in Eq. (5.17). The deduced spectroscopic factors are noted in Tables 5.18 and 5.19.

The DWBA predictions with molecular (solid curve), normal (dotted curve) and Michel (broken curves) potentials are compared to the data of the ground (1^+), 0.08 (2^+), 1.15(1^+), and 1.32 (2^+) MeV states in Fig. 5.38 and to the data of 1.75 (3^+), 2.66(2^+), 2.74 (1^+) and 3.00 (3^+) MeV states of ^{32}P in Fig. 5.39.

5.2.4.2. Microscopic DWBA calculation

The present microscopic analyses make use of three sets of spectroscopic amplitudes $\beta^{1/2}$, based on different nucleon-nucleon interactions. All three sets of spectroscopic amplitudes are obtained from [45]. The first set (MSDI) have been extracted using the modified surface delta interaction [152]; another set (RIP) have been calculated based on an effective interaction found by fitting to experimentally observed nuclear energy levels [153]. The third set (KB) which have been calculated assuming a Hamada-Johnston scattering potential [154]. All three amplitudes are furnished in Tables (5.20 – 5.22) along with the respective normalization constants deduced using Eq. (5.16) after fitting the experimental data using all three (molecular, normal optical and Michel) potentials.

All three sets of spectroscopic amplitudes are calculated in the model space of $1d_{5/2}2s_{1/2}1d_{3/2}$. The phase corrections to the spectroscopic amplitudes for inputting to the computer DWUCK4 are same as discussed in Sec. 5.2.2.2.

The bound-state wave functions for each of the transferred nucleons have been generated by assuming a real Woods-Saxon well with the geometry parameters r_0=1.25 fm and a_0=0.65 fm and the depth adjusted to reproduce the binding energy equal to the half of the separation of the transferred deuteron. A Thomas-Fermi spin-orbit term with λ=25 has also been used for the bound state wave functions.

A Gaussian form of the finite range correction in the LEA [39] has been investigated. Fig. 5.40 compares the microscopic DWBA calculations for the molecular type of α-^{30}Si potential using R=0.0 fm (dotted curves), 0.7 fm (solid curves) and 0.8 fm (broken curves) to the experimental data for ground (1^+), 0.08(2^+), 1.15 (1^+) and 1.32 (2^+) MeV states. As observed in the analysis of the reaction on ^{28,29}Si, R=0.7 fm gives the best overall fits to the data.

The effect of the three types of the α-^{30}Si potentials on the microscopic zero-range DWBA calculations with finite range correction R=0.7 fm has also been examined under the spectroscopic amplitudes calculated for all three interactions. Figs. 5.41–5.42 display the DWBA predictions for the molecular potentials using all three interactions MSDI (solid lines), RIP (dotted lines), and KB (broken lines). Figs. 5.43–5.44 and Figs. 5.45–5.46 exhibit in a similar way the DWBA predictions for the standard optical and Michel potentials using all three interactions.

Figs. 5.47 and 5.48 compare the experimental data with the microscopic DWBA predictions using the molecular (solid lines), standard optical (broken lines) and Michel

(dotted lines) potentials. In all the cases, the finite-range corrections using R =0.7 fm and spectroscopic amplitude due to MSDI have been used.

5.2.4.3. Calculations of the spectroscopic factors:

In case of the ^{30}Si(α,d)^{32}P reaction the theoretical spectroscopic factors S_L^{σ} for a state populated through (L,J) transfer are deduced using the Eq. (5.18), such as,

$$S_L^{\sigma} = \left| G_{LJ} \right|^2 \Big/ \left| 0.56 \Omega_{00} \right|^2$$

Here $G_{67} = 0.56\Omega_{00}$ represents the structure factor for an unobserved state with $J_f^{\pi} = 7^+$, which has the stretched configuration $(f_{7/2})^2$, and the spectroscopic amplitude $\beta^{1/2} = 1.0$ with the assumption that the target does not have a component $(f_{7/2})$ in its wave function. The total spectroscopic factors are calculated from Eq. (5. 19).

The spectroscopic factors S_L^{σ} and the total spectroscopic factors S^{σ}, using three sets of spectroscopic amplitudes $\beta^{\frac{1}{2}}$ from the MSDI, RIP and KB interactions [45] have been calculated and noted in Tables 5.18 and 5.19. The theoretically predicted spectroscopic factors are also compared to the experimentally deduced values using all three (molecular, normal optical and Michel) types of potentials in Tables 5.18 and 5.19.

Table 5.17. Potential parameters used in the DWBA calculations for the $^{30}Si(\alpha,d)^{32}P$ reaction. V is the depth of the potential adjusted to give the separation energy.

Channel		$\alpha+^{30}Si$		$d+^{32}P$	d+d	$d+^{30}Si$
Type	Molecular[a]	Michel[a]	Optical[a]	Optical[b]	Bound state[c]	
V_0 (MeV)	27.0	25.0	190.84	102.7	V	V
R_0 (fm)	5.52	5.20	-	-	-	-
r_0 (fm)	-	-	1.15	1.07	1.05	0.935
a_0 (fm)	0.34	0.46	0.73	0.852	0.50	0.997
V_1 (MeV)	42.5	-	-	-		
R_1 (fm)	2.90	-	-	-		
α	-	7.12	-	-		
ρ (fm)	-	6.45	-	-		
W_0 (MeV)	17.0	34.0	13.0	-		
R_W (fm)	4.1	4.05	-	-		
r_I(fm)	-	-	1.51	-		
a_I(fm)	-	0.65	0.87	-		
W_D (MeV)	-	-	-	16.10		
r_D (fm)	-	-	-	1.53		
a_D (fm)	-	-	-	0.574		
V_{so}(MeV)	-	-	-	6.0		
r_{so} (fm)	-	-	-	1.07		
a_{so} (fm)	-	-	-	0.852		
r_C (fm)	-	1.30	1.20	1.15	1.25	1.3
R_C (fm)	9.46	-	-	-	-	-

[a] Present work.
[b] Ref. [48].
[c] Ref. [18].

Table 5.18. Cluster spectroscopic factors of the $^{30}Si(\alpha,d)^{32}P$ reaction extracted by molecular, optical and Michel potentials are compared to the theoretical shell-model factors for the MSDI, RIP and KB interactions. Factors are calculated from the spectroscopic amplitudes $\beta^{1/2}$ of Ref.[45] by the method outlined in [37].

E_x	J^π	Cluster Config.	Cluster Spectroscopic Factor			Shell-model Spectroscopic Factor S_L^σ		
(MeV)		N,L	A_L (molecular)	A_L (optical)	A_L (Michel)	MSDI	RIP	KB
0.0	1^+	2,0	0.60±0.18	19.80±4.95	12.00 ±3.6	0.007	0.079	0.0004
		1,2	0.40±0.12	13.00±3.25	8.00±2.4	0.210	0.089	0.014
0.08	2^+	1,2	0.24±0.07	0.90±0.23	1.40±0.42	0.083	0.017	0.002
1.15	1^+	2,0	0.25±0.08	1.00±0.22	6.67±2.1	0.014	0.001	0.025
		1,2	0.25±0.08	1.00±0.25	6.67±2.1	0.001	0.011	0.061
1.32	2^+	1,2	0.09±0.03	2.60±0.70	1.40±0.42	0.0001	0.008	0.007
1.75	3^+	1,2	0.48±0.14	1.29±0.32	7.89±2.40	0.015	0.041	0.0002
		0,4	0.32±0.09	0.85±0.26	5.26±1.60	0.078	0.029	0.116
2.26	2^+	1,2	0.16±0.05	4.00±1.10	4.00±1.30	0.002	0.002	0.005
2.74	1^+	2,0	0.18±0.05	1.06±0.27	5.06±1.50	0.014	0.012	0.009
		1,2	0.29±0.09	1.60±0.32	7.60±2.30	0.154	0.018	0.030
3.00	3^+	0,4	0.02±0.006	0.21±0.05	0.29±0.09	0.006	0.037	0.007
		1,2	0.14±0.04	1.92±0.48	1.93±0.58	0.042	0.001	0.020

Table 5.19. Total spectroscopic factors of the $^{30}Si(\alpha,d)^{32}P$ reaction deduced from the macroscopic calculation using the molecular, normal optical and Michel potentials are compared to the total spectroscopic factors calculated with the spectroscopic amplitudes $\beta^{1/2}$ of three interactions (MSDI, RIP and KB) from Ref. [45] by the method outlined in Ref. [37].

E_x (MeV)	J^π	L	Total spectroscopic factors $\sum A_L$			Total spectroscopic factors S^a		
			Macroscopic calculations			Microscopic calculations		
			Molecular	Optical	Michel	MSDI	RIP	KB
0.0	1^+	0+2	1.00	32.80	20.00	0.217	0.168	0.014
0.08	2^+	2	0.24	0.90	1.40	0.083	0.017	0.002
1.15	1^+	0+2	0.50	2.00	13.34	0.015	0.012	0.086
1.32	2^+	2	0.09	2.60	1.40	0.0001	0.008	0.007
1.75	3^+	2+4	0.80	2.14	13.15	0.093	0.070	0.116
2.66	2^+	2	0.16	4.00	4.00	0.002	0.002	0.005
2.74	1^+	0+2	0.47	2.66	12.66	0.168	0.030	0.039
3.00	3^+	2+4	0.16	2.13	2.22	0.048	0.038	0.027

Table 5.20. Spectroscopic amplitudes and normalization constant for transitions in the $^{30}Si(\alpha,d)^{32}P$ reaction using molecular potential

E_x (MeV)	J^π	Interaction	Spectroscopic amplitudes [a]						Normalization constants **		
			$d_{5/2}d_{5/2}$	$d_{5/2}s_{5/2}$	$d_{5/2}d_{3/2}$	$s_{1/2}s_{1/2}$	$s_{1/2}d_{3/2}$	$d_{3/2}d_{3/2}$	N_{MSDI}	N_{RIP}	N_{KB}
0	1^+	MSDI	+0.117	-	+0.056	+0.029	+0.337	-0.215	4.0×10^3	-	-
		RIP	-0.228	-	+0.122	-0.097	-0.008	+0.204	-	2.5×10^3	-
		KB	+0.011	-	+0.028	+0.015	-0.170	-0.091	-	-	4.0×10^3
0.08	2^+	MSDI	+0.074	-	-0.063	-	-0.401	-	6.0×10^2	-	-
		RIP	+0.062	-	+0.244	-	-0.044	-	-	1.5×10^3	-
		KB	-0.020	-	-0.026	-	+0.098	-	-	-	6.0×10^3
1.15	1^+	MSDI	-0.067	-	-0.050	-0.220	-0.054	-0.275	4.0×10^3	-	-
		RIP	+0.137	-	-0.061	+0.017	+0.033	+0.380	-	3.5×10^3	-
		KB	+0.005	-	-0.002	+0.219	-0.207	+0.123	-	-	4.0×10^4

[Continued...]

Table 5.20. [continued..]

Spectroscopic amplitudes and normalization constant for transitions in the $^{30}Si(\alpha,d)^{32}P$ reaction using molecular potential

E_x (MeV)	J^π	Interaction	Spectroscopic amplitude [a)]						Normalization constants**		
			$d_{5/2}d_{5/2}$	$d_{5/2}s_{1/2}$	$d_{5/2}d_{3/2}$	$s_{1/2}s_{1/2}$	$s_{1/2}d_{3/2}$	$d_{3/2}d_{3/2}$	N_{MSDI}	N_{RIP}	N_{KB}
1.32	2^+	MSDI	-	-0.057	-0.091	-	+0.124	-	2.3×10^3	-	-
		RIP	-	-0.056	-0.015	-	-0.064	-	-	4.6×10^3	-
		KB	-	-0.019	+0.049	-	-0.129	-	-	-	1.4×10^3
1.75	3^+	MSDI	+0.011	-0.061	+0.140	-	-	+0.344	3.8×10^3	-	-
		RIP	-0.040	-0.115	+0.258	-	-	-0.067	-	8.0×10^3	-
		KB	-0.021	+0.017	-0.001	-	-	+0.388	-	-	2.8×10^3
2.66	2^+	MSDI	-	-0.027	-0.160	-	+0.188	-	7.0×10^2	-	-
		RIP	-	+0.048	-0.013	-	-0.084	-	-	2.1×10^4	-
		KB	-	+0.001	-0.139	-	+0.000	-	-	-	6.0×10^3

[Continued...]

Table 5.20. [continued..]

Spectroscopic amplitudes and normalization constant for transitions in the $^{30}Si(\alpha,d)^{32}P$ reaction using molecular potential

E_x (MeV)	J^+	Interaction	Spectroscopic amplitude [a]						Normalization Constants **		
			$d_{5/2}d_{5/2}$	$d_{5/2}s_{1/2}$	$d_{5/2}d_{3/2}$	$s_{1/2}s_{1/2}$	$s_{1/2}d_{3/2}$	$d_{3/2}d_{3/2}$	N_{MSDI}	N_{RIP}	N_{KB}
2.74	1^+	MSDI	-0.045	+0.032	-	-0.040	-0.309	+0.243	$1.7x10^3$	-	-
		RIP	+0.039	-0.111	-	+0.044	+0.173	+0..31	-	$1.8x10^3$	-
		KB	+0.049	-0.031	-	+0.104	+0.233	+0.142	-	-	$9.8x10^2$
3.00	3^+	MSDI	+0.028	-0.115	-0.084	-	-	+0.173	$1.5x10^3$	-	-
		RIP	+0.121	+0.154	+0.019	-	-	+0.004	-	$1.5x10^4$	-
		KB	+0.028	+0.100	+0.120	-	-	-0.086	-	-	$3.0x10^3$

a) [45]

**N_{MSDI} = Normalization Constant using molecular potential and Spectroscopic amplitudes extracted from MSDI interaction;
N_{RIP}= Normalization Constant using molecular potential and Spectroscopic amplitudes extracted from RIPinteraction;
N_{KB}= Normalization Constant using molecular potential and Spectroscopic amplitudes extracted from KB interaction

Table 5.21. Spectroscopic amplitudes and normalization constant for transitions in the $^{30}Si(\alpha,d)^{32}P$ reaction using normal optical potential

E_x (MeV)	J^+	Interaction	Spectroscopic amplitudes [a]						Normalization constants [**]		
			$d_{5/2}d_{5/2}$	$d_{5/2}s_{5/2}$	$d_{5/2}d_{3/2}$	$s_{1/2}s_{1/2}$	$s_{1/2}d_{3/2}$	$d_{3/2}d_{3/2}$	N_{MSDI}	N_{RIP}	N_{KB}
0	1^+	MSDI	+0.117	-	+0.056	+0.029	+0.337	-0.215	4.8×10^4	-	-
		RIP	-0.228	-	+0.122	-0.097	-0.008	+0.204	-	3.0×10^4	-
		KB	+0.011	-	+0.028	+0.015	-0.170	-0.091	-	-	5.8×10^4
0.08	2^+	MSDI	+0.074	-	-0.063	-	-0.401	-	6.0×10^3	-	-
		RIP	+0.062	-	+0.244	-	-0.044	-	-	1.6×10^4	-
		KB	-0.020	-	-0.026	-	+0.098	-	-	-	7.0×10^4
1.15	1^+	MSDI	-0.067	-	-0.050	-0.220	-0.054	-0.275	4.0×10^4	-	-
		RIP	+0.137	-	-0.061	+0.017	+0.033	+0.380	-	6.0×10^4	-
		KB	+0.005	-	-0.002	+0.219	-0.207	+0.123	-	-	3.0×10^4

[Continued...]

Table 5.21. [continued..]

Spectroscopic amplitudes and normalization constant for transitions in the $^{30}Si(\alpha,d)^{32}P$ reaction using normal optical potential

E_x (MeV)	J^π	Interaction	Spectroscopic amplitude [a)]						Normalization constants**		
			$d_{5/2}d_{5/2}$	$d_{5/2}s_{1/2}$	$d_{5/2}d_{3/2}$	$s_{1/2}s_{1/2}$	$s_{1/2}d_{3/2}$	$d_{3/2}d_{3/2}$	N_{MSDI}	N_{RIP}	N_{KB}
1.32	2^+	MSDI	-	-0.057	-0.091	-	+0.124	-	2.0×10^4	-	-
		RIP	-	-0.056	-0.015	-	-0.064	-	-	4.2×10^4	-
		KB	-	-0.019	+0.049	-	-0.129	-	-	-	1.2×10^4
1.75	3^+	MSDI	+0.011	-0.061	+0.140	-	-	+0.344	8.0×10^3	-	-
		RIP	-0.040	-0.115	+0.258	-	-	-0.067	-	2.2×10^4	-
		KB	-0.021	+0.017	-0.001	-	-	+0.388	-	-	2.8×10^3
2.66	2^+	MSDI	-	-0.027	-0.160	-	+0.188	-	7.0×10^3	-	-
		RIP	-	+0.048	-0.013	-	-0.084	-	-	2.0×10^5	-
		KB	-	+0.001	-0.139	-	+0.000	-	-	-	6.5×10^4

[Continued...]

Table 5.21. [continued..]

Spectroscopic amplitudes and normalization constant for transitions in the $^{30}Si(\alpha,d)^{32}P$ reaction using normal optical potential

E_x (MeV)	J^+	Interaction	Spectroscopic amplitude [a]						Normalization Constants **		
			$d_{5/2}d_{5/2}$	$d_{5/2}s_{1/2}$	$d_{5/2}d_{3/2}$	$s_{1/2}s_{1/2}$	$s_{1/2}d_{3/2}$	$d_{3/2}d_{3/2}$	N_{MSDI}	N_{RIP}	N_{KB}
2.74	1^+	MSDI	-0.045	+0.032	-	-0.040	-0.309	+0.243	$1.5x10^4$	-	-
		RIP	+0.039	-0.111	-	+0.044	+0.173	+0..31	-	$1.5x10^4$	-
		KB	+0.049	-0.031	-	+0.104	+0.233	+0.142	-	-	$1.0x10^4$
3.00	3^+	MSDI	+0.028	-0.115	-0.084	-	-	+0.173	$7.0x10^3$	-	-
		RIP	+0.121	+0.154	+0.019	-	-	+0.004	-	$9.0x10^4$	-
		KB	+0.028	+0.100	+0.120	-	-	-0.086	-	-	$2.2x10^3$

a) [45]

**N_{MSDI} = Normalization Constant using normal optical potential and Spectroscopic amplitudes extracted from MSDI interaction;
N_{RIP}= Normalization Constant using normal optical potential and Spectroscopic amplitudes extracted from RIP interaction;
N_{KB}= Normalization Constant using normal optical potential and Spectroscopic amplitudes extracted from KB interaction

Table 5.22. Spectroscopic amplitudes and normalization constant for transitions in the $^{30}Si(\alpha,d)^{32}P$ reaction using Michel potential

E_x (MeV)	J^π	Interaction	Spectroscopic amplitudes [a]						Normalization constants [**]		
			$d_{5/2}d_{5/2}$	$d_{5/2}s_{5/2}$	$d_{5/2}d_{3/2}$	$s_{1/2}s_{1/2}$	$s_{1/2}d_{3/2}$	$d_{3/2}d_{3/2}$	N_{MSDI}	N_{RIP}	N_{KB}
0	1^+	MSDI	+0.117	-	+0.056	+0.029	+0.337	-0.215	6.0×10^4	-	-
		RIP	-0.228	-	+0.122	-0.097	-0.008	+0.204	-	3.9×10^4	-
		KB	+0.011	-	+0.028	+0.015	-0.170	-0.091	-	-	5.2×10^4
0.08	2^+	MSDI	+0.074	-	-0.063	-	-0.401	-	8.0×10^3	-	-
		RIP	+0.062	-	+0.244	-	-0.044	-	-	2.2×10^4	-
		KB	-0.020	-	-0.026	-	+0.098	-	-	-	6.0×10^4
1.15	1^+	MSDI	-0.067	-	-0.050	-0.220	-0.054	-0.275	6.0×10^4	-	-
		RIP	+0.137	-	-0.061	+0.017	+0.033	+0.380	-	6.0×10^4	-
		KB	+0.005	-	-0.002	+0.219	-0.207	+0.123	-	-	4.0×10^4

[Continued...]

Table 5.22. [continued..]

Spectroscopic amplitudes and normalization constant for transitions in the $^{30}Si(\alpha,d)^{32}P$ reaction using Michel potential

E_x (MeV)	J^π	Interaction	Spectroscopic amplitude [a)]						Normalization constants**		
			$d_{5/2}d_{5/2}$	$d_{5/2}s_{1/2}$	$d_{5/2}d_{3/2}$	$s_{1/2}s_{1/2}$	$s_{1/2}d_{3/2}$	$d_{3/2}d_{3/2}$	N_{MSDI}	N_{RIP}	N_{KB}
1.32	2^+	MSDI	-	-0.057	-0.091	-	+0.124	-	3.0×10^4	-	-
		RIP	-	-0.056	-0.015	-	-0.064	-	-	6.0×10^4	-
		KB	-	-0.019	+0.049	-	-0.129	-	-	-	2.0×10^4
1.75	3^+	MSDI	+0.011	-0.061	+0.140	-	-	+0.344		6.0×10^3	- -
		RIP	-0.040	-0.115	+0.258	-	-	-0.067	-	1.4×10^4	-
		KB	-0.021	+0.017	-0.001	-	-	+0.388	-	-	4.1×10^3
2.66	2^+	MSDI	-	-0.027	-0.160	-	+0.188	-	1.5×10^4	-	-
		RIP	-	+0.048	-0.013	-	-0.084	-	-	5.0×10^5	-
		KB	-	+0.001	-0.139	-	+0.000	-	-	-	1.7×10^5

[Continued...]

Table 5.22. [continued..]

Spectroscopic amplitudes and normalization constant for transitions in the $^{30}Si(\alpha,d)^{32}P$ reaction using Michel potential

E_x (MeV)	J^+	Interaction	Spectroscopic amplitude [a]						Normalization Constants **		
			$d_{5/2}d_{5/2}$	$d_{5/2}s_{1/2}$	$d_{5/2}d_{3/2}$	$s_{1/2}s_{1/2}$	$s_{1/2}d_{3/2}$	$d_{3/2}d_{3/2}$	N_{MSDI}	N_{RIP}	N_{KB}
2.74	1^+	MSDI	-0.045	+0.032	-	-0.040	-0.309	+0.243	2.5×10^4	-	-
		RIP	+0.039	-0.111	-	+0.044	+0.173	+0..31	-	3.0×10^4	-
		KB	+0.049	-0.031	-	+0.104	+0.233	+0.142	-	-	1.8×10^4
3.00	3^+	MSDI	+0.028	-0.115	-0.084	-	-	+0.173	3.0×10^3	-	-
		RIP	+0121	+0.154	+0.019	-	-	+0.004	-	1.5×10^5	-
		KB	+0.028	+0.100	+0.120	-	-	-0.086	-	-	6.0×10^3

a) [45]

**N_{MSDI} = Normalization Constant using Michel potential and Spectroscopic amplitudes extracted from MSDI interaction;
N_{RIP}= Normalization Constant using Michel potential and Spectroscopic amplitudes extracted from RIP interaction;
N_{KB}= Normalization Constant using Michel potential and Spectroscopic amplitudes extracted from KB interaction

Table 5.23. Comparison of the normalization constants extracted by zero-range DWBA calculations for $^{29}Si(\alpha,d)^{31}P$ and $^{30}Si(\alpha,d)^{32}P$ reactions by using the spectroscopic amplitudes of MSDI, RIP, and KB interactions.

(a) Normalization Constants for $^{29}Si(\alpha,d)^{31}P$ Reaction

E_x MeV,	Molecular			Normal optical			Michel		
	N_{MSDI}	N_{RIP}	N_{KB}	N_{MSDI}	N_{RIP}	N_{KB}	N_{MSDI}	N_{RIP}	N_{KB}
0.0	55	100	2200	900	9500	1500	550	7000	12000
1.27	500	1700	8000	6000	2200	8900	3200	1100	40000
2.23	400	460	3000	6500	7300	50000	1900	2100	17000
3.13	80	610	50	1200	1500	500	550	19000	300
3.30	180	270	2300	4000	90000	8000	2200	4400	43000
3.41	800	18000	1100	14000	280000	20000	800	40000	1000
3.51	1100	700	1300	15000	11000	16000	80000	7000	8000
4.19	3800	4500	1500	500000	500000	18000	22000	30000	10000
4.26	590	2500	3400	11000	40000	58000	5900	25000	34000

(b) Normalization Constants for $^{30}Si(\alpha,d)^{32}P$ Reaction.

E_x MeV,	Molecular			Normal optical			Michel		
	N_{MSDI}	N_{RIP}	N_{KB}	N_{MSDI}	N_{RIP}	N_{KB}	N_{MSDI}	N_{RIP}	N_{KB}
0.0	4000	2500	4000	48000	30000	58000	60000	39000	52000
0.08	600	1500	6000	6000	16000	70000	8000	22000	60000
1.15	4000	3500	40000	40000	60000	30000	60000	60000	40000
1.32	2300	4600	1400	20000	42000	12000	30000	60000	20000
1.75	3800	8000	2800	8000	22000	2800	6000	14000	4100
2.66	700	21000	6000	7000	200000	65000	15000	$5x10^5$	170000
2.74	1700	1800	980	15000	15000	10000	30000	25000	30000
3.00	1500	15000	3000	7000	90000	2200	3000	150000	6000

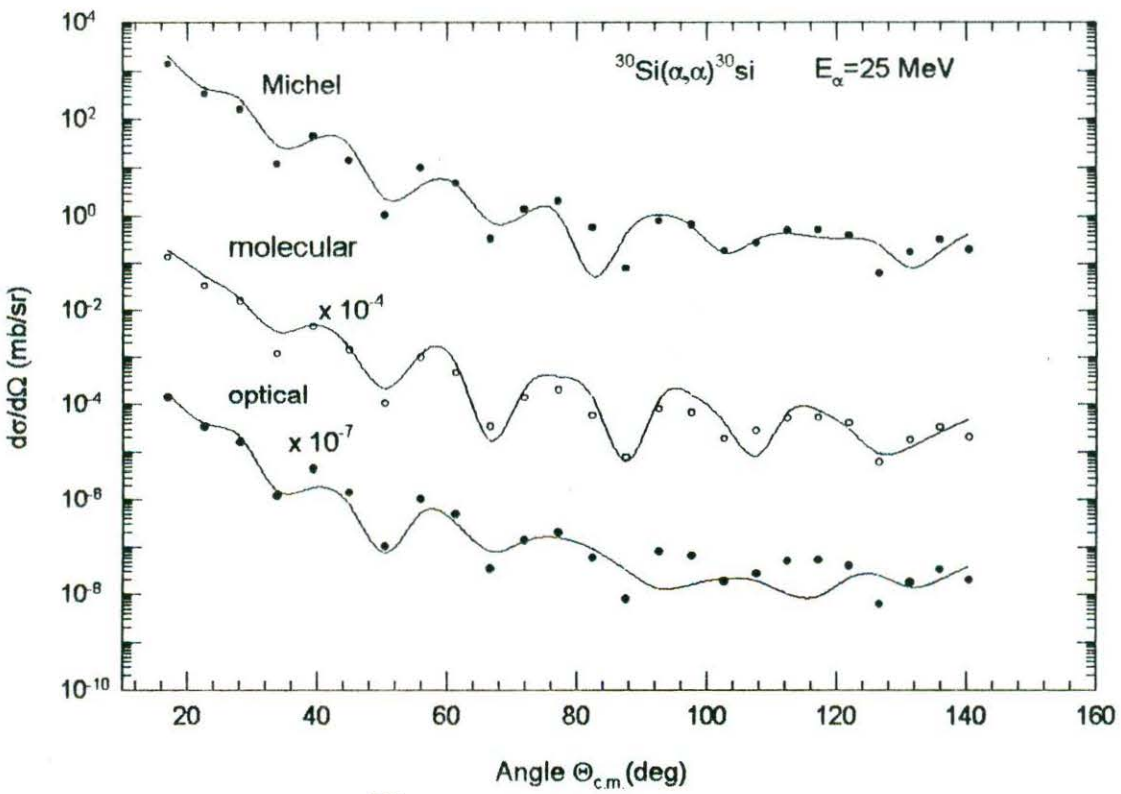

Fig. 5. 37. Fits to the α-^{30}Si elastic scattering data at 25 MeV (lab) with the Michel, molecular and normal optical potentials. Data are from [45]

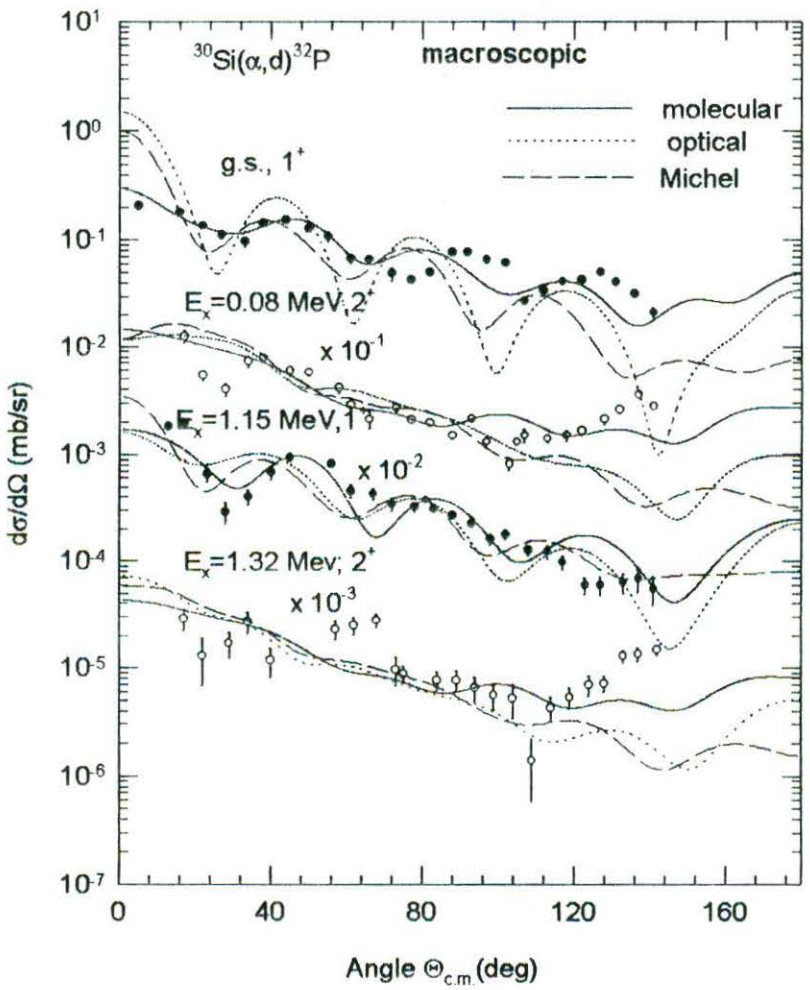

Fig. 5. 38. Comparison of the full finite-range macroscopic DWBA calculations for the ^{30}Si(α,d)^{32}P reaction at 25 MeV leading to ground (1$^+$), 0.08 (2$^+$), 1.15 (1$^+$), and 1.32(2$^+$) MeV states of ^{32}P to the differential cross-section data. The solid, dotted and broken curves are the predictions using the molecular, nórmal optical and Michel α-^{29}Si potentials respectively. Data are from [48].

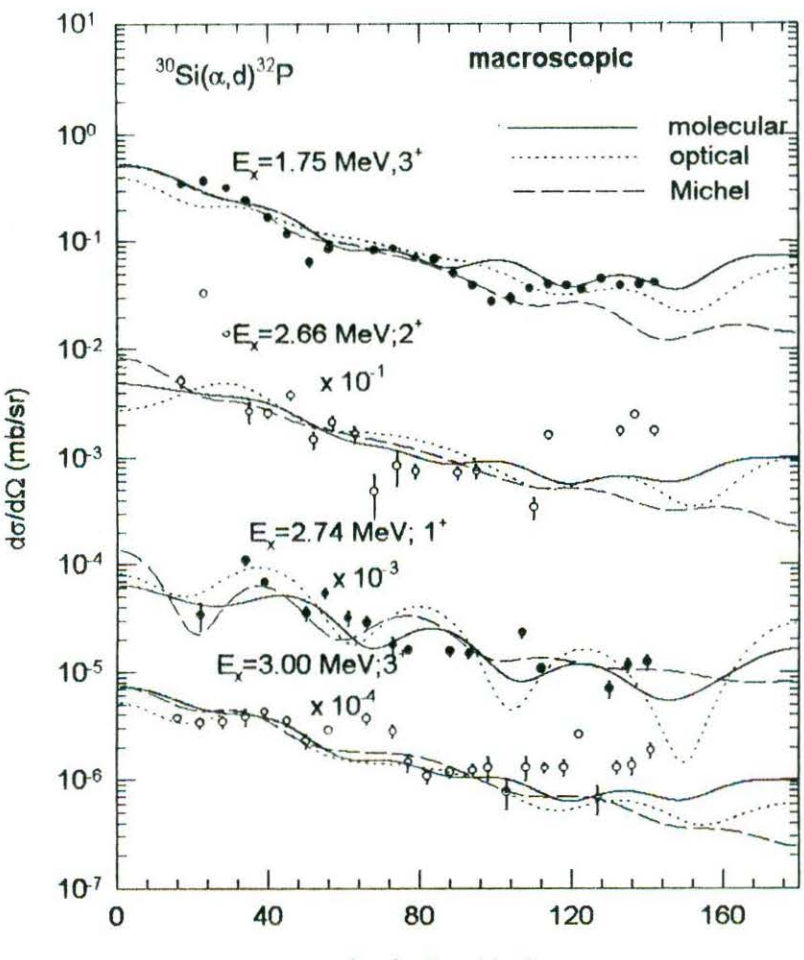

Fig.5.39. Same as in Fig. 5.38 for 1.75 (3^+), 2.66 (2^+), 2.74 (1^+) and 3.00(3^+) MeV states of ^{32}P. Data are from [48].

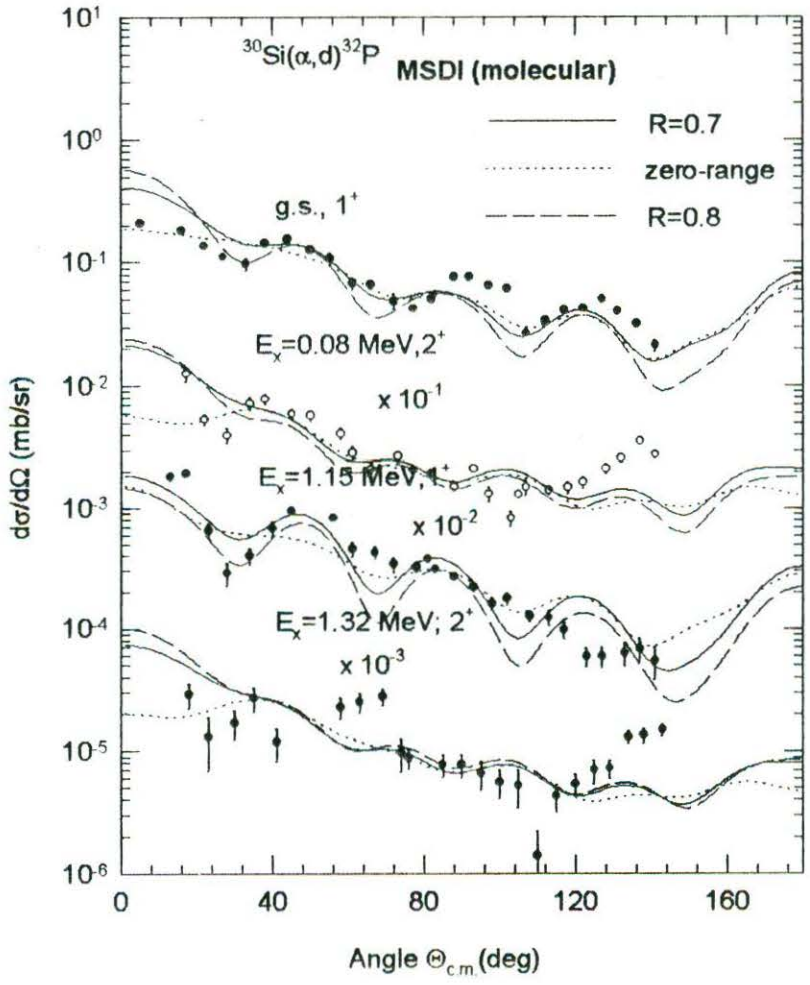

Fig.5.40. Comparison of the zero-range microscopic DWBA calculations using the MSDI spectroscopic amplitudes and the molecular potential in the α-channel for the ^{30}Si(α,d)^{32}P reaction at 25 MeV leading to the ground (1^+), 0.08 (2^+), 1.15(1^+), and 1.32 (2^+) MeV states of ^{32}P to the differential cross-section data. The solid curves are the predictions using the finite-range (FR) correction with R=0.7 fm. The broken and the dotted curves are the predictions with R=0.0 and 0.85 fm. respectively. Data are from [48].

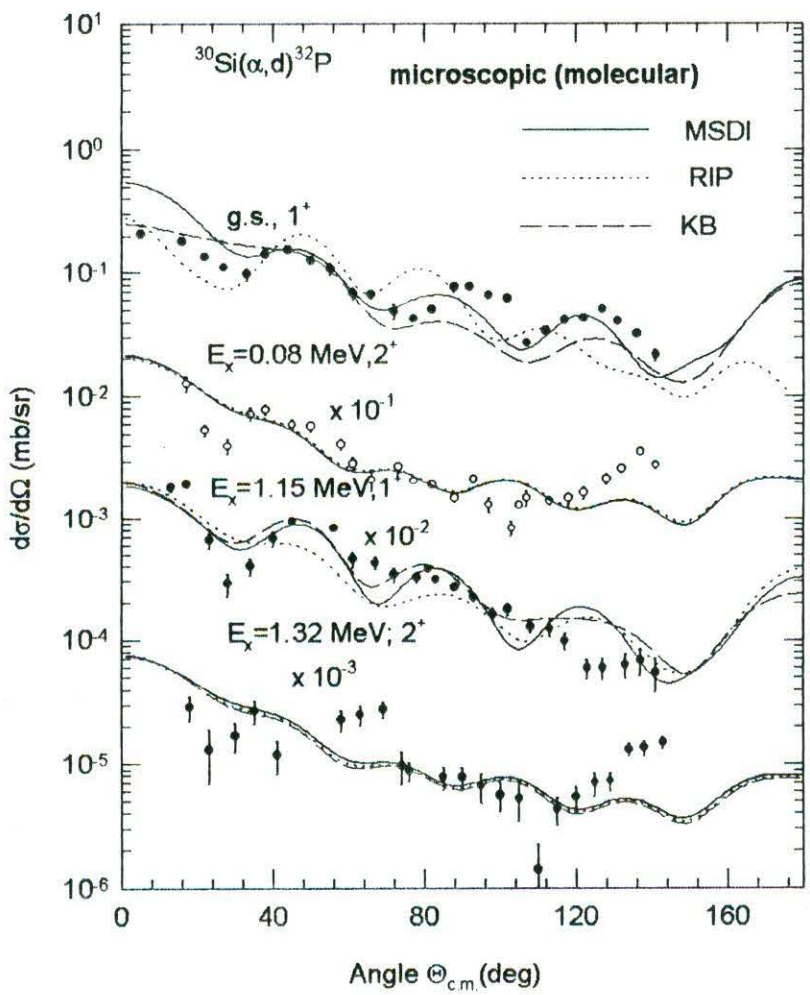

Fig. 5.41. Comparison of the zero-range microcopic DWBA calculations with FR correction (R=0.7 fm.) and the molecular potential for ^{30}Si(α,d)^{32}P reaction leading to the g.s. (1^+), 0.08 (2^+), 1.15(1^+), and 1.32 (2^+) MeV states of ^{32}P to the differential cross-section data. The solid broken and dotted curves are the predictions using the MSDI, RIP, and KB interactions respectively. Data are from [48].

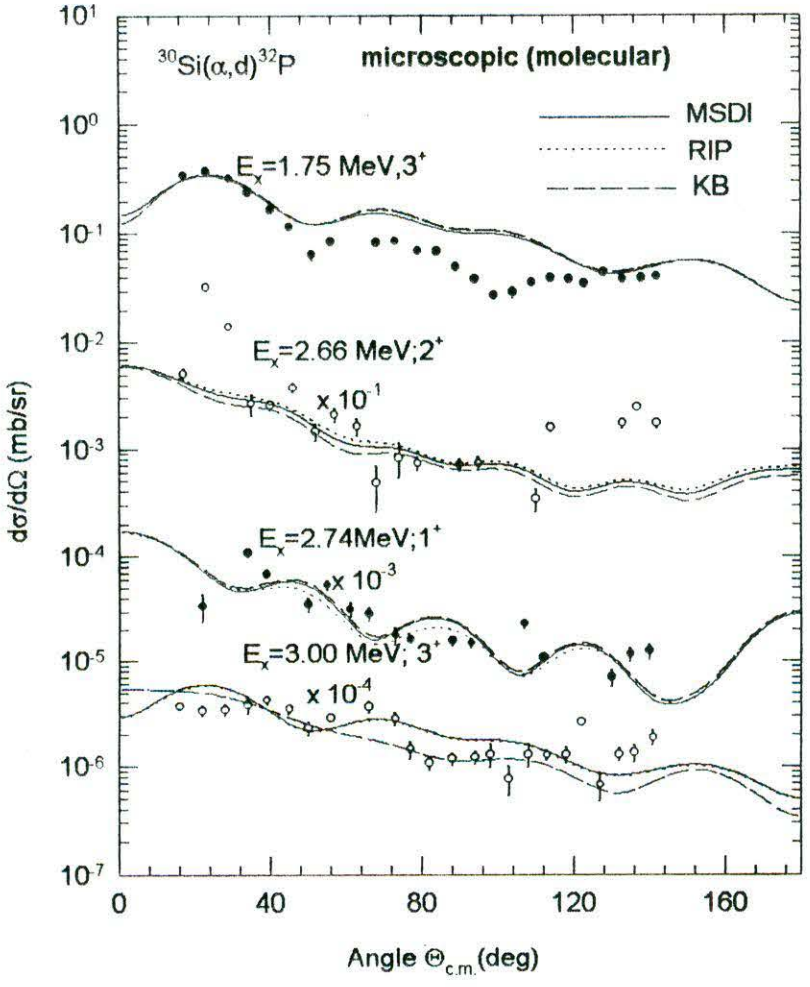

Fig. 5.42. Same as in Fig. 5.41 for the 1.75(3^+), 2.66(2^+) and 3.00(3^+) MeV states of ^{32}P. Data are from [48].

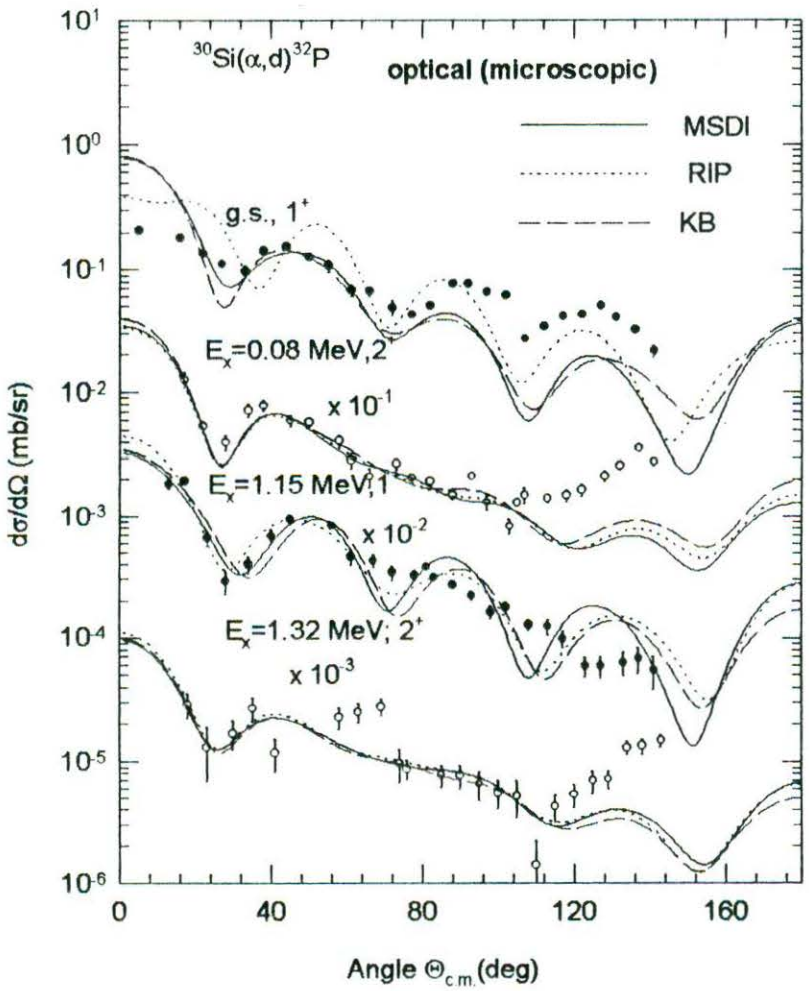

Fig. 5.43. Same as in Fig. 5.41 using normal optical potential. Data are from [48].

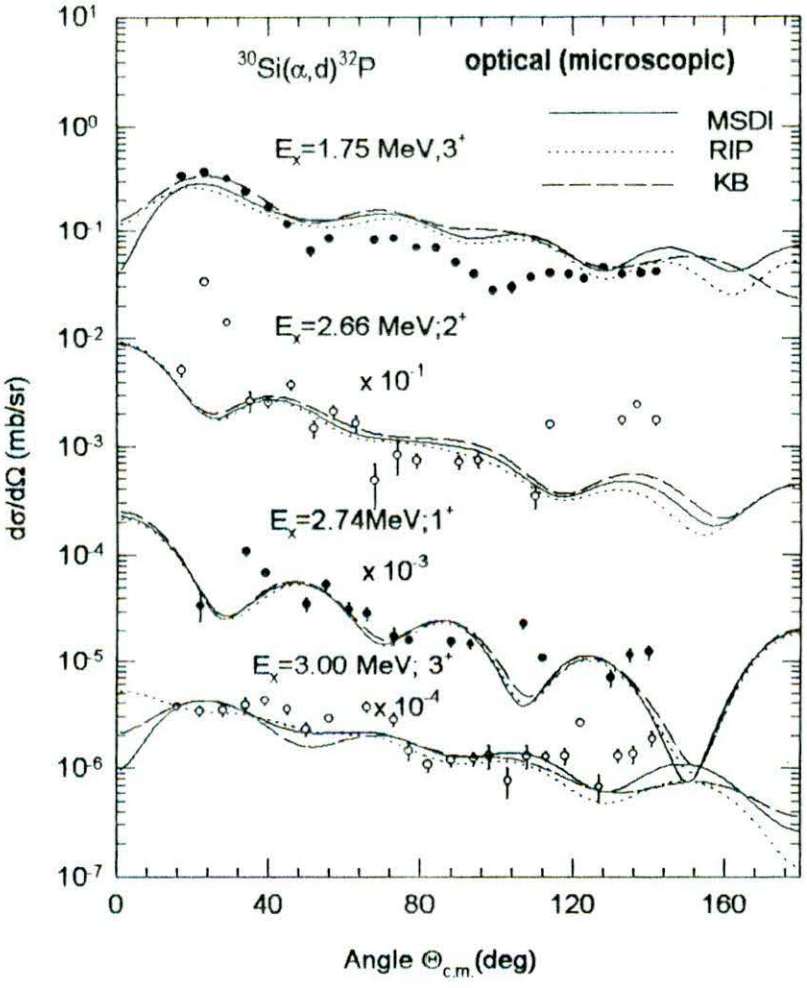

Fig. 5. 44. Same as in Fig. 5.42 using normal optical potential. Data are from [48].

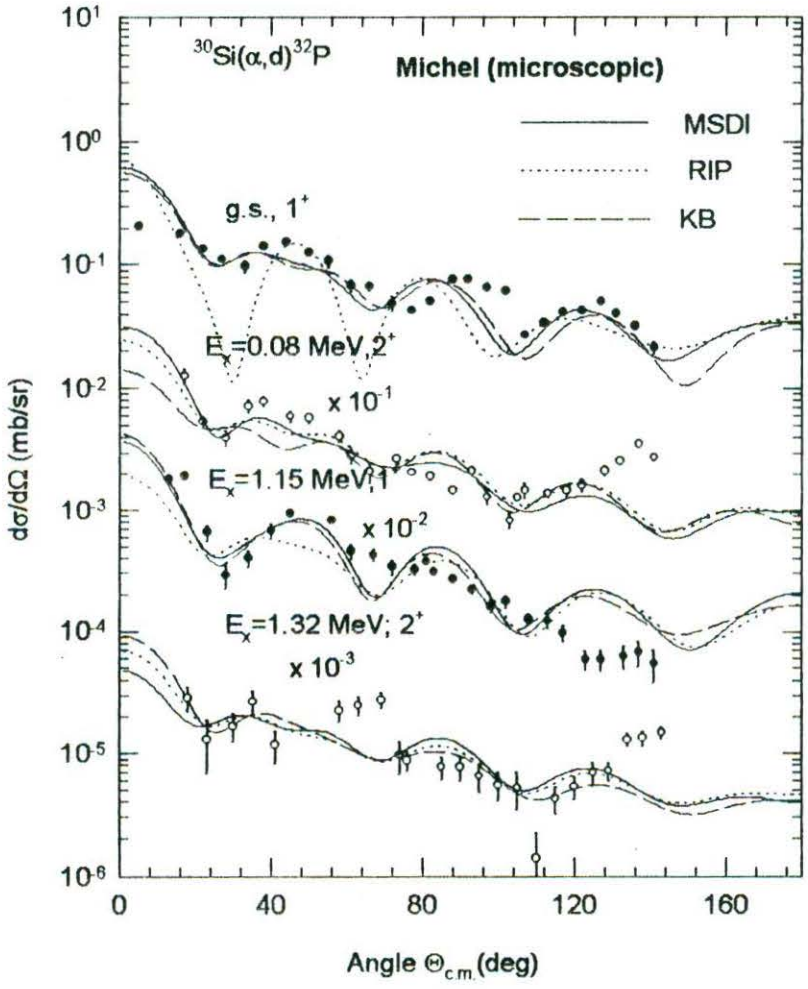

Fig.5.45. Same as in Fig. 5. 41 using Michel potential. Data are from [48].

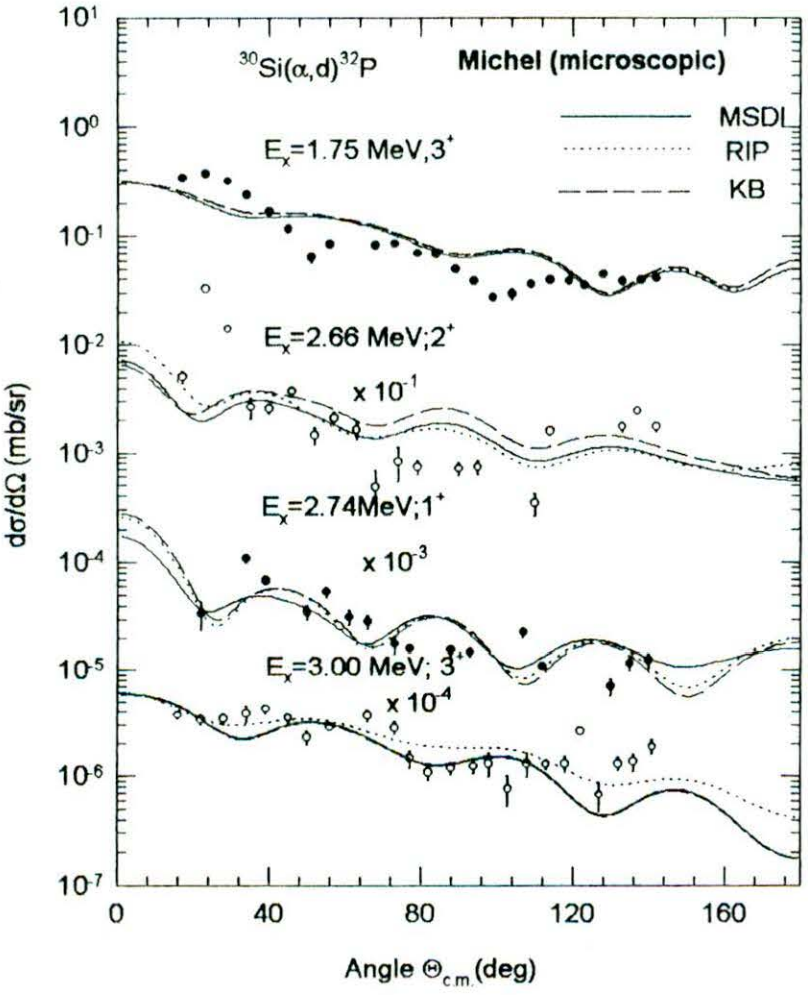

Fig. 5. 46. Same as in Fig. 5. 42 using Michel potential. Data are from [48].

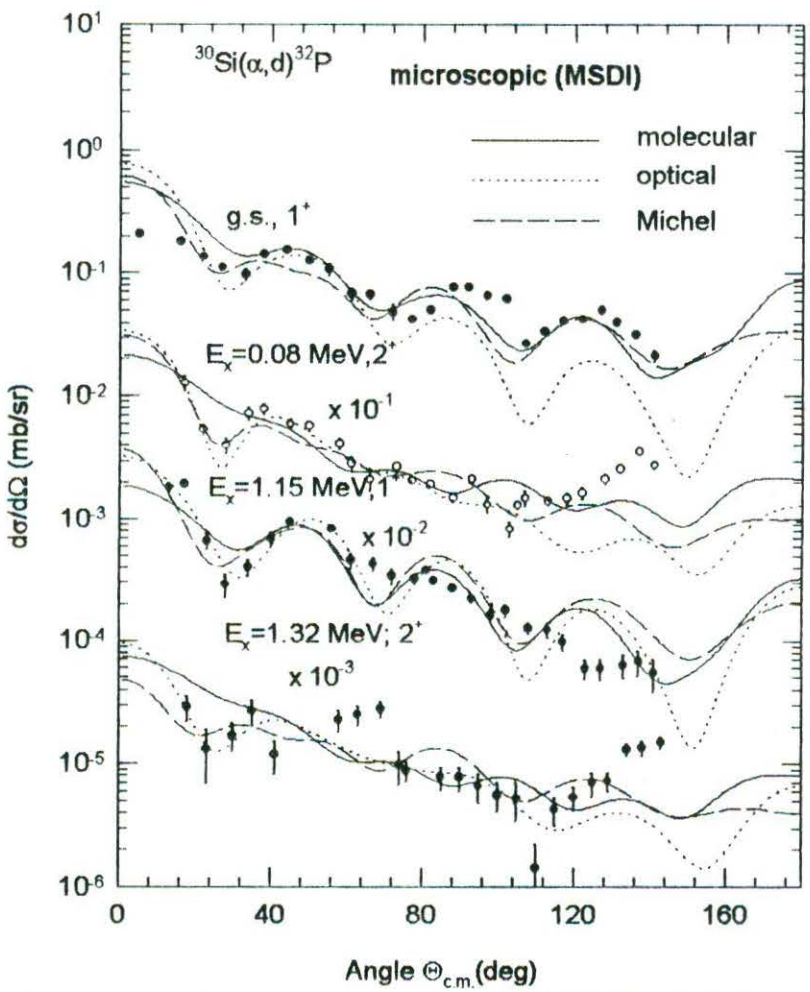

Fig. 5. 47. Comparison of the zero-range microscopic DWBA calculations using the MSDI spectroscopic amplitudes and the molecular, normal optical and Michel potentials in the α-channel for the ^{30}Si(α,d)^{32}P reactions at 25 MeV leading to the ground (1^+), 0.08 (2^+), 1.15(1^+), and 1.32(2^+) MeV states of ^{32}P to the differential cross-section data. The solid, dotted and broken curves are the predictions using the molecular, normal optical and Michel potentials respectively. Data are from [48].

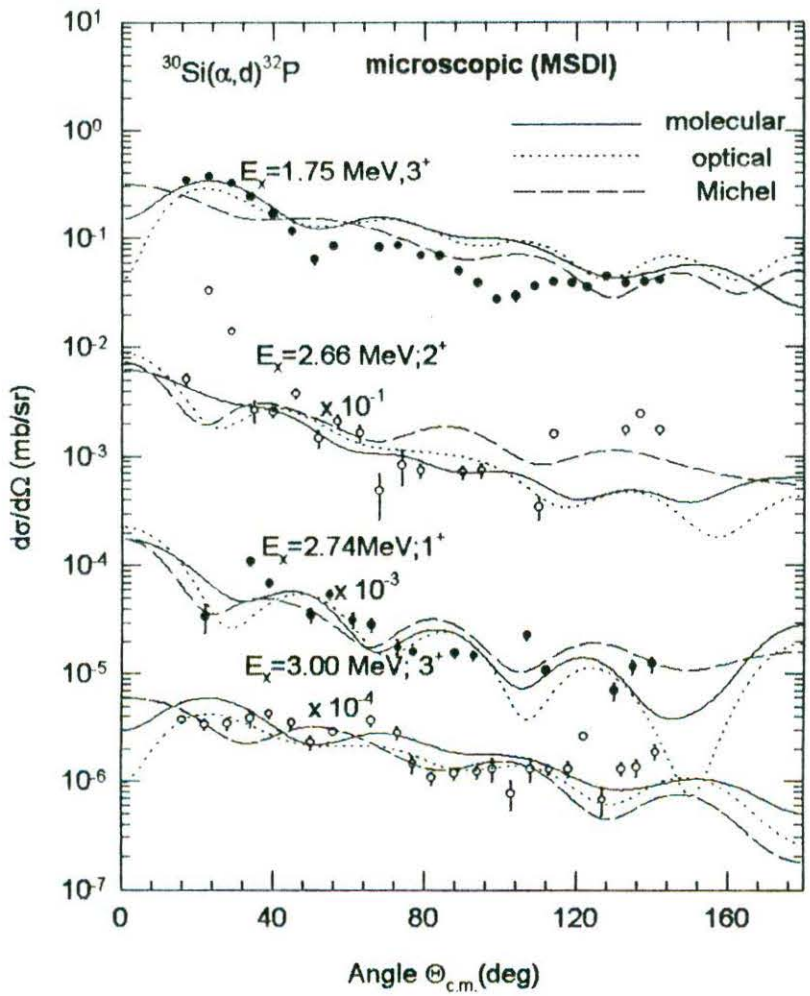

Fig. 5. 48. Same as in Fig. 5. 47. for 1.75(3^+), 2.66(2^+), 2.74(1^+), and 3.00(3^+) MeV states. Data are from [48].

5.2.5. DWBA analysis of the $^{28}Si(\alpha,p)^{31}P$ reaction

The zero-range DWBA calculations have been performed using the code DWUCK4 [39]. The potential parameters in the distorting incident channel used in the DWBA calculations are noted in Table 5.24 for all four potentials. The bound state wave function for the transferred triton, considered as a point cluster, has been generated by assuming a real Woods-Saxon well with its depth adjusted to reproduce the separation energy. These parameters along with the proton optical potential are also noted in Table 5.43. Corrections due to non-locality [32,39] of potential in the conventional form have been applied using the non-locality ranges $\beta(\alpha)$=0.2, $\beta(t)$=0.2 and $\beta(p)$=0.85 fm. The correction in the triton-bound state form-factor is found to produce little effect on the cross-section. The calculations using all four potentials for the $^{28}Si(\alpha,p)^{31}P$ reaction leading to the ground $1/2^+$, 1.266 MeV $3/2^+$ and 2.234 MeV $5/2^+$ states are compared with the data of Jankowski *et al.*[18] in Fig. 5.49.

To test the validity of using the molecular potential, the full finite-range DWBA calculations have been carried out using the code DWUCK5 [39]. The (t+p) bound state geometry for the FFR calculations is shown in Table 5.24. The FFR predictions are compared to the data in Fig. 5.50. The spectroscopic factors S for the cluster transfer have been deduced from the expression [39]

$$\left(\frac{d\sigma}{d\Omega}\right)_{expt} = \frac{\left(2J_f+1\right)}{\left(2J_i+1\right)} C^2 Ss \left(\frac{d\sigma}{d\Omega}\right)_{DWUCK5} \qquad (5.22)$$

Here $\left(\frac{d\sigma}{d\Omega}\right)_{expt}$ and $\left(\frac{d\sigma}{d\Omega}\right)_{DWUCK5}$ are, respectively, the experimental cross-section and that predicted by DWUCK5. J_f and J_i are the total spins of the final and initial nuclei, respectively. s=2.0 is the light particle spectroscopic factor. C^2 is the isospin Clebsch-Gordon coefficient. The deduced S-values are listed in Table 5.25. The normalization constant D_0^2 for the t-cluster transfer in the ZR calculations has been estimated from the expression [39].

$$\left(\frac{d\sigma}{d\Omega}\right)_{expt} = \frac{(2J_f+1)}{(2J_i+1)(2j+1)} D_0^2 C^2 S \left(\frac{d\sigma}{d\Omega}\right)_{DWUCK4} \qquad (5.23)$$

Here $\left(\frac{d\sigma}{d\Omega}\right)_{DWUCK4}$ predicted cross-section by DWUCK4. The deduced D_0^2 values and the average $D_0^2 = 2.25 \times 10^4$ MeV^2 fm^3 have been shown in Table 5.25.

It is evident, from Fig.5.50, that the FFR calculations do not improve fits over the ZR predictions and reduce the cross-sections at larger reaction angles even more. Nevertheless, the FFR calculations allow us to extract the spectroscopic factors.

5.2.6. CCBA analysis of the $^{28}Si(\alpha,p)^{31}P$ reaction

The CCBA calculations using the molecular potential have been carried out using the code CHUCK3 [39]. The coupling scheme which associates the deformation parameters β_2 = -0.18 and β_4 = +0.08 for ^{28}Si is shown in Fig.5.51. In the CCBA calculations, the depth of the imaginary part of the molecular potential (Table 5.24) has been decreased to 10.5 MeV in order to reproduce the angular distribution for the elastic scattering. All possible relative phases and various relative transition amplitudes a_R in the

rearrangement paths have been tried in the simplest possible coupling scheme. The transition strength in a two-step path is proportional to the square of $|\beta a_R|$. The CCBA predictions using the relative spectroscopic amplitudes noted in Table 5.25 for the ground ($1/2^+$), 1.266 ($3/2^+$), 2.234 ($5/2^+$) and 3.415 ($7/2^+$) MeV state transitions have been compared to the data in Fig.5.50.

Table 5.24. Parameters of the α-^{28}Si potentials used in the DWBA calculations for $^{28}Si(\alpha,p)^{31}P$ reaction are given in columns 1 to 5. The parameters of proton optical-model potential, and bound states of ($t+^{28}Si$) and ($t+p$) systems are noted in columns 6-8, respectively. V is adjusted to give the separation energy.

Channel	$\alpha + ^{28}Si$				$p + ^{31}P$	$t + ^{28}Si$	$t + p$
Potential Type	Molecular [a]	Michel [a]	Deep [a] Optical	Shallow [b] Optical	Optical [c]	Bound [b] State	Bound [b] State
V_o(MeV)	26.0	21.0	216.0	55.0	53.3 - 0.55 E_p	V	V
R_o (fm)	5.35	5.00	3.70	5.16	-	-	-
r_o (fm)	-	-	-	-	1.25	0.929	1.05
a_o (fm)	0.340	0.60	0.67	0.505	0.65	0.921	0.50
V_1(MeV)	42.0	-	-	-	-	-	-
R_1 (fm)	2.80	-	-	-	-	-	-
α	-	8.39	-	-	-	-	-
ρ (fm)	-	6.25	-	-	-	-	-
W_o(MeV)	14.5	33.1	22.4	8.64	-	-	-
R_I (fm)	-	3.85	3.98	5.16	-	-	-
a_I (fm)	-	0.65	0.67	0.505	-	-	-
R_W (fm)	4.00	-	-	-	-	-	-
W_D(MeV)	-	-	-	-	13.5	-	-
r_D (fm)	-	-	-	-	1.25	-	-
a_D (fm)	-	-	-	-	0.47	-	-
R_C (fm)	9.35	3.95	4.07	3.95			
r_c (fm)					1.30	1.30	1.25

a) Ref. [19]
b) Ref.[18].
c) Ref.[156].

Table 5.25. Cluster transfer configurations (n: number of nodes, L: angular momentum) used in the CCBA are shown in columns 3 to 6. Column 7 indicates the relative spectroscopic factors used in calculations of the $^{28}Si(\alpha,p)^{31}P$.

E_x (^{31}P)	J^π	Cluster transfer configuration					Spect. Factor S	$D_o^2 \times 10^4$ MeV^2 fm^3
		One-step	Two-step			Relative Spect. Amplitudes		
		nL_d	nL_{t1}	nL_{t2}	nL_{t3}			
0.0	$1/2^+$	3S	1G	-	-	+01:+15	0.070	2.00 ± 0.50
1.266	$3/2^+$	2D	2D	3S	-	+01:+05:-05	0.031	2.56 ± 0.64
2.234	$5/2^-$	2D	2D	3S	1G	+01:+01:+02:-01	0.004	-
3.415	$7/2^-$	2G	3D	4S	-	+01:+06:+02	0.003	-

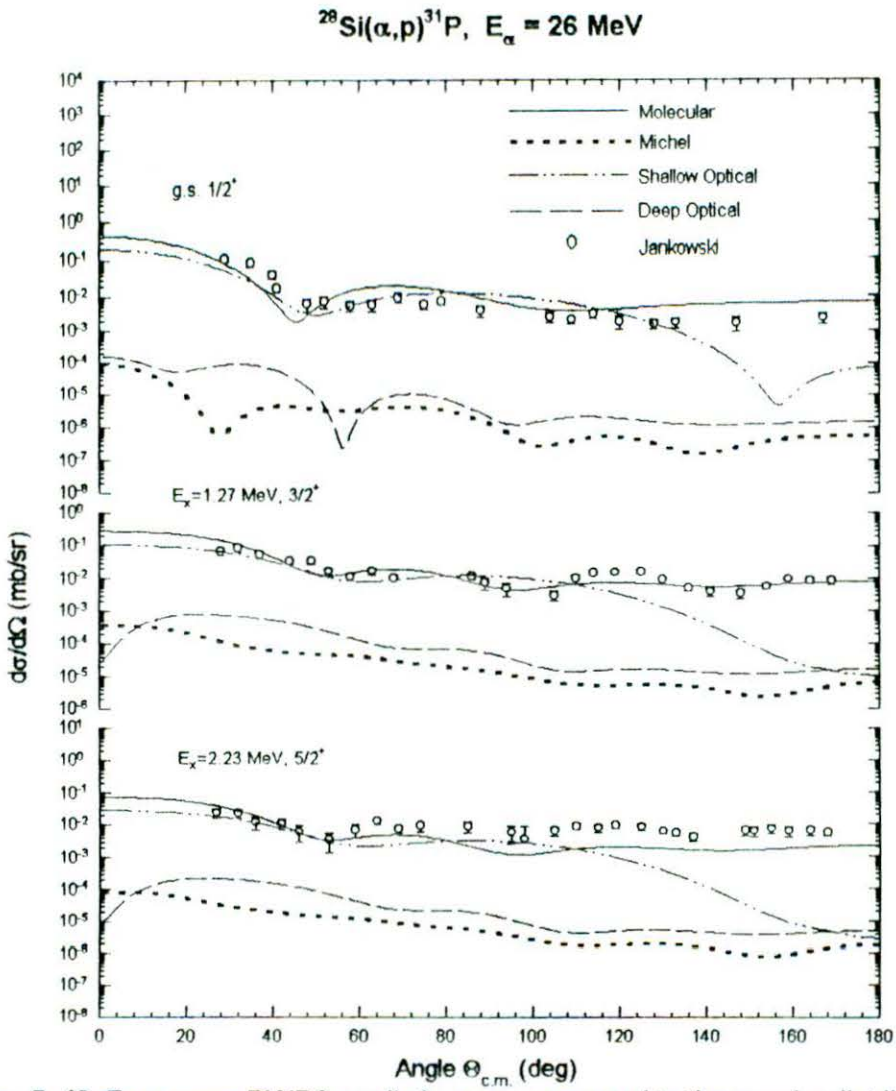

Fig. 5. 49. Zero-range DWBA predictions are compared to the angular distribution of cross-sections for the $^{28}Si(\alpha,p)^{31}P$ reaction at 26 MeV leading to the ground($1/2^+$), 1.27 ($3/2^+$), and 2.234 ($5/2^+$) MeV states. Solid, dotted, dashed and dash-dotted curves are the predictions for the molecular, Michel, deep and shallow normal optical potentials respectively, in the α-channel. Data are from [18].

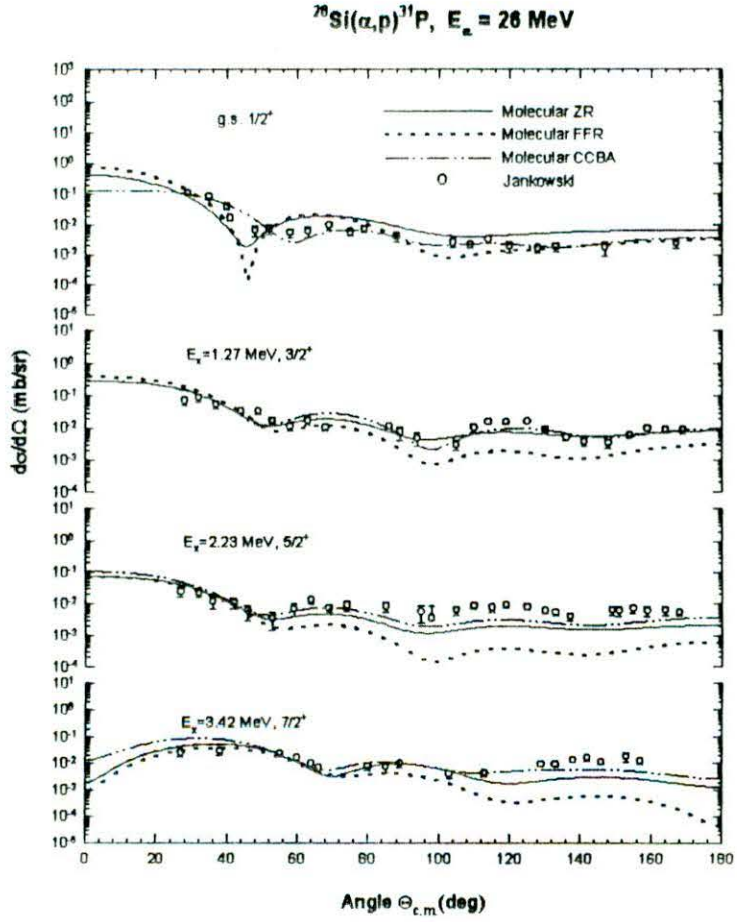

Fig.5.50. Zero-range (solid), full finite-range(dotted lines) and CCBA (dashed lines) predictions of the transfer reaction using the molecular potential are compared to the data for the $^{28}Si(\alpha,p)^{31}P$ reaction at 26 MeV leading to the ground ($1/2^+$), 1.27 ($3/2^+$), 2.23 ($5/2^+$), 3.42 ($7/2^+$) MeV states. Data are from [18].

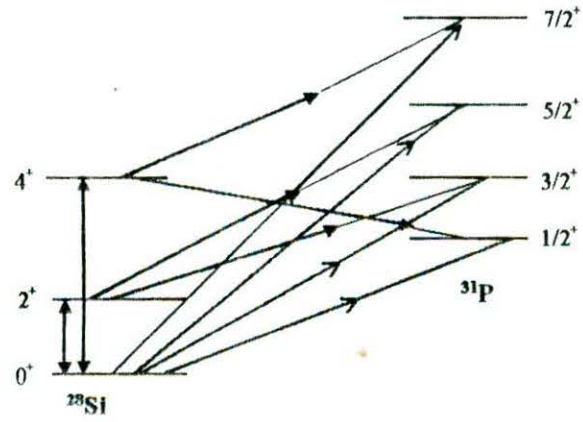

Fig. 5. 51 Coupling scheme in the CCBA calculations..

CHAPTER 6

RESULTS AND DISCUSSION

The molecular and Michel potential fits to the $^{27}Al(\alpha,\alpha)^{27}Al$ data (Fig. 5.1) as well as fits to the $^{29,30}Si(\alpha,\alpha)^{29,30}Si$ data using the molecular, normal optical and Michel potential in the present work (Figs. 5.20, 5.37) are more or less of the same quality. All three cases lack experimental data at the large angles. But, the elastic data on ^{28}Si has a wide angular range. The large angle behaviour of angular distribution including ALAS which cannot be accounted for by the normal (WS) optical potential [4,9], has been shown to be a sensitive probe for determining the α-nucleus potential [6,19-21,28,29,56]. However, the initial potential parameters for elastic scattering on $^{29,30}Si$ are scaled from the parameters of the α-^{28}Si potential deduced on the basis of seven-point angular distributions spanning the 14.47–45.0 MeV incident energy range and covering a wide angular range in the elaborate work of Tariq *et al.* [19]. So, the parameters of the α-$^{29,30}Si$ potential parameters are expected to be reasonable. On the other hand, the molecular and Michel α-^{27}Al potentials, deduced in the present work on the basis of a narrow angular distribution ($\theta_{c.m} < 80^0$) at one-point incident energy of 64.5 MeV which is outside the energy range of the work of Tariq *et al.* [19], may not be final. In spite of the possible limitations of the α-^{27}Al potential, the DWBA analyses in the present work on the $^{27}Al(\alpha,t)^{28}Si$, $^{28,29,30}Si(\alpha,d)^{30,31,32}Si$ and $^{28}Si(\alpha,p)^{31}P$ reactions using the parameters of all three (molecular, normal optical and Michel) form of potentials reveal some valuable

facts. The following sections exhibit step by step the results and the relevant discussion on these.

6.1. The $^{27}Al(\alpha,t)^{28}Si$ reaction

In the present study, 53 transitions have been analyzed with all three types of potentials. The analyses involve: (i) 4 transitions with the l=2 transfers (Fig. 5.4) leading to the ground, 4.98 and 6.69 MeV states with the unique j=5/2 transfer and the 12.33 MeV state which is assumed to be populated *via* j=3/2; (ii) 11 transitions with l=3 (Fig.5.5); (iii) 9 transitions with l=4 (Fig. 5.6); (iv) 11 transitions with the admixture l=0+2 (Fig. 5.7); (v) 7 transitions with the admixture l=1+3 (Fig. 5.8); (vi) 1 transition with l=2+3 (Fig. 5.8) populating probably two unresolved states with opposite parities at about E_x =6.88 MeV and (vii) 11 transitions with the admixture l=2+4 (Fig. 5.9). The data of the transition to the 11.97 MeV state are compared to the DWBA predictions twice, one in Fig. 5.8 for the l=1+3 transfer and another in Fig. 5.9 for the l=2+4 transfer, as both transfers produce similar quality and acceptable fits to the data.

In Fig. 5.3 the FFR and ZR calculations are compared to the angular distribution data for transitions to the ground and E_x= 11.58 MeV states. The improvement of the fits due to predictions of the former over those of the latter underlines the importance of the FFR calculations.

It is evident from Figs. 5.4-5.9 that the full finite-range DWBA analyses using the molecular and normal optical potentials, fit quite satisfactorily the experimental data of the 44 transitions out of 53 with 9 other states fitted moderately. In general, the fits with

the molecular and normal optical potentials seem to be of the same quality, but the fits with the Michel potential are comparatively poor. At forward scattering angles < 20^0 or so, all three potentials yield, to some extent, the same results. But, at larger scattering angles, for the bound state transitions with the excitation energies up to 11.58 MeV, the molecular potential provides a better fit, although the normal optical potential competes reasonably well and the Michel potential seems to be inferior. However, all three types of potentials reproduces the absolute cross-sections, as reflected in the deduced spectroscopic factors [Table 5.2]. For the continuum states with the excitation energies above 11.58 MeV both the molecular and normal optical potentials yield again comparable results with quite reasonable fits to the data, but the Michel potential seems inadequate. At reaction angles larger than 30^0, the difference in the predictions due to the three distorting α-nucleus potentials, becomes very prominent and increases with the reaction angle. It is also to be mentioned that for transitions to the 4.98, 6.69, 8.54, 10.21 and 12.24 MeV states, neither of the three types of potentials could produce good fits to the angular distributions, indicating the probable contribution of reaction mechanisms other than the direct one that may be involved in these cases.

Yasue *et al.* [44] reported that an admixture of l=1, 2 and 3 was needed to fit the data of the levels at E_x = 6.88 and 6.89 MeV, but in the present study an admixture of l=2 and 3 suffices to fit satisfactorily the angular distributions of these unresolved levels (Fig. 5.8). Furthermore, they [44] used the l=0+2+4 admixture for the 7.93 and 8.26 MeV transitions, while in the present work l=0+2 seems to be sufficient to fit the data quite well (Fig. 5.7). Moreover, as mentioned earlier, Yasue *et al.* [44] associated the 15.02,

15.85 and 16.11 MeV transitions with the l=3 transfer, but the comparison of the predictions in the present analyses for l=3 and 4 in Fig. 5.10 for each of the three potentials, show that the angular distributions for these transitions are better fitted by the l=4 transfer. It is also obvious from Fig. 5.10 that the predictions with the molecular potential bring out the difference more distinctly between the angular patterns for the l=3 and l=4 transfers.

The spectroscopic factors (Table 5.2) extracted using the molecular potential are comparable to those obtained using the normal optical potential, but are a bit larger for some cases. In general, the spectroscopic factors deduced from using the Michel potential are even larger. Considering the quality of fits, the spectroscopic factors obtained with the Michel potential are expected to be less reliable.

The spectroscopic strengths extracted from the use of the molecular potential are compared to those calculated from the shell-model [143] in Table 5.3. The predicted and deduced strengths agree for most of the l=2 transitions except that for the the 6.89 MeV state. The extracted strengths for the l=0 transitions to the 1.78, 6.28 and 9.32 MeV states are much weaker than the predicted values. This may partly be ascribed to the fact that the matching l-transfer, $|k_iR_i - k_fR_f|$ (k's and R's are respectively the momenta and interaction distances in the reaction channels) lies in the range 2-4 over E_x = 0.0 - 14.36 MeV of the final nucleus and hence l=0 is a mismatched transfer. Furthermore, l=0 shell-model wave functions used in [143] may not be good due to truncation.

The extracted sum of strengths for all l=2 as well as for all l=0 transitions has a factor of 2 missing from the expected magnitude e.g. the effective number of proton-

holes in the transfer-orbits. This is surprising when one considers the states of ^{28}Si, resulting from the $j^{\pi} = 1/2^{+}$, $3/2^{+}$, $5/2^{+}$ transfers in the reaction, are highly improbable to exist at $E_x > 16.50$ MeV. The spherical shell-model cannot probably take up the whole of the transition strength and some of the strength drains off as a result of deformation. For the transition to each of the 6^{-} states at E_x=11.58 MeV and 14.36 MeV, the predicted strength G=0.083, calculated on the basis of deformed shell-model [140,141], is not adequate enough to explain the observed values (Table 5.3). The band mixing effects due to Coriolis coupling [146] may have significant effects on these transition strengths and is worth further investigation..

6.2. The $^{28}Si(\alpha,d)^{30}P$ reaction

Both the molecular and Michel types of α-nucleus potential have been used, for the first time, for the analyses of the data for the two-nucleon transfer (α,d) reaction. The data for the even-parity states up to E_x=3.02 MeV, have been analyzed both in terms of the FFR DWBA with the cluster form-factor and the ZR DWBA with the microscopic form-factors. In the latter calculations, the FPSDI and CW [37] as well as MSDI [18] spectroscopic amplitudes derived from the wave functions of Wildenthal and his collaborators [144,145] and Ref. [20] cited in the work of de Meijer *et al.* [37]. The data of the odd-parity states are analyzed only in terms of the macroscopic FFR calculations.

In both microscopic and macroscopic DWBA calculations, the molecular potential (Figs. 5.12-5.14 and 5.17-5.19) produces the best description of the data for all the transitions studied. The Michel potential, which has been shown to describe

satisfactorily the elastic $\alpha+^{28}Si$ data [19], is found inadequate not only in accounting for the pattern of the angular distributions (Figs. 5.12-5.14, 5.17), but also in reproducing the right order of magnitude for the cross section data. The normal optical potential, on the other hand, which can fit the angular distribution at forward reaction angles and predicts the same order of cross sections as the molecular one does, is found inadequate in describing the data at large scattering angles (Figs. 5.12-5.14, 5.17).

The finite-range correction to the ZR microscopic calculations produces significant effects on the pattern of the angular distributions and improves substantially the fits to the data as can be seen in Fig. 5.16. This confirms the observation made by Bencze and Zimanyi [157]. The best-fit value for the finite-range parameter found is R=0.70 fm for the reaction.

In the literature, an ambiguity in the spin-parity assignment for the 3.93 MeV state is noted. The comparison of the macroscopic DWBA predictions for $J^{\pi}=2^{-}$ (solid curve) and 3^{+} (dotted curve) in Fig. 5.15 with the experimental data favours the former, confirming the assignment of Jankowski *et al.* [19] and opposing that of de Meijer *et al.* [37].

The macroscopic spectroscopic factors A_L for the transitions to the final states up to E_x=5.42 MeV are deduced by comparing the macroscopic DWBA calculations to the data. Table 5.5 compares the deduced spectroscopic factors A_L to those obtained at the 50 MeV incident energy by de Meijer *et al.* [37] and also to those extracted using the same data as of the present work by Jankowski *et al.* [18]. The results of Jankowski *et al.* [18] are not expected to be reliable as they included the compound nucleus contributions in

the analyses. The results of de Meijer *et al.* are based on the zero-range calculations. Nevertheless, their A_L values for the transitions involving one L-transfer leading to, particularly, the 1.454 (2^+) and 4.62 MeV (3^-) states are remarkably close to those of the present work.

The A_L values for the even-parity states have been compared to the model dependent theoretical spectroscopic factors S_L^{σ} in Table 5.5. It can be noticed that apart from the ground state (1^+), 1.454 (2^+) and 2.72 MeV (2^+) transitions, the total spectroscopic factors $\sum A_L$ agrees with the calculated total S^{σ} for the CW amplitudes. On the other hand, the FPSDI predictions for the S^{σ} values are closer to the experimental $\sum A_L$ for the ground and 1.45 MeV states. Neither of the FPSDI and CW amplitudes reproduces the experimental A_L for the 2.72 MeV state. It can also be noticed from Table 5.5 that FPSDI yields larger spectroscopic strengths compared to CW. This is also reflected in the deduced values of relative normalization constants $\aleph_{rel}$ in Table 5.7, where FPSDI needs in general smaller $\aleph$-values to get to the data. None of the three interactions *viz.* FPSDI, CW and MSDI has been able to yield consistent values of the normalization constants for transitions to the even-parity states. However, the model-independent $\aleph$=722±25 is obtained from the data of the 7.20 MeV (7^+) state, where the spectroscopic amplitude is believed to be unity.

6.3. The $^{29}Si(\alpha,d)^{31}P$ reaction

The macroscopic FFR DWBA calculations performed for $^{29}Si(\alpha,d)^{31}P$ reaction using all three potentials e.g. molecular, normal optical and Michel potentials have been

compared to the experimental data in Figs. 5.21-5.23. It is evident from Fig. 5.21 that for ground ($1/2^+$), 1.27 ($3/2^+$), and 2.23 ($5/2^+$) MeV states of ^{31}P, the quality of fits are moderate for all three potentials. For the ground state transition, the molecular and normal potentials generate a bit better fit in the large angle region in comparison to that in the forward angles, whereas, the Michel potential reproduces the angular distribution up to $\theta_{cm}= 40^0$-50^0 in a better way, but beyond that it is unable to reproduce satisfactorily. For both 1.27 ($3/2^+$) and 2.23 ($5/2^+$) MeV states, the normal optical and Michel potentials yield a bit better fit at the forward-angle region in comparison to the molecular one. The macroscopic DWBA predictions by the molecular potential reproduce the experimental data for the 3.13 ($1/2^+$), 3.30 ($5/2^+$), 3.51($3/2^+$), 4.19 ($5/2^+$) and 4.26 ($3/2^+$) MeV states (Fig. 5.22-5.23) in an excellent way over the whole range of angular distribution. On the other hand, the DWBA fits due to the normal optical and Michel potentials for these states are comparable to those of the molecular one at forward angles only, but not of the same quality at the more backward angles. For the 3.41 ($7/2^+$) MeV state the fit to the experimental data is not satisfactory for any of the three potentials.

The effect of finite-range correction to the ZR DWBA microscopic calculations using the molecular potential and the MSDI spectroscopic amplitudes for the ground ($1/2^+$), 1.27 ($3/2^+$) and 2.23 ($5/2^+$) MeV states has been exhibited in Fig. 5.24. The finite-range parameter value R=0.7 fm improves the fits to the data substantially.

The microscopic ZR DWBA calculations with finite range correction (R=0.7 fm.) using the molecular potential (Figs. 5.25-5.27), normal optical (Figs. 5.28-5.30) and Michel (Figs. 5.31-5.33) potentials and the MSDI, RIP and KB spectroscopic amplitudes

are compared to the experimental data. Fig. 5.25 shows that the fits to the data of the 1.27 ($3/2^+$) and 2.23 ($5/2^+$) MeV states are quite reasonable for the molecular potential using the spectroscopic amplitudes from all three MSDI, RIP, and KB interactions. But the molecular potential fits using the RIP and KB amplitudes are not so satisfactory for the ground ($1/2^+$) state (Fig. 5.25); but the same potential using MSDI accounts for the data of the state in a bit better way. For the 3.13 ($1/2^+$) and 3.30 ($5/2^+$) MeV states (Fig. 5.26) the fits from the molecular potential using all three interaction amplitudes are very good with MSDI doing again the best. But for the 3.41 ($7/2^+$) MeV state, the fits from the molecular potential for all three interactions are moderate. The fits to the 3.51 ($3/2^+$), 4.19 ($5/2^+$) and 4.26 ($3/2^+$) MeV states (Fig. 5.27) are excellent over the whole range of angular distribution using the molecular potential and the spectroscopic amplitudes of all three MSDI, RIP, and KB interactions. So, it is observed that in the ZR DWBA microscopic calculations, the molecular potential successfully reproduce the experimental data of almost all the positive parity states using the spectroscopic amplitudes of all three interactions. It is not easily possible to distinguish the preference of any one of the interactions to the other. Nevertheless, a careful scrutiny will give MSDI a favour.

From Fig. 5.28, it is obvious that the normal optical potential accounts for the ground state ($1/2^+$) reasonably well at far backward angles but fails to do so at the forward angles. For the 1.27 ($3/2^+$) and 2.23 ($5/2^+$) MeV states (Fig. 5.28), the fits are satisfactory at the forward angles, but not good at the backward angles. For the 3.13 ($1/2^+$), 3.30 ($5/2^+$) and 3.41 ($7/2^+$) MeV states (Fig. 5.29) as well as for the 3.51 ($3/2^+$), 4.19 ($5/2^+$) and 4.26 ($3/2^+$) MeV states (Fig. 5.30), the fits are as good as those due to the

molecular potential except at the backward angles for some states. As noted earlier, the reaction data have been reproduced satisfactorily by the potential parameters without adjustments over those generated by fitting elastic data as shown in Fig. 5.20. It can be seen from the Figs. 5.28-5.30 that the microscopic ZR DWBA calculations using the normal optical potential without adjustment of any parameter reproduce at least the same quality fits, if not better compared to the previous study [48], where some of the potential parameters are changed over those from the fitting the elastic data, to forge fits to the reaction data.

Fig. 5.31 shows that, the ZR DWBA fits to the ground ($1/2^+$) state data is not so satisfactory using the Michel potential with any of the three interactions. For the 1.27 ($3/2^+$) and 2.23 ($5/2^+$) MeV states (Fig. 5.31) the fits are moderate at the forward angles, but worse at the more backward angles. The fits to the data of the 3.13 ($1/2^+$), 3.30 ($5/2^+$), 3.51 ($3/2^+$), 4.19 ($5/2^+$) and 4.26 ($3/2^+$) MeV states (Figs. 5.32-5.33), using the Michel potential and the spectroscopic amplitudes of all three MSDI, RIP, and KB interactions are quite good; but the fit to the 3.41 ($7/2^+$) MeV state (Fig. 5.32) is not satisfactory.

Figs. 5.34-5.36 compare the fits of the microscopic DWBA calculations to the experimental data of all the positive parity states of ^{31}P using the molecular (solid lines), normal optical (broken lines) and Michel (dotted lines) potentials, each coupled to the MSDI spectroscopic amplitudes. It is evident without ambiguity from Figs. 5.34-5.36 that the molecular potential reproduces a better overall fit to angular distribution data in comparison to the other two potentials.

The spectroscopic factors (Tables 5.12-5.13) deduced from the macroscopic calculations using all the three molecular, normal optical and Michel potentials when compared to the theoretical spectroscopic factors calculated from the MSDI, RIP and KB spectroscopic amplitudes with the method outlined in [150], give some distinct features of the potential used. The total spectroscopic factors ΣA_L for each of the transitions deduced using the molecular potential agrees well with the calculated total spectroscopic factor S^σ, although the individual A_L values have some differences with S_L^σ for the corresponding transitions. On the other hand, both the normal optical and Michel potentials could not reproduce the right order of differential cross-sections. The calculated cross-sections from these two potentials are underestimated by one to two orders of magnitude. This is reflected in the magnitude of the experimental spectroscopic factors for both the normal optical and Michel potentials, which are overestimated by the same orders over the theoretical spectroscopic factors S^σ (Tables 5.12-5.13). In this connection, it is also to be noted that the theoretical spectroscopic factors S^σ (Table 5.12) using the spectroscopic amplitudes of MSDI, RIP, and KB interactions are not also consistent with one another. So, it is not possible to decide which interaction is capable of reproducing the correct order of cross-sections.

The normalization constants in Eq. (5.16) extracted by comparing the theoretical cross-sections with the experimental ones using three potentials for all the states are noted in Table 5.23a. Two inferences come out from the deduced normalization constants. Firstly, the normalization constants yielded by neither of the potentials is equal for all the transitions and secondly, the normalization constants generated by the normal

optical and Michel potentials are higher than those by the molecular potential for the corresponding transitions by 1-2 orders of magnitude, again reflecting the underestimation of the predicted cross-sections by the latter two potentials. No conclusive inference can be drawn for the normalization constant of the (α,d) reaction from the inconsistency in the deduced values.

6.4. The $^{30}Si(\alpha,d)^{32}P$ reaction

The predictions from the macroscopic FFR DWBA analyses performed using the molecular, normal optical and Michel potentials are compared to the experimental data in Figs. 5.38-5.39. It is obvious from Figs. 5.38-5.39 that the fits using the molecular potential, to data of the ground (1^+) and 1.75 (3^+) MeV states are excellent over the whole range of angular distribution. The DWBA predictions using the molecular potential for the 0.08 (2^+), 1.15 (1^+), 1.32 (2^+), 2.66 (2^+), 2.74 (1^+) and 3.00 (3^+) MeV states are also in very good agreement with the experimental data.

On the other hand, both the normal optical and Michel potentials seem to be inadequate in reproducing the experimental data of the ground (1^+) and 0.08 (2^+) MeV states. For the 1.15 (1^+), 1.32 (2^+), 1.75 (3^+), 2.66 (2^+), 2.74 (1^+) and 3.00 (3^+) MeV states, the normal optical and Michel potentials produce reasonable fits at forward angles, but can not do so at the more backward angles.

The finite-range correction to the ZR microscopic calculations for the ground (1^+), 0.08 (2^+), 1.15 (1^+) and 1.32 (2^+) MeV states are shown in Fig. 5.40. The best-fit value for the finite-range parameter found is R=0.70 fm which conforms to the value obtained for the reaction on $^{28,29}Si$.

Figs. 5.41-5.42 show the comparison of the microscopic ZR DWBA predictions using the molecular potential and spectroscopic amplitudes due to the MSDI, RIP, or KB interaction with the experimental data. It is evident from Fig. 5.41 that for the ground (1^+) state, the DWBA calculations using the molecular potential coupled with MSDI amplitudes gives better agreement with the experimental data than those with the RIP and KB amplitudes. The calculations for the molecular potential coupled with either of the three MSDI, RIP, and KB amplitudes reproduce the data for the 0.08 (2^+), 1.15 (1^+), 1.32 (2^+), 2.74 (1^+) and 3.00 (3^+) MeV states reasonably well. The fits to the 1.75 (3^+) and 2.66 (2^+) MeV states are unsatisfactory, although the data for the latter two states are satisfactorily described by the macroscopic calculations (Fig. 5.39). Nevertheless, considering the overall situation, it is evident that the MSDI spectroscopic amplitudes provide a better description of the data compared to the other two.

Figs. 5.43-5.44 show the microscopic DWBA predictions due to the normal optical potential using the MSDI, RIP and KB spectroscopic amplitudes. It is to be noted here that the potential parameters generated from the elastic fit have been used here unaltered. For the ground (1^+) state, the fits are not satisfactory beyond the scattering angle $\theta_{cm}= 80^0$. The fits to the 0.08 (2^+), 1.25 (2^+), 1.32 (2^+), 2.66 (2^+), 2.74 (1^+) and 3.00 (3^+) MeV states are quite good up to the angle of about 120^0. For the 1.75 (3^+) MeV state the fit is moderate.

Figs. 5.45-5.46 display the microscopic calculations using the MSDI, RIP and KB amplitudes coupled with the Michel potential. For the ground state (1^+), the MSDI and KB amplitudes using the Michel potential describe the data well, whereas, the RIP

amplitudes do poorly at forward angles. The DWBA calculations for the 0.08 (2^+), 1.15 (1^+), 1.32 (2^+), 2.74 (1^+) and 3.00 (3^+) MeV states, using all three MSDI, RIP, and KB amplitudes and the same potential reproduce the data reasonably well up to about θ_{cm} = 120^0. The fits to the 1.75 (3^+) and 2.66 (2^+) MeV states are not satisfactory.

The comparison of the fits for all the states using the molecular, standard optical and Michel potentials coupled with the MSDI amplitudes for each of the potentials (Figs. 5.47-5.48) obviously show that the normal optical potential produces a lesser quality fits on the whole in comparison to those using the molecular and Michel potential.

The experimental spectroscopic factors A_L deduced from the macroscopic calculations using the molecular, normal optical and Michel potentials are tabulated along with the theoretical spectroscopic factors S_L^a in (Tables 5.18-5.19). It is obvious from the tables that the calculated theoretical shell-model spectroscopic factors due to all three MSDI, RIP and KB amplitudes are different by orders of magnitude. The values of the total spectroscopic factors S^a extracted from both the RIP and KB amplitudes are lesser compared to those from the MSDI ones. The experimental spectroscopic factors deduced for the molecular potential are comparable with those calculated from the MSDI spectroscopic amplitudes for the L=2 transition to the ground (1^+) and 2.74 (1^+) MeV states. For all other states, the experimentally deduced spectroscopic factors due to the molecular potential are a bit higher but comparable to the theoretical ones. On the other hand, the total spectroscopic factors ΣA_L deduced using the normal optical and Michel potentials are one to two orders higher than the theoretical S^a values for all the transitions. This means that the macroscopic DWBA predictions using both the normal

optical and Michel potentials underestimate the magnitude of cross-sections by one to two orders for the different final states.

Tables 5.20-5.23 containing the spectroscopic amplitudes from the three MSDI, RIP and KB interactions and the corresponding normalization constants for different transitions reveal two facts. (1) The normalization constants are not consistent and not same for all states and not even for the same final state for different distorting α-nucleus potentials and interactions responsible for the spectroscopic amplitudes. (2) The normalization constants deduced from the data of any state using the normal optical and Michel potentials are larger by one to two orders of magnitude than the corresponding ones due to the molecular potential.

6.5. The $^{28}Si(\alpha,p)^{31}P$ reaction

The present work reports for, the first time, the analyses of a three-nucleon transfer reaction using both the molecular, deep WS and shallow WS and Michel potentials. The DWBA calculations for the three-nucleon transfer (α,p) reaction to the ground ($1/2^+$), 1.27 MeV ($3/2^+$) and 2.23 MeV ($5/2^+$) states of the final nucleus, using the molecular potential reproduce the data both in magnitude and in angular dependence, rather well. The calculations using the deep optical and Michel potentials are underestimated by 2 to 4 orders of magnitude in each case, although the angular patterns are reasonably reproduced. The calculations using the shallow potential reproduce the magnitude of cross-sections up to 100^0 or so, but then predict a sharp decrease at large

angles. Thus, the molecular potential is the only one to account for the data for the ground ($1/2^+$), 1.27 MeV ($3/2^+$) and 2.23 MeV ($5/2^+$) final states over the entire angular distributions. Moreover, the present analysis indicates that the data for the reaction can be successfully described without the addition of any compound nucleus contribution, which has been included in the analysis by Jankowski *et al.* [18], but is highly improbable at the incident energy considered. Furthermore, the fits to the data are reproduced without having to adjust any of the parameters of the molecular potential, obtained from the elastic data.

The CCBA calculations for the $^{28}Si(\alpha,p)^{31}P$ reaction using the molecular potential improve the fits over the ZR and FFR calculations (Fig. 5.50). The inelastic 4^+ state at E_x = 4.618 MeV in ^{28}Si plays a major role in the CCBA calculations in reproducing the ground state data. The coupling to the inelastic 2^+ state to the ground state of ^{28}Si is also significant in improving the data for the 1.266 and 2.234 MeV states of ^{31}P. The CCBA calculations confirm the deformed shape of the ^{28}Si nucleus.

6.6. Summing up

One may summarize the discussion on the study of the $^{27}Al(\alpha,t)^{28}Si$, $^{28,29,30}Si(\alpha,d)^{30,31,32}P$ and $^{28}Si(\alpha,p)^{31}P$ reactions in the following way:

The one-nucleon transfer (α,t) reaction on ^{27}Al at the 64.5 MeV incident energy can be reasonably described by the molecular and Michel potentials. The performance of these two types of potential is as satisfactory as the normal WS potential in the description of the reaction data at forward angles. However, the substantial difference in the DWBA predictions for those three types of potential occurs at large reaction angles

suggesting that the large angle data for the reaction may be used as a sensitive probe to decide the nature the α-nucleus potential.

The macroscopic FFR DWBA and microscopic ZR DWBA analyses of the (α,d) on the alpha-cluster ^{28}Si nucleus and the non-alpha-cluster ^{29,30}Si nuclei bring out clearly three facts. (1) The compound nucleus effect is insignificant at the energy considered as opposed to that reported by Jankowski *et al.* [18]. (2) The molecular potential reproduces the experimental data of the (α,d) reactions quite reasonably and convincingly without having to adjust any of the parameters of the potential obtained from elastic fit. (3) The Michel potential, which can account for the ALAS effect of the α-^{28}Si elastic scattering as good as the molecular one if not better, could not reproduce, like the normal optical potential, the angular distribution as well as magnitude of cross-sections of the (α,d) reactions on the silicon-isotopes at the energy considered.

The analyses of the ^{28}Si(α,p)^{31}P reaction ensure emphatically that the molecular potential shows its clear preference to the normal optical and Michel potentials. It also affirms the conjecture that the compound nucleus effect is least probable at the incident energies near to E_α=26 MeV. The molecular potential reproduces the experimental data of the ^{28}Si(α,p)^{31}P reaction reasonably well in magnitude and angular oscillations.

Now, a pertinent question arises as to why the Michel potentials which has been so successful in accounting for ALAS in the elastic scattering on many targets [56-61], seems to fail in reproducing the data of the ^{28,29,30}Si(α,d)^{30,31,32}P and ^{28}Si(α,p)^{31}P reactions. The reason of success of molecular and apparent failure of Michel potentials may lie within the following facts.

The molecular and Michel potentials have two distinctive features. The Michel (square-Woods-Saxon) potential is a deep and monotonic potential and on the other hand, the molecular potential is a shallow and non-monotonic one. The molecular potential model has its root in a many body theory utilizing the Energy Density Functional (EDF) formalism, which incorporates the effects of Pauli's exclusion principle [28]. As a consequence, the molecular potential may have inherent strength of describing the physical situation of α-nucleus interaction in more details. The success of the molecular potential conforms to Baye's [160] assertion that amongst the phase equivalent potentials, the shallow one with a singularity, which is borne by the molecular potential with its the repulsive core, eliminates the states forbidden by the Pauli principle and is, therefore, expected to give better result in the description of transfer reactions. On the contrary, the Michel potential concentrates on and emphasizes the physical phenomena related to surface processes and hence may lack the ability of describing the processes dependent on the nuclear interior. So, although the two potentials widely divergent in their forms, provide a more or less equally good description of α-elastic scattering from light nuclei in the ALAS energy-region as well as at higher energies, because the effective part of the potentials responsible for elastic scattering are similar. But, when the non-elastic processes like the (α,d) and (α,p) reactions come into the scenario, a more detailed contribution from the nuclear interior may dominate the feature. The molecular potential represents a more realistic situation of the phenomena.

Furthermore, one may also note that the two potentials differ significantly in defining the Coulomb radius. In case of the molecular potential, the Coulomb radius R_C is

the distance where ^{28}Si barely touches the α particle. The observed density distribution, $\rho(r)$ for ^{28}Si is given by [90]

$$\rho(r) = \rho(0)\left[1 + \exp\frac{r-c}{d}\right]^{-1}$$

with c=3.14 fm and d=0.537 fm. Thus, at r=6 fm, this leads to $\rho(r) = 0.005\rho(0)$. A reasonable density distribution function for α particle is $4\left(\frac{\gamma}{\pi}\right)^{3/2} \exp\left(-\gamma r^2\right)$ with γ =0.5 [158]. This is about 0.001 at r=3.35 fm. Thus, a reasonable value of R_C is (6.00+3.35) =9.35 fm., which is used in the molecular potential. The Michel potential, on the other hand, uses R_C= 3.95 fm. At this distance, the two nuclei have inter-penetrated each other substantially. In the DWBA theory, the stripped particles from the projectile are assumed to drop on the nuclear surface and hence, the treatment may be somewhat sensitive to the actual value of R_C.

The present study of the ^{27}Al(α,t)^{28}Si, ^{28,29,30}Si(α,d)^{30,31,32}P and ^{28}Si(α,p)^{31}P reactions strengthens Satchler's contention [31] that the real test of a potential generated from the analysis of elastic scattering data lies in its ability in reproducing the non-elastic data. Hence, the success of the molecular α-nucleus potential in describing the angular distributions of the (α,d), and (α,p) reactions on the silicon-isotopes and the one-nucleon transfer (α,t) reaction on ^{27}Al in addition to the elastic scattering on various targets in different mass regions, justifies its clear-cut superiority over the normal WS and the Michel potentials.

CHAPTER 7

CONCLUSION

The present study reveals some convincing successes of the molecular potential and inadequacy of the Michel one in describing α-induced two-nucleon transfer (α,d) and three-nucleon transfer (α,p) reactions on the mid sd-shell targets, although both are strong contenders to explain the ALAS effects in the α-elastic scattering and to account for the angular distribution of one-nucleon transfer (α,t) reaction. It is worth mentioning, in this relation, that the normal optical potential has been proven inadequate in describing the ALAS effect in the α-elastic scattering on targets of different mass regions.

Although, the molecular and Michel types of α-nucleus potentials produce more or less the same quality fits to the $^{27}Al(\alpha,\alpha)^{27}Al$ scattering (Fig.5.1) and both of them are able to describe reasonably the data of the $^{27}Al(\alpha,t)^{28}Si$ reaction at small reaction angles, they lead to significantly different scenario in generating the predictions at large reaction angles. The three potentials generate diverse predictions at large angles, offering the large-angle data of the one-nucleon transfer reaction as a sensitive probe of the α-nucleus potential.

The macroscopic FFR DWBA and microscopic ZR DWBA analyses of the (α,d) reaction on $^{28\text{-}30}Si$ establish convincingly the fact that the molecular potential reproduces the experimental data in magnitude and in angular oscillations quite satisfactorily. The Michel and normal optical potentials, on the other hand, underestimate the cross-sections by one to two orders of magnitude in addition to giving poorer fits to the angular distribution. The molecular potential can also give adequate accounts of the absolute

magnitude and angular pattern of the three-nucleon transfer (α,p) reaction on ^{28}Si. The Michel potential underestimates the cross-section of the reaction by 2-4 orders of magnitude. The normal optical WS potential cannot simultaneously reproduce the absolute magnitude of cross-sections and the angular distribution, in conformity with the observation of Brunner *et al.* [161] and Hamill and Kunz [162].

In addition, the present work strongly put forward some important observations. Firstly, this study in conjunction with the previous studies of α-elastic scattering on ^{24}Mg and ^{28,30}Si by Tariq *et al.* [19] supports the observations asserted by Budzanowski *et al.* [159] that elastic data of either at forward angle or at backward angles only are insufficient to determine the potential parameters. So, the present work emphasizes the essentiality of the elastic and non-elastic scattering data of wide angular range extending to the large backward angles to determine the parameters of potentials more reliably. Secondly, the present study conforms to Satchler's contention [31] that the real test of a potential set generated from the analyses of elastic scattering data lies in its ability to reproduce the non-elastic data.

Both the (α,d) and (α,p) reactions, because of their high negative Q-value, are spin-selective and favour the transitions to maximum spins. However, since these reactions have large angular momentum mismatch, there will be a substantial contribution from the nuclear interior, resulting in sensitivity of the calculated cross-sections to the nature of the α-nucleus interaction. The molecular-type potential gives satisfactory account of the (α,d) and (α,p) reactions even for the large angle data. Thus, the present work suggests that the molecular potential paves the way for more prolific use of these two reactions for spectroscopic studies.

The present study also invoke some endeavour to dig into the deeper essence of the fact that while the Michel potential enjoys so much successes in accounting for the ALAS effect in the elastic processes on various targets of different nuclear mass regions [57,61], the cluster structure in ^{44}Ti [58,59] and oscillations in the fusion excitation function [60,163], it is found inadequate in describing the (α,d) and (α,p) reactions. The success of molecular potential, on the other hand, lays a strong foothold for the Energy Density Functional formalism. This may pave the way for introducing newer steps in the hope of resolving some astrophysical problems, related to neutron star density [164].

The success of molecular potential in accounting for the α-elastic and α-induced non-elastic data, is certainly a leap forward and ushers in the long cherished hope of Hodgson [22] for obtaining a satisfactory global α-nucleus potential. But even then, the present work suggests that the molecular potential with its simple parametrization needs further examination with targets in other mass regions before being accepted as a global one.

References:

[1] J.C. Correlli, E. Bleuler and J. Tandem, Phys. Rev. **116**, 1184 (1959).

[2] C.R. Gruhn and N.S. Wall, Nucl.Phys. **81**, 161 (1966).

[3] G. Gaul, H. Lüdecke, R. Santo, H. Schmeing and R. Stock , Nucl.Phys. **A137**, 177 (1969).

[4] A. Bobrowska, A. Budzanowski, K. Grotowski, L. Jarczyk, S. Micek, H. Niewodniczanski, A. Strzalkowski and Z. Wróbel, Nucl. Phys. **A126**, 361 (1969).

[5] H. Eickhoff, D. Frekers, H. Lönner, K. Poppensieker, R. Santo, G. Gaul, C. Mayer-Böricke and P. Turek, Nucl. Phys. **A252**, 333 (1975).

[6] H. Abele, H.J. Hauser, A. Körber, W. Leitner, R. Neu, H. Plappert, T. Rohwer, G. Staudt, M. Straßer, S. Welte, M. Walz, P.D. Eversheim and F. Hinterberger, Z. Phys. A **326**, 373 (1987).

[7] H. Oeschler, H. Schroter, H. Ficjs, L. Baum, G. Gaul, H. Ludecki, R. Santo and R. Stock, Phys. Rev. Lett. **28**, 694 (1972).

[8] Å. Bredbacka, M. Brenner, K.M. Källman, P. Manngård, Z. Máté, S. Szilágyi and L. Zolnai, Nucl. Phys. **A574**, 397 (1994).

[9] L. Jarczyk, B. Maciuk, M. Siemaszko and W. Zipper, Acta Phys. Pol. **B7**, 531 (1976).

[10] A.W. Obst and K.W. Kemper, Phys. Rev. **C 6**, 1705 (1972).

[11] A.E. Antropov, S.I. Vasilev, P. Zurabin and B.N. Orlov, Izv. Akad. Nauk. SSSR, Ser. Fiz. **38**, 2175 (1974); **37**, 1873 (1973).

[12] B. Xiumin, L. Shiming, W. Yuanda, Y. Rongfang, H. Bingyin and S. Zuxun, Chin. Phys. **6**, 645 (1986).

[13] H. Kitazawa, Y. Harima and N. Mukai, Nucl. Phys. **A510**, 429 (1990).

[14] W. Trombik, K.A. Eberhard and J.S. Eck, Phys. Rev. C **11**, 685 (1975).

[15] A.M. Kobos, B, A. Brown, R. Lindsay and G.R.Satchler, Nucl. Phys. **A425**, 205 (1984).

[16] F. Schmittroth, W. Tobocman and A.A. Golestanch, Phys. Rev.C **1**, 377 (1970).

[17] H.-J. Apell, W. Gemeinhardt, R. Stock, R.R. Betts, O. Hansen, A. Sperduto, H. Fuchs

[18] K. Jankowksi, A. Grzeszczuk, M. Siemanszko, A. Surowiec, W. Zipper, A. Budzanowski and E. Kozik, Nucl. Phys. **A426**, 1 (1984).

[19] A.S.B. Tariq, A.F.M.M. Rahman, S.K. Das, A.S. Mondal, M.A. Uddin, A.K. Basak,

H.M.Sen Gupta and F.B.Malik, Phys. Rev. C **59**, 2558 (1999).

[20] F. Michel, J. Albinski, P. Belery, Th. Delbar, Gh. Grégoire, B. Tasiaux and G. Reidemeister., Phys. Rev.C **28**,1904(1983).

[21] F. Michel, G. Reidemeister and S. Ohkubo, Phys. Rev. Lett. **57**, 1215 (1986).

[22] P. E. Hodgson, Oxford Report , OUNP-94-09(1994).

[23] W. Wuhr, A. Hoffman and G. Phillipp, Z. Phys. 269, 365(1974).

[24] F. Michel, Vanderpoorten, Phys. Lett. 82B, 183 (1979).

[25] B. Block and F.B. Malik, Phys. Rev. Lett. **19**, 239 (1967).

[26] R.J. Munn, B. Block and F.B. Malik, Phys. Rev. Lett. **21**, 159 (1968).

[27] F.B. Malik and I. Reichstein, in *Clustering Phenomena in Atoms and Nuclei*, eds.M. Brenner, T. Lönnroth and F.B. Malik (Springer-Verlag Berlin, Heidelberg, 1992),p126.

[28] I. Reichstein and F.B. Malik, Phys. Lett. **B 37**, 344 (1971).

[29] P. Manngård, M. Brenner, M.M. Alam, I. Reichstein and F.B. Malik, Nucl. Phys. **A504**, 130 (1989).

[30] W. Hauser and H. Feshbach, Phys. Rev. **87**, 366 (1952).

[31] G.R. Satchler, *Int'l Conf. on Reactions between Complex Nuclei,* Nashville North-Holland, Amsterdam, (1974)p171.

[32] N.K. Glendenning in *Nuclear Spectroscopy and Reactions, Part D,* ed.J. Cerny (Academic Press, New York, 1975) p. 319.

[33] H. Nann, W.S. Chieu, A. Saha and B.H. Wildenthal, Phys. Lett. **60B**, 32 (1975).

[34] A. Van der Woude and R. J. de Meijer, Nucl. Phys. **A258**, 199 (1976).

[35] R.M. DelVecchio *et al.*, Nucl.Phys. **A265**, 220 (1976).

[36] H. Nann, W.S. Chien, A. Saha and B. H. Wildenthal, Phys. Rev.C **15**, 1959 (1977).

[37] R. J. de Meijer, L.W. Put, J.J. Akerman, J.C. Vermeulen and C.R. Binham, Nucl. Phys.**A386**, 200 (1982).

[38] G.R. Satchler, Nucl. Phys. **55**, 1 (1964).

[39] P.D. Kunz, The Codes DWUCK4, DWUCK5 & CHUCK3, *private communication*.

[40] F.G. Perey, *Proc. Conf. Direct Reactions and Nuclear Reaction Mechanism*

(Gordon and Breach, New York, 1963) p. 125.

[41] F. James and M. Roos. Comp. Phys. Comm. **10**, 343 (1975).

[42] P. E. Hodgson, Lecture at La Rabida, Spain (1985).

[43] H. Oberhummer, Nuovo Cimento, 55A, 253(1980).

[44] M. Yasue, T. Tanabe, S. Kubono, J. Kokame, M. Sugitani, Y. Kadota, Y. Taniguchi and M. Igarashi, Nucl.Phys.A391,377(1982).

[45] N. J. Davis and J. M. Nelson, *Private communication.*

[46] C.M. Vincent and H.T. Fortune, Phys. Rev. C **2,** 793(1970).

[47] C.M. Vincent and H.T. Fortune, Phys. Rev. C **7,** 865(1973).

[48] N. J. Davis and J. M. Nelson, Nucl. Phys. A**458,** 475 (1986).

[49] P. E. Hodgson, *The optical model of elastic scattering,* Oxford University Press, Oxford, (1963).

[50] I. Ulehla, L. Gomalcak and Z. Pluhao, *Optical model of the atomic nucleus,* Academic Press, New York, (1964).

[51] C.M. Perey and F.G. Perey, Atomic and Nuclear Data Tables **17**, 1 (1976).

[52] G. R. Satchler, *Direct Nuclear Reaction,* Clarendon Press, Oxford, Oxford University Press, New York, (1983).

[53] P. E. Hodgson, *Conferences on Applied Nuclear Theory and Nuclear Model Calculations for Nuclear Technology Applications,* Trieste, Italy, (15 Feb.- 19 March, 1988).

[54] R. D. Woods and D. S. Saxon, Phys. Rev. 95, 577(1954).

[55] C. Eckart, Phys. Rev. 35, 1303(1930).

[56] Th. Delbar, Gh. Grégoire, G. Paic, R. Ceuleneer, F. Michel, R. Vanderpoorten, R. Budzanowski, H. Dabrowski, L. Friendl, K, Grotoski, S. Micek, R. Planeta, A. Strzalkowski and A. Eberhard, Phys. Rev. C **18**, 1237 (1978).

[57] F. Michel, J. Albinski, P. Belery, Th. Delbar, Gh. Grégoire, B. Tasiaux and G. Reidemeister., Phys. Rev. C **28**, 1904 (1983).

[58] F. Michel, G. Reidemeister and S. Ohkubo, Phys. Rev. Lett. **57,** 1215 (1986).

[59] F. Michel, G. Reidemeister and S. Ohkubo, Phys. Rev. C**37,** 292(1988).

[60] F. Michel, G. Reidemeister and S. Ohkubo, Phys. Rev. C34, 1248 (1986).

[61] F. Michel, G. Reidemeister and Y. Kondo, Phys. Rev. C **51**, 3290 (1995).

[62] T. Wada and H. Horiuchi, Phys. Rev. Lett. **58**, 2190 (1987).

[63] T. Wada and H. Horiuchi, Phys. Rev. C **38**, 2063 (1988).

[64] L. Rickertsen B. Block, J. W. Clark and F. B. Malik, Phys. Rev. Lett. **22**, 951(1969).

[65] K. Brueckner, J.R. Buchler and M.M. Kelly, Phys. Rev. 173,944 (1968).

[66] Q. Haider and F. B. Malik, *Proc. Int'l Conference on Resonance behavior of Heavy-Ion,* Greece 1981, ed. G. Vourpoulos, (Demokritos, Athens, 1981) p925.

[67] I. Reichstein and F.B. Malik, *Proc. Workshop on High Resolution, Heavy-Ion Physics*, eds. M. Martinot and C. Volant (CEN/Saclay Publication, 1978).

[68] Q. Haider and F. B. Malik, J. Phys.G 7, 1661(1981).

[69] N. Ohtsuka, R. Linden, A. Faessler and F. B. Malik, Nucl. Phys. A**465**, 550 (1987).

[70] M. A. Hooshyar, B. Compai-Tabizi and F. B. Malik, *Proc. Int'l Conference on Nuclear Reaction Mechanism,* ed. E. Gadioli (U. of Milani Press,1988)p385.

[71] W. Scheid, R. Lingensa and W. Greiner, Phys. Rev. Lett. 21, 1479(1968).

[72] M. M. Alam and F.B. Malik,*Clustering Phenomena in Atoms and Nuclei,* eds.M. Brenner, T. Lönnroth and F.B. Malik (Springer-Verlag Berlin, Heidelberg, 1992),p144.

[73] D. R. Alexander and F. B. Malik, Phys. Lett. 42B, 412(1972).

[74] P. Gombas, Ann. Phys. (Liepzig)10, 253(1952).

[75] R. A. Berg and L. Wilets, Phys. Rev. 101, 1805(1956).

[76] L. Wilets, Rev. Mod. Phys. 30, 542 (1958).

[77] K. A. Brueckner, J. R. Buchlar, S. Jorna and R. J. Lombard, Phys. Rev. 171, 1188(1968).

[78] K. A. Brueckner, J. R. Buchlar, and M. M. Kelly, Phys. Rev. 173, 944(1968).

[79] K. A. Brueckner, J. R. Buchlar, R. C. Clark and R. J. Lombard, Phys. Rev. 181, 1543(1969).

[80] K. A. Brueckner, S. A. Coon and J. Dabrowski, Phys. Rev. 168, 1184(1968).

[81] H. A. Bethe, Phys. Rev. 167, 879(1968).

[82] P. Hohenberg and W. Kohn, Phys. Rev. 136, B864 (1964).

[83] R. J. Lombard, Ann. Phys. (N. Y.), 77, 380 (1973).

[84] I. Reichstein and F.B. Malik, Ann. Phys. (N. Y.), 98, 322(1976).

[85] K. A. Brueckner, J. L. Gammel, Phys. Rev. 109, 1023(1958).

[86] J. R. Buchler and L. Ingber, Nucl. Phys. **A170**, 1 (1971).

[87] D. C.Peaslee, Phys. Rev. 95, 717(1959).

[88] I. Reichstein and F. B. Malik, Condensed Matter Theory 1, 291(1985).

[89] H. de Vries, C.W. de Jager and C. de Vries, At.Data Nucl.Data Tables **36**, 495 (1987).

[90] A. H. Wapstra and G. Audi, Nucl. Phys. A432, 1 (1985).

[91] W. D. Myers and W. J. Swiatecki, Nucl. Phys. 81, 1(1966).

[92] H. Ngô and Ch. Ngô, Nucl. Phys. A348, 140(1980).

[93] I. Reichstein and F.B. Malik, *Superheavy Element,* ed. M. A. K. Lodhi (Pergamon Press, 1978).

[94] P. Manngård *et al., Proc. 5th Int'l Conference on Nuclear Reaction Mechanisms,* Värena, ed. E. Gadioli, (1988)p385.

[95] J. R. Oppenheimer and M. Phillips, Phys. Rev. 48, 500(1935).

[96] H. B. Burrows, W. M. Gibson and J. Rotblat, Phys. Rev. 80, 1095(1950).

[97] S. T. Butler, Proc. Roy. Soc. A208, 559(1951).

[98] R. Ruby, Nature 166,552 (1950).

[99] N. Austern, *Direct Nuclear Reaction Theories*, Wiley and Sons, New York (1970).

[100] N. Austern, Phys. Lett. 90B, 33(1980).

[101] H. Feshbach, Ann. Revs. Nucl. Sci., 8, 1959(1959).

[102] A. Kerman and S. Koonin, Ann. Phys. (N. Y.), 125, 429(1980).

[103] W. Tobocman, *Theory of Direct Nuclear Reaction,* Oxford University Press, (1961).

[104] N. K. Glendenning, Phys.Rev. **137**, B102 (1965).

[105] I. S. Towner and J.C. Hardy, Adv.in Phys. **18**, 401 (1969).

[106] N. K. Glendenning, *Direct Nuclear Reaction,* Academy Press, New York, (1983).

[107] B. F. Bayman and A. Kallio, Phys. Rev., 156, 1121 (1967).

[108] G. R. Satchler, Nucl. Phys. 18, 67 (1960).

[109] G. H. Rawitscher and S. N. Mukherjee, Phys. Rev. 181, 1518 (1969).

[110] D. M. Brink and G. R. Satchler, *Angular Momentum,* Oxford University Press, New York, (1962).

[111] J. B. French, *Nuclear Spectroscopy, Part B,* ed. F. Ajzenberg-Selove, Academic Press, New York, (1960).

[112] H. M. Macfarlane and J. B. French, Revs. Mod. Phys., 32, 567 (1960).

[113] M. Hull and G. Breit, *Encyclopedia of Physics*, vol.-41, ed. S. Flügge (Spinger-Verlag, Berlin) (1959).

[114] F. Perey and B. Buck, Nucl. Phys. 32, 353 (1962).

[115] N. K. Glendenning, Annu. Rev. Nucl. Sci. (Palo Alto) 13, 191 (1963).

[116] N. K. Glendenning, Phys. Rev.156, 1344 (1967).

[117] A. De Shalit and I. Talmi, *Nuclear Shell Theory,* Academy Press, New York, (1963).

[118] I. Talmi, Helv. Phys. Acta 25, 185(1952).

[119] M. Moshinsky, Nucl. Phys. 13, 104(1959).

[120] T. A. Brody and M. Moshinsky, *Monographias del Instituto de Fisica,* Mexico (1960); T. A. Brody, G. Jacob, and M. Moshinsky, Nucl. Phys. 17, 16(1960).

[121] N. K. Glendenning, Atomic Data and Nucl. Data Tables16, 1 (1975).

[122] R. M. Drisko and F. Rybicki, Phys. Rev. Lett. 16, 275 (1966).

[123] R. Muthukrishnan and M. Baranger, Phys. Lett. 18, 160 (1965).

[124] J. R. Rook and D. Mitra, Nucl. Phys. 51, 96(1964).

[125] J. M. Nelson and B. E. F. Macefield, *Write up for DWBA Code* NELMAC, University of Birmingham (Dept. of Physics), Rep. No. 74-9.

[126] P. M. Lewis, O. Karban, J. M. Barnwell, J. D. Brown, P. V. Drumm,

J. M. Nelson and S. Roman, Nucl. Phys. A**404**, 205 (1983).

[127] F. Hoyler, H. Oberhummer, T. Rohwer, G. Staudt and H. V. Klapdor, Phys. Rev. C31, 17 (1985).

[128] H. Oberhummer, W. Pfeifer, F. Brunner and H. H. Müller, Nucl. Phys. A401, 415 (1983).

[129] H. Guyer, V. Meyer, H. H. Müller, W. Reichart, H. Oberhummer, P. Reichs, R. Wagner and W. Pfeifer, Phys. Rev. C18, 1626 (1978).

[130] N. S. Chant and N. F. Mangelson, Nucl. Phys. A140, 81 (1970).

[131] Y. M. Smirnov, Nucl. Phys. 27, 177 (1961); 39, 346 (1962).

[132] S. K. Penny and G. R. Satchler, Nucl. Phys. 53, 145 (1964).

[133] P. J. Iano and N. Austern, Phys. Rev. 151, 853(1966).

[134] T. Tamara, Physics Reports, 14C, 59 (1974).

[135] O. Bersillon, The Code SCAT2, NEA 0829, *private communication.*

[136] V.M. Lebedev, A.V. Spassky, I.B. Teplov, L.N. Fateeva and L.Z. Ismail, Nucl. Phys. **A298**, 206(1978).

[137] J.M. Barnwell *et al.*, Nucl. Phys. **A388**, 542 (1982).

[138] G. Hauser, G. Nowicki, H. Rebel, G. Schatz, G. Schweimer, J. Specht, Nucl. Phys. **A182**, 1 (1972).

[139] P. J. Brussaards and P. W. Glaudemans, *Shell-Model Applications in Nuclear Spectroscopy,* North-Holland, Amsterdam, (1977).

[140] G.R. Satchler, Ann. Phys. **3**, 275 (1958).

[141] B. Cujec, Phys. Rev. **136**, B1305 (1964).

[142] P. Davidson, *Collective Models of the Nucleus* (Academic, New York,1968).

[143] H. J. A De Voigt and B.H. Wildenthal, Nucl. Phys. A206, 305 (1973).

[144] B.H. Wildenthal, J.B. McGrory, E.C. Halbert and H.D. Graber, Phys.Rev.C **4**, 1708 (1971).

[145] B.H. Wildenthal and J.B. McGrory, Phys. Rev. C **7**, 714 (1973).

[146] F.B. Malik and W. Scholz, Phys. Rev. **147**, 836 (1966); Phys. Rev. **150**, 919 (1966); Phys. Rev. **153**, 1071 (1967).

[147] M. K. Pal, *Theory of Nuclear Structure* (Affiliated East-Wesr Press, New Delhi, 1982).

[148] W. Fitz, J. Heger, R. Santo and S. Wenneis, Nucl.Phys. **A143**, 113 (1970).

[149] L.A. Charlton, Phys.Rev. C **8**, 146 (1978).

[150] I. Skwirczynska, E. Kozik, A. Budzanowski, J. Ploskonka and A. Strzalkowski, Nucl. Phys. **A371**, 288 (1981).

[151] P.M. Endt and C. Van der Leun, Nucl.Phys. **A310**, 1(1978).

[152] P. W. Glaudemann, P.J. Brussaard and B. H. Wildenthal, Nucl. Phys. A102, 593 (1967).

[153] E. C. Halbert, J. B. McGrory, B. H. Wildenthal and S. P. Pandya, Adv. in Nucl. Phys. 4, 31 (1971).

[154] T. T. S. Kuo, *Fourth Symposium on the Structure of low-medium mass nuclei,* ed. J. P. Davidson (1970)p75.

[155] S.K. Das, A.S.B. Tariq, A.F.M.M. Rahman, P.K. Roy, M.N. Huda, A.S. Mondal, A.K. Basak, H.M. Sen Gupta and F. B. Malik, Phys. Rev. C **60**, 044617-1 (1999).

[156] F.G. Perey, *Proc. Conf. on Direct Interactions and Nuclear Reaction Mechanisms* (Gordon and Breach, New York, 1963), p.125; Phys. Rev. **131**, 755 (1963).

[157] Gy. Bencze and J. Zimanyi, Nucl.Phys. **88**, 76 (1966).

[158] L.R.B. Elton, *Nuclear Sizes* (Oxford Univ. Press, 1961).

[159] A. Budzanowski, L. Jarczyk, L. Kamys and A. Kapuscik, Nucl. Phys. A256, 495 (1976).

[160] D. Baye, Phys. Rev. Lett. 58, 2738(1987).

[161] F. Brunner, H. H. Müller, C. Dorninger and H. Oberhummer, Nucl. Phys. A398,84 (1983).

[162] J. J. Hamill and P. D. Kunz, Phys. Lett. 129B, 5 (1983).

[163] S. Ohkubo, Phys. Rev. C **36,** 551(1987).

[164] I. Reichstein and F. B. Malik, to be published.

APPENDIX

Effect of α-nucleus potential on the ^{27}Al$(\alpha,t)^{28}$Si reaction

S. K. Das,[1] A. S. B. Tariq,[1] A. F. M. M. Rahman,[1] P. K. Roy,[1] M. N. Huda,[1] A. S. Mondal,[1] A. K. Basak,[1] H. M. Sen Gupta,[2] and F. B. Malik[3]

[1]*Department of Physics, University of Rajshahi, Rajshahi, Bangladesh*

[2]*Department of Physics, University of Dhaka, Dhaka, Bangladesh*

[3]*Department of Physics, Southern Illinois University, Carbondale, Illinois 62901*

(Received 15 June 1999; published 16 September 1999)

Full finite-range distorted-wave Born approximation calculations have been performed using molecular, Michel, and normal optical potentials to analyze the angular distributions of cross sections for the 53 transitions populating the bound and unbound states of ^{28}Si via the (α,t) reaction. The parameters of these three potentials have been determined from analyses of the elastic scattering data in the entrance channel at the incident energy involved. The molecular and optical potentials are found to produce satisfactory fits to the data, but the Michel potential seems to be inadequate. For all three potentials in the entrance channel, the deduced l transfers for the transitions to the 15.02, 15.85, and 16.11 MeV states differ from the assignments previously reported. The extracted spectroscopic factors are compared with shell-model predictions. [S0556-2813(99)02510-8]

PACS number(s): 25.55.Ci, 21.10.Jx, 24.10.Eq, 24.50.+g

I. INTRODUCTION

Since the first observation of anomalous large angle scattering (ALAS) by Correlli *et al.* [1] in the elastic scattering of α particles by ^{16}O and ^{32}S, it has also been found to occur in other elastic and nonelastic processes [2–4] induced by α particles. The normal optical-model potentials are found to be consistently inadequate in reproducing ALAS in elastic and inelastic scattering as well as transfer reactions induced by α particles [5–9]. Two alternative types of potential have been proposed to explain ALAS. The first one, advocated by Michel *et al.* [10,11], is a special type of optical potential with a squared Woods-Saxon (WS) geometry. The second one is a molecular type of complex potentials [12–14], having a repulsive core in its real part. Both potentials have been successful in reproducing ALAS in the elastic scattering of α particles [10–15] by some $2s$-$1d$ nuclei. Nonelastic processes have so far been, in most cases, treated within the framework of direct-reaction theory using normal optical potentials in the distorted channels. The anomalies in the data of (α,d) and (α,p) reactions on ^{28}Si [9] have, so far, been analyzed in terms of an incoherent sum of the distorted-wave Born approximation (DWBA) contribution calculated with normal optical potentials and the compound nucleus contribution calculated on the basis of the Hauser-Feshbach model [16]. The method has enjoyed a limited success. In particular, the elastic and transfer data could not be fitted with the same optical potential. To the best of our knowledge there is no available report dealing with the single particle transfer processes using both the molecular- and Michel-type potentials, although these potentials could explain successfully the elastic α-scattering data for a number of $2s$-$1d$ targets [15]. The normal optical model, on the other hand, has failed to explain these data. One may also note that the molecular type of potential has been able reasonably to reproduce [17] the angular distributions of the cross section for the ^{28}Si$(\alpha,p)^{31}$P reaction leading to the ground and excited states. The present study is motivated with a view to test the two potentials in analyzing the one-nucleon transfer reaction on a target, as a part of a series of investigations to find the nature of the α-nucleus interaction which can explain all collision processes involving α-particles including particle transfer reactions. With this objective in mind we have chosen the experimental data of Yasue *et al.* [18] for the ^{27}Al$(\alpha,t)^{28}$Si reaction at $E_\alpha = 64.5$ MeV leading to 56 transitions with an energy resolution of about 35 keV. The DWBA analyses in the work of Yasue *et al.* [18] do not use the appropriate form factor as well as the full finite-range (FFR) calculations for the transitions to states in the unbound region. We have investigated the effect of a FFR using the normal optical, Michel-type, and molecular potentials for particle transfers to bound as well as the unbound states using the resonance form factor, formulated by Vincent and Fortune [19,20]. One may note, however, the lack of reaction data in the analysis at scattering angles greater than about 60° (c.m.) which might be important in determining the details of the potentials. The form of the three types of

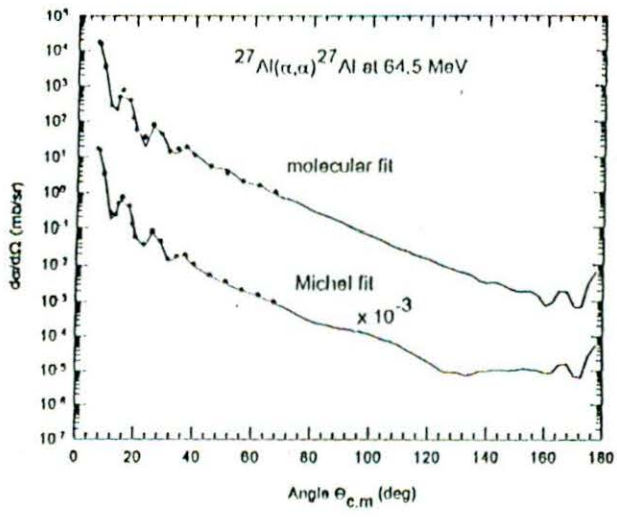

FIG. 1. Fits to the α-^{27}Al elastic scattering data at 64.5 MeV with molecular and Michel potentials. Data are from [18].

TABLE I. Potential Parameters. V adjusted to give the separation energy.

Channel	$\alpha+^{27}$Al			$t+^{28}$Si	$p+^{27}$Al	$t+p$	
				Optical			
Potential type	Optical	Michel	Molecular	set 1	set 2	Bound state	Bound state
V_0 (MeV)	218.0	80.20	52.81	143.82	56.30	V	V
r_0 (fm)	1.24	1.617	1.55	1.19	1.40	1.25	1.25
a_0 (fm)	0.68	0.60	0.57	0.682	0.72	0.70	0.65
V_1 (MeV)			68.46				
R_1 (fm)			2.84				
α		7.40					
ρ (fm)		2.90					
W_0 (MeV)	25.6	55.20	58.13	31.30	50.10		
r_I (fm)	1.24	1.53		1.28	1.40		
a_I (fm)	0.68	0.52		0.999	0.72		
R_w (fm)			3.35				
W_D (MeV)							
r_D (fm)							
a_D (fm)							
$V_{s.o.}$ (MeV)				4.65		$\lambda=25$	$\lambda=25$
$r_{s.o.}$ (fm)				0.996			
$a_{s.o.}$ (fm)				0.280			
r_c (fm)						1.25	1.25
R_c (fm)	5.10	3.90	9.30	3.94	3.94		
	a			b	c	d	d

[a]Reference [34].
[b]Reference [35].
[c]Reference [36].
[d]Reference [27].

α-nucleus potential used in the present work is discussed in Sec. II. Section III gives briefly the salient aspects of the DWBA theory relevant to the present analyses. The DWBA analyses are furnished in Sec. IV. Section V discusses the l transfers involved in populating the various final states, in particular l assignments that differ from the previously reported values [18] for some of the transitions. The conclusions are given in Sec. VI.

II. α-NUCLEUS POTENTIALS

The squared WS Michel potential [10,11] including the Coulomb term $V_c(r)$ is comprised of the following forms [10] of the real $V(r)$ and imaginary $W(r)$ parts:

$$V_M(r) = -V_0\left\{1+\alpha\exp\left[-\left(\frac{r}{\rho}\right)^2\right]\right\} \times\left[1+\exp\left(\frac{r-R_R}{2a_R}\right)\right]^{-2}+V_c(r), \quad (1)$$

$$W_M(r) = -W_0\left[1+\exp\left(\frac{r-R_I}{2a_I}\right)\right]^{-2}, \quad (2)$$

with

$$V_c(r) = \left[\frac{Z_1Z_2e^2}{2R_c}\right]\left[3-\frac{r^2}{R_c^2}\right] \quad (\text{for } r\le R_c) \quad (3)$$

$$= \frac{Z_1Z_2e^2}{r} \quad (\text{for } r>R_c), \quad (4)$$

where $R_C=r_CA_T^{1/3}$ is the Coulomb radius.

This phenomenological form of the potential has been shown to be approximately similar to the equivalent local potential [21] obtained from the microscopic analysis using resonating group method [21,22].

The molecular potential is embedded in the early works of Block and Malik [23] and others [24,25] who recognized this as the manifestation of the role of the Pauli exclusion principle in heavy ion scattering. The potential is obtained from a many body theory utilizing the energy-density functional method [25,26]. This potential has the following forms [14] for the real, $V_m(r)$, and imaginary, $W_m(r)$, parts:

$$V_m(r) = -V_0\left[1+\exp\left(\frac{r-R_0}{a_0}\right)\right]^{-1} + V_1\exp\left[-\left(\frac{r}{R_1}\right)^2\right]+V_c(r), \quad (5)$$

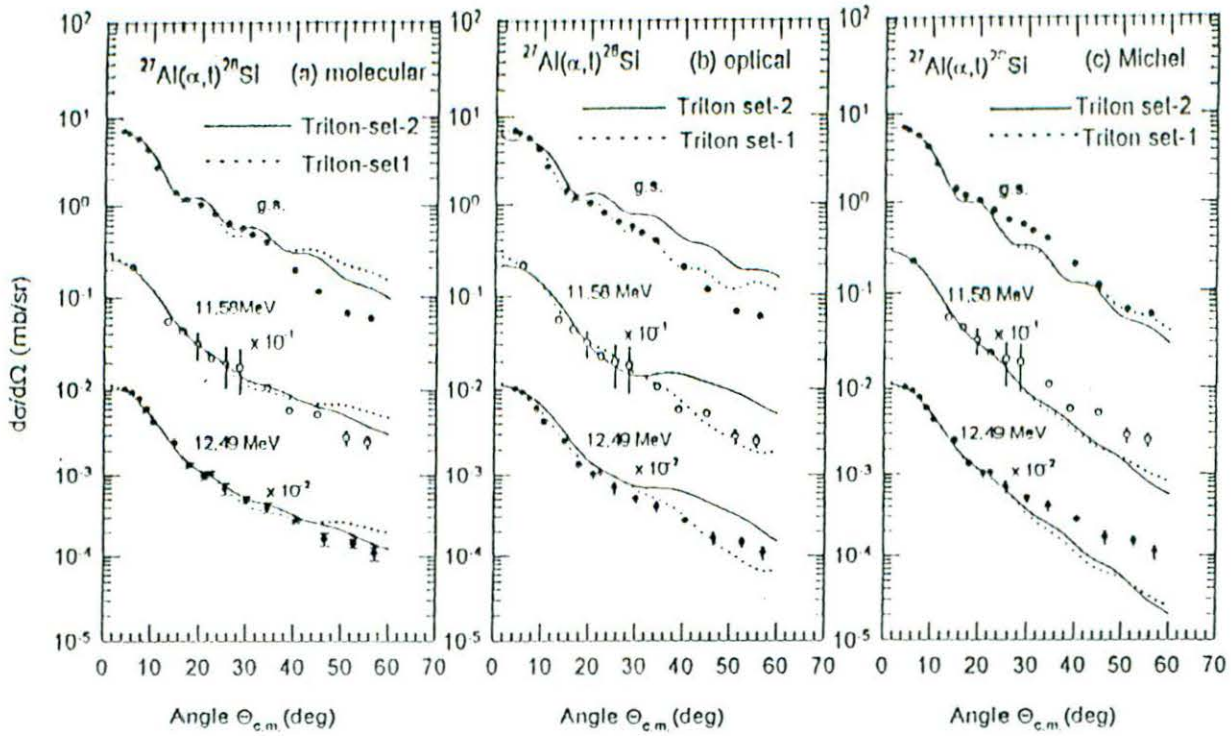

FIG. 2. Full finite-range DWBA predictions compared to data [18] for three transitions using (a) molecular, (b) normal optical, and (c) Michel potentials with set 1 and set 2 (Table I) of triton potentials in the exit channel.

$$W_m(r) = -W_0 \exp\left[-\frac{r}{R_W}\right]^2. \tag{6}$$

Thus the real part is nonmonotonic with a short-range repulsion. The Coulomb radius is scaled [14,15] according to $R_C = R_\alpha + r_C A_T^{1/3}$, R_α being the contribution from α particles.

The normal optical potential for the α-nucleus system including the Coulomb term is given by [27]

$$V(r) = V_c - Vf(x_0) - i\left[Wf(x_W) - 4W_D \frac{d}{dx} f(x_D)\right], \tag{7}$$

where $f(x_i) = (1+e^{x_i})^{-1}$ with $x_i = (r - r_i A^{1/3})/a_i$ and the subscript $i = 0$, W, and D. The Coulomb radius is given by $R_C = r_C A_T^{1/3}$.

III. THEORY OF DWBA FORMALISM

The differential cross section for a transfer reaction with a particular j transfer in the DWBA theory [28] is given by

$$\frac{d\sigma}{d\Omega} = \frac{\mu_i \mu_f}{(2\pi\hbar^2)^2} \frac{k_f}{k_i} \frac{1}{(2J_i+1)(2s_a+1)} \sum |T_{fi}|^2, \tag{8}$$

where J_i and s_a are the spins of the target and the projectile, respectively. μ's and k's are, respectively, the reduced masses and wave numbers. The subscripts i and f refer to the incident and outgoing channels, respectively. Σ denotes the sum over all magnetic substates. T_{fi} is the transition amplitude, having the form

$$T_{fi} = J \int d^3\mathbf{r}_a \int d^3\mathbf{r}_b \chi_f^{(-)*}(\mathbf{k}_b, \mathbf{r}_b) V_{fi}(\mathbf{r}) \chi_i^{(+)}(\mathbf{k}_a, \mathbf{r}_a). \tag{9}$$

Here J is the Jacobian of the transformation to the relative coordinates. $\chi_i^{(+)}$ and $\chi_f^{(-)}$ are the distorted waves in the initial and final channels, respectively, with outgoing and incoming boundary conditions. $\mathbf{r}_a$ and $\mathbf{r}_b$ are the coordinates of the outgoing and incoming particles a and b relative to the center of mass of the system. $\mathbf{k}_a$ and $\mathbf{k}_b$ are the momenta of the projectile and ejectile, respectively. The distorted waves $\chi(\mathbf{k},\mathbf{r})$ are generated from the Schrödinger equation [28]

$$\left\{\nabla^2 + k^2 - \left(\frac{2\mu}{\hbar^2}\right)[V(r) + V_c(r)]\right\}\chi(\mathbf{k},\mathbf{r}) = 0, \tag{10}$$

where $V(r)$ is the distorting potential and μ is the reduced mass of the pair. The distorting potential may be the normal optical, Michel, or molecular potential. The V_{fi} is the transition matrix having the form [28]

$$V_{fi} = \langle \psi_f \psi_b | V | \psi_i \psi_a \rangle. \tag{11}$$

Equation (11) can be, under certain circumstances, factored into (i) the overlap integral $\langle \psi_f | \psi_i \rangle$ containing the spectroscopic amplitude and the information on the nuclear struc-

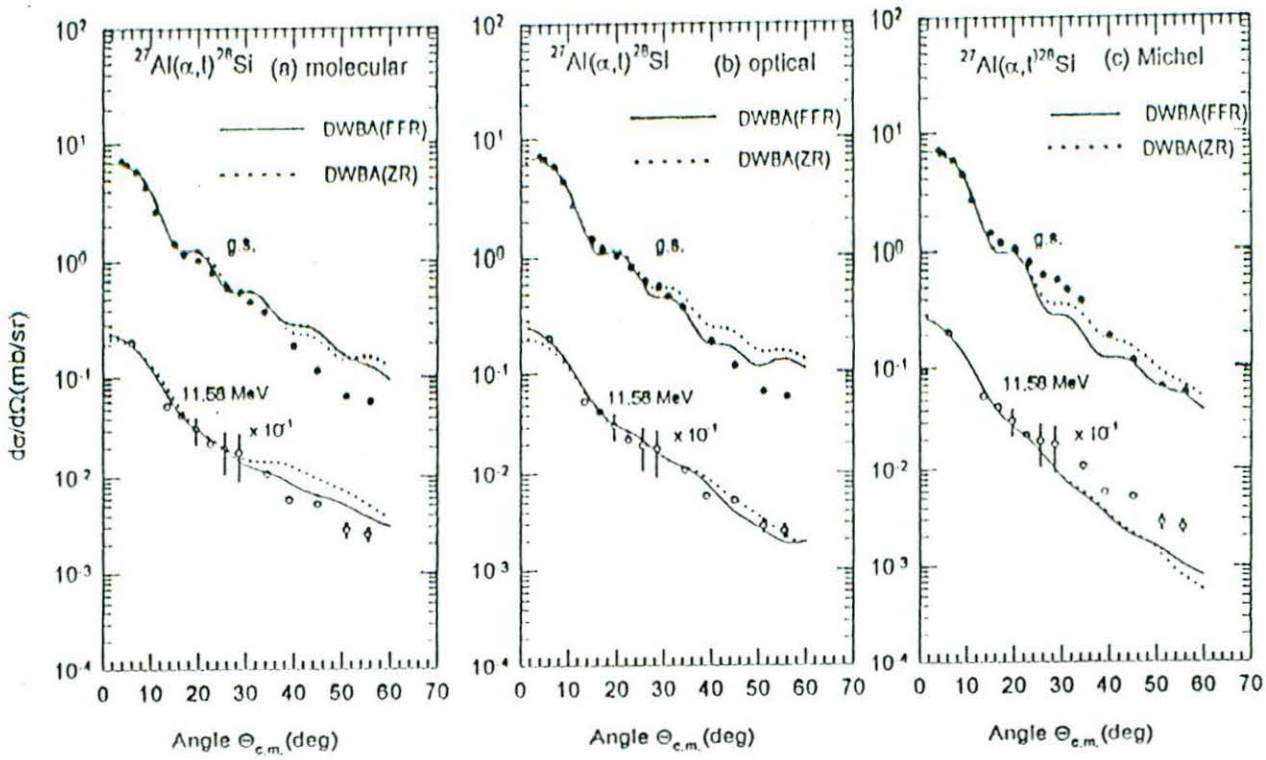

FIG. 3. Full finite-range (solid curves) and zero-range (dotted curves) DWBA predictions using (a) molecular, (b) normal optical, and (c) Michel potentials for the g.s. and $E_x = 11.58$ MeV transitions are compared to data. Data are from [18].

ture and (ii) the effective interaction $\langle \psi_a | V | \psi_b \rangle$ responsible for the transition from the initial channel to the final channel [28]. In the analysis of single nucleon stripping reactions, it is assumed that the transferred nucleon is picked up from the projectile and deposited into a shell-model state of the final nucleus. Thus the DWBA calculations in the present analysis involve the single particle proton wave function in the final nucleus as well as that in the incident α particle.

In the isospin representation, Eq. (8) can be reduced into a more tractable form for the calculation of the cross section of the stripping reaction in FFR calculations [30]:

$$\left(\frac{d\sigma}{d\Omega}\right)_{\text{expt}} = \frac{2J_f+1}{2J_i+1} C^2 S s \left(\frac{d\sigma}{d\Omega}\right)_{\text{DWUCK5}}. \tag{12}$$

$(d\sigma/d\Omega)_{\text{DWUCK5}}$ means the cross section calculated with the computer code DWUCK5, C^2 is the isospin Clebsch-Gordon coefficient, and S and s are, respectively, the heavy and light particle spectroscopic factors. J_f and J_i are the total spins of the final and initial nuclei, respectively. The corresponding expression [30] for a zero-range (ZR) approximation is

$$\left(\frac{d\sigma}{d\Omega}\right)_{\text{expt}} = \frac{(2J_f+1)}{(2J_i+1)(2j+1)} D_0^2 C^2 S \left(\frac{d\sigma}{d\Omega}\right)_{\text{DWUCK4}}. \tag{13}$$

D_0^2 is the normalization constant, and $(d\sigma/d\Omega)_{\text{DWUCK4}}$ is the cross section calculated with DWUCK4.

For the analyses of the data for the unbound states of the final nucleus, the resonance form factor formulated by Vincent and Fortune [19,20] is applied. It is assumed that the resonance has a Breit-Wigner shape, and in such a case the differential cross section is given [20] by

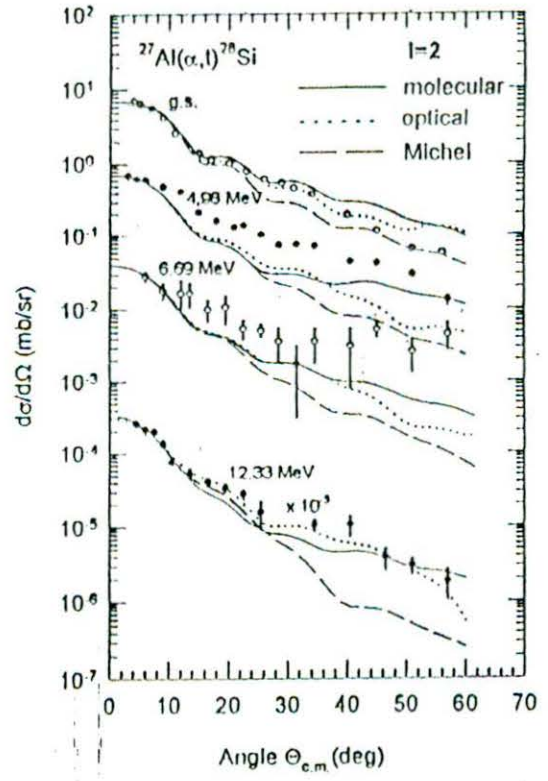

FIG. 4. Full finite-range DWBA predictions using molecular (solid curves), normal optical (dotted curves), and Michel (dashed curves) potentials for the transitions with l values indicated are compared to data (solid or open circles). The triton potential of set 1 has been used with the normal optical and Michel potentials, and that of set 2 with the molecular potential in the α channel. Data are from [18].

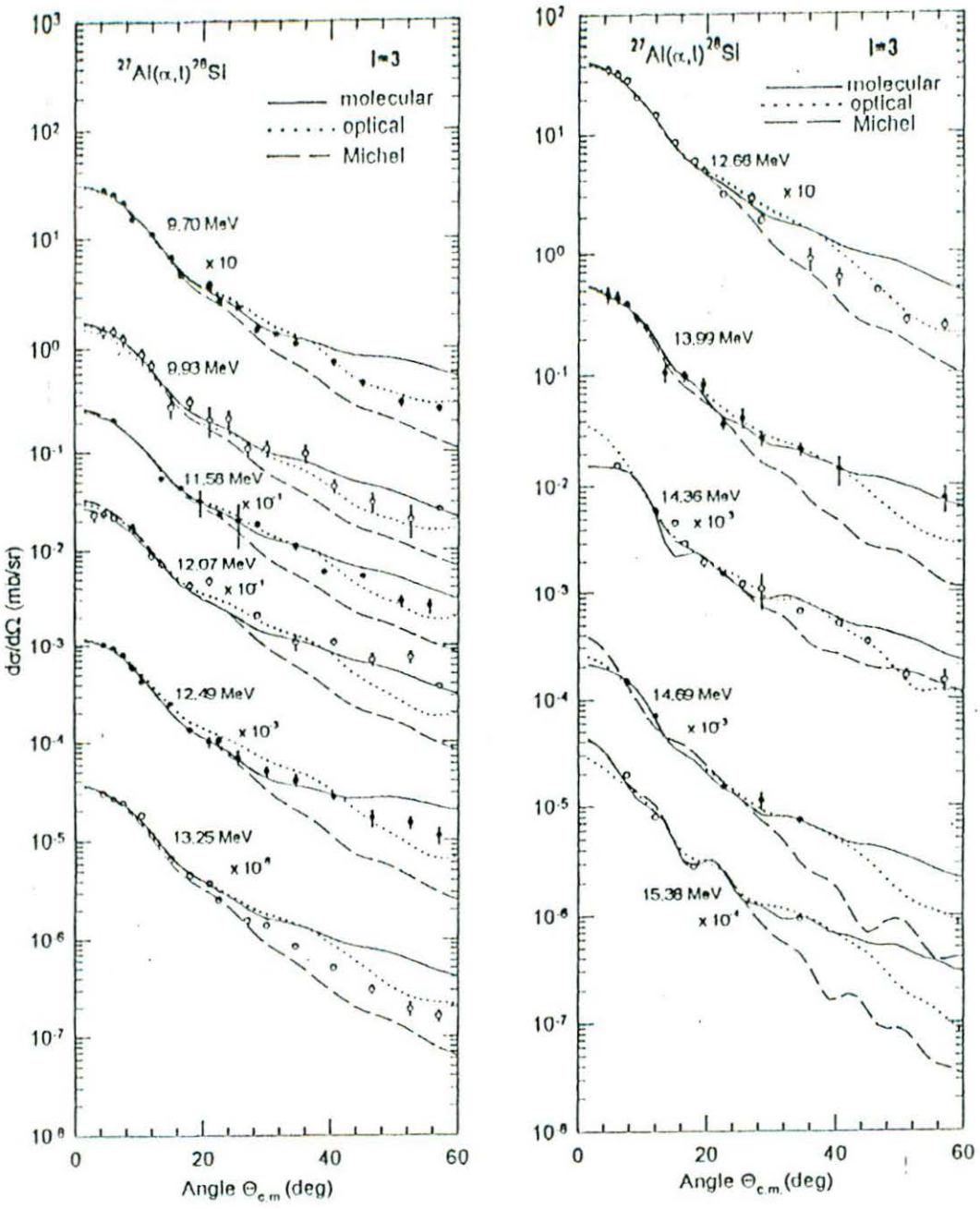

FIG. 5. Same as in Fig. 4.

$$\frac{d\sigma}{d\Omega} = \frac{\Gamma \mu k}{\hbar} \frac{d\sigma^{F}}{d\Omega}. \tag{14}$$

Here $d\sigma^{F}/d\Omega$ is the cross section predicted at the energy of resonance (the positive energy of the transferred proton relative to the core). Γ is the width of the resonance, μ is the reduced mass of the transferred proton and the target nucleus, and k is the wave number of the proton at the resonance energy. Γ is estimated from the relation [20]

$$\frac{2}{\Gamma} = \frac{2\mu}{\hbar^2 k}\left[\int_0^{R_{\max}} |u(r)|^2 dr + \frac{G}{2k}\frac{d}{dk}\left(\frac{G'}{G}\right)\right]. \tag{15}$$

Here $u(r)$ is the radial wave function of proton in the field of target core and $r = R_{\max}$ is the distance beyond which nuclear potentials are assumed to be zero. G and G' are the irregular Coulomb function and its derivative at $r = R_{\max}$, respectively.

IV. DWBA ANALYSIS

The ZR and FFR DWBA calculations for the angular distributions have been performed using the computer codes DWUCK4 and DWUCK5 [30], respectively. Both codes are modified to include Michel and molecular potentials. For the ZR calculations, a Gaussian form of finite-range correction in the local energy approximation [29,30] with the correction parameter $R = 0.7$ fm has been used. Corrections due to the nonlocality [30,31] of potentials in the conventional form have been applied using the nonlocality parameters $\beta(\alpha) = 0.2$ and $\beta(p) = 0.85$ fm. The FFR analyses have been performed for both bound and unbound regions

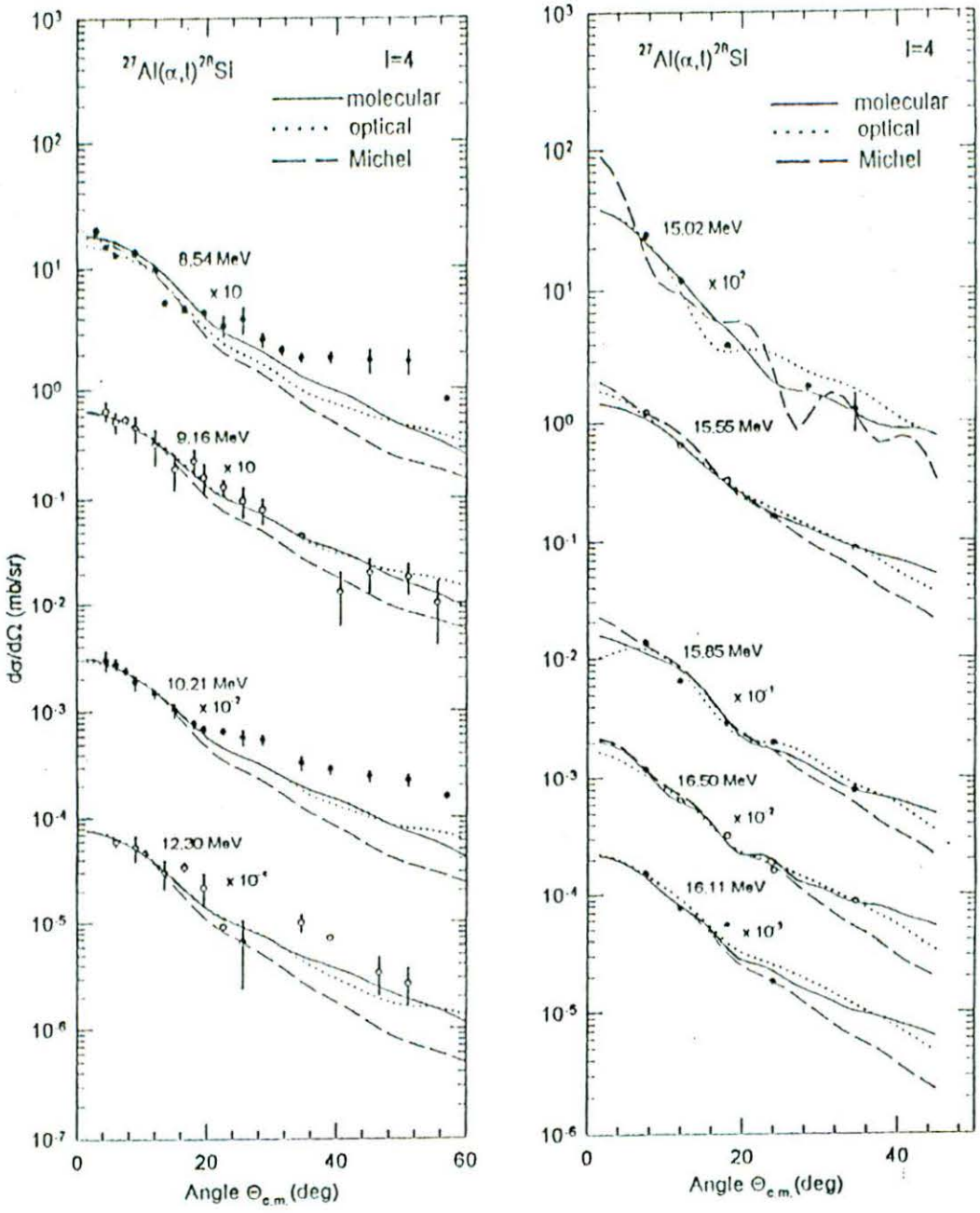

FIG. 6. Same as in Fig. 4.

using the Michel, molecular, and normal optical model types of potentials.

A. Choice of potential parameters

For the entrance channel, the parameters of the molecular and Michel types of potential are generated by fitting the angular distributions of elastic data [18] using the chi-squared minimization code MINUIT [32] in conjunction with the optical-model code SCAT2 [33] modified to incorporate the Michel and molecular potentials. The fits to the elastic data are shown in Fig. 1. The normal optical-potential-parameter set used in the present analysis is taken from [34]. The parameters of all three types of potentials are given in Table I. The bound state geometry parameters are also noted in Table I. For a bound state of ^{28}Si for both the FFR and ZR calculations, as well as for the bound state of the α for the FFR calculations, the single proton transfer wave function has been computed adjusting the WS potential well depth so that its eigenvalue equals the separation energy [29].

For the triton potential in the exit channel, different sets of triton potentials have been tried. Two sets of triton potentials, labeled set 1 and set 2 in Table I, have been found to fit the data reasonably well with the molecular, normal optical, or Michel potential in the entrance channel as can be seen in Figs. 2(a)–2(c). Set 2 of triton potentials produces a slightly better fit at the larger scattering angle region when the molecular potential is employed in the α channel [Fig. 2(a)]. On the other hand, the normal optical potential in the α channel produces a good fit to the data for set 1 of triton potentials in the exit channel [Fig. 2(b)]. We have, therefore, finally chosen set 2 of triton potentials with the molecular potential and

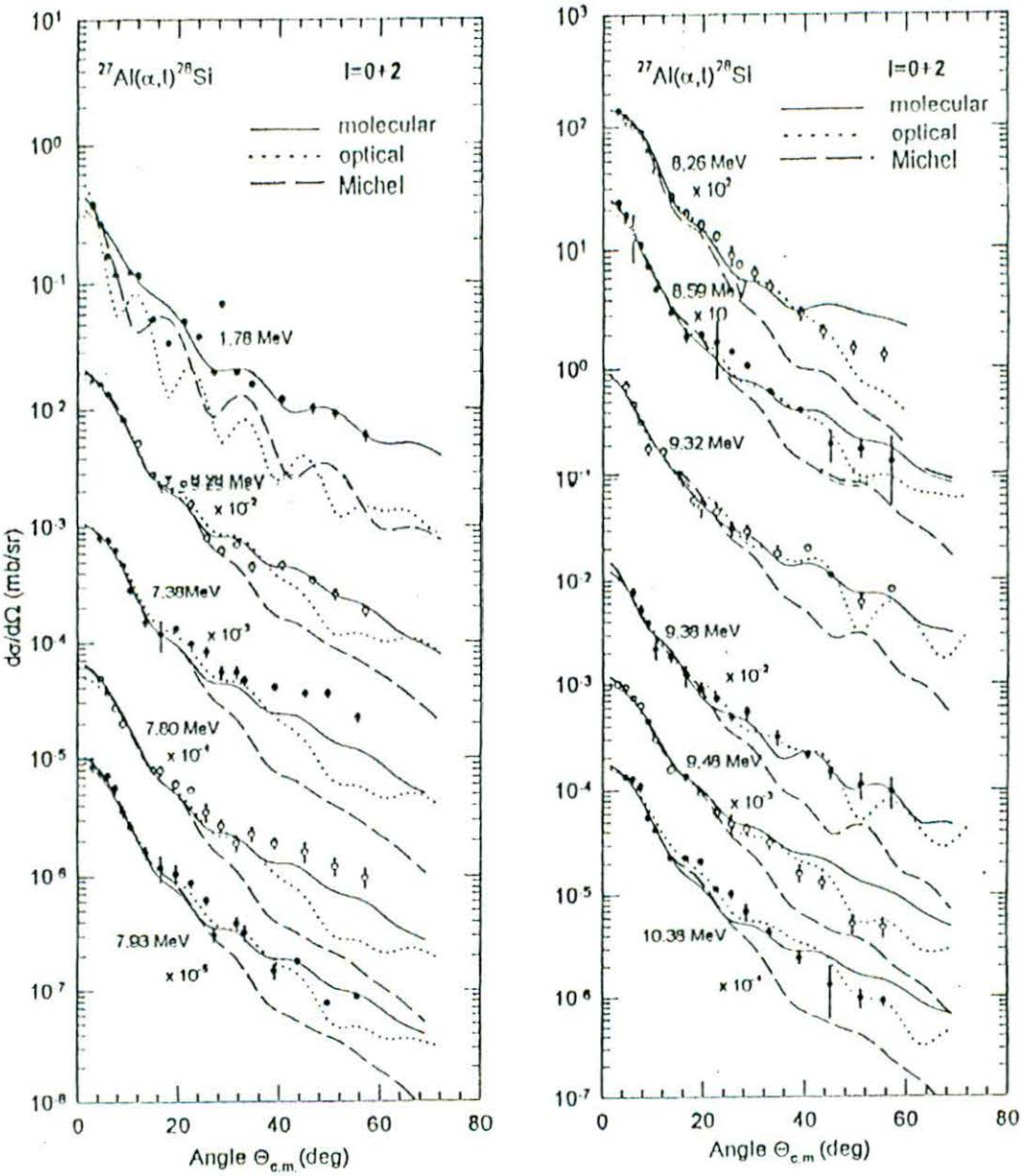

FIG. 7. Incoherent sums of full finite-range DWBA predictions using molecular (solid curves), normal optical (dotted curves), and Michel (dashed curves) potentials for the transitions with l values indicated are compared to data (filled or open circles). Data are from [18].

set 1 of the triton potentials with the Michel or normal optical potential in the α channel for the analyses of the data. It is to be noted that the sensitivity of the predicted cross sections to the triton potential seems to be much stronger in the case of the normal optical potential in the entrance [Fig. 2(b)] than for cases with the other two potentials.

B. Angular distributions

The comparison of the ZR and FFR DWBA calculations of the angular distributions for the ground state (g.s.) and the state at the excitation energy $E_x = 11.58$ MeV using the molecular, Michel, and normal optical potentials for the best fits to the experimental data are shown in Figs. 3(a)–3(c).

The FFR DWBA calculations for angular distributions for the best fits to the data using all three types of α-nucleus potentials for various l transfers are compared to the experimental data in Figs. 4–9 for all levels. The levels in Figs. 4–9 are grouped according to the associated l transfers. The levels populated through the $l=2$, 3, and 4 transfers are shown in Figs. 4–6, respectively. On the other hand, the levels which have been obtained through the incoherent sum of more than one l transfer such as $l=0+2$, $1+3$, and $2+4$ are shown, respectively, in Figs. 7–9. The DWBA fit to the unresolved group at $E_x = 6.88$ MeV is also shown in Fig. 8 with the total incoherent contribution from $l=2+3$. In the previous study, Yasue *et al.* associated an $l=3$ transfer for fitting 15.02, 15.85, and 16.11 MeV transitions, but in the present study, it seems to be $l=4$. The predicted angular distributions using each of the molecular, Michel, and normal optical potentials for both l transfers ($l=3$ and $l=4$) are compared to the data in Fig. 10. Clearly, the $l=4$ transfer is preferred in all three cases.

C. Spectroscopic strengths

The spectroscopic strengths of a reaction for a transition to a final state $(J_f;T_f)$ with the transferred configuration (lj) is related to the spectroscopic factor S_{lj} [38] by

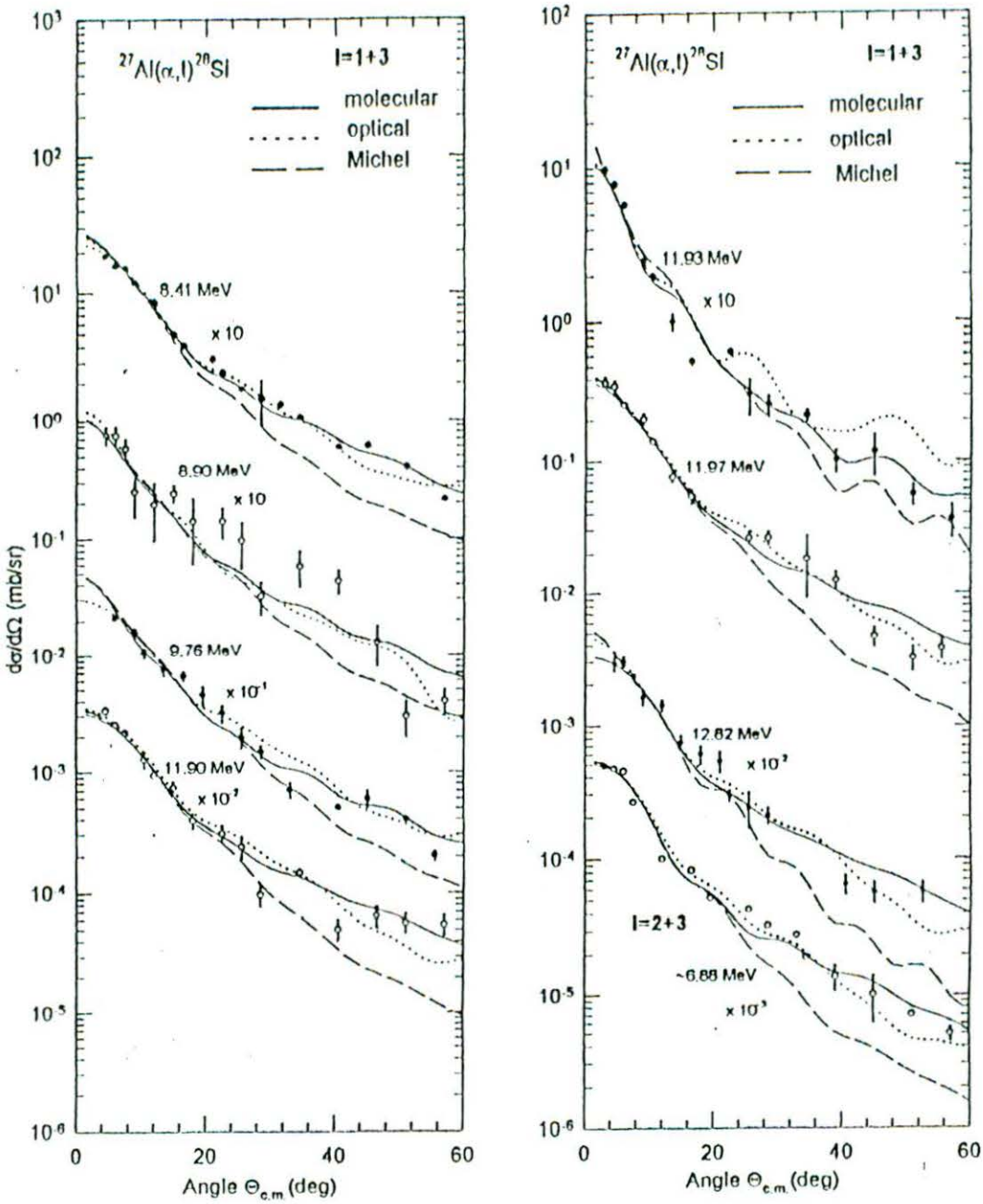

FIG. 8. Same as in Fig. 7. The data of the 6.88 MeV transition are compared to the $l=2+3$ DWBA predictions.

$$G_{lj}=\frac{(2J_f+1)}{(2J_i+1)}C^2S_{lj}, \tag{16}$$

where C is the Clebsch-Gordon coefficient involving isospins of the target and the final nucleus.

The sum rule for the spectroscopic strength in the case of the ^{27}Al$(\alpha,t)^{28}$Si reaction can then be expressed [38] by

$$\sum_{J_f} G_{lj}=\frac{1}{2}\langle n \text{ holes}\rangle \quad (\text{for } T_f=1)$$

$$=\frac{1}{2}\langle p \text{ holes}\rangle-\frac{1}{2}\langle n \text{ holes}\rangle \quad (\text{for } T_f=0),$$

where $\langle p$ holes$\rangle$ and $\langle n$ holes$\rangle$ are, respectively, the effective number of proton holes and neutron holes in the orbit (lj).

The total strength comprising transitions with $T_f=0$ and 1 is then

$$\sum_{J_f,T_f} G_{lj}=\langle p \text{ holes}\rangle. \tag{17}$$

The deduced sum of strengths for all $l=2$ transitions with $j=3/2,5/2$ transfers and $T_f=0,1$ is $\Sigma G=2.33$. This is almost half of the sum rule strength 5.0, the number of proton holes in the $1d_{5/2}$ and $1d_{3/2}$ orbits. Similarly, the sum of all $l=0$ transition strengths for both $T_f=0$ and 1 has been found to be $\Sigma G=0.96$, which is again 50% of the expected sum of 2.0.

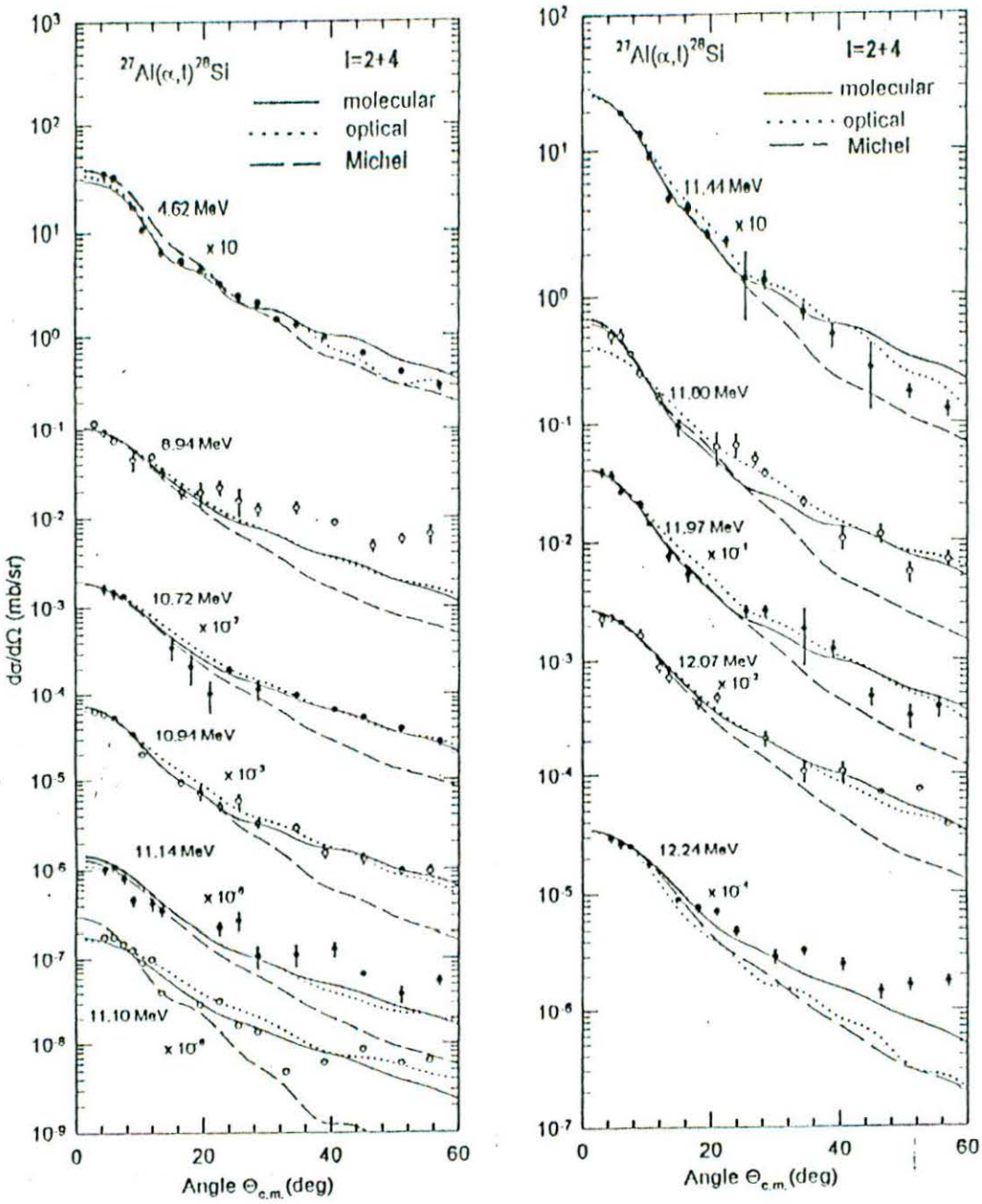

FIG. 9. Same as in Fig. 7.

The extracted transition strengths for the $(6^-;0)$ state at $E_x = 11.58$ MeV and $(6^-;1)$ state at $E_x = 14.36$ MeV, which have the stretched configuration $(1d_{5/2}^{-1}, 1f_{7/2})$ in the shell model, are 0.14 and 0.23, respectively, which is small compared to the expected full strength of 1.08 for each. If one considers, however, the fragmentation of 6^- strengths as due to the deformed structure of the ^{28}Si core, using the assumptions that (i) the vibrational state of the core does not change in the transition, (ii) the core has negative deformation, and (iii) the proton-hole configuration in the target is $|j_i = 5/2, \Omega_i = 1/2\rangle$—i.e., the target has $J_i = 5/2$ and $K_i = 1/2$—one may calculate the spectroscopic strength due to deformation using the expression [39,40]

$$G = \frac{(2J_f+1)}{(2J_i+1)} C^2S = g^2 C^2 \langle J_i K_i j \Omega | J_f K_f \rangle^2 C_{Nlj}(\Omega\omega\alpha)^2, \tag{18}$$

where $C_{Nlj}(\Omega\omega\alpha)$ as defined in [39,40] are the coefficients connecting a deformed single particle state to spherical eigenstates, and g^2 is unity as $K_i \neq 0$. The values of these coefficients have been taken from [41]. Equation (18) with $K_f = 4$ results in a strength of $G = 0.083$ for each of the $(6^-;0)$ and $(6^-;1)$ states, which is, indeed, small.

V. DISCUSSION

In the present study, 53 transitions have been analyzed with all three types of potentials. The analyses involve (i) 4 transitions with the $l = 2$ transfers (Fig. 4), leading to the ground, 4.98, and 6.69 MeV states with the unique $j = 5/2$ transfer and the 12.33 MeV state which is assumed to be populated via $j = 3/2$, (ii) 11 transitions with $l = 3$ (Fig. 5), (iii) 9 transitions with $l = 4$ (Fig. 6), (iv) 11 transitions with

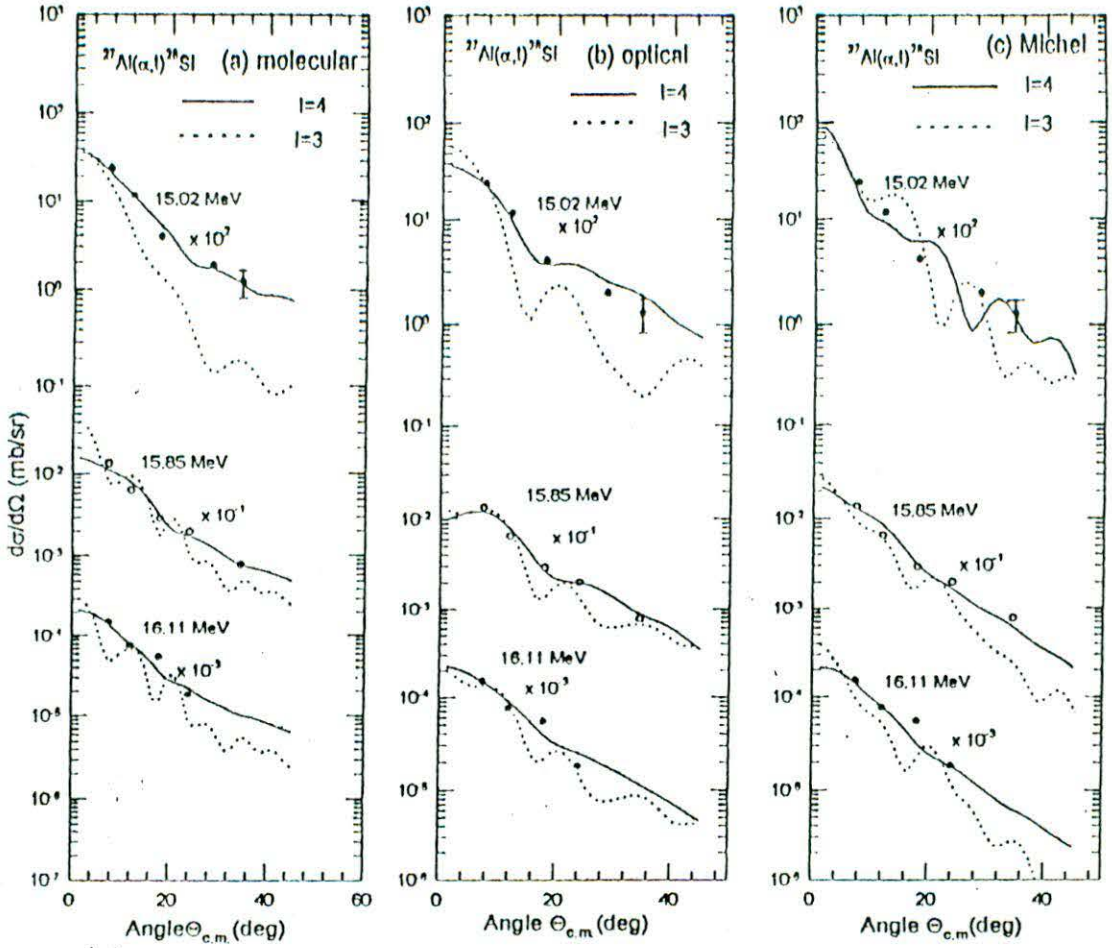

FIG. 10. Full finite-range DWBA predictions for transitions with $l=4$ (solid curves) and $l=3$ (dotted curves) values are compared to data for three transitions using (a) molecular, (b) normal optical, and (c) Michel potentials. Data are from [18].

the admixture $l=0+2$ (Fig. 7), (v) 7 transitions with the admixture $l=1+3$ (Fig. 8), (vi) 1 transition with $l=2+3$ (Fig. 8) populating probably two unresolved states with opposite parities at about $E_x=6.88$ MeV, and (vii) 11 transitions with the admixture $l=2+4$ (Fig. 9) transfer. The data of the transition to the 11.97 MeV state are compared to the DWBA predictions twice, once in Fig. 8 for the $l=1+3$ transfer and again in Fig. 9 for the $l=2+4$ transfer as both transfers produce acceptable fits to the data.

In Fig. 3 the FFR and ZR calculations are compared to the angular distribution data for transitions to the g.s. and the state at $E_x=11.58$ MeV. The improvement of the fits due to predictions of the former over those of the latter underlines the importance of the FFR calculations.

It is evident from Figs. 4–9 that the full finite-range DWBA analyses using the molecular and normal optical potentials fits quite satisfactorily the experimental data of the 44 transitions out of 53 with 9 other states fitted moderately. In general, the fits with the molecular and normal optical potentials seem to be of the same quality, but the fits with the Michel potential are comparatively poor. At forward scattering angles $<20°$ or so, all three potentials yield, to some extent, the same results. But at larger scattering angles, for the bound state transitions with excitation energies up to 11.58 MeV, the molecular potential provides a better fit, although the normal optical potential competes reasonably well, while the Michel potential fails completely. For the continuum states with excitation energies above 11.58 MeV both molecular and normal optical potentials yield again comparable results with quite reasonable fits to the data, but the Michel potential fails again. At reaction angles larger than 30°, the difference in the predictions due to the three distorting α-nucleus potentials becomes very prominent and increases with the reaction angle. It is also to be mentioned that for some transitions, e.g., the 4.98, 6.69, 8.54, 10.21, and 12.24 MeV states, neither of the three types of potentials could produce good fits to the angular distributions, indicating probably that reaction mechanisms other than the direct one may be involved in these cases.

Yasue *et al.* [18] reported that an admixture of $l=1$, 2, and 3 was needed to fit the data of the level 6.88 and 6.89 MeV, but in the present study an admixture of $l=2$ and 3 suffices to fit satisfactorily the angular distributions of these unresolved levels (Fig. 8). Furthermore, they [18] used the $l=0+2+4$ admixture for the 7.93 and 8.26 MeV transitions, while in the present work $l=0+2$ seems to be sufficient to fit the data quite well (Fig. 7). Moreover, as mentioned earlier, Yasue *et al.* [18] associated the 15.02, 15.85, and 16.11 MeV transitions with the $l=3$ transfer, but the comparison of the predictions in the present analyses for $l=3$ and 4 in Fig. 10 for each of the three potentials shows that the angular distributions for these transitions are better

TABLE II. States of ^{28}Si observed in the ^{27}Al(α,t) reaction at E_α = 64.5 MeV.

			$(2J_f+1)C^2Ss^a$ Present work			
E_x (MeV)	$J^\pi;T$ b	$l(nlj)$	c	d	e	f,g
g.s	$0^+;0$	$2(0d_{5/2})$	4.8	4.5	4.5	4.6
1.78	$2^+;0$	(0+2)	0.7, 1.08	0.84, 1.26	0.672, 1.008	1.7, 1.2
4.62	$4^+;0$	(2+4)	2.13, 0.022	2.90, 0.396	2.22, 0.117	2.5, 0.04
4.98	$0^+;0$	$2(0d_{5/2})$	0.42	0.6	0.75	0.48
6.28	$3^+;0$	(0+2)	0.138, 1.24	0.36, 2.04	0.63, 1.47	0.39, 1.4
6.69	$0^+;0$	$2(0d_{5/2})$	0.03	0.048	0.048	0.04
6.88	$3^-;0$	(2+3)	0.27, 0.03	0.57, 0.03	0.456, 0.024	0.65, 1.1, 2.6
6.89	$4^+;0$					
7.38	$2^+;0$	(0+2)	0.06, 0.86	0.3, 1.2	0.276, 1.104	0.15, 0.90
7.42	$2^+;0$					
7.80	$3^+;0$	(0+2)	0.26, 0.396	0.357, 0.663	0.315, 0.585	0.22, 0.35
7.93	$2^+;0$	(0+2)	0.27, 0.672	0.63, 1.17	0.441, 0.819	0.7, 0.65, 0.06
8.26	$2^+;0$	(0+2)	0.30, 1.20	0.15, 1.65	0.38, 1.5	0.13, 1.1
8.41	$4^-;0$	(1+3)	0.48, 0.72	0.9, 0.9	0.9, 0.9	0.45, 1.0
8.54	$6^+;0$	4	0.48	0.78	0.9	0.13
8.59	$3^+;0$	(0+2)	1.0, 1.51	2.85, 2.85	1.8, 1.8	0.8, 1.9
8.90	$1^-;0$	(1+3)	0.048, 0.072	0.076, 0.032	0.055, 0.023	0.018, 0.048
8.94	$4^+;0$	(2+4)	0.054, 0.023	0.022, 0.086	0.022, 0.086	0.11, 0.06
	$5^-;0$	or 3	0.054	0.066	0.036	0.06
9.16	$4^+;0$	4	0.02	0.03	0.03	0.06
9.32	$3^+;1$	(0+2)	1.176, 0.50	1.95, 1.05	1.365, 0.735	1.5, 0.49
9.38	$2^+;1$	(0+2)	1.33, 0.88	3.36, 1.44	3.84, 0.96	1.6, 1.0
9.48	$2^+;0$	(0+2)	0.52, 0.90	1.5, 1.5	1.026, 0.054	0.2, 0.24
9.70	$5^-;0$	3	1.20	1.8	1.8	1.8
9.76	$(2,3)^-;0$	(1+3)	0.038, 0.113	0.576, 0.144	0.385, .096	0.06, 0.17
9.93	$(1,2)^-;0$	3	0.60	1.17	0.99	0.11
10.21	$(2-4)^+;0$	4	0.096	0.126	0.126	0.17
10.38	$3^+;1$	(0+2)	0.66, 1.98	1.13, 3.38	0.75, 2.25	0.65, 2.3
10.72	$1^+;0+1$	(2+4)	0.113, 0.038	1.92, 0.48	0.144, 0.036	0.11, 0.009
10.94	+	(2+4)	0.70, 0.08	1.37, 0.072	1.083, 0.057	0.32
11.10		(2+4)	0.105, 0.045	0.108, 0.072	0.072, 0.048	0.1, 0.04,
11.14	2^+	(2+4)	0.363, 0.297	0.274, 0.068	0.168, 0.042	0.02, 0.06
11.44	$2^+,3^+,4^+;(0,1)$	(2+4)	2.96, 0.16	5.99, 0.315	3.99, 0.21	3.8, 0.39
11.45	$1^+;1$					
11.58	$6^-;0$	3	1.41	1.86	1.68	2.1
11.80	+	2+4	0.19, 0.157	0.36, 0.36	0.5, 0.22	0.13, 0.12
11.90	$3^-;0$	(1+3)	0.4, 0.08	0.126, 0.294	0.099, 0.231	0.49, 0.17
11.93	−	1+3	3.70, 0.195	5.67, 0.63	4.28, 0.23	4.7
11.97	$(2^+,4^+);0$	2+4	0.59, 0.066	0.972, 0.108	0.11, 0.066	0.5, 0.09
	or $3^-;0$	or 1+3	0.41, 0.221	0.655, 0.353	0.43, 0.23	0.4, 0.3
12.07	$(2^\pm);0$	2+4	0.21, 0.09	0.315, 0.135	0.252, 0.108	0.3, 0.09
		or 3	0.21	0.36	0.24	0.2
12.24	$3^++4^+;0$	2+4	0.1, 0.06	0.144, 0.216	0.144, 0.216	0.27, 0.12
12.30	$2^+;0$	4	0.39	0.51	0.51	0.06
12.33	$1^+;1$	2	0.72	1.32	0.9	0.55
12.49	$3^-;0$	3	0.84	1.2	1.14	1.0
12.66	$4^-;1$	3	3.00	5.4	4.2	3.8
12.82	$1^-;0$	1+3	0.14, 0.32	0.20, 0.46	0.15, 0.36	0.03, 0.32
13.25	$5^-;1$	3	3.30	5.4	4.2	3.6

TABLE II. *(Continued).*

			$(2J_f+1)C^2Ss^a$ Present work			
E_x (MeV)	$J^\pi;T$ b	$l(nlj)$	c	d	e	f,g
13.99	--	3	0.63	1.02	0.78	1.6
14.36	$6^-;1$	3	2.40	2.88	2.7	3.7
14.69	–	3	0.24	0.51	0.33	0.39
15.02	–	4	0.15	0.21	0.21	0.70
15.38	–	3	0.45	0.78	0.57	0.55
15.55	+	4	0.12	0.21	0.15	0.09
15.85	–	4	0.11	0.222	0.156	0.36
16.11	–	4	0.48	0.24	0.48	0.41
16.50	+	4	0.14	0.24	0.18	0.07

[a] $s=2.0$ is the light particle spectroscopic factor.
[b] Reference [37].
[c] Optical.
[d] Michel.
[e] Molecular.
[f] Reference [18].
[g] Light particle spectroscopic factor is not mentioned in [18].

fitted by the $l=4$ transfer. It is also obvious from Fig. 10 that the predictions with the molecular potential bring out the difference more distinctly in the angular patterns for $l=3$ and $l=4$.

The spectroscopic factors (Table II) extracted using the molecular potential are comparable to those obtained using the normal optical potential, but are a bit larger for some cases. In general, those deduced from using the Michel potential are even larger. Considering the quality of the fits, the spectroscopic factors obtained with the Michel potential are expected to be less reliable.

The spectroscopic strengths extracted from the use of the molecular potential are compared to those calculated from the shell model [42] in Table III. The predicted and deduced strengths agree for most of the $l=2$ transitions except that for the 6.89 MeV state. The extracted strengths for the $l=0$ transitions to the 1.78, 6.28, and 9.32 MeV state are much weaker than the predicted values. This may be partly ascribed to the fact that the matching l transfer $|k_iR_i - k_fR_f|$ (k's and R's are, respectively, the momenta and interaction distances in the reaction channels) lies in the range 2–4 over $E_x=0.0$–14.36 MeV of the final nucleus and hence $l=0$ is a mismatched transfer. The $l=0$ shell-model wave functions used in [42] may not be good due to truncation.

The extracted sum of strengths for all $l=2$ as well as for all $l=0$ transitions has a factor of 2 missing from the expected magnitude, e.g., the effective number of proton holes in the transfer orbits. This is surprising when one considers that the states of ^{28}Si resulting from the $j^\pi=1/2^+$, $3/2^+$, $5/2^+$ transfers in the reaction are highly improbable to exist at $E_x>16.50$ MeV. The spherical shell model cannot probably take up the whole of the transition strength, and some of the strength drains off as a result of deformation. For the transition to each of the 6^- states at $E_x=11.58$ and 14.36

TABLE III. Comparison of the deduced spectroscopic strengths to the shell-model predictions.

			$G=\frac{(2J_f+1)}{(2J_i+1)}C^2S$	
E_x (MeV)	$J^\pi;T$ a	$l(nlj)$	Present work[b]	Shell model[c]
g.s.	$0^+;0$	$2(0d_{5/2})$	0.375	0.53
1.78	$2^+;0$	(0 + 2)	0.06, 0.08	0.38, 0.06
4.62	$4^+;0$	(2 + 4)	0.19, 0.01	0.33, 0.00
4.98	$0^+;0$	$2(0d_{5/2})$	0.06	0.05
6.28	$3^+;0$	(0 + 2)	0.05, 0.12	0.34, 0.14
6.69	$0^+;0$	$2(0d_{5/2})$	0.004	0.005
6.88	$3^-;0$	3	0.002	0.0
6.89	$4^+;0$	2	0.038	0.27
7.38	$2^+;0$	(0 + 2)	0.02, 0.09	0.02, 0.17
7.42	$2^+;0$			
7.80	$3^+;0$	(0 + 2)	0.03, 0.05	0.357, 0.663
7.93	$2^+;0$	(0 + 2)	0.04, 0.07	0.00, 0.13
8.59	$3^+;0$	(0 + 2)	0.15, 0.15	0.035, 0.21
9.32	$3^+;1$	(0 + 2)	0.11, 0.06	0.38, 0.06
9.38	$2^+;1$	(0 + 2)	0.32, 0.08	0.23, 0.05
10.38	$3^+;1$	(0 + 2)	0.06, 0.19	0.01, 0.20
10.72	$1^+;0+1$	(2 + 4)	0.012, 0.006	0.015, 0.00
11.58	$6^-;0$	3	0.14	0.083[d]
14.36	$6^-;1$	3	0.23	0.083[d]

[a] Reference [37].
[b] Molecular potential.
[c] Reference [42].
[d] Deformed shell model [39,40].

MeV, the predicted strength $G=0.083$, calculated on the basis of deformed shell model [39,40], is not adequate enough to explain the observed values (Table III). The band mixing effects due to Coriolis coupling [43] may have significant effects on these transition strengths and is worth further investigation.

VI. CONCLUSIONS

In the present work, both the molecular and Michel types of α-nucleus potential producing the same quality fit to the α-^{27}Al elastic data have been used to analyze one-nucleon transfer data to the bound and unbound states of ^{28}Si. The present work shows that full finite-range DWBA analyses with the molecular potential can describe the angular distributions of the transitions to the bound and unbound states in ^{28}Si at least as satisfactorily, if not somewhat better, as those obtained using the normal optical potential. On the other hand, the Michel potential is, in general, inadequate to explain the data. Furthermore, at reaction angles greater than about 30°, the DWBA calculations using the three types of α-nucleus potentials become significantly different and, hence, the experimental data at larger angles appear to be essential to decide the nature of the α-nucleus potential. To determine the parameters of the potential more accurately, elastic scattering data at large angles would also be helpful.

ACKNOWLEDGMENTS

This work is partially supported by Grant No. INT-9808892 of the U.S. National Science Foundation and a grant from Rajshahi University. The authors thankfully acknowledge the grants. The authors are also thankful to Professor P. D. Kunz of the University of Colorado for making the codes DWUCK4 and DWUCK5 available to us. One of us, S.K.D. is thankful to Shahjalal University of Science and Technology, Bangladesh, for the study leave grant and to the American Institute for Bangladesh Studies for a travel grant to the U.S.

[1] J. C. Correlli, E. Bleuler, and J. Tandem, Phys. Rev. **116**, 1184 (1959).
[2] H. Oeschler, H. Schroter, H. Ficjs, L. Baum, G. Gaul, H. Ludechi, R. Santo, and R. Stock, Phys. Rev. Lett. **28**, 694 (1972).
[3] Å. Bredbacka, M. Brenner, K. M. Källman, P. Manngård, Z. Máté, S. Szilágyi, and L. Zolnai, Nucl. Phys. **A574**, 397 (1994).
[4] L. Jarczyk, B. Maciuk, M. Siemaszko, and W. Zipper, Acta Phys. Pol. B **7**, 531 (1976).
[5] H. Kitazawa, Y. Harima, and N. Mukai, Nucl. Phys. **A510**, 429 (1990).
[6] B. Xiumin, L. Shiming, W. Yuanda, Y. Rongfang, H. Bingyin, and S. Zuxun, Chin. Phys. **6**, 645 (1986).
[7] A. W. Obst and K. W. Kemper, Phys. Rev. C **6**, 1705 (1972).
[8] A. E. Antropov, S. I. Vasilev, P. Zurabin, and B. N. Orlov, Izv. Akad. Nauk. SSSR, Ser. Fiz. **38**, 2175 (1974) [Bull. Acad. Sci. USSR, Phys. Ser. **37**, 1873 (1973)].
[9] K. Jankowksi, A. Grzeszczuk, M. Siemanszko, A. Surowiec, W. Zipper, A. Budzanowski, and E. Kozik, Nucl. Phys. **A426**, 1 (1984).
[10] F. Michel, J. Albinski, P. Belery, Th. Delbar, Gh. Grégoire, B. Tasiaux, and G. Reidemeister, Phys. Rev. C **28**, 1904 (1983).
[11] F. Michel, G. Reidemeister, and S. Ohkubo, Phys. Rev. Lett. **57**, 1215 (1986).
[12] F. Schmittroth, W. Tobocman, and A. A. Golestanch, Phys. Rev. C **1**, 377 (1970).
[13] I. Reichstein and F. B. Malik, Phys. Lett. **37B**, 344 (1971).
[14] P. Manngård, M. Brenner, M. M. Alam, I. Reichstein, and F. B. Malik, Nucl. Phys. **A504**, 130 (1989).
[15] A. S. B. Tariq, A. F. M. M. Rahman, S. K. Das, A. S. Mondal, M. A. Uddin, A. K. Basak, H. M. Sen Gupta, and F. B. Malik, Phys. Rev. C **59**, 2558 (1999).
[16] W. Hauser and H. Feshbach, Phys. Rev. **87**, 366 (1952).
[17] S. K. Das, A. K. Basak, K. Banu, A. S. Mondal, A. S. B. Tariq, A. F. M. M. Rahman, H. M. Sen Gupta, and F. B. Malik (unpublished).
[18] M. Yasue, T. Tanabe, S. Kubono, J. Kokame, M. Sugitani, Y. Kadota, Y. Taniguchi, and M. Igarashi, Nucl. Phys. **A391**, 377 (1982).
[19] C. M. Vincent and H. T. Fortune, Phys. Rev. C **2**, 793 (1970).
[20] C. M. Vincent and H. T. Fortune, Phys. Rev. C **7**, 865 (1973).
[21] T. Wada and H. Horiuchi, Phys. Rev. C **38**, 2063 (1988).
[22] T. Wada and H. Horiuchi, Phys. Rev. Lett. **58**, 2190 (1987).
[23] B. Block and F. B. Malik, Phys. Rev. Lett. **19**, 239 (1967).
[24] R. J. Munn, B. Block, and F. B. Malik, Phys. Rev. Lett. **21**, 159 (1968).
[25] K. Bruekner, J. R. Buchler, and M. M. Kelly, Phys. Rev. Lett. **19**, 239 (1967).
[26] F. B. Malik and I. Reichstein, in *Clustering Phenomena in Atoms and Nuclei*, edited by M. Brenner, T. Lönnroth, and F. B. Malik (Springer-Verlag, Berlin, 1992), p. 327.
[27] C. M. Percy and F. G. Percy, At. Data Nucl. Data Tables **17**, 1 (1976).
[28] G. R. Satchler, Nucl. Phys. **55**, 1 (1964).
[29] N. K. Glendenning, in *Nuclear Spectroscopy and Reactions*, edited by J. Cerny (Academic, New York, 1975), Part D, p. 319.
[30] P. D. Kunz, Computer codes DWUCK4, DWUCK5, and CHUCK3 (private communication).
[31] F. G. Percy, in *Proceedings of the Conference on Direct Reactions and Nuclear Reaction Mechanism*, edited by E. Clemental and C. Villi (Gordon and Breach, New York, 1963), p. 125.
[32] F. James and M. Roos, Comput. Phys. Commun. **10**, 343 (1975).
[33] O. Bersillon, Computer code SCAT2, NEA 0829 (private communication).
[34] V. M. Lebedev, A. V. Spassky, I. B. Teplov, L. N. Fateeva, and L. Z. Ismail, Nucl. Phys. **A298**, 206 (1978).
[35] J. M. Barnwell *et al.*, Nucl. Phys. A388, 542 (1982).
[36] G. Hauser *et al.*, Nucl. Phys. A142, 1 (1972).
[37] P. M. Endt and C. Van der Leun, Nucl. Phys. **A310**, 1 (1978).
[38] P. J. Brussaards and P. W. Glaudemans, *Shell-model Applica-*

tions in Nuclear Spectroscopy (North-Holland, Amsterdam, 1977).
[39] G. R. Satchler, Ann. Phys. (N.Y.) 3, 275 (1958).
[40] B. Cujec, Phys. Rev. 136, B1305 (1964).
[41] P. Davidson, *Collective Models of the Nucleus* (Academic, New York, 1968).
[42] H. J. A. De Voigt and B. H. Wildenthal, Nucl. Phys. A206, 305 (1973); B. H. Wildenthal and J. B. McGrory, Phys. Rev. C 7, 714 (1973).
[43] F. B. Malik and W. Scholz, Phys. Rev. 147, 836 (1966); 150, 919 (1966); 153, 1071 (1967).

Effect of α-nucleus potential on the ^{28}Si$(\alpha, d)^{30}$P reaction

S. K. Das[1], A. S. B. Tariq[1], M. A. Uddin[1], A. S. Mondal[1], A. K. Basak[1],
K. M. Rashid[2], H. M. Sen Gupta[3] and F. B. Malik[4]
[1] *Department of Physics, University of Rajshahi, Rajshahi, Bangladesh*
[2] *Department of Applied Physics and Electronics, University of Rajshahi, Rajshahi, Bangladesh*
[3] *Department of Physics, University of Dhaka, Dhaka, Bangladesh*
[4] *Department of Physics, Southern Illinois University, Carbondale, Illinois 62901, U.S.A.*
(April 6, 2000)

Microscopic and macroscopic distorted wave Born approximation calculations have been performed using molecular, Michel and normal optical potentials to analyze the angular distributions of cross-sections for 12 transitions populating the 0.0, 0.709, 1.454, 1.974, 2.538, 2.72, 2.84, 3.02, 3.93. 4.62, 5.42 and 7.20 MeV states of ^{30}P via the (α, d) reaction. Only the molecular potential is able to produce satisfactory fits to the data, but the normal optical potential is found to be inadequate in accounting for the large-angle data and the Michel potential is just unsatisfactory. The spectroscopic factors for the d-cluster transfer are deduced from the full finite-range distorted-wave Born approximation and compared to the shell-model predictions for the even-parity states.The spin-parity assignment of the 3.93 MeV state is confirmed. The best-fit value for the finite-range parameter for the zero-range DWBA calculations is also deduced.

PACS number(s): 25.55.Fm, 24.50.+g, 21.10.Jx

I. INTRODUCTION

Since the early observation of an unusual enhancement of cross section at large angles, commonly known as anomalous large angle scattering (ALAS), by Corelli *et al.* [1] in α elastic scattering by ^{16}O and ^{32}S nuclei, it has also been noted in other elastic [2–8] as well as the non-elastic [7–13] processes involving α-particles. The normal optical potentials are found to be consistently inadequate in reproducing ALAS in the similar phenomena induced by α particles [13–17]. Two simple local potentials [18], with a minimum number of varying parameters, have been proposed to explain ALAS. The first one with a squared Woods-Saxon (WS) geometry, advocated by Michel and his collaborators [19–22], is a special type of optical potential, which is referred to as Michel potential [18]. The second one is a molecular type of complex potential [18,23,24] having a repulsive core in its real part. Both the potentials have been successful in reproducing ALAS in the elastic scattering of α-particles [18–24] by some *sd*-shell nuclei. Non-elastic processes have so far been, in most cases, treated within the framework of direct-reaction theory using the normal optical potentials in the distorted channels, except a recent study by Das *et al.* [25] who have examined the effects of the molecular and Michel potentials in one-nucleon transfer reaction to the states of ^{28}Si.

ALAS, observed in (α, d) and (α, p) reactions on ^{28}Si [17] and (α, d) on ^{27}Al [26] have, so far, been analyzed in terms of an incoherent sum of the distorted-wave Born approximation (DWBA) contribution calculated with normal optical potentials and the compound nucleus contribution predicted on the basis of the Hauser-Feshbach model [27]. The method has, however, enjoyed a limited success. In particular, the elastic and transfer-data could not be fitted with the same optical potential.

The (α, d) reaction has been shown to be a valuable spectroscopic tool for locating two-particle states [28–32]. Because of the large negative Q-value involved, the reaction favors the transitions to states coupled to the maximum allowed spin. Moreover, unlike the one-nucleon transfer reaction, the (α, d) reactions involving two-nucleon transfer are dependent on the coherence property *e.g.* the relative signs of the different components of the wave-functions. The (α, d) reactions enjoy another advantage in that these can be analyzed in terms of both the macroscopic (cluster transfer) and the microscopic approaches in the form-factor calculations. Another important feature of the (α, d) reactions lies in populating states with the $T = 0$ transfer. Moreover, if the relative angular momentum of the two transferred nucleons is 0 and remains so in the reaction process only the L-transfer $L = J$ is allowed for the natural parity states, but two L-transfers $L = J \pm 1$ are permitted for exciting the unnatural parity states, the spin transfer $S = 1$ being unique.

The present study is undertaken to examine the influences of the normal optical, molecular and Michel potentials in analyzing the two-nucleon transfer reaction ^{28}Si$(\alpha, d)^{30}$P at 26 MeV incident energy, with the target and energy chosen for the substantial ALAS effect [18]. The latter two potentials have not been tested for a two-nucleon transfer reaction. The work is a part of a series of investigations on other non-elastic processes including the (α, t) on ^{27}Al [25], the (α, p) on ^{28}Si [33] and the (α,α') on ^{24}Mg and ^{28}Si [34] to find the nature of the α-nucleus interaction which

can explain all the collision processes involving α-particles. In Sec. II, the forms of the three α-nucleus potentials used in the present work, is presented. The DWBA formalism and analyses are dicussed in Secs. III and IV, respectively. Section V deals with the discussion on the results of the analyses. The conclusion is given in Sec. VI.

II. α-NUCLEUS POTENTIALS

The squared WS Michel potential [20,21] including the Coulomb term $V_C(r)$ comprises of the following forms [18,20] of the real $V_M(r)$ and imaginary $W_M(r)$ parts:

$$V_M(r) = -V_0 \left[1 + \alpha exp\left\{-\left(r^2/\rho^2\right)\right\}\right] \left[1 + exp\left\{\left(r - R_R\right)/2a_R\right\}\right]^{-2} + V_C(r) \tag{1}$$

$$W_M(r) = -W_0 \left[1 + exp\left\{\left(r - R_I\right)/2a_I\right\}\right]^{-2}, \tag{2}$$

with

$$V_C(r) = \left[\frac{Z_1 Z_2 e^2}{2R_C}\right] \left[3 - \frac{r^2}{R_C^2}\right] \text{ for } r \leq R_C \tag{3}$$

$$= \frac{Z_1 Z_2 e^2}{r} \qquad \text{for } r > R_C. \tag{4}$$

In Eqs. (1)-(4) $R_i = r_i A_T^{1/3}$ with $i = R, I$ and C, has been defined in terms of the usual radius parameter.

The molecular potential, which is generated from a many-body theory utilizing the energy-density functional method [23,24], has the following forms [18,24,25] for the real, $V_m(r)$ and imaginary, $W_m(r)$ parts:

$$V_m(r) = -V_0 \left[1 + exp\left\{\left(r - R_0\right)/a_0\right\}\right]^{-1} + V_1 exp\left\{-\left(r^2/R_1^2\right)\right\} + V_C(r) \tag{5}$$

$$W_m(r) = -W_0 exp\left\{-\left(r^2/R_W^2\right)\right\}. \tag{6}$$

Thus, the real part is non-monotonic with a short-range repulsion. The Coulomb and nuclear radii are scaled [18,24] according to $R_i = R_{oi} + r_0 A_T^{1/3}$ with $i = 0, 1, C, W$ and $r_0 = 1.35$ fm.

The normal optical potential for the alpha-nucleus system including the Coulomb term is given by [27]

$$V(r) = V_C - Vf(x_0) - i\left[Wf(x_W) - 4W_D \frac{d}{dx} f(x_D)\right], \tag{7}$$

where, $f(x_i) = \left(1 + e^{x_i}\right)^{-1}$ with $x_i = \left(r - r_i A^{1/3}\right)/a_i$ and the subscript $i = 0, W$ and D.

III. THEORY OF DWBA FORMALISM

In absence of spin-orbit interactions, the differential cross-section for an (α, d) reaction on a spin-0 target with a particular J-transfer in the DWBA theory [35] is given by,

$$\frac{d\sigma}{d\Omega} = \frac{\mu_i \mu_f}{\left(2\pi\hbar^2\right)^2} \frac{k_f}{k_i} (2J+1) \sum_{LM} \left| \sum_{\rho_1 \rho_2} \beta^{1/2} \left[\rho_1 \rho_2; J0\right] \begin{bmatrix} l_1 & l_2 & L \\ \frac{1}{2} & \frac{1}{2} & 1 \\ j_1 & j_2 & J \end{bmatrix} B_M^L \right|^2, \tag{8}$$

where, μ's and k's are, respectively, the reduced masses and wave numbers. The subscripts i and f refer to the incident and outgoing channels, respectively. $\rho_1 = [n_1 l_1 j_1]$ and $\rho_2 = [n_2 l_2 j_2]$ denote the orbital quantum numbers for the transferred nucleons in the final nucleus. $\beta^{1/2}\left[\rho_1 \rho_2; J0\right]$ are the spectroscopic amplitudes in the jj-coupling for an angular momentum transfer J and an isospin transfer $T = 0$. The large square brackets in Eq. (8) refer to the normalized 9-j symbol, the LS-jj transformation factor [36]. B_M^L describes the kinematical aspects of the reaction. In Eq. (8) the light particle spectroscopic factor $c^2 s = 1.0$ for (α, d) reactions has been used.

In the macroscopic DWBA calculations, no information on the structure of the cluster is required except the quantum numbers (N, L) as defined by

$$2\left(n_1 + n_2\right) + l_1 + l_2 = 2N + L, \tag{9}$$

where the quantum numbers $\nu = 0$ and $\lambda = 0$ are assumed for the relative $0s$-state internal motion of the transferred cluster. The expression for cross section in terms of the cluster quantum numbers (N, L) parallel to Eq. (8) is given [36] by

$$\frac{d\sigma}{d\Omega} = \frac{\mu_i \mu_f}{\left(2\pi\hbar^2\right)^2} \frac{k_f}{k_i} (2J+1) \sum_{LM} \left| G_{LJ} \Re_M^L \right|^2 . \tag{10}$$

In Eq. (10), only one N-value is considered to contribute, the two nucleons in the cluster being in the relative $0s$-state. The structure amplitude G_{LJ}, as defined by Glendenning [36] is expressed as

$$G_{LJ} = \sum_{\rho_1 \rho_2} (2 - \delta_{\rho_1 \rho_2})^{1/2} \beta^{1/2} [\rho_1 \rho_2; J0] \begin{bmatrix} l_1 & l_2 & L \\ \frac{1}{2} & \frac{1}{2} & 1 \\ j_1 & j_2 & J \end{bmatrix} \Omega_{00} \langle 00, NL : L \mid n_1 l_1, n_2 l_2 : L \rangle. \tag{11}$$

In Eq. (11), Ω_{00} denotes the overlap of the spatial wave function of relative motion of the two particles in the transferred cluster with the corresponding part in the incident α particle. $\langle \mid \rangle$ represents the Brody-Moshinsky bracket [35–37].

Denoting the macroscopic cross sections calculated for the L-transfer with the FFR code DWUCK5 [38] by $\left(\frac{d\sigma}{d\Omega}\right)^L_{DW5}$ and taking advantage of the incoherent sum over the L-transfer(s) as in Eqs. (8) and (10), one can write the experimental cross sections for this reaction as

$$\left(\frac{d\sigma}{d\Omega}\right)_{exp} = (2J+1) \left[A_{L1} \left(\frac{d\sigma}{d\Omega}\right)^{L1}_{DW5} + A_{L2} \left(\frac{d\sigma}{d\Omega}\right)^{L2}_{DW5} \right] \tag{12}$$

On the other hand, the experimental cross-sections are related to the microscopic cross-sections $\left(\frac{d\sigma}{d\Omega}\right)^L_{DW4}$ calculated with the ZR code DWUCK4 [38] by

$$\left(\frac{d\sigma}{d\Omega}\right)_{exp} = \aleph \left(\frac{d\sigma}{d\Omega}\right)_{DW4} . \tag{13}$$

$\aleph$ in Eq. (13) is the normalization constant for the (α, d) reactions. The form of Eq. (12) shows that A_{L1} and A_{L2} are the spectroscopic factors [26,32] for the $L1$ and $L2$ transfers, respectively. The spectroscopic factor [26] A_L in Eq. (12) for each of the L-transfers and the normalization constant $\aleph$ in Eq. (13) can be extracted from fitting the experimental cross sections.

IV. DWBA ANALYSIS

The microscopic zero-range and macroscopic full finite-range (FFR) DWBA calculations for the angular distributions have been performed using the computer codes DWUCK4 and DWUCK5 [38], respectively. Both the codes are modified to include the Michel potential. Corrections due to non-locality [38,39] of potentials in the conventional form have been applied using the non-locality parameters $\beta(\alpha) = 0.2$ and $\beta(p) = 0.85$ fm. In both the microscopic ZR and macroscopic FFR calculations, the molecular, Michel, and normal optical types of α-^{28}Si potential and the optical d-^{30}P potential have been employed. The parameters of the molecular and Michel potentials are taken from the work of Tariq *et al.* [18], and those of the normal optical potentials for the incident channel are from Jankowski *et al.* [17]. Several sets of the d-^{30}P optical potentials including that from Ref. [17] have been tried, but the one from the work of Fitz *et al.* [40] produces the best fit. All the potential parameters employed in the present analyses are displayed in Table I.

A. Macroscopic DWBA calculations

The macroscopic analyses have been performed using the full finite-range DWBA code DWUCK5 [38]. The bound-state geometries for the d-d and d-^{28}Si Woods-Saxon (WS) potentials, shown in Table I are taken from [17]. The bound state wave funtions for the transferred deuteron in alpha as well as the final nucleus have been generated by adjusting the deuteron separation energies. At the start of calculations, the accuracy parameters used in the code DWUCK5 have been assigned appropriate values, to define effective width of wave numbers [38,41] in the expansion

of the distorted waves in terms of plane waves for making the zero-range calculations identical to those from the code DWUCK4 [38]. This ensures the necessary *covergence* for the integral for the zero-range form-factor, defined in Eq. (3.9) of Charlton [41].

The cluster configurations of the transferred deuteron for the different states of excitation are shown in Table II. For the final states with natural parity, populated by one L-transfer, the DWBA predictions are normalized to the data to yield the relevant spectroscopic factor A_L as defined in Eq. (12). On the other hand, for the transitions involving two L-transfers, leading to the final states with unnatural parity, the spectroscopic factors are obtained by minimizing the value of χ^2 defined by

$$\chi^2 = \sum_i \left[\frac{\sigma_{exp}(\theta_i) - \sigma_{DW}(\theta_i)}{\Delta\sigma_{exp}(\theta_i)} \right]^2, \tag{14}$$

where $\sigma_{exp}(\theta_i) = \left(\frac{d\sigma}{d\Omega}\right)_{exp}(\theta_i)$ and $\Delta\sigma_{exp}(\theta_i)$ are, respectively, the experimental cross section, as defined in Eq. (12), and its error at the scattering angle θ_i. $\sigma_{DW}(\theta_i)$ is the cross section predicted by the DWBA theory.

The DWBA predictions with the molecular (solid curves), normal optical (broken curves), and Michel (dotted curves) potentials are compared to the data of the ground (1^+), 0.709 (1^+), 1.454 (2^+), 2.72 (2^+) and 3.02 MeV (2^+) states in Fig. 1; to the data of the 1.974 (3^+), 2.538 (3^+), and 2.84 MeV (3^+) in Fig. 2; and to the data of the 3.93 (2^-), 4.63 (3^+) and 5.42 MeV (2^+) states of ^{30}P in Fig. 3. It is amply clear from Figs. 1-3 that the calculations with the molecular potential produces the best fits to data for all the transitions. Furthermore, the Michel potential generates cross sections, which are lower by 1 to 2 orders of magnitude than those predicted by either the normal optical or the molecular potential. Table III gives the comparison of the total spectroscopic factors for the cluster transfer for the three types of potentials.

The compiled work of Endt and van der Leun [44] suggests alternative spin-parity for the 3.93 MeV state as $J^\pi = 1^+, 2^-$ or 3^+. While de Meijer *et al.* [32] assigned $J^\pi = 3^+$ for the state, Jankowski *et al.* [17] suggested 2^-. The DWBA calculations with the molecular potential for both $J^\pi = 2^-$ and 3^+, are compared to the experimental cross sections in Fig. 4. The $J^\pi = 2^-$ assignment is clearly favored, confirming the observation of Jankowski *et al.*

B. Microscopic DWBA calculations

The microscopic calculations have been performed using the zero-range code DWUCK4 for the positive parity states with the transferred particles stripped to the *sd*-shell. The present analyses make use of three sets of spectroscopic amplitudes $\beta^{1/2}$, two sets based on the FPSDI and MSDI hamiltonians as defined in Wildenthal *et al.* [42] and the shell-model wave functions of the ^{28}Si and ^{30}P nuclei given by Wildenthal *et al.* [42,43] and the third one, labeled by CW [32], derived from the wave functions of Chung and Wildenthal referred to in [32]. The FPSDI and CW amplitudes are taken from de Meijer *et al.* [32], while the MSDI amplitudes are from Jankowski *et al.* [17]. All the three sets of spectroscopic amplitudes are calculated in the model space of $0d_{5/2}$-$1s_{1/2}$-$0d_{3/2}$. Since the codes DWUCK4 and DWUCK5 assume that the spherical harmonics carry a time reversal phase of i^l, a factor not used in the phase conventions adopted in the calculations of the spectroscopic amplitudes [32], the amplitudes have been multiplied by an extra phase of $i^{l_1+l_2-L}$ before feeding these to the codes.

The bound state wave functions for each of the transferred nucleons have been generated by assuming a real Woods-Saxon well with the geometry parameters $r_0 = 1.25$ fm and $a_0 = 0.65$ fm and the depth adjusted to produce the binding energy equal to half the separation energy of the transferred deuteron. A Thomas-Fermi spin-orbit term with $\lambda = 25$ has also been used for the bound state wave functions.

A Gaussian form of finite range correction in the local energy approximation [38] has been investigated. Fig. 5 compares the microscopic DWBA calculations for the molecular type of α-^{28}Si potential using the range parameter $R = 0.0$ fm (broken curves), 0.7 fm (solid curves) and 0.85 fm (dotted curves) to the experimental data for the transfer to the ground (1^+), 2.53 (3^+), 2.84 (3^+) and 3.02 MeV (2^+) states. The finite-range correction with $R = 0.7$ fm improves the fits to the data.

The effect of the three types of the α-^{28}Si potential on the microscopic DWBA calculations has also been examined using the spectroscopic amplitudes calculated from the FPSDI interaction. Fig. 6 displays the DWBA predictions for the molecular (solid curves), normal optical (broken curves) and Michel (dotted curves) potentials, which are compared to the data for the ground (1^+), 0.71 (1^+), 1.45 (2^+) and 1.97 MeV (3^+) states of ^{30}P. As in the case of the macroscopic analyses, the molecular potential provides the best description of the data and the Michel gives the worst. Moreover, the predicted cross sections with the Michel potential are so small that they need normalization factors (Table III), larger by orders of magnitude compared to those for the molecular and normal optical potentials.

Figs. 7 and 8 display the comparison of the microscopic DWBA calculations with the finite-range parameter $R = 0.7$ fm and the molecular α-^{28}Si potential, for the FPSDI (solid curves), CW (broken curves) and MSDI (dotted curves) interactions. The calculations with the three interactions produce more or less the same quality of fits to the transfer data to the ground (1^+), 0.709 (1^+), 1.454 MeV (2^+) states (Fig. 7). The FPSDI and CW amplitudes produce identical predictions for the 2.72 MeV (2^+) state (Fig. 7) and 2.84 MeV (3^+) state (Fig. 8) and the same quality of fits to the 1.97 (3^+) and 2.538 (3^+) MeV states (Fig. 8). For the 3.02 MeV state, FPSDI gives a better description at large scattering angles than CW does (Fig. 7). Nonetheless, the spectroscopic amplitudes from the three interactions produce completely different spectroscopic factors S_L, as listed in Table II. Moreover, the experimental cross sections for the reaction leading to the ground (1^+), 0.709 (1^+), 1.454 (2^+), 1.974 (3^+), 2.538 (3^+), 2.72 (2^+), 2.84 (3^+) and 3.02 MeV (1^+) states of ^{30}P, need normalization constants as listed in Table IV, which are widely different and inconsistent.

The 7.20 MeV (7^+) state is considered to have a pure stretched $\left(0f_{7/2}\right)^2$ configuration leading to the spectroscopic amplitude for the (α, d) reaction as $\beta^{1/2} = 1.0$ [30,32]. This model independent value of $\beta^{1/2}$ has been used to deduce the normalization constant for the reaction as $\aleph = 722 \pm 25$, which compares closely with $\aleph = 870 \pm 20$ and 650 ± 20 obtained, following two methods for calculating the form-factors, by de Meijer *et al.* [32]. But only a few of the extracted $\aleph$-values for other states given in Table IV are close to the model independent-value, deduced from the reaction data for the 7.20 MeV state. None of the FPSDI, CW and MSDI interactions produce a consistent set of values for the normalization constant.

C. Spectroscopic factors

The model dependent spectroscopic factors are calculated from the FPSDI, CW and MSDI spectroscopic amplitudes $\beta^{1/2}$ by the method outlined in [32]. Since the spectroscopic factor for the 7.20 MeV state is unity, the spectroscopic factors for other transitions are obtained by

$$S_L = \frac{|G_{LJ}|^2}{|G_{67}(7.20)|^2}, \tag{15}$$

where the structure factor G_{LJ} is expressed through Eq. (11) and $G_{67}(7.20) = 0.56\Omega_{00}$ denotes the value of the structure factor for the 7.20 MeV state. The S_L values, which are listed in Table II, are taken from de Meijer *et al.* [32] for the FPSDI and CW spectroscopic amplitudes. For the MSDI interaction, the S_L values are calculated using Eq. (15) from the MSDI spectroscopic amplitudes from Jankowski *et al.* [17]. The theoretical spectroscopic factors S_L are compared to the experimental spectroscopic factors A_L, deduced from the macroscopic analysis in Table II.

V. DISCUSSION

In the present work, both the molecular and Michel types of α-nucleus potential have been used, for the first time, for the analyses of two-nucleon transfer data. The data for the even-parity states up to $E_x = 3.02$ MeV, have been analyzed both in terms of the FFR DWBA with the cluster form-factor and the ZR DWBA with the microscopic form-factors. In the latter calculations, the FPSDI and CW [32] as well as MSDI [17] spectroscopic amplitudes derived from the wave functions of Wildenthal and his collaborators [42,43] and Ref. [20] cited in the work of de Meijer *et al.* [32]. The data of the odd-parity states are analyzed only in terms of the macroscopic FFR calculations.

In both microscopic and macroscopic DWBA calculations, the molecular potential [Figs. 1-3 and 7,8] produces the best description of the data for all the transitions studied. The Michel potential, which has been shown to describe satisfactorily the elastic α+^{28}Si data [18], is found inadequate not only in accounting for the pattern of the angular distributions [Figs. 1-3, 6], but also in reproducing the right order of magnitude for the cross section data. The normal optical potential, on the other hand, which can fit the angular distribution at forward scattering angles and predicts the the same order of cross sections as the molecular one does, is found inadequate in describing the data at large scattering angles [Figs. 1-3, 6].

The finite-range correction to the ZR microscopic calculations produces substantial effects on the pattern of the angular distributions and improves substantially the fits to the data as can be seen in Fig. 5. This confirms the observation made by Bencze and Zimanyi [45]. The best fit value for the finite-range parameter found is $R = 0.70$ fm for the reaction.

In the literature, an ambiguity in the spin-parity assignment for the 3.93 MeV state is noted. The comparison of the macroscopic DWBA predictions for $J^\pi = 2^-$ (solid curve) and 3^+ (dotted curve) in Fig. 4 to the experimental data favors the former, confirming the assignment of Jankowski *et al.* [17] and opposing that of de Meijer *et al.* [32].

The spectroscopic factors A_L for the transitions to the final states up to $E_x = 5.42$ MeV are deduced by comparing the macroscopic DWBA calculations to the data. Table II compares the deduced spectroscopic factors A_L to those obtained at 50 MeV incident energy by de Meijer *et al.* [32] and those extracted using the same data as of the present work by Jankowski *et al.* [17]. The results of Jankowski *et al.* are not reliable as they included the compound nucleus contributions in their analyses. The results of de Meijer *et al.* are based on the zero-range calculations. Nevertheless, their A_L values for the transitions involving one L-transfer leading to, particularly, the 1.454 (2^+) and 4.62 MeV (3^-) states are remarkably close to those of the present work.

The A_L values for the even-parity states and the model dependent theoretical spectroscopic factors S_L, defined in Eq. (15), are compared in Table II. It can be noticed that apart from the ground state (1^+), 1.454 (2^+) and 2.72 MeV (2^+) transitions, the total spectroscopic factors $\sum A_L$ agree with $\sum S_L$ for the CW interactions. On the other hand, the FPSDI predictions for $\sum S_L$ values are closer to the experimental $\sum A_L$ for the ground and 1.45 MeV states. Neither of the FPSDI and CW interactions reproduces the experimental A_L for the 2.72 MeV state. It can also be noticed from Table III that FPSDI yields larger spectroscopic strengths compared to CW. This is also reflected in the deduced values of relative normalization constants $\aleph_{rel}$ in Table IV, where FPSDI needs in general smaller $\aleph$-values to get to the data. None of the three interactions *viz.* FPSDI, CW and MSDI is able to yield consistent values to account for the even-parity states. However, the model-independent $\aleph = 722 \pm 25$ is obtained from the data of the 7.20 MeV (7^+) state, where the spectroscopic amplitude is believed to be unity.

VI. CONCLUSION

Both the macroscopic and microscopic DWBA analyses suggest that the molecular type of the α-^{28}Si potential is undoubtedly the best of the three types of potentials considered. The success of the present analyses lies in observing that the experimental cross-sections for all the transitions are reproduced over the entire angular range without the addition of compound nucleus contributions, which are unlikely to happen at the incident energy considered herein.

The present work in conjunction with the previous studies of the α-elastic scattering on ^{24}Mg and ^{28,30}Si by Tariq *et al.* [18], of the (α, t) reaction on ^{27}Al [25] and the (α, p) reaction on ^{28}Si [33] by Das *et al.*, and of the α-inelastic scattering on ^{24}Mg and ^{28}Si by Rahman *et al.* [34] confirms that the molecular potential is the best of the three types of α-nucleus interactions including the Michel and the normal optical potentials, in describing the elastic, inelastic and rearrangement collision processes on the *sd*-shell nuclei. This ushers in hopes for finding a global α-nucleus potential, as observed by Hodgson [46]. It remains to be examined whether the molecular type of potentials are capable of accounting for collision processes involving α particle and other light and medium-light nuclei. For this purpose, it would be extremely helpful to have complete angular distributions for different processes involving a particular nucleus.

VII. ACKNOWLEDGMENTS

This work is partly supported by the grant INT-9808892 of the U.S. National Science Foundation and a grant from the Ministry of Science and Technology, Government of Bangladesh, which are thankfully acknowledged. One of the authors, SKD, is thankful to Shahjalal University of Science and Technology, Bangladesh for the study leave grant. The authors are also thankful to Professor P.D. Kunz of the University of Colorado for making the codes DWUCK4 and DWUCK5 available to them.

[1] J.C. Correlli, E. Bleuler and D.J. Tendam, Phys. Rev. **116**, 1184 (1959).
[2] C.R. Gruhn and N.S. Wall, Nucl. Phys. **81**, 161 (1966).
[3] G. Gaul, H. Lüdeke, R. Santo, H. Schmeing and R. Stock, Nucl. Phys. **A137**, 177 (1969).
[4] A. Bobrowska, A. Budzanowski, K. Grotowski, L. Jarczyk, S. Micek, H. Niewodniczanski, A. Strzalkowski and Z. Wróbel, Nucl. Phys. **A126**, 361 (1969).
[5] H. Eickhoff, D. Frekers, H. Lönner, K. Poppensieker, R. Santo, G. Gaul, C. Mayer-Böricke and P. Turek, Nucl. Phys. **A252**, 333 (1975).
[6] H. Abele, H.J. Hauser, A. Körber, W. Leitner, R. Neu, H. Plappert, T. Rohwer, G. Staudt, M. Straßer, S. Welte, M. Walz, P.D. Eversheim and F. Hinterberger, Z. Phys. A **326**, 373 (1987).

[7] W. Trombik, K.A. Eberhard and J.S. Eck, Phys. Rev. C **11**, 685 (1975).
[8] A.M. Kobos, B, A. Brown, R. Lindsay and G.R. Satchler, Nucl. Phys. **A425**, 205 (1984).
[9] H. Oeschler, H. Schroter, H. Ficjs, L. Baum, G. Gaul, H. Ludechi, R. Santo and R. Stock, Phys. Rev. Lett. **28**, 694 (1972).
[10] Å. Bredbacka, M. Brenner, K.-M. Källman, P. Månngard, Z. Máté, S. Szilágyi and L. Zolnai, Nucl. Phys. **A574**, 397 (1994).
[11] L. Jarczyk, B. Maciuk, M. Siemaszko and W. Zipper, Acta Phys. Pol. **B7**, 531 (1976).
[12] H.-J. Apell, W. Gemeinhardt, R. Stock, R.R. Betts, O. Hansen, A. Sperduto, H. Fuchs and R. Santo, Nucl. Phys. **A246**, 477 (1975).
[13] A.W. Obst and K.W. Kemper, Phys. Rev. C **6**, 1705 (1972).
[14] H. Kitazawa, Y. Harima and N. Mukai, Nucl. Phys. **A510**, 429 (1990).
[15] B. Xiumin, L. Shiming, W. Yuanda, Y. Rongfang, H. Bingyin and S. Zuxun, Chin. Phys. **6**, 645 (1986).
[16] A.E. Antropov, S.I. Vasilev, P. Zurabin and B.N. Orlov, Izv. Akad. Nauk. SSSR, Ser. Fiz. **38**, 2175 (1974); **37**, 1873 (1973).
[17] K. Jankowski, A. Grzeszczuk, M. Siemaszko, A. Surowiec, W. Zipper, A. Budzanowski and E. Kozik, Nucl. Phys. **A426**, 1 (1984).
[18] A.S.B. Tariq, A.F.M.M. Rahman, S.K. Das, A.S. Mondal, M.A. Uddin, A.K. Basak, H.M. Sen Gupta and F.B. Malik, Phys. Rev. C **59**, 2558 (1999).
[19] Th. Delbar, Gh. Grégoire G. Paic, R. Ceuleneer, F. Michel, R. Vanderpoorten, R. Budzanowski, H. Dabrowski, L. Friendl, K, Grotoski, S. Micek, R. Planeta, A. Strzalkowski and A. Eberhard, Phys. Rev. C **18**, 1237 (1978).
[20] F. Michel, J. Albinski, P. Belery, Th. Delbar, Gh. Grégoire, B. Tasiaux and G. Reidemeister, Phys. Rev. C **28**, 1904 (1983).
[21] F. Michel, G. Reidemeister and S. Ohkubo, Phys. Rev. Lett. **57**, 1215 (1986).
[22] F. Michel, G. Reidemeister and Y. Kondo, Phys. Rev. C **51**, 3290 (1995).
[23] I. Reichstein and F.B. Malik, Phys. Lett. **37B**, 344 (1971).
[24] P. Manngård, M. Brenner, M.M. Alam, I. Reichstein and F.B. Malik, Nucl. Phys. **A504**, 130 (1989).
[25] S.K. Das, A.S.B. Tariq, A.F.M.M. Rahman, P.K. Roy, M.N. Huda, A.S. Mondal, A.K. Basak, H.M. Sen Gupta and F. B. Malik, Phys. Rev. C **60** (1999), *in press.*
[26] I. Skwirczynska, E. Kozik, A. Budzanowski, J. Ploskonka and A. Strzalkowski, Nucl. Phys. **A371**, 288 (1981).
[27] W. Hauser and H. Feshbach, Phys. Rev. **87**, 366 (1952).
[28] H. Nann, W.S. Chien, A. Saha and B.H. Wildenthal, Phys. Lett. **60B**, 32 (1975).
[29] A. Van der Woude and R.J. de Meijer, Nucl. Phys. **A258**, 199 (1976).
[30] R.M. Del Vecchio, R.T. Kouzes and R. Sherr, Nucl. Phys. **A265**, 220 (1976).
[31] H. Nann, W.S. Chien, A. Saha and B.H. Wildenthal, Phys. Rev. C **15**, 1959 (1977).
[32] R.J. de Meijer, L.W. Put, J.J. Akerman, J.C. Vermeulen and C.R. Binham, Nucl. Phys. **A386**, 200 (1982).
[33] S.K. Das, A.K. Basak, K. Banu, A.S. Mondal, A.S.B. Tariq, A.F.M.M. Rahman, H.M. Sen Gupta and F.B. Malik, *submitted to* Physical Review C.
[34] A.F.M.M. Rahman, A.S. Mondal, S.K. Das, A.S.B. Tariq, A.K. Basak, H.M.Sen Gupta and F.B.Malik, *to be submitted to* Physical Review C.
[35] I.S. Towner and J.C. Hardy, Adv. Phys. **18**, 401 (1969).
[36] N.K. Glendenning, Phys. Rev. **137**, B102 (1965).
[37] M.K. Pal, *Theory of Nuclear Structure*, (Affiliated East-West Press, New Delhi, 1982).
[38] P.D. Kunz, The codes DWUCK4, DWUCK5 and CHUCK3, private communication.
[39] N.K. Glendenning in *Nuclear Spectroscopy and Reactions, Part D*, ed. J. Cerny (Academic Press, New York, 1975), p. 319.
[40] W. Fitz, J. Heger, R. Santo and S. Wenneis, Nucl. Phys. **A143**, 113 (1970).
[41] L.A. Charlton, Phys. Rev. C **8**, 146 (1978).
[42] B.H. Wildenthal, J.B. McGrory, E.C. Halbert and H.D. Graber, Phys. Rev. C **4**, 1708 (1971).
[43] B.H. Wildenthal and J.B. McGrory, Phys. Rev. C **7**, 714 (1973).
[44] P.M. Endt and C. van der Leun, Nucl. Phys. **A310**, 1 (1978).
[45] Gy. Bencze and J. Zimanyi, Nucl. Phys. **88**, 76 (1966).
[46] P.E. Hodgson, Oxford Report, OUNP-94-09 (1994).

TABLE I. Potential parameters for DWBA calculations. The potential depth V for the bound states is adjusted to give the separation energy.

Channel	$\alpha + {}^{28}$Si			$d + {}^{30}$P	$d + d$	$d + {}^{28}$Si
Potential type	Molecular[a]	Michel[a]	Optical[b]	Optical[c]	Bound state[a]	
V_0 (MeV)	26.0	21.0	50.42	102.7	V	V
R_0 (fm)	5.35	5.00	-	-	-	-
r_0 (fm)	-	-	1.699	1.07	1.05	0.935
a_0 (fm)	0.34	0.60	0.505	0.852	0.50	0.997
V_1 (MeV)	42.0	-	-	-	-	-
R_1 (fm)	2.80	-	-	-	-	-
α	-	5.82	-	-	-	-
ρ (fm)	-	6.25	-	-	-	-
W_0 (MeV)	15.0	28.9	10.34	-	-	-
R_W (fm)	4.0	3.85	-	-	-	-
r_I (fm)	-	-	1.699	-	-	-
a_I (fm)	-	0.65	0.505	-	-	-
W_D (MeV)	-	-	-	16.10	-	-
r_D (fm)	-	-	-	1.53	-	-
a_D (fm)	-	-	-	0.574	-	-
V_{SO} (MeV)	-	-	-	6.0	-	-
r_{SO} (fm)	-	-	-	1.07	-	-
a_{SO} (fm)	-	-	-	0.852	-	-
r_C (fm)	-	1.30	1.30	1.15	1.25	1.3
R_C (fm)	9.35	-	-	-	-	-

[a] Ref. [18].
[b] Ref. [17].
[c] Ref. [40].

TABLE II. Cluster specstroscopic factors are compaared to the theoretical shell-model factors for the FPSDI, CW and MSDI interactions. FPSDI and CW spectroscopic factors are taken from Ref. [32]. MSDI factors are calculated from the spectroscopic amplitudes $\beta^{1/2}$ of Ref. [17] by the method outlined in Ref. [32]. S_L values are normalized to the value of $\left|G_{67}^{7.20}\right|^2$ for the 7.20 MeV state.

E_x	J^π	Cluster configuration	Cluster spectroscopic factor			Shell model spectroscopic factor $S_L = \|G_{LJ}\|^2 / \left\|G_{67}^{7.20}\right\|^2$		
(MeV)		N, L	A_L [a]	A_L [b]	A_L [c]	FPSDI	CW	MSDI
0.0	1^+	2,0	0.23 ± 0.07	1.76 ± 0.20	0.28	0.448	0.043	0.168
		1,2	0.23 ± 0.07	[d]	0.56	0.237	0.121	0.031
0.709	1^+	2,0	0.16 ± 0.07	1.45 ± 0.20	-	0.029	0.030	0.020
		1,2	0.24 ± 0.08	[d]	0.85	0.617	0.274	0.038
1.454	2^+	1,2	0.25 ± 0.05	0.20 ± 0.04	0.32	0.372 [a]	0.081	7.8×10^{-4}
1.974	3^+	1,2	0.11 ± 0.04	0.72 ± 0.13	-	0.041	0.078	0.004
		0,4	0.09 ± 0.03	0.47 ± 0.20	-	6.1×10^{-4}	0.134	1.5×10^{-3}
2.538	3^+	1,2	0.16 ± 0.04	0.67 ± 0.14	-	0.015	0.165	-
		0,4	0.07 ± 0.03	< 0.25	-	0.426	0.076	-
2.72	2^+	1,2	0.28 ± 0.05	0.12 ± 0.02	0.34	0.058	0.045	-
2.84	3^+	1,2	0.08 ± 0.02	0.16 ± 0.07	-	0.007	0.007	-
		0,4	0.09 ± 0.02	0.33 ± 0.11	-	0334	0.254	-
3.02	1^+	2,0	0.03 ± 0.02	0.51 ± 0.15	0.27	9.7×10^{-4}	0.319	-
		1,2	0.32 ± 0.05	0.06 ± 0.10	0.35	1.4×10^{-3}	0.021	-
3.93	2^-	2,1	0.11 ± 0.04	-	0.32	-	-	-
		1,3	0.18 ± 0.04	-	-	-	-	-
	(3^+)	(1,2)	(0.06 ± 0.05)	(0.14 ± 0.05)	-	-	-	-
		(0,4)	(0.08 ± 0.05)	(0.05 ± 0.06)	-	-	-	-
4.62	3^-	2,1	0.15 ± 0.04	0.17 ± 0.02	0.30	-	-	-
5.42	2^-	2,1	0.54 ± 0.09	-	-	-	-	-
		1,3	0.06 ± 0.03	-	0.86	-	-	-

[a] Present work.
[b] Ref. [32].
[c] Ref. [17].
[d] Too small a value to quote.

TABLE III. Comparison of deduced total specstroscopic factors from the macroscopic and normalization factors for the microscopic FPSDI calculations using the molecular, normal optical and Michel potentials. Total spectroscopic factor is the sum of the spectroscopic factors for the two L-transfers for the unnaturalparity states.

E_x (MeV)	J^π	L	Total spectroscopic factors			Normalization constant $\aleph$		
			Macroscopic calculations			Microscopic calculations		
			Molecular	Optical	Michel	Molecular	Optical	Michel
0.0	1^+	0+2	0.46	0.74	23.4	280	480	7000
0.709	1^+	0+2	0.40	1.33	30.0	70	85	8000
1.454	2^+	2	0.25	0.50	11.0	270	950	1800
1.974	3^+	2+4	0.20	0.57	20.0	1500	2000	35000

TABLE IV. Normalization constant $\aleph$ for the microscopic zero-range calculations for different shell-model interactions. $\aleph_{rel}$ is the value relative to the model independent $\aleph = 722$ for the 7.20 MeV state.

E_x (MeV)	J^π	L	Normalization constant $\aleph$			Relative normalization constant $\aleph_{rel}$		
			Interaction			Interaction		
			FPSDI	CW	MSDI	FPSDI	CW	MSDI
0.0	1^+	0+2	280	4000	800	0.388	5.540	1.108
0.709	1^+	0+2	70	180	1500	0.096	0.249	2.08
1.454	2^+	2	270	850	5500	0.374	1.177	7.618
1.974	3^+	2+4	1500	500	7000	2.077	0.692	9.965
2.538	3^+	2+4	220	900	-	0.304	1.246	-
2.72	2^+	2	550	4500	-	0.762	6.233	-
2.84	3^+	2+4	350	450	-	0.484	0.623	-
3.02	1^+	0+2	14000	450	-	19.39	0.623	-

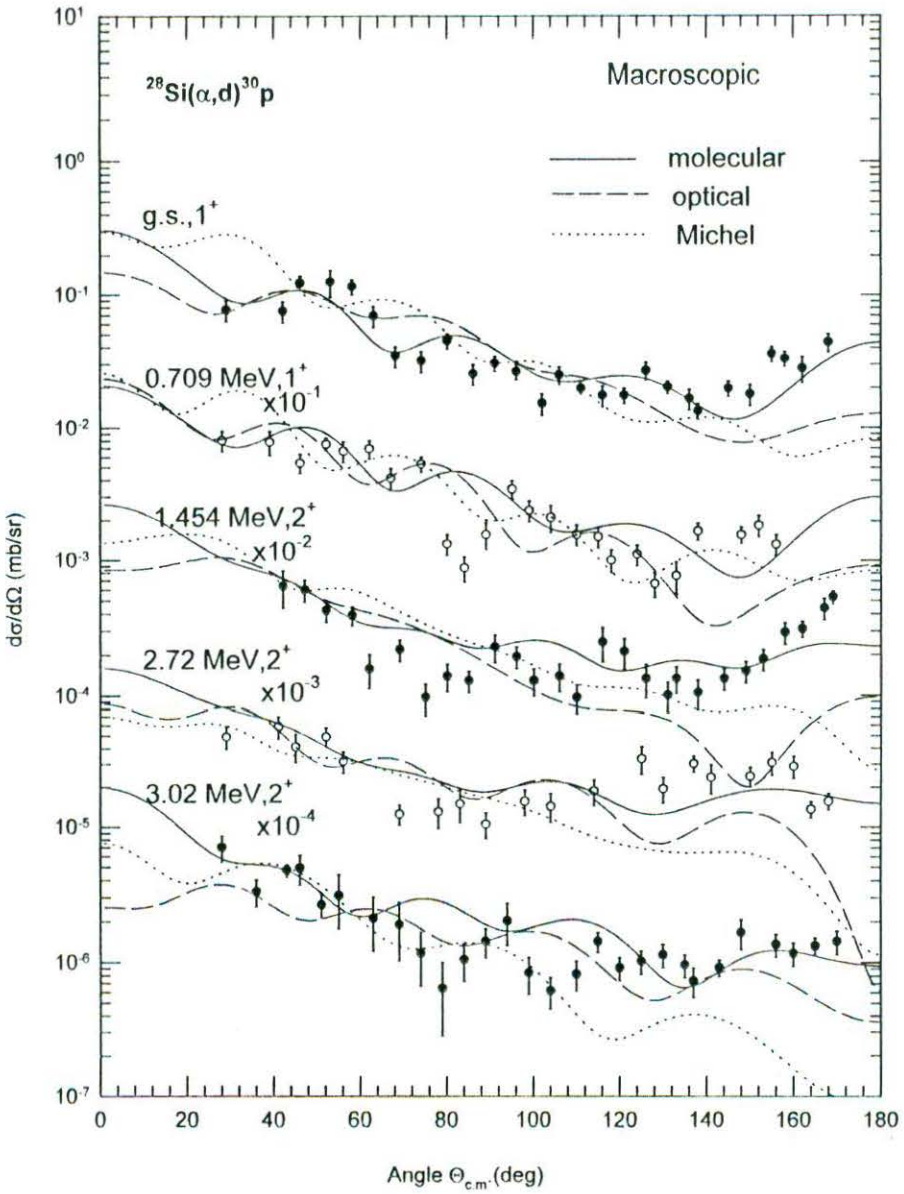

Fig.1. Comparison of the full finite-range macroscopic DWBA calculations for the ^{28}Si(α,d)^{30}P reaction at 26 MeV leading to the 1^+ and 2^+ states of ^{30}P to the differential cross-section data. The solid, broken and dotted curves are the predictions using the molecular, normal optical and Michel α-^{28}Si potentials, respectively. The data are from [17].

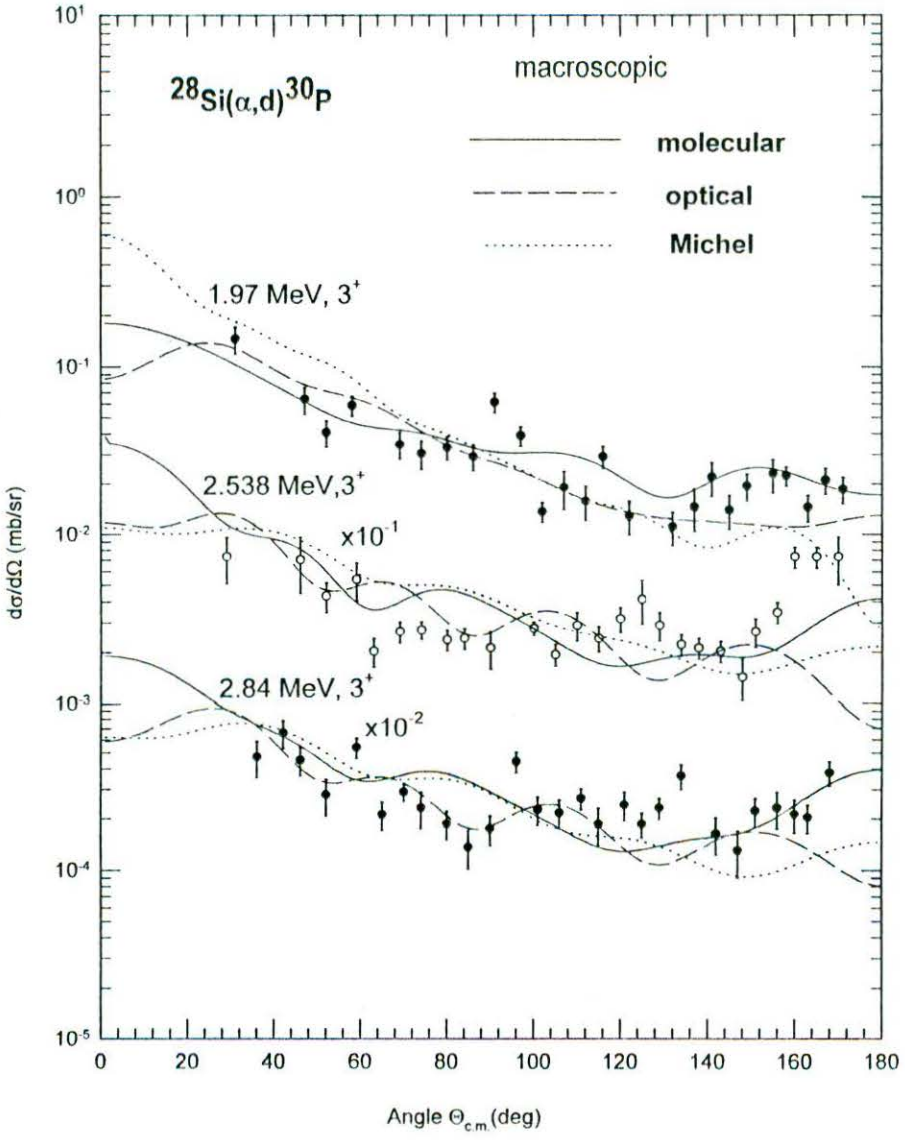

Fig.2. Same as in Fig.1 for the transition to the 3^+ states of ^{30}P. The data are from [17].

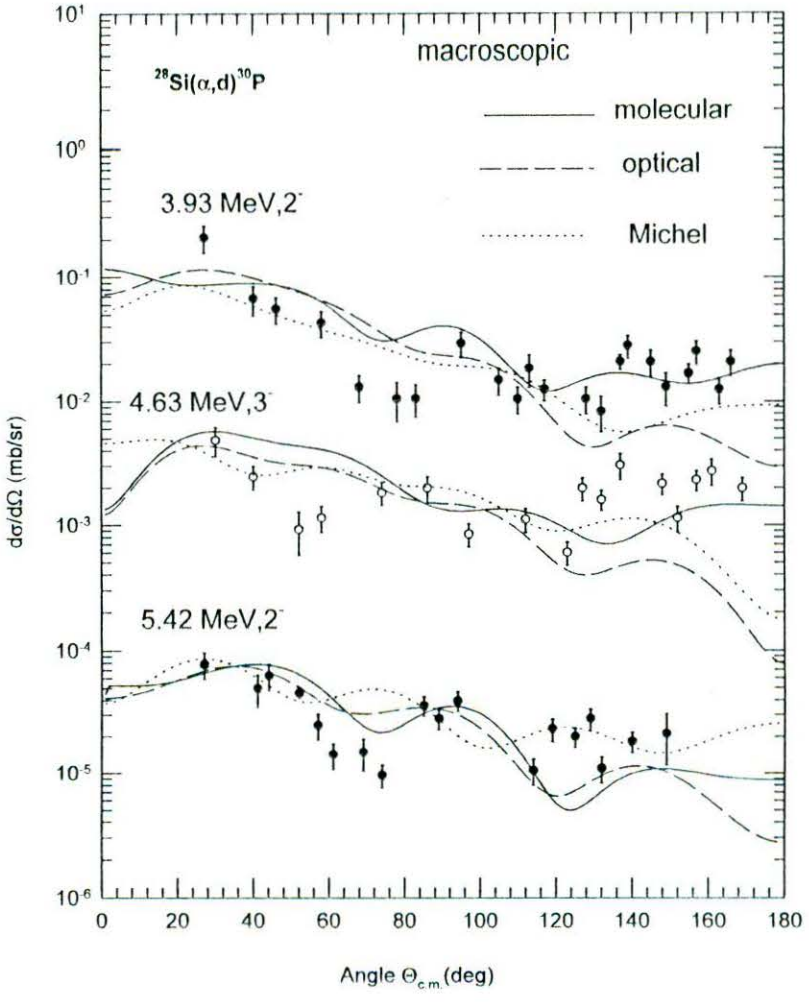

Fig. 3. Same as in Fig.1 for the transition to the 2^- and 3^- states of ^{30}P. The data are from [17].

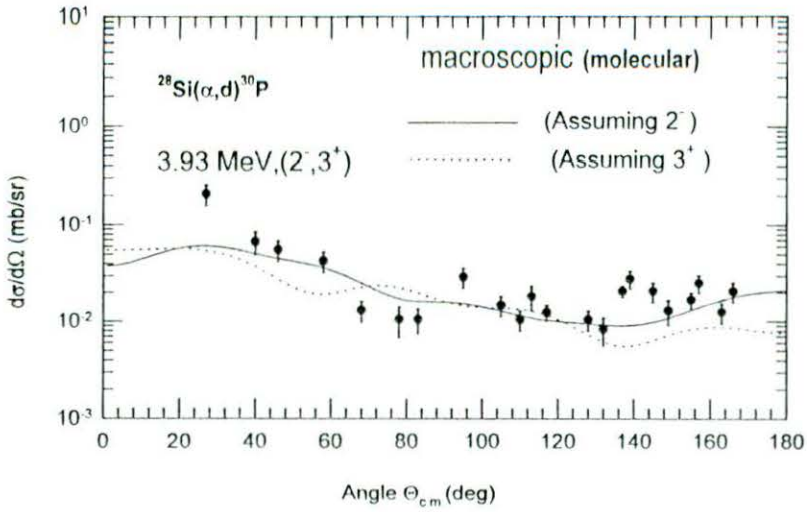

Fig. 4. Full finite-range macroscopic DWBA calculations using the molecular α-^{28}Si potential for the 3.93 MeV state assuming the spin-parity $J^{\pi}=2^-$ (solid curve) and 3^+ (dotted curves) are compared to the data. The data are from [17]

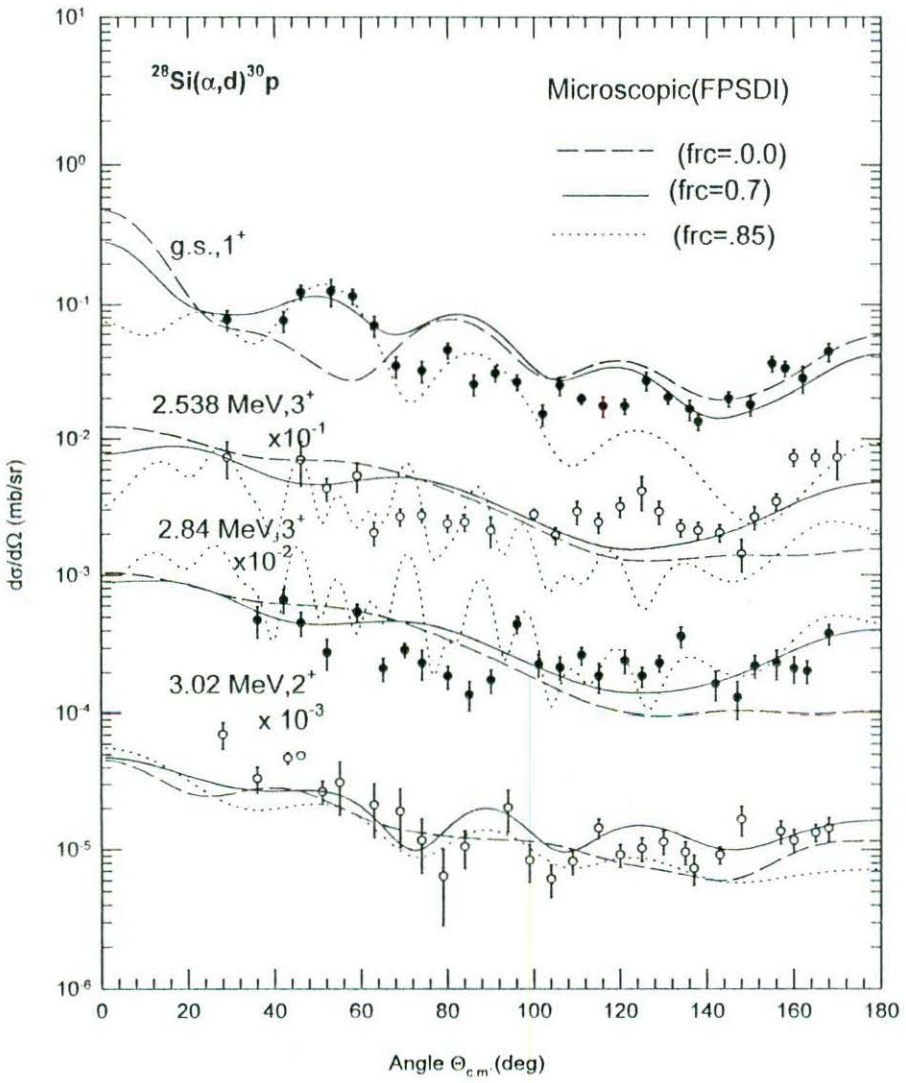

Fig. 5. Comparison of the zero-range microscopic DWBA calculations using the FPSDI spectroscopic amplitudes and the molecular potential in the α-channel for the ^{28}Si(α,d)^{30}P reaction at 26 MeV leading to the ground (1^+), 2.538(3^+), 2.84(3^+) and 3.02 (2^+) MeV states of ^{30}P to the differential cross-section data. The solid curves are the predictions using the finite-range (FR) correction with FR parameter R=0.7 fm. The broken and dotted curves are the predictions with R=0.0 and 0.85 fm, respectively. The data are from [17].

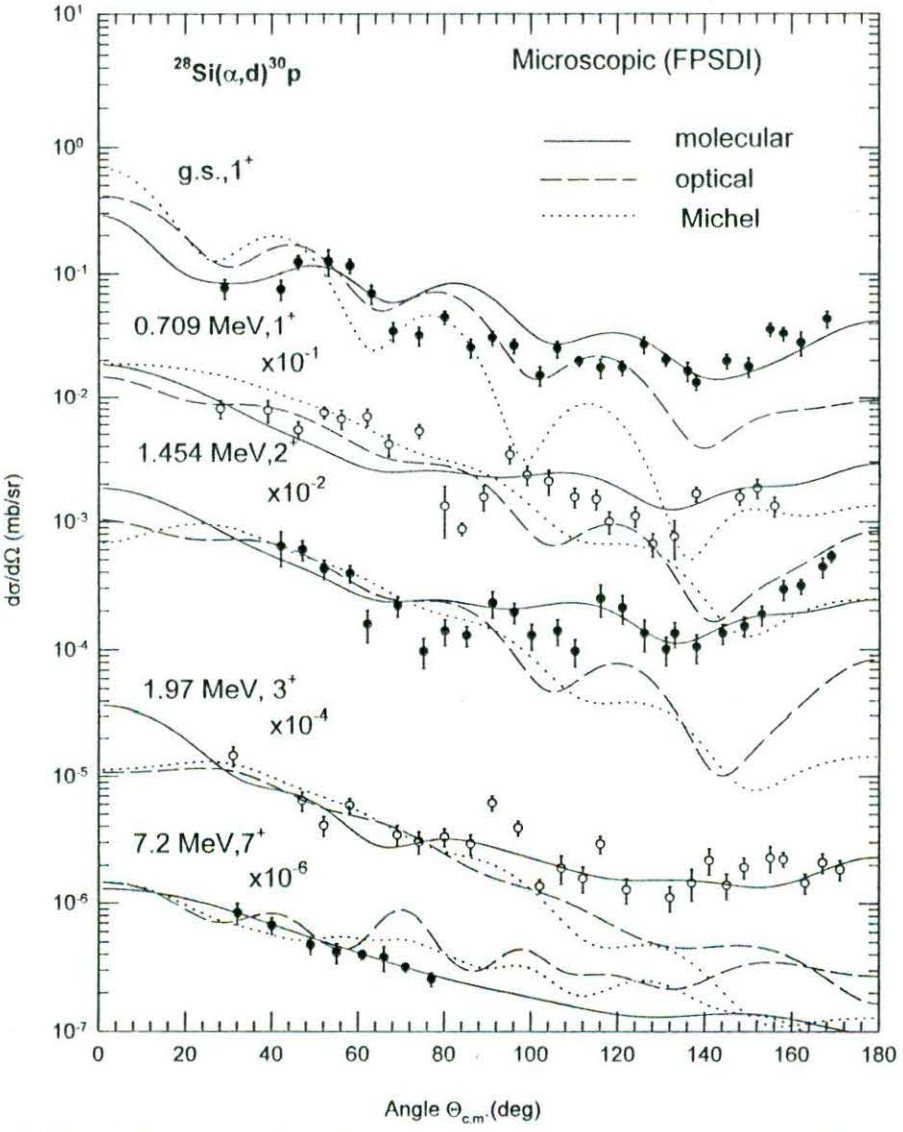

Fig. 6. Comparison of zero-range microscopic DWBA calculations with FR correction for the ^{28}Si(α,d)^{30}P reaction at 26 MeV leading to the ground (1$^+$), 0.709(1$^+$), 1.454(2$^+$), 1.93(3$^+$), and 7.20 (7$^+$) MeV states of ^{30}P to the differential cross-section data. The solid, broken and dotted curves are the predictions using the molecular, optical and Michel α-^{28}Si potentials, respectively. The data are from [17]

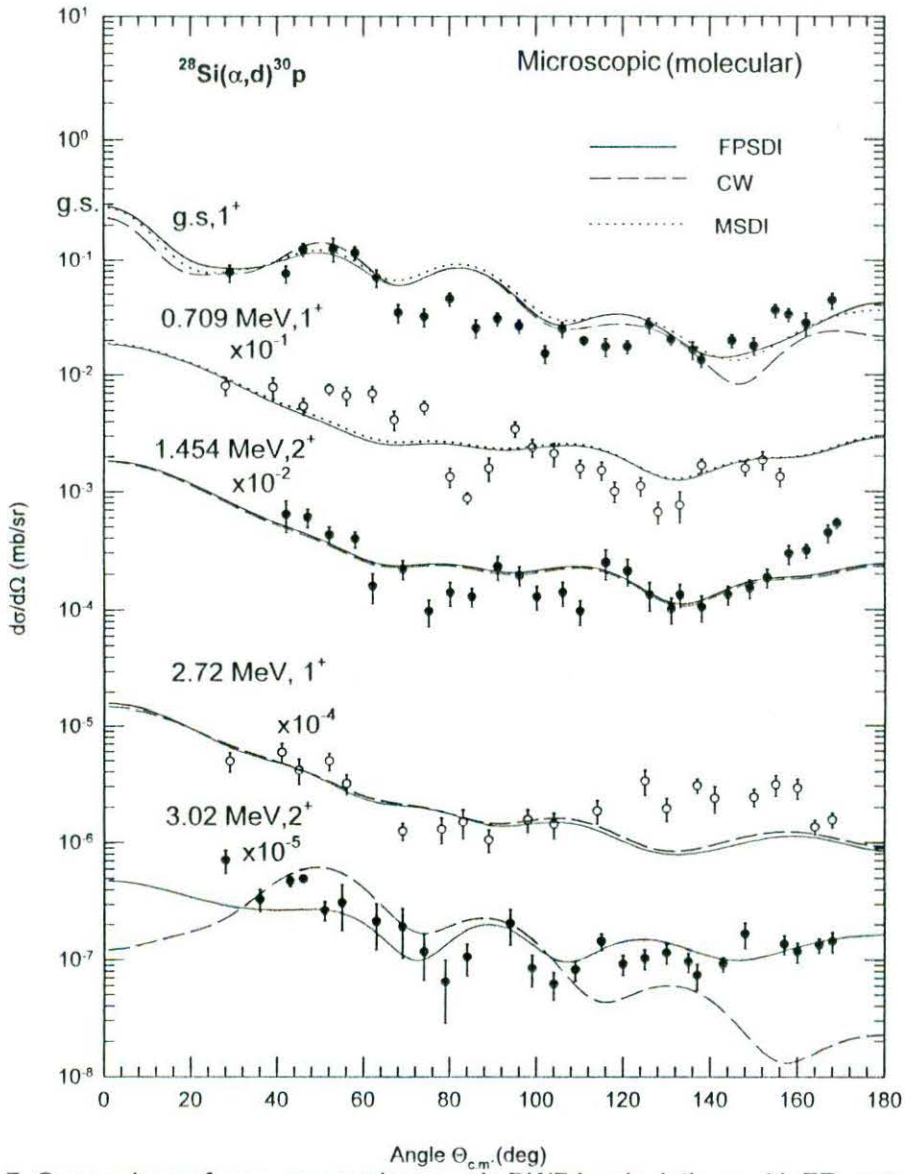

Fig. 7. Comparison of zero-range microscopic DWBA calculations with FR correction and the molecular potential for the ^{28}Si(α,d)^{30}P reaction at 26 MeV, leading to the 1^+ and 2^+ states of ^{30}P to the differential cross-section data. The solid, broken and dotted curves are the predictions using the FPSDI, CW and MSDI spectroscopic amplitudes. The data are from [17].

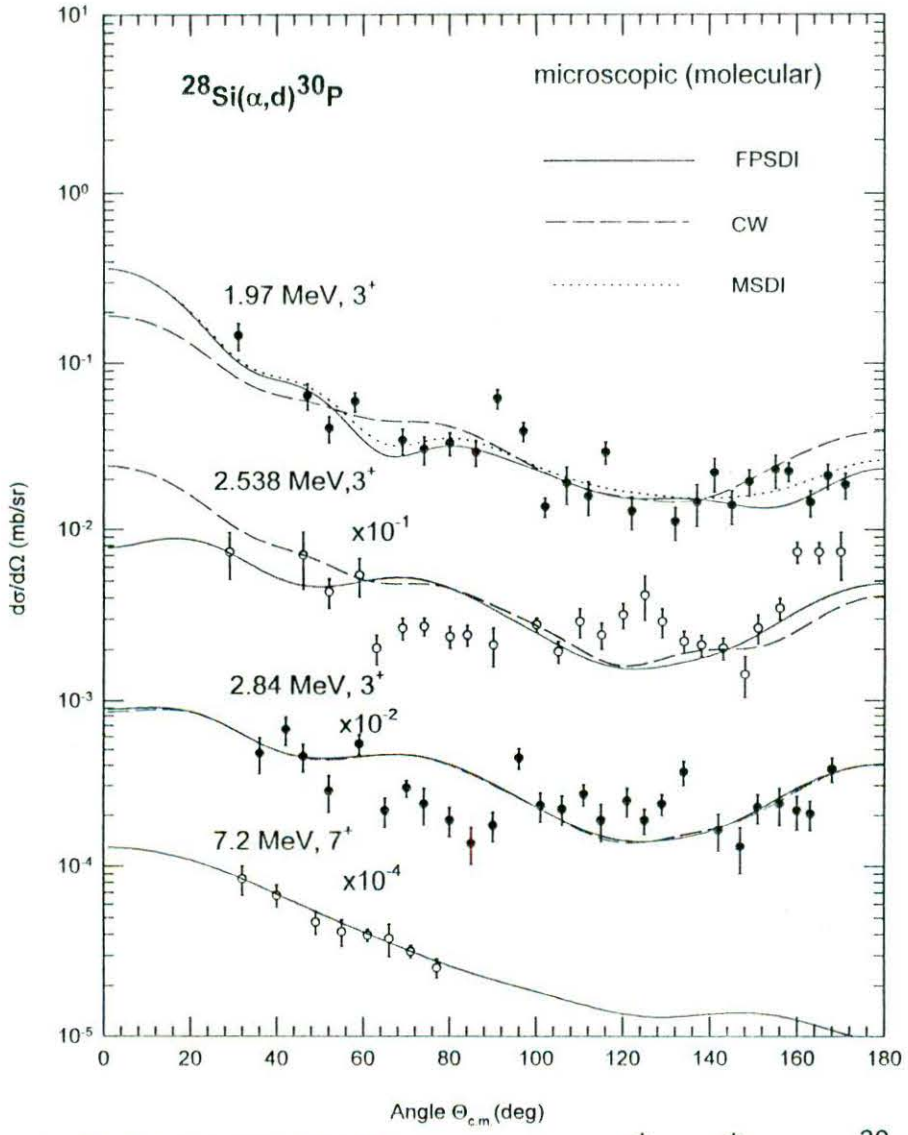

Fig.8. Same as in Fig. 7 for transitions to the 3^+ and 7^+ states of ^{30}P. The data are from [17].

Effect of α-nucleus potential on the ^{28}Si$(\alpha,p)^{31}$P reaction

S. K. Das[1], A. K. Basak[1], K. Banu[1], A. S. Mondal[1], A. S. B. Tariq[1], A. F. M. M. Rahman[1], H. M. Sen Gupta[2] and F. B. Malik[3]

[1] *Department of Physics, University of Rajshahi, Rajshahi, Bangladesh*

[2] *Department of Physics, University of Dhaka, Dhaka, Bangladesh*

[3] *Department of Physics, Southern Illinois University, Carbondale, Illinois 62901, U.S.A.*

(March 26, 2000)

The differential cross-section of the ^{28}Si$(\alpha,p)^{31}$P reaction for 26 MeV incident energy has been analyzed in DWBA with zero and full-finite range using a deep and shallow optical, Michel and molecular potentials in the incident channel and a usual optical model potential for proton in the final channel. The parameters of potential in the entrance channel are determined from the elastic scattering data. The calculations done with the deep optical and Michel potentials reproduce the structure of the angular distributions reasonably well, but fail to account for the absolute magnitudes by a few orders. The shallow optical one is satisfactory up to about $\theta_{cm} = 100^{\circ}$. The molecular potential, on the other hand, reproduces both the absolute cross-sections and the pattern of the angular distributions. CCBA calculations improve fits to the data over the DWBA predictions.

PACS number(s) : 25.55.Hp, 21.10.Jx, 24.50.+g, 27.30.+t

I. INTRODUCTION

Anomalous large angle scattering (ALAS), observed in the elastic scattering of alpha-particles by light and medium-light nuclei [1–3], have recently been analyzed successfully for ^{24}Mg, ^{28}Si, ^{30,32}S targets in terms of a complex molecular [4,5] and a special type of optical potential with a squared Woods-Saxon geometry, advocated by Michel and his collaborators [6,7]. The latter is, henceforth, referred to as the Michel potential. Both of these potentials describe equally well the elastic scattering data in a wide energy range with a small set of parameters changing systematically with energies.

The ALAS effects have also been observed in the non-elastic processes [2,3,8–13]. Schmittroth *et al.* [11] have established that the use of a complex molecular potential could enhance the back angle scattering in a single-nucleon transfer reaction involving heavy ion. Similarly, ALAS has also been observed by Jankowski *et al.* [14] in the two- and three-particle transfer reactions on the ^{28}Si target. The large-angle behavior of the data in the latter work has been analyzed in terms of an incoherent sum of the distorted-wave Born approximation (DWBA) contribution calculated with the normal optical potentials and the compound nucleus contribution predicted on the basis of the Hauser-Feshbach model [15]. The method has, however, enjoyed a limited success.

The three-nucleon transfer in (α,p) reactions is a complex process. In addition to probable contributions from compound nucleus, pre-compound and multi-step sequential transfer processes, the direct part of the reaction mechanism may comprise triton stripping, knock-on and heavy-particle stripping [16–18]. Of these triton stripping has been found to be the dominant one [16]. Although calculations in DWBA using the usual optical potential in the incident channel can, quite often, reproduce the general pattern of angular distribution, but the absolute cross-section is understimated by two to three orders of magnitude [19]. The normalization problem also persists in (α,p) reactions [20–23]. Walz *et al.*'s [24] claim to reduce the discrepancy between the data and calculation to 20% for the (p,α) case using a double-folded α-nucleus potential, has been contradicted by Kajihara *et al.* [25], who failed to reproduce the Walz *et al.*'s calculations and found an enhancement factor $\epsilon = 4$ instead of 1.2. The purpose of the present study is, therefore, to examine the extent to which the molecular, Michel and optical potentials can account for the pattern, magnitude and ALAS observed in the three-nucleon transfer (α,p) reaction on ^{28}Si. The study is also a part of our broader goal of finding the nature of α-nucleus potential capable of explaining a number of physical phenomena involving an alpha particle and a light nucleus, in this case ^{28}Si. As evidenced from a number of investigations including the single-nucleon (α,p) transfer reaction on ^{28}Si by Das *et al.* [12], it is important to select data having fairly complete angular distributions in order to differentiate the effects of α-nucleus potential on a reaction process. With this in mind, we have selected the experimental cross-section data of Jankowski *et al.* [14] for the ^{28}Si$(\alpha,p)^{31}$P reaction covering a wide range in angular distribution including those at large angles, which are expected to be sensitive to the nature of α-nucleus potential.

The investigation has been carried out within the framework of zero-range (ZR) DWBA formalism with a simple process of triton-cluster transfer using shallow, deep, Michel and molecular optical potentials in the incident alpha-channel.The full finite-range (FFR) DWBA and the coupled-channels Born approximation (CCBA) calculations for

the molecular potential have also been performed to determine the viability of the latter two potentials. This investigation further reinforces the past assertion that data having a wide range of angular distribution are important for understanding the physical process involving α-particle and light nuclei.

Section II discusses the α-nucleus potentials used in the analyses. The DWBA and CCBA analyses are furnished in Sections III and IV respectively. Section V deals with the discussion and the conclusions.

II. α-NUCLEUS POTENTIALS

$V_m(r)$, the real and $W_m(r)$, the imaginary parts of the complex molecular potential, which has its root in the energy-density functional study of the reaction [4,26] are given by

$$V_m(r) = -V_0 \left[1 + exp\left\{(r - R_0)/a_0\right\}\right]^{-1} + V_1 exp\left\{-\left(r^2/R_1^2\right)\right\}$$
$$W_m(r) = -W_0 exp\left\{-\left(r^2/R_W^2\right)\right\} \tag{1}$$

The real $V_M(r)$ and imaginary $W_M(r)$ parts, of the Michel potential which is an approximate form of the non-local potential expected from the resonating group method (RGM) as applied to the α-cluster system [27,28] are given by

$$V_M(r) = -V_0 \left[1 + \alpha exp\left\{-\left(r^2/\rho^2\right)\right\}\right] \left[1 + exp\left\{(r - R_0)/2a_0\right\}\right]^{-2}$$
$$W_M(r) = -W_0 \left[1 + exp\left\{(r - R_I)/2a_I\right\}\right]^{-2} \tag{2}$$

The real and imaginary parts of the normal optical potential, $V(r)$ and $W(r)$ are given, respectively, by

$$V(r) = -V_0 \left[1 + exp\left\{(r - R_0)/a_0\right\}\right]^{-1}$$
$$W(r) = -W_0 \left[1 + exp\left\{(r - R_I)/a_I\right\}\right]^{-1} \tag{3}$$

The Coulomb part for all three types of potentials is given by

$$V_C(r) = \left[\frac{Z_1 Z_2 e^2}{2R_C}\right]\left[3 - \frac{r^2}{R_C^2}\right] \text{ for } r \leq R_C \tag{4}$$
$$= \frac{Z_1 Z_2 e^2}{r} \qquad \text{for } r > R_C \tag{5}$$

In case of the Michel and optical potentials, R_C is quite often written as $= r_C A_T^{1/3}$, where A_T is the target mass number. On the other hand, in case of the molecular potential, R_C is the sum of the alpha and ^{28}Si radii when they barely touch each other.

Although the normal optical model has not been very successful in reproducing the elastic scattering data over the energy range investigated by Jankowski *et al.* [14] and Jarczyk *et al.* [10], it is possible to find a set of parameters producing a reasonable fit to the elastic scattering data at 26 MeV. Observing that the energy-density functional approach in the special adiabatic approximation may lead to a shallow optical potential [26], a search for such a potential has also been made and included in the study.

The parameter search has been carried out using the code SCAT2 [29] modified by us to incorporate molecular and Michel potentials. The parameters obtained from the best fit to the elastic scattering data of α-particle by ^{28}Si at 26 MeV incident energy are listed in Table I. The fits to the elastic data are shown in Fig. 1. In general, the fits with all four potentials are reasonable, although the shallow optical potential fit is somewhat poorer than those of the rest. Parameters of the molecular and Michel potentials are the same as the ones in Ref. [5].

III. DWBA ANALYSIS

The zero-range DWBA calculations have been performed using the code DWUCK4 [30] which has been modified to include the Michel potential in the distorting channels. The potential parameters in the distorting incident channel used in the DWBA calculations are noted in Table 1 for all four potentials. The bound state wave function for the transferred triton, considered as a point cluster, has been generated by assuming a real Woods-Saxon well with its depth adjusted to reproduce the separation energy. These parameters along with the proton optical potential are also noted in Table 1. Corrections due to non-locality [31] of potential in the conventional form have been applied

using the non-locality ranges $\beta(\alpha) = 0.2$, $\beta(p) = 0.85$ and $\beta(t) = 0.2$ fm. The correction in the triton-bound state form-factor is found to produce little effect on the cross-section. The calculations using all four potentials for the ^{28}Si$(\alpha,p)^{31}$P reaction leading to the $1/2^+$ ground, 1.266 MeV $3/2^+$ and 2.234 MeV $5/2^+$ states are compared with the data of Jankowski *et al.* [14] in Fig. 2.

To test the validity of using the molecular potential, the full finite-range DWBA calculations have been carried out using the code DWUCK5 [22]. The (t+p) bound state geometry for the FFR calculations is shown in Table 1. The FFR predictions are compared to the data in Fig.3. The spectroscopic factors S for the cluster transfer have been deduced from the expression [30]

$$\left(\frac{d\sigma}{d\Omega}\right)_{expt} = \frac{2J_f + f}{2J_i + 1} C^2 S s \left(\frac{d\sigma}{d\Omega}\right)_{DWUCK5} \tag{6}$$

Here $\left(\frac{d\sigma}{d\Omega}\right)_{expt}$ and $\left(\frac{d\sigma}{d\Omega}\right)_{DWUCK5}$ are, respectively, the experimental cross-section and that predicted by DWUCK5. J_f and J_i are the total spins of the final and initial nuclei, respectively. $s = 2.0$ is the light particle spectroscopic factor. C^2 is the isospin Clebsch-Gordon coefficient. The deduced S-values are listed in Table 2. The normalization constant D_0^2 for the t-cluster transfer in the ZR calculations has been estimated from the expression [22]

$$\left(\frac{d\sigma}{d\Omega}\right)_{expt} = \frac{(2J_f + 1)}{(2J_i + 1)\,(2j + 1)} D_0^2 C^2 S \left(\frac{d\sigma}{d\Omega}\right)_{DWUCK4} \tag{7}$$

Here $\left(\frac{d\sigma}{d\Omega}\right)_{expt}$ and $\left(\frac{d\sigma}{d\Omega}\right)_{DWUCK4}$ are, respectively, the experimental cross-section and that predicted by DWUCK4. The deduced D_0^2 values and the average $D_0^2 = 2.25 \times 10^4$ MeV^2 fm^3 have been shown in Table 2. It is evident, from Fig.3, that the FFR calculations do not improve fits over the ZR predictions and reduce the cross-sections at larger reaction angles even more. Nevertheless, the FFR calculations allow us to extract the spectroscopic factors.

IV. CCBA ANALYSIS

The CCBA calculations using the molecular potential have been carried out using the code CHUCK3 [30], with the coupling scheme shown in Fig.4 and the deformation parameters $\beta_2 = -0.18$ and $\beta_4 = +0.08$ for ^{28}Si. In the CCBA calculations, the depth of the imaginary part of the molecular potential (Table 1) has been decreased to 10.5 MeV in order to reproduce the angular distribution for the elastic scattering. All possible relative phases and various relative transition amplitudes a_R in the rearrangement paths have been tried in the simplest possible coupling scheme. The transition strength in a two-step path is proportional to the square of βa_R. The CCBA predictions using the relative spectroscopic amplitudes given in Table 2 for the $1/2^+$ ground, 1.266 MeV $3/2^+$, 2.234 MeV $5/2^+$ and 3.415 MeV $7/2^+$ state transitions have been compared to the data in Fig. 3. The CCBA calculations improve the fits over the ZR and FFR calculations. The inelastic 4^+ state at $E_x = 4.618$ MeV in ^{28}Si plays a major role in the CCBA calculations in reproducing the ground state data. The coupling to the inelastic 2^+ state to the ground state of ^{28}Si is also significant in improving the fits to the data for the 1.266 and 2.234 MeV states of ^{31}P. The CCBA calculations seem to confirm the deformed shape of the ^{28}Si nucleus.

V. DISCUSSION AND CONCLUSION

The present work reports, for the first time, the analyses of a three-nucleon transfer reaction using the molecular type potential. While the patterns of the angular distributions for the reaction to the ground ($1/2^+$), 1.27 MeV ($3/2^+$) and 2.23 MeV ($5/2^+$) states of the final nucleus, are reasonably reproduced by the DWBA calculations using the deep optical and Michel potentials, the predicted cross-sections are off by 2 to 4 orders of magnitudes in each case. This agrees with the results of Refs. [21,23] for the calculation with the deep optical potential and those of Xiumin *et al.* [36] who failed to reproduce the data for the ^{40}Ca$(\alpha,p)^{43}$Sc reaction with the squared WS potential used by the Michel group [32]. However, the DWBA and CCBA calculations using the molecular potential and assuming a simple triton-cluster transfer mechanism, reproduce not only the angular oscillations more satisfactorily, but also the correct order of absolute cross-sections for each of the four final states including the one at 3.42 MeV excitation of ^{31}P. The calculation using the shallow potential reproduces the magnitudes up to 100° or so, but then decreases sharply at large angles. Thus, the molecular potential is the only one to account for the data for the ground ($1/2^+$), 1.27 MeV ($3/2^+$) and 2.23 MeV ($5/2^+$) final states over the entire angular distributions. Furthermore, the present analysis

indicates that the data for the reaction can be successfully described without any compound nucleus contribution, as included by Jankowski *et al.* [14], which is highly improbable at the incident energy considered here.

A pertinent question arises as to why the Michel potential, which has been so successful in accounting for ALAS in the elastic scattering on many targets [6,7,32,33] including ^{28}Si in the present work, fails to reproduce the data of the ^{28}Si$(\alpha,p)^{31}$P reaction. The Michel potential has also been found to be inadequate for the one-nucleon transfer reaction [12]. Aside from the fact that the Michel potential is monotonic, whereas the molecular is non-monotonic, one may note that the two potentials differ significantly in defining the Coulomb radius. In case of the molecular potential, the Coulomb radius R_C is the distance where ^{28}Si barely touches the α particle. The observed density distribution, $\rho(r)$ for ^{28}Si is given by [34]

$$\rho(r) = \rho(0)\left[1 + exp\frac{r-c}{d}\right]^{-1} \tag{8}$$

with $c = 3.14$ fm. and $d = 0.537$ fm. Thus, at $r = 6$ fm., $\rho(r) = 0.005\rho(0)$. A reasonable density distribution for α particle is $4\left(\frac{\gamma}{\pi}\right)^{3/2}\exp\left(-\gamma r^2\right)$ with γ=0.5 [35]. This is about 0.001 at r=3.35 fm. Thus, a reasonable value of R_C is (6.00+3.35)=9.35 fm., which is used in the molecular potential. The Michel, on the other hand, uses R_C=3.95 fm. At this distance, the two nuclei have inter-penetrated each other substantially. In the DWBA theory, the stripped particles from the projectile are assumed to drop on the nuclear surface and hence, the treatment may be somewhat sensitive to the actual value of R_C.

One may summarize from the displays in Figs. 1 to 3 that, while the molecular, the Michel with the squared WS geometry and the normal optical potentials produce more or less the similar quality of fits to the elastic data, their use in describing the transfer data for the (α,p) reactions leads to significantly different results, with only the molecular one accounting for the observed data in terms of both absolute cross-sections and angular distribution. This supports Satchler's contention [37] that the real test of a potential set generated from the analysis of elastic scattering data lies in its ability in reproducing the non-elastic data. The present work seems to suggest preference for the molecular potential over other forms of the alpha-nucleus potential in describing the angular distribution of the (α,p) reaction on ^{28}Si at 26 MeV. The finding demands further investigation with other targets.

ACKNOWLEDGMENTS

The interests and assistance of Professor M. Brenner are gratefully acknowledged. This research work is made possible by the grant INT-9808892 of the U.S. National Science Foundation and a grant from the Ministry of Science & Technology, Government of Bangladesh, which are thankfully acknowledged. One of us, SKD, is also thankful to the American Institute for Bangladesh Studies for a travel grant to U.S.A. The authors are also thankful to Professor P.D. Kunz of the University of Colorado for making codes DWUCK4, DWUCK5 and CHUCK3 available to them.

[1] J.C. Correlli, E. Bleuler and D.J. Tendam, Phys. Rev. **116**, 1184 (1959).
[2] H. Oeschler, H. Schröter, H. Ficjs, L. Baum, G. Gaul, H. Lüdecke, R. Santo and R. Stock, Phys. Rev. Lett. **28**, 694 (1972).
[3] Å. Bredbacka, M. Brenner, K.-M. Källman, P. Månngard, Z. Máté, S. Szilágyi and L. Zolnai, Nucl. Phys. **A574**, 397 (1994).
[4] P. Manngård, M. Brenner, M.M. Alam, I. Reichstein and F.B. Malik, Nucl. Phys. **A504**, 130 (1989).
[5] A.S.B. Tariq, A.F.M.M. Rahman, S.K. Das, A.S. Mondal, M.A. Uddin, A.K. Basak, H.M. Sen Gupta and F.B. Malik, Phys. Rev. C **59**, 2558 (1999).
[6] F. Michel, J. Albinski, P. Belery, Th. Delbar, Gh. Grégoire, B. Tasiaux and G. Reidemeister., Phys. Rev. C **28**, 1904 (1983).
[7] F. Michel, G. Reidemeister and S. Ohkubo, Phys. Rev. Lett. **57**, 1215 (1986).
[8] W. Trombik, K.A. Eberhard and J.S. Eck, Phys. Rev. C **11**, 685 (1975).
[9] A.M. Kobos, B, A. Brown, R. Lindsay and G.R. Satchler, Nucl. Phys. **A425**, 205 (1984).
[10] L. Jarczyk, B. Maciuk, M. Siemaszko and W. Zipper, Acta Phys. Pol. **B7**, 531 (1976).
[11] F. Schmittroth, W. Tobocman and A.A. Golestaneh, Phys. Rev. C **1**, 377 (1970).
[12] S.K. Das, A.S.B. Tariq, A.F.M.M. Rahman, P.K. Roy, M.N. Huda, A.S. Mondal, A.K. Basak, H.M. Sen Gupta and F. B. Malik, Phys. Rev. C **60**, □□□□□ (1999).

[13] H.-J. Apell, W. Gemeinhardt, R. Stock, R.R. Betts, O. Hansen, A. Sperduto, H. Fuchs and R. Santo, Nucl. Phys. **A246**, 477 (1975).
[14] K. Jankowski, A. Grzeszczuk, M. Siemaszko, A. Surowiec, W. Zipper, A. Budzanowski and E. Kozik, Nucl. Phys. **A426**, 1 (1984).
[15] W. Hauser and H. Feshbach, Phys.Rev. **87**, 366 (1952).
[16] P.E. Hodgson, Lecture at Int. Summer School, La Rabida, Spain (1985).
[17] E. Gadioli and P.E. Hodgson, Rep. Prog. Phys. **52**, 247 (1989)
[18] R.Bonetti, F. Crespi and K. -I. Kubo, Nucl. Phys. **A499**, 381 (1989).
[19] H. Oberhummer, Nuov. Cim. **55A**, 253 (1980).
[20] N. S. Chant and N. F. Mangelson, Nucl. Phys. **A140**, 81 (1970).
[21] F. Brunner, H.H. Müller, C. Dorninger and H. Oberhummer, Nucl. Phys. **A398**, 84 (1983).
[22] F. Hoyler, H. Oberhummer, T. Rohwer, G. Staudt and H. V. Klapdor,Phys. Rev. C **31**, 17 (1985).
[23] J.J. Hamill and P.D. Kunz, Phys. Lett. **129B**, 5 (1983).
[24] M. Walz, R. Neu, G. Staudt, H. Oberhummer and H. Cech, J. Phys. **G14**, L91 (1988).
[25] T. Kajihara, Y. Yamamoto and K.-I. Kubo, Nucl. Phys. **A568**, 499 (1994).
[26] I. Reichstein and F.B. Malik, Phys. Lett. **37B**, 344 (1971).
[27] T. Wada and H. Horiuchi, Phys. Rev. Lett. **58**, 2190 (1987).
[28] T. Wada and H. Horiuchi, Phys. Rev. C **38**, 2063 (1988).
[29] O. Bersillon, The Code SCAT2, NEA 0829, private communication.
[30] P.D. Kunz, The Codes DWUCK4, DWUCK5 and CHUCK3, private communication.
[31] F.G. Perey, *Proc. Conf. on Direct Interactions and Nuclear Reaction Mechanisms* (Gordon and Breach, New York, 1963), p.125; Phys. Rev. **131**, 755 (1963).
[32] Th. Delbar, Gh. Grégoire G. Paic, R. Ceuleneer, F. Michel, R. Vanderpoorten, R. Budzanowski, H. Dabrowski, L. Friendl, K, Grotowski, S. Micek, R. Planeta, A. Strzalkowski and A. Eberhard, Phys. Rev. C **18**, 1237 (1978).
[33] F. Michel, G. Reidemeister and Y. Kondo, Phys. Rev. C **51**, 3290 (1995).
[34] H. de Vries, C.W. de Jaeger and C. de Vries, At. Data Nucl. Data Tables **36**, 495 (1987).
[35] L.R.B. Elton, *Nuclear Sizes*, (Oxford Univ. Press, 1961).
[36] B. Xiumin, L. Shuming, W. Yuanda, Y. Rongfang, H. Bingyin and S. Zuxun, Chin. J. Nucl. Phys. **7(3)**, 226 (1985).
[37] G.R. Satchler, in *Proceedings International Conference on Reactions between Complex Nuclei*, edited by R.L. Robinson *et al.* (North-Holland, Amsterdam, 1974), p.171.

TABLE I. Parameters of the α-^{28}Si potentials given by Eqs. (1), (2) and (3) used in the calculations shown in Fig. 1 are given in columns 1 to 5. The parameters of proton optical-model potential, and bound states of (t+^{28}Si) and (t+p) systems are noted in columns 6-8, respectively. V is adjusted to give the separation energy.

Channel	α + ^{28}Si				p + ^{31}P	t + ^{28}Si	t + p
Potential Type	Molecular[a]	Michel[a]	Deep Optical	Shallow[b] Optical	Optical[c]	Bound State[b]	Bound State[b]
V_0 (MeV)	26.0	21.0	216.0	55.0	53.3 - 0.55E_p	V	V
R_0 (fm)	5.35	5.00	3.70	5.16	-	-	-
r_0 (fm)	-	-	-	-	1.25	0.929	1.05
a_0 (fm)	0.34	0.60	0.67	0.505	0.65	0.921	0.50
V_1 (MeV)	42.0	-	-	-	-	-	-
R_1 (fm)	2.80	-	-	-	-	-	-
α	-	8.39	-	-	-	-	-
ρ (fm)	-	6.25	-	-	-	-	-
W_0 (MeV)	14.5	33.1	22.4	8.64	-	-	-
R_I (fm)	-	3.85	3.98	5.16	-	-	-
a_I (fm)	-	0.65	0.67	0.505	-	-	-
R_W (fm)	4.00	-	-	-	-	-	-
W_D (MeV)	-	-	-	-	13.5	-	-
r_D (fm)	-	-	-	-	1.25	-	-
a_D (fm)	-	-	-	-	0.47	-	-
R_C (fm)	9.35	3.95	4.07	3.95	-	-	-
r_C (fm)	-	-	-	-	1.30	1.30	1.25

[a]Ref. [5].
[b]Ref. [14].
[c]Ref. [31].

TABLE II. Cluster transfer configurations (n: number of nodes, L: angular momentum) used in the CCBA are shown in columns 3 to 6. Column 7 indicates the relative spectroscopic amplitudes used in calculations shown in Fig. 3. Columns 8 and 9 are, respectively, the spectroscopic factors deduced from the FFR calculations and the normalization constant for the (α,p) reaction for the DWBA calculations.

E_x	J^π	Cluster transfer configuration					Spect.	$D_0^2 \times 10^4$
(^{31}P)		One-step	Two-step			Relative Spect.	Factor	MeV^2 fm^3
MeV		nL_d	nL_{t_1}	nL_{t_2}	nL_{t_3}	Amplitudes	S	
0.0	1/2+	3S	1G	-	-	+01:+15	0.070	2.00±0.50
1.266	$3/2^+$	2D	2D	3S	-	+01:+05:-05	0.031	2.56±0.64
2.234	$5/2^-$	2D	2D	3S	1G	+01:+01:+02:-01	0.004	-
3.415	$7/2^-$	2G	3D	4S	-	+01:+06:+02	0.003	-

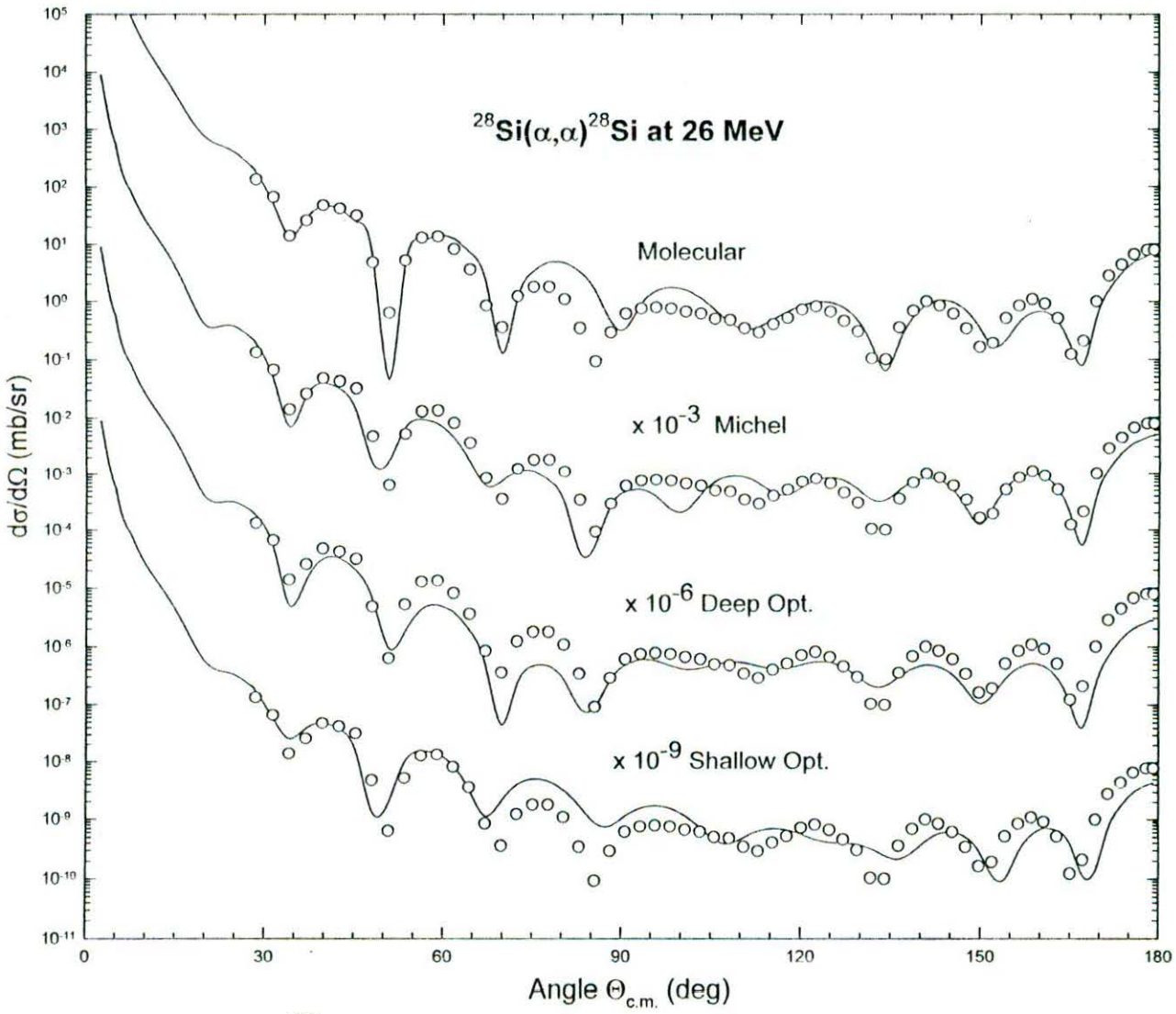

Fig.1. Fits to the α-^{28}Si elastic scattering data at 26 MeV (lab.) with the molecular, Michel, deep and shallow normal optical potentials. Data are from [9]

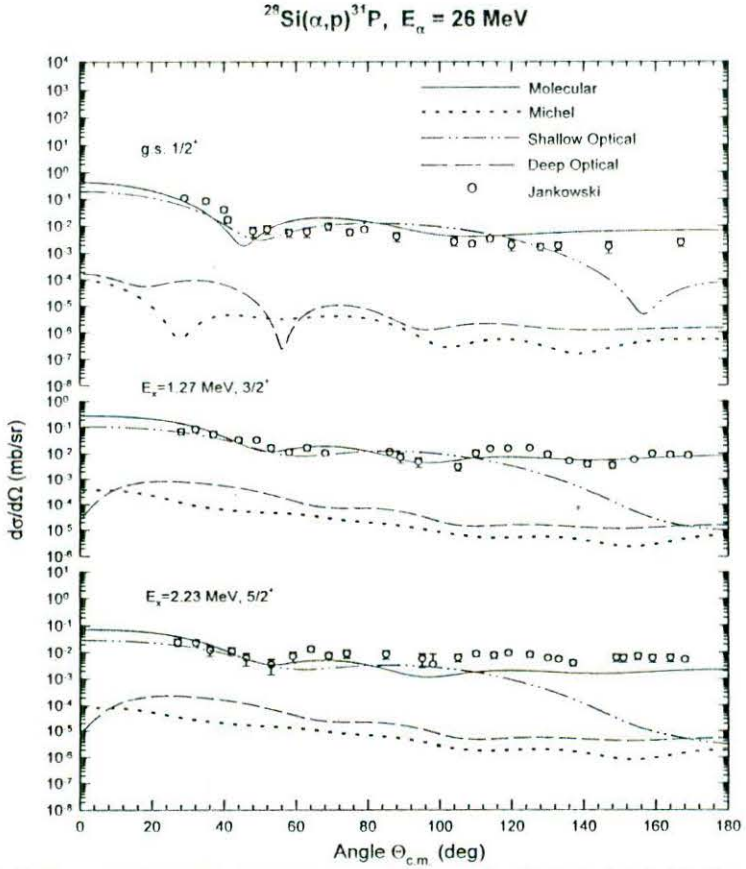

Fig.2. Zero-range DWBA predictions are compared to the angular distribution of cross-sections for the $^{28}Si(\alpha,p)^{31}P$ reaction at 26 MeV leading to the ground($1/2^+$), 1.27 ($3/2^+$), and 2.234 ($5/2^+$) MeV states. Solid, dotted, dashed and dash-dotted curves are the predictions for the molecular, Michel, deep and shallow normal optical potentials respectively, in the α-channel. The data are from [14].

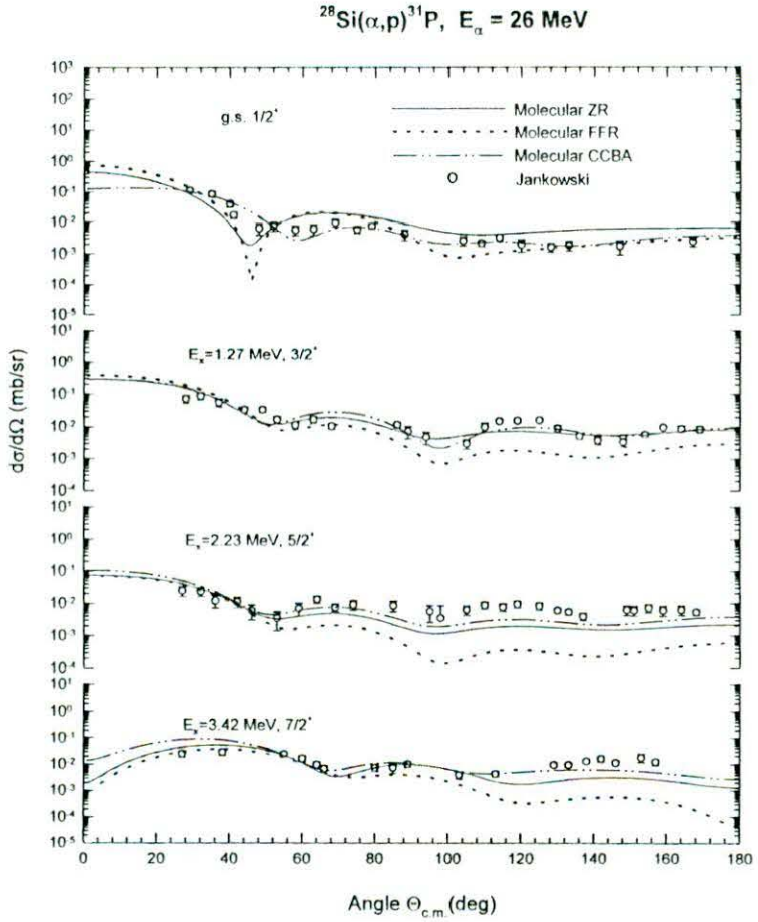

Fig.3. Zero-range (solid), full finite-range(dotted lines) and CCBA (dashed lines) predictions of the transfer reaction using the molecular potential are compared to the data for the $^{28}Si(\alpha,p)^{31}P$ reaction at 26 MeV leading to the ground ($1/2^+$), 1.27 ($3/2^+$), 2.23 ($5/2^+$), 3.42 ($7/2^+$) MeV states. The data are from [14].

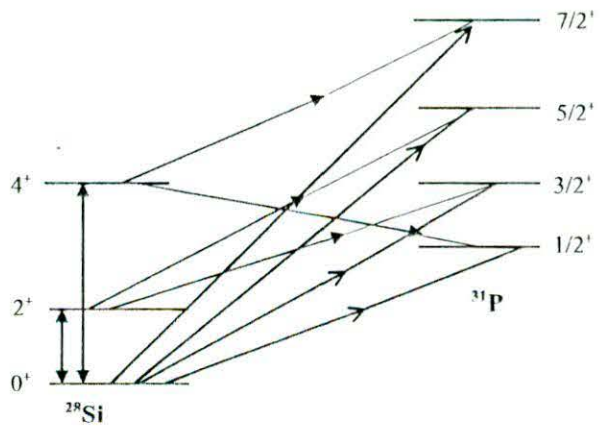

Fig. 4. Coupling scheme in the CCBA calculations..